DISSERTATION

NOVEL FOULING RESISTANT MAGNETICALLY-RESPONSIVE MEMBRANES FOR TREATMENT OF IMPAIRED WATER

Submitted by

Heath Henry Himstedt

Department of Chemical and Biological Engineering

In partial fulfillment of the requirements

For the Degree of Doctor of Philosophy

Colorado State University

Fort Collins, Colorado

Fall 2012

Doctoral Committee:

Advisor: S. Ranil Wickramasinghe

Travis Bailey
Xianghong Qian
Mathias Ulbricht
Reagan Waskom

ABSTRACT

NOVEL FOULING RESISTANT MAGNETICALLY-RESPONSIVE MEMBRANES FOR TREATMENT OF IMPAIRED WATER

The focus of this dissertation research is the development of novel fouling resistant magnetically-responsive micromixing filtration membranes. Maintenance and replacement costs account for well over half the total cost of membrane processes. Fouling limits membrane performance by reducing membrane flux and lifetime. Specialized stimuli-responsive membranes have been investigated as a means to combat fouling; however, stimuli such as pH, solution ionic strength, and temperature require changes to the entire feedstream to impart a response. This is time consuming and expensive. The novel membranes presented in this dissertation combat fouling through active hydrodynamic disruption of the filtration boundary layer via instant activation by an external magnetic field without the need to adjust feedstream conditions. The fouling resistant properties of these membranes were tested by using them to treat oily wastewaters from oil and gas production, known as produced water.

Chapter 1 introduces concepts referenced throughout the dissertation narrative including basic principles of pressure-driven membrane technology; the principles of membrane fouling and fouling resistant membranes; a review of applications of (super)paramagnetic nanoparticles; and a discussion of produced water and the treatment challenges it presents. Chapters 2 through 6 are published, or soon to be submitted, scientific papers which chronicle the development and application of these novel membranes. Chapter 2 discusses the concepts behind magnetically-activated micromixing and presents initial proof-of-concept nanofiltraiton membranes. Chapter 3 employs track-etched membranes to characterize the modification protocol and the magnitude

of the magnetic response, as well as the relationship between the two. Chapter 4 determines the effect of modification grafting density on mixing efficacy and membrane filtration properties. Chapter 5 shows the improvements to membrane performance and lifetime attributable to magnetically-activated mixing during filtration of model produced water and realistic produced water. Chapter 6 builds upon Chapter 5 by using treated realistic produced water permeate as irrigation water. Chapters 7 and 8 summarize the research findings and present possible direction for future research, respectively.

This work presents the development and one potential application of novel magnetically-activated micromixing membranes. These membranes reduce membrane fouling by inducing hydrodynamic mixing in an alternating magnetic field. These membranes could lead to improved membrane performance and lifetime when treating highly fouling feedstreams. This would significantly decrease membrane maintenance and replacement costs and could lead to new clean water product streams.

Chapters 2 and 3 have been published in scientific journals, and Chapter 4 is currently in revision for publication. See the curriculum vitae in Appendix A6 for additional detail.

ACKNOWLEDGEMENTS

The love and support of my family was invaluable throughout the past four years. I could not have succeeded without H3, Ok, and It.

My secondary families helped me feel at home in Colorado: the Difrancos, the Wittmeyers, Boy Scout Troop 12 and Venture Crew 12, and Meadowlark Church of Christ and First Presbyterian Church.

My time at CSU would not have been the same without my advisor, Dr. Ranil Wickramasinghe. He provided me much guidance, challenged me to better myself, introduced me and my work to countless members of industry and academia, and taught me many valuable lessons for my future career in academia.

I sincerely thank Dr. Wickramasinghe and Dr. Dandy for allowing me to finish my last year at CSU and Dr. Snow for allowing me to continue my experiments in his lab.

My dissertation research was funded by a Department of Defense National Defense Science and Engineering Graduate (NDSEG) Fellowship. I am extremely grateful for the financial support and the flexibility it afforded me.

My faith is a huge part of my personal fabric, and the comfort of GOD's love and the peace it gave helped me to persevere through the difficult times.

Special mention must be given to the wilderness of Colorado. I often escaped and immersed myself in its beauty and serenity to keep me sane.

.

TABLE OF CONTENTS

LIST OF TABLES

LIST OF FIGURES

CHAPTER 1

INTRODUCTION AND BACKGROUND

The research presented in this dissertation focuses on modifying commercially available membranes to be responsive to a magnetic field. These membranes generate small-scale mixing in the presence of an alternating magnetic field. Their development and one potential application are presented in Chapters 2-6. In order to fully understand the research presented here, knowledge of a few key subjects is required.

1.1 Membrane Fouling and Fouling Resistant Membranes

Membrane filtration offers many advantages over more traditional engineering unit operations. Membranes can operate in continuous or batch mode, are relatively flexible in terms of feed composition, require less energy, have a smaller footprint, and do not generate excess amounts of secondary waste from added (pre)treatment chemicals[1-3]. In pressure-driven filtration, the membrane acts as a barrier which rejects suspended and dissolved compounds in the feed under a pressure driving force. The four major types of pressure-driven membrane filtration are reverse osmosis (RO), nanofiltration (NF), ultrafiltration (UF), and microfiltration (MF). These are used to remove compounds larger than a few angstroms, few nanometers, tens of nanometers, and hundreds of nanometers, respectively[1-3].

Membrane fouling limits the efficacy and lifetime of any membrane system. Fouling is the deposition of compounds onto the membrane surface, via physical or chemical interactions[1-8]. Fouling can be grouped into three major categories: scaling of inorganics when they exceed

saturation concentration, particulate or colloidal fouling where colloids physically deposit on the surface, and biofouling from formation of biofilms such as extra cellular matrices[1-5,8,9]. Over time fouling can reduce membrane flux (throughput) and can reduce the selectivity of the membrane, resulting in a poorer separation. Membrane maintenance and replacement costs are the largest expense of most, if not all, membrane systems[1-5,8]. This is mostly due to fouling, which requires preventative steps to abate or cleaning procedures to reverse. Both of these can be expensive due to the use of chemical additives and loss of production time while maintenance is being performed. More fouling resistant membranes would yield improved membrane performance, longer membrane lifetimes, and better economics for membrane filtration systems. Attempts to develop fouling resistant and/or more easily cleaned membranes represent a large fraction of the total research involving membranes[1,3,5,8,10]. There are three strategies used to reduce membrane fouling.

1.1.1. Alter Feed Characteristics

Because the composition of the feed is the primary factor which determines the propensity for fouling it is possible to reduce the potential for fouling by altering characteristics of the feed through the use of chemical additives and/or pretreatment. Additives can include flocculants, dispersants, or biocides to lesson biofouling. Pretreatment can include removal of certain feed components, altering the pH, or heating/cooling the feed. Although both of these techniques can be very effective in certain cases, they are undesirable due to the increased operational cost and the addition of another process step. Ideal membranes would be able to handle a variety of feeds without any additives or pretreatment.

1.1.2. Modify Membrane Surface Properties

The second most important factor in the severity of membrane fouling is the nature of the membrane surface. Considerations include the hydrophilicity of the surface, surface roughness, effective surface charge, and chemical groups present on the surface. Many studies have characterized the effects of membrane surface properties on fouling[4,5,9,10]. These studies suggest that, in general, the two most important membrane characteristics related to fouling are hydrophilicity and surface roughness[4,5,9,10]. Charge also plays a significant role in RO and NF, where repulsion of charges and diffusion, in addition to strictly size exclusion, more accurately describe membrane rejection[1-3,6-8].

Studies on membrane hydrophilicity have shown that fouling, particularly fouling of hydrophobic compounds such as proteins, is greatly reduced for more hydrophilic surfaces during filtration of aqueous solutions[4,5,9,10]. More hydrophilic surfaces can be obtained by either crafting more hydrophilic membranes or establishing a hydrophilic layer on the membrane surface post-manufacture. Modifying the entire membrane during production can be challenging because membrane stability and integrity must not be compromised by the addition of the new material. This also limits uses of the membrane to operate best only in certain feeds; however, modifying post-manufacture allows a single base membrane to be easily modified for various applications. Modifying existing membranes typically involves grafting a layer of polymer or polyelectrolyte on the surface. Polymers can be grafted on the surface via grafting-to or grafting-from methods. Grafting-to involves growing a polymer in solution and attaching the assembled polymer to the membrane surface. The major downfall with this method is the potential for large polymer chains to interfere with one another, limiting the density at which the polymer chains can be attached[11-14]. Grafting-from methods, which are used in this dissertation, involve creating

an initiation site on the membrane surface from which polymers can be grown via monomer addition. Higher grafting densities are possible with grafting-from methods[11-15]. A number of polymerization methods can be used during grafting-from modification. These include UV-initiated polymerization, atom transfer radical polymerization (ATRP), anionic polymerization, reversible addition fragmentation chain transfer (RAFT) polymerization, and nitroxide-mediated radical polymerization (NMP)[11-15]. Surface-initiated ATRP (SI-ATRP) was utilized in this research because it allows independent variation of grafting density (initiator density) and chain length (reaction time), yields chain lengths with very small polydispersity, employs relatively mild reaction conditions, and is compatible with a wide range of monomers[11-13,15].

1.1.3. Improve Hydrodynamics

The final possibility for limiting membrane fouling is to improve the hydrodynamics above the membrane surface. This is most often achieved by optimizing the operating conditions of the membrane system by introducing a cross-flow velocity, building spacers which can direct flow and generate turbulence, adjusting the physical orientation of the membrane (flat sheet, spiral-wound, or hollow fiber), back-flushing the membrane periodically, or even having the entire membrane assembly revolve or shake[1-3,16-19]. The goal of these techniques is to generate turbulence (mixing) at the separation boundary layer—a thin layer above the membrane surface where species rejected by the membrane are concentrated[1-3, 16-19]. If no turbulence is present, the rejected species concentrate near the membrane surface, increasing the risk of fouling. This increasing solute concentration as one nears the surface is known as concentration polarization. Hydrodynamic mixing reduces the severity of concentration polarization, ensuring that the effective solute concentration at the membrane surface is similar to the concentration in the bulk feed[1-3, 16-19]. This dissertation focuses on reducing fouling via hydrodynamic mixing since it is

an active and direct method. Adjustment of feed characteristics is less than desirable due to the increased costs, and membrane surface modification is only a passive improvement in fouling resistance. A modified membrane surface which could actively generate hydrodynamic mixing would be a very powerful and versatile technology, particularly because only hydrodynamic methods can actively reduce concentration polarization. A unique class of modified membranes known as stimuli-responsive membranes has the potential to accomplish this.

1.2 Stimuli-responsive Membranes

1.2.1. Properties of Stimuli-responsive Membranes

Stimuli-responsive membranes alter their properties in response to an applied stimulus [20-22]. One manner of producing a stimuli-responsive membrane is to graft responsive nanostructures to the membrane surface. For example, this is accomplished by modifying the membrane (during or post-production) with certain polymers. When a stimulus is applied, changes in the polymer confirmation bring about changes in the membrane properties such as hydrophilicity or surface charge. By selectively applying the stimulus, the filtration properties of the membrane can be tuned to maximize membrane performance and/or minimize fouling.

1.2.2. Examples of Employed Stimuli

The two most commonly used stimuli are solution pH and temperature[20-22]. Responsive membranes based on these stimuli have shown improved membrane performance; however, the entire feedstream must be altered in order to enact the response. This is a costly proposition due to the time necessary to change the properties of the entire feed, the cost of the energy required, and the chemicals which must be added. Furthermore, changes in solution pH or temperature could have an adverse effect on the end product.

Responsive membranes which employ stimuli from external fields do exist. Such stimuli do not require changes to the bulk feed and will therefore instantaneously evoke a response. These membranes often respond to UV radiation (photoresponsive); however, membranes responsive to an electrical or magnetic field have been developed as well[20-22]. Photoresponsive membranes are often difficult to use in practice since the UV radiation must reach the membrane surface. Application of an electrical or magnetic field is very enticing and promising. The generation of the stimulus can be built outside of the membrane housing (which must be compatible with the type of radiation), and electromagnetic radiation is rarely detrimental to the membrane structure or chemistry. These stimuli offer the best possibility to create a membrane which can quickly and actively reduce concentration polarization (and thus fouling) via hydrodynamic mixing.

1.2.3. Hypothesis for Magnetically-responsive Membranes

It was hypothesized that membranes could be modified to generate hydrodynamic mixing in the presence of a magnetic field. A design for such a magnetically-responsive membrane was developed. Polymer brushes were grafted from the membrane surface using SI-ATRP. Superparamagnetic nanoparticles (SPNPs) were then attached to the end of the polymer chains. In a field the nanoparticles will generate a force and torque which will rotate the polymer chains. If the field alternated orientation the chains would rotate back-and-forth. This movement, similar to the behavior of bacterial cilia[23], generates mixing which reduces concentration polarization. SPNPs have been used to generate small scale mixing previously[23-28]. The critical difference in previous studies and the proposed study of this dissertation is the attachment of the SPNPs to filtration membranes. Previous micromixers have been freely dispersed in solution, whether linked chains of SPNPs or SPNPs linked to polymers[23-28]. Attaching SPNPs to filtration

membranes while retaining membrane performance and SPNP response to a field was challenging. The benefit of attached SPNP complexes would be concentrated mixing directly above the membrane surface rather than randomly throughout the feed. Mixing at the membrane surface will actively disrupt concentration polarization, improving membrane performance. The development of these membranes in presented in Chapters 2-6.

1.3 Superparamagnetic Nanoparticles

1.3.1. Theory and Characteristics of Superparamagnetic Nanoparticles

The defining characteristic of superparamagnetic nanoparticles (SPNPs or simply NPs) is that they have an average magnetic moment of zero in the absence of an external magnetic field[29-31]. In a field, the moments within the particles align with the direction of the field practically instantaneously. Furthermore, when the particles are sufficiently small (few nanometers in diameter, depending on the material), the particles are single domain, meaning they have a single large magnetic moment and act as small permanent magnets[29-31]. SPNPs also show no hysteresis, meaning there is no remanance in the magnetic moment when field direction is changed. Thus, when the field is removed, the particles will freely disperse in solution with no magnetic interaction between particles[29-31]. These factors make SPNPs ideal candidates for magnetically-responsive membranes. A brief review of SPNP uses is given below.

SPNPs can be used to generate heat or movement in a material, determined by the relaxation the particle experiences when an external field in applied or removed. Néel relaxation time refers to the time it takes for the magnetic moments of the nanoparticles to orient randomly once an external magnetic field is removed—or conversely to align with an applied external field—without actual physical rotation. This relaxation can generate large amounts of heat, but

would not be able to move any material coupled to the NP[29-32]. Brownian relaxation on the other hand refers to randomization of the magnetic moments by Brownian motion once an external field is removed or applied. Brownian relaxation could cause a material coupled to a NP to move, with little heat generation, if it was the dominant form of relaxation[29-32]. The frequency of the external field and the particle diameter determine the dominant form of relaxation[29-32].

1.3.2. Uses of Superparamagnetic Nanoparticles

1.3.2.1. Hyperthermia Treatment

One of the most promising uses for SPNPs is the localized treatment of hyperthermia. NPs are placed at the injured area, often through direct injection, and excited with an alternating magnetic field. By controlling the frequency of the field, Néel relaxation is maximized causing the NPs to generate large amounts of heat[29,33-38]. If larger particles are used, additional heating is achieved via magnetic hysteresis as the moments attempt to align with the alternating field. This could be used to treat cases of hyperthermia as well as destroy cancerous tumors, which are more sensitive to changes in temperature than healthy cells. Many groups are investigating this technology, and it appears that concerns such as appropriate NP size and biocompatibility will be addressed in the foreseeable future[29,33-38].

1.3.2.2. Magnetically-Enhanced Separations

SPNPs could be used to improve separations of catalysts, proteins, or biopharmaceuticals, among other compounds[39-47]. NPs could be modified so they either bound to or are taken up by the desired compounds. A magnetic field could be applied causing the NP-compound conjugates to migrate, resulting in a high purity separation. SPNPs modified with grafted dopamine have been used to selectively immobilize proteins containing nitrilotriacetic acid[43,44]. Tan *et al* have

used this technique to detect and separate minute amounts of DNA and mRNA which differed by as little as a single-base pair[45-47]. Hu *et al* showed marked improvement in catalysis recovery compared to other technologies, particularly when the catalysts were few microns or smaller[42]. SPNPs offer a unique approach for separating compounds which cannot be effectively removed using traditional techniques, and SPNP usage will likely continue to increase as the demand for highly specific separations in areas such as biotechnology continues to rise.

1.3.2.3. Gas Separation

A specific subset of magnetically-enhanced separations has received much attention: the separation of gaseous species based on their magnetic behavior. The most studied example is selective separation of O_2 (paramagnetic) and N_2 (diamagnetic) from air[48-55]. Cai *et al* showed that O_2 could be separated from N_2 when air is bombarded with a magnetic field gradient[50-52]. Gwak *et al* developed ceramic membranes containing iron- and cobalt-particles which showed an improvement in membrane selectivity in an external field[53,54]. Strzelewicz and Grzywna[49] and Rybak *et al* [55] investigated polymeric membranes containing dispersed magnetic powders and achieved O_2 enrichment of > 50% with one pass. Madaeni *et al* expanded upon this by incorporating magnetic materials into polyethersulfone membranes[48]. They showed that O_2 and N_2 permeance (and thus selectivity) changed with application of a magnetic field and decreased feed pressure due to the additional magnetic materials presenting more interaction sites for the paramagnetic O_2. Separation of other gaseous species based on differing magnetic properties is possible as well. This technology presents a unique opportunity to selectively separate gases which have otherwise similar physical characteristics.

1.3.2.4. Improved Catalysis

A previous section described a method which improved overall reaction efficiency by improving catalyst recycle[42]. Beyond improved separations, NPs could be used to develop new and more efficient catalysts where the NPs would be coated in catalytic species. The NP could be used to steer the catalyst to a desired site for improved reactivity and/or recovery of spent catalysts. Additionally, NPs could be created so the magnetic core is itself catalytic. Reaction activity could be immediately activated or halted via application or removal of an external field. These two ideas have already been used to improve hydrogenation of organics[56,57] and ring-closing and cross-coupling reactions involving alkyl halides[58], respectively. Finally, catalysts could be immobilized onto a support structure which has been made superparamagnetic as presented by Lu *et al* [59,60]. Palladium catalyst was immobilized onto a carbon matrix containing magnetic cobalt NPs. Improved activity and easier separation of catalyst was shown. Improved catalytic activity and easier catalyst recycling could have a large industrial effect.

1.3.2.5. Drug Delivery

Drug delivery utilizing SPNPs can be divided into two categories: active delivery and encapsulation. Active delivery, first proposed nearly forty years ago[61], involves coupling drugs to the NPs. The NPs are steered to the local injured area. Once the effect of the drug is complete, the NPs can be removed from the site and the body via steering. Active delivery is capable of delivering a controlled high concentration of drug to a specific site, without risking damage to other parts of the body[33,62], similar in theory to hyperthermia treatments described previously. Active drug delivery could be particularly useful in treatment of cancer. By limiting radiation therapy to only the cancerous tissue, the many negative side effects of radiation therapy

on the patient could be reduced. Combined with the possibility of heating in an alternating field, as described above, treatment of cancer could be greatly improved. There are however many concerns before this technology gains widespread usage including questions of biocompatibility of the NPs, stability of drug binding to NPs, and the appropriate size of NPs to be effective[33,62].

Encapsulation also seeks to deliver a concentrated drug dose to only the injured area. A polymeric capsule, or membrane, is formed around a dose of drug. The capsule lining contains a number of SPNPs and acts as a barrier to prevent diffusion of the drug into the body. Once the capsule containing the drug arrives at the injured area, either through direct injection or transported through the body (via a pill, etc), an external field is used to cause the polymeric capsule to open[63-65]. The drug is then free to dissolve out of the capsule and affect the injured area. The empty capsule is then removed as waste by the body. Typically, an alternating field is applied which causes the SPNPs to destroy the capsule lining via degradation of the polymer through magnetic heating or agitation. Unfortunately this almost always irreparably damages the capsule eliminating the possibility of reuse. Biocompatibility is still a concern, as is assuring the capsule is transported to the correct area and properly dispenses the drug on command.

1.3.2.6. Small-scale Mixing

As mentioned previously, SPNPs have been proposed or used as very small scale mixers[23-28]. Khatavkar *et al* [23] proposed the idea of micromixers based on the movement of bacterial cilia. They proposed coupling chains of nanoparticles to the walls of a fluid vessel. They postulated that certain chemistries could be used which could be excited by an electrical or magnetic field. The resulting movement of the nanoparticle chains should result in mixing of the fluid. The membranes developed and studied in this dissertation take this concept and expand it

by attaching SPNPs to the end of flexible polymer chains since more flexible chains have been shown to generate greater mixing[24,25].

Biswal and Gast[24,25] chemically linked chains of paramagnetic nanoparticles using polyethylene glycol connections to form flexible chains. They showed that more flexible chains and increased rotating field frequency generated greater mixing; however, a maximum effective frequency was found, after which mixing was diminished. Franke *et al* [26] confined SPNPs within lipid vesicles which could be steered within a small volume. With the application of a rotating external field, the aligning SPNPs caused the vesicles to agitate the surrounding fluid. A relationship was observed between mixing efficiency and field frequency. Stronger fields were also applied to cause the vesicles to rupture, exposing the rotating SPNP directly to the surrounding fluid. Lu *et al* [27] deposited layers of various metals onto hard substrates to create very small magnetic bars. In a rotating field the bars behaved similarly to laboratory magnetic stir bars. These bars were small enough to be dispersed in a liquid to generate fluid mixing. Similarly, Singh *et al* [28] coated polystyrene beads with layers of polyelectrolytes and magnetic nanoparticles. Single beads generated small amounts of mixing; however, rigid chains of coated beads generated greater mixing.

It is apparent that magnetically-activated mixing on very small scales is a proven concept. The challenge for this dissertation research was to anchor flexible magnetically-responsive chains to a filtration membrane without adversely affecting the performance of the membrane. It is argued that in an alternating field the mixing generated by the flexible chains at the membrane surface will be significant enough to decrease concentration polarization resulting in more fouling-resistant membranes.

1.4 PRODUCED WATER TREATMENT

1.4.1. Produced Water Characteristics and Conventional Treatment Methods

Produced water (PW) is an oily wastewater byproduct produced during oil and gas operations. It is by far the largest byproduct of oil production; billions of barrels are produced annually in the U.S.[66-71]. PW is also generated when water is injected into rock formations to improve oil or natural gas yield. The water helps release more oil and gas from the rock formation by serving as a carrier for the oil or gas. PW is therefore a complex mixture of natural and artificial compounds including organics, inorganics, metals, additives, salts, dissolved gases, and oils. The exact composition varies with geography and the age of the operation[66-71]. Of the roughly 250 million barrels produced daily, the vast majority of PW is either discharged into surface waters or reinjected into geological formations. Neither of these is ideal due to detrimental effects of PW on the environment. Additionally, increasingly stringent discharge criteria mean this is often not possible without pretreatment[66-71]. Therefore, treatment and management of PW have become a large factor in virtually every oil and gas operation. Treatment of PW for beneficial reuse is rapidly gaining interest; however, the significant treatment needed is often difficult to accomplish.

Traditionally PW treatment has focused on removing oil and grease, suspended solids, salts, and heavy metals. Many technologies in use today are not ideal because they can generate secondary waste, such as sludge, cannot effectively handle PW composition without extensive pretreatment, or cannot achieve the desired treatment level without further downstream processing[66-71]. There is currently no single technology which can treat all PW compositions. Treatment technologies typically used include multistage flash/distillation, evaporation ponds,

centrifugation, ion exchange, flotation or flocculation, media filtration, and/or adsorption. Ashaghi *et al*[66], Igunnu and Chen[67], Mastouri *et al*[68], and the National Research Council[69] have recently presented reviews of the available PW treatment technologies and their shortcomings.

1.4.2. Membranes for Produced Water Treatment

Membranes have been considered to replace or augment existing PW treatment technologies. The benefits of membrane filtration are decreased energy consumption, a smaller footprint, adaptability to changing feed conditions, and no added chemicals (except possibly during cleaning and/or pre-treatment)[66-73]. NF and RO have shown the most promise to be able to treat a wide variety of feeds with higher levels of contaminants; however, MF and UF have been shown to be applicable for less contaminated PW compositions or as a pretreatment before NF/RO. The greatest limitation to membrane efficacy in PW treatment and widespread membrane usage is loss of membrane performance due to membrane fouling[66-73]. Membrane modification, including stimuli-responsive membranes, and the use of ceramic rather than polymeric membranes have been studied as means to reduce fouling during PW treatment. Membrane modification has been effective in limited scope. Fouling remains a concern as does the addition of chemicals or heat to evoke a change in certain responsive membranes. Ceramic membranes have been very effective in treating certain PW compositions[66,69,70,73]; however, they are currently difficult and expensive to produce[1-3]. Additionally, ceramic membranes cannot achieve the same degree of separation as NF or RO membranes. The research presented in this dissertation focuses on modifying polymeric membranes to actively combat membrane fouling during treatment of PW via magnetically-activated mixing. It is believed this mixing will be significant enough to prevent scaling, reduce colloidal deposition, and disrupt oil emulsions, leading to improved membrane lifetimes and economics.

REFERENCES

1. R. W. Baker, Membrane technology and applications, 2nd ed, 2004, Chichester: Wiley.
2. W. S. W. Ho, K. K. Sirkar, Eds. Membrane Handbook, 1992, Norwell: Kluwer.
3. N. N. Li, A. G. Fane, W. S. W. Ho, T. Matsuura, Eds. Advanced membrane technology and applications, 2008, Hoboken: J. Wiley & Sons.
4. C. H. Koo, A. W. Mohammad, F. Suja, M. Z. M. Talib, Review of the effect of selected physicochemical factors on membrane fouling propensity based on fouling indices, Desalination, 287 (2012) 167-177.
5. W. Guo, H. H. Ngo, J. Li, A mini-review on membrane fouling, Bioresour. Tech., 122 (2012) 27-34.
6. D. Paul, A. r. M. Abanmy, Reverse osmosis: membrane fouling – the final frontier, Ultra Pure Water, 7 (1990) 25-36.
7. A. Drews, C.-H. Lee, M. Kraume, Membrane fouling – a review on the role of EPS, Desalination, 200 (2006) 186-188.
8. A. V. R. Reddy, J. J. Trivedi, C. V. Devmurari, D. J. Mohan, P. Singh, A. P. Rao, S. V. Joshi, P. K. Ghosh, Fouling resistant membranes in desalination and water recovery, Desalination, 183 (2005) 301-306.
9. J. S. Baker, L. Y. Dudley, Biofouling in membrane systems – a review, Desalination, 118 (1998) 81-90.
10. M. C. Wilbert, Enhancement of membrane fouling resistance through surface modification, water treatment technology program report no. 22. U.S. Dept. of the Interior, March 1997.
11. S. Edmondson, V. L. Osborne, W. T. S. Huck, Polymer brushes via surface-initiated polymerizations, Chem. Soc. Rev., 33 (2004) 14-22.
12. M. Ulbricht, Advanced functional polymer membranes, Polymer, 47(2006) 2217-2262.
13. W. A. Braunecker, K. Matyjaszewski, Controlled/living radical polymerization: features, developments, and perspectives, Prog. Polym. Sci., 32 (2007) 93-146.
14. A. Bhattacharya, B. N. Misra, Grafting: a versatile means to modify polymers. Techniques, factors, and applications, Prog. Polym. Sci., 29 (2004) 767-814.
15. K. Matyjaszewski, Atom transfer radical polymerization (ATRP): current status and future perspectives, Macromolecules, 45 (2012) 4015-4039.
16. M. S. H. Bader, P. A. Jennings, Concentration polarization phenomena in turbulent flow: review and modification, J. Envir. Sci. Health, A27 (1992) 463-483.
17. A. S. Khair, T. M. Squires, Fundamental aspects of concentration polarization arising from nonuniform electrokinetic transport, Phy. Fluids, 20 (2008) 087102 1-20.
18. N. A. Mishchuk, Concentration polarization of interface and non-linear electrokinetic phenomena, Adv. Colloid Inter. Sci., 160 (2010) 16-39.
19. S. S. Sablani, M. F. A. Goosen, R. Al-Belushi, M. Wilf, Concentration polarization in ultrafiltration and reverse osmosis: a critical review, Desalination, 141(2001) 269-289.
20. D. Wandera, S.R. Wickramasinghe, S.M. Husson, Stimuli-responsive membranes, J. Mem. Sci. 357 (2010) 6-35.
21. M.A. Stuart, W.T. Huck, J. Genzer, M. Müller, C. Ober, M. Stamm, G.B. Sukhorukov, I. Szleifer, V.V. Tsukruk, M. Urban, F. Winnik, S. Zauscher, I. Luzinov, S. Minko, Emerging applications of stimuli-responsive polymer materials. Nat. Mat. 9 (2010) 101-113.
22. L.-Y. Chu, Smart membrane materials and systems, 2011, Zhejiang, Zhejiang University Press.

23. V. V. Khatavkar, P. D. Anderson, J. M. J. den Toonder, H. E. H. Meijer, Active micromixer based on artificial cilia, Phy. Fluids, 19 (2007) 083605 1-19.
24. S. L. Biswal, A. P. Gast, Micromixing with linked chains of paramagnetic particles, Anal. Chem., 76 (2004) 6448-6455.
25. S. L. Biswal, A. P. Gast, Rotational dynamics of semiflexible paramagnetic particle chains, Phys. Review E, 69 (2004) 041406 1-9.
26. T. Franke, L. Schmid, D. A. Weitz, A. Wixforth, Magneto-mechanical mixing and manipulation of picoliter volumes in vesicles, Lab Chip, 9 (2009) 2831-2835.
27. L.-H. Lu, K. S. Ryu, C. Liu, A magnetic microstirrer and array for microfluidic mixing, JMEMS, 11 (2002) 462-469.
28. H. Singh, P. E. Laibinis, T. A. Hatton, Rigid, superparamagnetic chains of permanently linked beads coated with magnetic nanoparticles. Synthesis and rotational dynamics under applied magnetic fields, Langmuir, 21 (2005) 11500-11509.
29. A.-H. Lu, E. L. Salabas, F. Schüth, Magnetic nanoparticles: synthesis, protection, functionalization, and application, Angew. Chem. Int. Ed., 46 (2007), 1222-1244.
30. N. Pamme, Magnetism and microfluidics, Lab Chip, 6 (2006) 24-38.
31. Q. Song, Section 1.3: Superparamagnetism of magnetic nanomaterials, in: Size and shape controlled synthesis and superparamagnetic properties of spinel ferrites nanocrystals. Ph. D. Dissertation, Georgia Institute of Technology, 2005.
32. R. Kötitz, W. Weitschies, L. Trahms, W. Semmler, Investigation of Brownian and Néel Relaxation in magnetic fluids. J. Magn. Magn. Mat. 201 (1999) 102-104.
33. A. K. Gupta, M. Gupta, Synthesis and surface engineering of iron oxide nanoparticles for biomedical applications, Biomaterials, 26 (2005) 3995-4021.
34. S. Mornet, S. Vasseur, F. Grasset, P. Verveka, G. Goglio, A. Demourgues, J. Portier, E. Pollert, E. Duguet, Magnetic nanoparticles design for medical application, Prog. Solid State Chem. 34 (2006) 237-247.
35. S. Mornet, S. Vasseur, F. Grasset, E. Duguet, J. Mater. Chem., 14 (2004), 2161-2175.
36. C. C. Berry, A. S. G. Curtis, Topical review: functionalisation of magnetic nanoparticles for applications in biomedicine, J. Phys. D, 36 (2003), R198-R206.
37. R. Hiergeist, W. Andrä, N. Buske, R. Hergt, I. Hilger, U. Richter, W. Kaiser, Application of magnetite ferrofluids for hyperthermia, J. Magn. Magn. Mat., 201 (1999) 420-422
38. R. Hergt, S. Dutz, R. Müller, M. Zeisberger, Magnetic particle hyperthermia: nanoparticle magnetism and materials development for cancer therapy, J. Phys. Cond. Mat., 18 (2006) S2919-S2934.
39. S. Giri, B. G. Trewyn, M. P. Stellmaker, V. S.-Y. Lin, Stimuli-responsive controlled-release delivery system based on mesoporous silica nanorods capped with magnetic nanoparticles, Angew. Chem., 117 (2005), 5166-5172.
40. C. Bergemann, D. Müller-Schulte, J. Oster, L. Brassard, A. S. Lubbe, Magnetic ion-exchange nano- and microparticles for medical, biochemical and molecular biological applications, J. Magn. Magn. Mat., 194 (1999) 45-52.
41. L. Nuñez, M. D. Kaminski, Transuranic separation using organophosphorus extractants adsorbed onto superparamagnetic carriers, J. Magn. Magn. Mat., 194 (1999) 102-107.
42. A. Hu, G. T. Yee, W. Lin, Magnetically-recoverable chiral catalysts immobilized on magnetite nanoparticles for asymmetric hydrogenation of aromatic ketones, J. Am. Chem. Soc., 127 (2005) 12486-12487.

43. C. Xu, K. Xu, H. Gu, R. Zheng, H. Liu, X. Zhang, Z. Guo, B. Xu, Dopamine as a robust anchor to immobilize functional molecules on the orion oxide shell of magnetic nanoparticles, J. Am. Chem. Soc., 126 (2004), 9938-9939.
44. L. X. Chen, T. Liu, M. C. Thurnauer, R. Csencsits, T. Rajh, Fe2O3 nanoparticle structures investigated by x-ray absorption near-edge structure, surface modifications, and model calculations, J. Phys. Chem. B, 106 (2002) 8539-8546.
45. I. Safarik, M. Safarikova, Use of magnetic techniques for the isolation of cells, J. Chrom. B, 722 (1999) 33-53.
46. X. Zhao, R. Tapec-Dytioco, K. Wang, W. Tan, Collection of trace amounts of DNA/mRNA molecules using genomagnetic nanocapturers, Anal. Chem., 75 (2003) 3476-3483.
47. H. Gu, K. Xu, C. Xu, B. Xu, Biofunctional magnetic nanoparticles for protein separation and pathogen detection, Chem. Comm., (2006) 941-949.
48. S. S. Madaeni, E. Enayati, V. Vatanpour, Separation of nitrogen and oxygen gases by polymeric membrane embedded with magnetic nano-particle, Polym. Adv. Technol., 22 (2011) 2556-2563.
49. A. Strzelewicz, Z. J. Grzywna, Studies on the air membrane separation in the presence of a magnetic field, J. Mem. Sci., 294 (2007) 60-67.
50. J. Cai, L. Wang, P. Wu, Oxygen separation from atmospheric air by using gradient magnetic field, Jpn. J. App. Phys., 45 (2006) 1039-1041.
51. J. Cai, L. Wang, P. Wu, Oxygen enrichment from air by using the interception effect of gradient magnetic field on oxygen molecules, Phys. Lett. A, 362 (2007) 105-108.
52. J. Cai, L. Wang, P. Wu, Z. Li, L. Tong, S. Sun, Study on oxygen enrichment from air by application of the gradient magnetic field, J. Magn. Magn. Mat., 320 (2008) 171-181.
53. J. Gwak, A. Ayral, V. Rouessac, L. Cot, J.-C. Grenier, J.-H. Choy, Synthesis and characterization of porous ferromagnetic membranes, Micro. Meso. Mat., 63 (2003) 177-184.
54. J. Gwak, A. Ayral, V. Rouessac, K. H. Kim, J.-C. Grenier , L. Cot, J.-H. Choy, Porous ceramic membranes exhibiting ferri/ferromagnetic properties for separation, Sep. Purif. Tech., 46 (2005) 118-124.
55. A. Rybak, Z. J. Grzywna, W. Kaszuwara, On the air enrichment by polymer magnetic membranes, J. Mem. Sci., 336 (2009) 79-85.
56. J.-I. Park, J. Cheon, Synthesis of "solid solution" and "core-shell" type cobalt-platinum magnetic nanoparticles via transmetalation reactions, J. Am. Chem. Soc., 123 (2001) 5743-5746.
57. C.-H. Jun, Y. J. Park, Y.-R. Yeon, J. Choi, W. Lee, S. Ko, J. Cheon, Demonstration of a magnetic and catalytic Co@Pt nanoparticle as a dual-function nanoplatform, Chem. Comm., (2006) 1619-1621.
58. R. B. Bedford, M. Betham, D. W. Bruce, S. A. Davis, R. M. Frost, M. Hird, Iron nanoparticles in the coupling of alkyl halides with aryl Grignard reagents, Chem. Comm., (2006) 1398-1400.
59. A.-H. Lu, W. Schmidt, N. Matoussevitch, H. Bönnermann, B. Spliethoff, B. Tesche, E. Bill, W. Kiefer, F. Schüth, Nanoengineering of a magnetically-separable hydrogenation catalyst, Angew. Chem., 116 (2004) 4303-4306.
60. A.-H. Lu, W. Li, A. Kiefer, W. Schmidt, E. Bill, G. Fink, F. Schüth, Fabrication of magnetically-separable mesostructured silica with an open pore system, J. Am. Chem. Soc., 126 (2004) 8616-8617.

61. K. J. Widder, A. E. Senyei, D. G. Scarpelli, Magnetic microspheres: a model system for site specific drug delivery in vivo, Proc. Soc. Exp. Biol. Med., 58 (1978), 141-146.
62. T. Neuberger, B. Schöpf, H. Hofmann, M. Hofmann, B. von Rechenberg, Superparamagnetic nanoparticles for biomedical applications: possibilities and limitations of a new drug delivery system, J. Magn. Magn. Mat., 293 (2005) 483-496.
63. E. R. Edelman, J. Kost, H. Bobeck, R. Langer, Regulation of drug release from polymer matrices by oscillating magnetic fields, J. Biomed. Mat. Res., 19 (1985) 67-83.
64. T. Hoare, J. Santamaria, G. F. Goya, S. Irusta, D. Lin, S. Lau, R. Padera, R. Langer, D. S. Kohane, A magnetically-triggered composite membrane for on-demand drug delivery, Nano Lett., 9 (2009) 3651-3657.
65. T. Hoare, B. P. Timko, J. Santamaria, G. F. Goya, S. Irusta, S. Lau, C. F. Stefanescu, D. Lin, R. Langer, D. S. Kohane, Magnetically-triggered nanocomposite membranes: a versatile platform for triggered drug release, Nano Lett., 11 (2011) 1395-1400.
66. K. S. Ashaghi, M. Ebrahimi, P. Czermak, Ceramic ultra- and nanofiltration membranes for oilfield produced water treatment: a mini review, Open Environ. Sci., 1(2007), 1-8.
67. E. T. Igunnu, G. Z. Chen, Produced water treatment technologies, Int. J. Low-Carbon Techn. 1 (2012) 1-21.
68. R. Mastouri, F. Nadim, N. Kargari, 2010: A time to review the produced water treatment technologies, a time to look forward for new management policies, Not published, Islamic Azad University, Arak, Iran.
69. National Research Council of the National Academies, Management and effects of coalbed methane produced water in the western United States, 2010, Washington D.C.: The National Academies Press.
70. T. Bilstad, E. Espedal, Membrane separation of produced water, Wat. Sci. Tech., 34 (1996) 239-246.
71. B. Van der Bruggen, C. Vandecasteele, T. V. Gestel, W. Doyen, R. Leysen, A review of pressure-driven membrane processes in wastewater treatment and drinking water production, Env. Prog., 22 (2003) 46-56.
72. A. Asatekin, A. M. Mayes, Oil industry wastewater treatment with fouling resistant membranes containing amphiphilic comb copolymers, Environ. Sci. Tech., 43 (2009) 4487-4492.
73. M. Cakmakci, N. Kayaalp, I. Koyuneu, Desalination of produced water from oil production fields by membrane processes. Desalination, 222 (2008) 176-186.

CHAPTER 2

MAGNETICALLY-ACTIVATED MICROMIXERS FOR SEPARATION MEMBRANES

This chapter describes the membrane modification protocol, alternating magnetic field apparatus, theory behind magnetically-activated micromixing filtration membranes, and the first successful membranes employing this idea.

I developed the modification protocol, performed the filtration experiments, characterized the modification using XPS and FESEM, and studied the magnetic response using PIV. Guidance was provided by the co-authors throughout the study. Dr. Yang and Dr. Dasi assisted greatly during the development of the modification protocol and the design and use of the PIV system, respectively.

SUMMARY

Presented here is a radically novel approach to reduce concentration polarization and, potentially, also fouling by colloids present in aqueous feeds: magnetically-responsive micromixing membranes. Hydrophilic polymer chains, poly(2-hydroxyethyl methacrylate) (polyHEMA), were grafted via controlled surface-initiated atom transfer radical polymerization (SI-ATRP) on the surface of polyamide composite nanofiltration (NF) membranes and then end-capped with superparamagnetic iron oxide magnetite (Fe_3O_4) nanoparticles. The results of all modification steps, i.e., immobilization of bromide initiator, SI-ATRP, conversion of polyHEMA endgroups from bromide to amine, and carboxyl-functional Fe_3O_4 nanoparticle immobilization via peptide coupling, have been confirmed by X-ray photoelectron spectroscopy (XPS) and field emission scanning electron microscopy (FESEM). These nanoparticles experience a magnetic force as well as a torque under an oscillating external magnetic field. It has been shown, using particle image velocimetry (PIV), that the resulting movement of the polymer brushes at certain magnetic field frequencies induces mixing directly above the membrane surface. Furthermore, it was demonstrated that with such membranes the NF performance could significantly be improved (increase of flux and salt rejection) by an oscillating magnetic field, which can be explained by a reduced concentration polarization in the boundary layer. However, the proof-of-concept presented here for the active alteration of macroscopic flow via surface-anchored micromixers based on polymer-nanoparticle conjugates has much broader implications.

Financial support for this work was provided by the Strategic Environmental Research and Development Program (USA), WP-1670. The authors would like to thank Prof. Dr. M. J. Semmens for his helpful suggestions.

2.1. INTRODUCTION

Synthetic membranes have become important tools for separation and reaction engineering, and the development of advanced membranes is a very dynamic field of materials science and engineering.[1] Presumably the most important driving force for development of advanced membrane technologies is the need for more efficient technologies to produce and recycle pure water; membranes for the pressure-driven desalination (reverse osmosis, RO, nanofiltration, NF) or ultrafiltration (UF) play a crucial role.[2] However, in many applications, concentration polarization and fouling limit membrane selectivity, capacity, and productivity.[3] Concentration polarization occurs during membrane filtration, and it is due to convection of rejected species to the membrane surface by the permeate flow. Concentration polarization may be reduced by inducing mixing at the membrane surface in order to disrupt the boundary layer that forms. Fouling is the reduction of membrane performance due to deposition of matter on or in the selective barrier of the membrane. Fouling can be accelerated by concentration polarization. Countermeasures against fouling include optimizing module design or inducing mixing during operation (cross-flow velocity, back pulsing), pretreatment of the feed, and surface modification of the membrane. The latter approach can largely reduce the adsorption or adhesion strength of colloidal foulants, leading to less deposition and/or easier removal of fouling layers. The post-modification of established membranes has become an important approach which is also frequently used in industry.[1] Numerous examples for efficient anti-fouling modification can be found in the literature, for instance, based on grafting thin layers of hydrophilic polymers to the surface of RO, NF or UF membranes.[4,5] While such membranes typically have "static" properties, more sophisticated strategies are based on so called responsive membranes: Fouling could be reduced or cleaning can be facilitated by surface properties (e.g.,

hydrophilicity, charge, modulus) which can be changed by external stimuli, e.g., pH value or temperature.[1,6,7] However, with all such modified or even responsive membranes, concentration polarization can not be influenced directly.

Presented here is a radically novel approach to reduce concentration polarization and, potentially, also fouling by colloids present in aqueous feeds: magnetically-responsive micromixing membranes. Hydrophilic polymer chains are grafted via controlled surface-initiated atom transfer radical polymerization (SI-ATRP) on the surface of NF membranes and then end-capped with superparamagnetic iron oxide magnetite (Fe_3O_4) nanoparticles. These nanoparticles experience a magnetic force as well as a torque under an oscillating external magnetic field. It was expected that the nanoscale movement of the nanoparticle-capped chains could lead to mixing on the micro- and macroscales. Importantly the method proposed here could be scaled up to large surface areas using membrane modules (Figure 2.1a).

(Super)paramagnetic nanoparticles have been used to create micromixers previously; however, these micromixers were free in solution and could only induce mixing on extremely small scales.[8-13] By anchoring these micromixers to the surface of a membrane, it should be possible to induce mixing across the entire membrane surface in the presence of an oscillating magnetic field. This mixing would be analogous to that of bacterial cilia.[14] Thus, one could activate and improve the performance of the membrane at any time during filtration. Other responsive membranes have shown promise for reducing fouling using stimuli such as pH and temperature; however, these require changes to the bulk feed to obtain a membrane response.[4,6,15,16] Magnetically-responsive membranes can be activated through an external stimulus; therefore characteristics of the bulk feed are unaffected. Membranes responsive to an external magnetic field have been presented before, which were created by embedding magnetic

nanoparticles in a polymeric matrix to create "gating" membranes for drug delivery but not filtration.[17-19] This, however, is quite different from the novel responsive NF membranes described in this study.

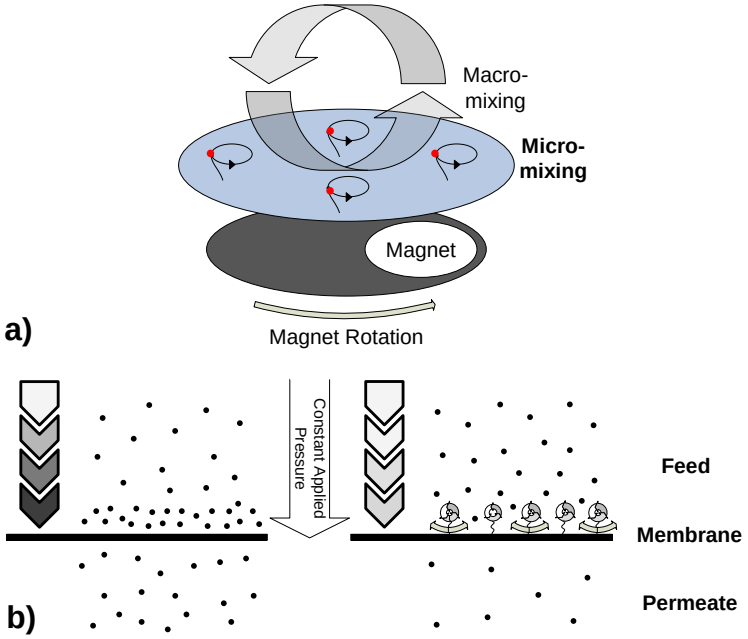

Figure 2.1. Schematic depiction of micromixing concept; (A) Micromixers on the membrane surface activated by oscillating magnetic field, here a magnet rotating with a certain frequency, cause macromixing; (B) Concentration polarization, leading to an increased concentration of rejected species in the boundary layer (left), and reduction of concentration polarization by mixing induced at the membrane surface (right); in NF processes with a given feed and trans-membrane pressure, concentration polarization causes a higher permeate concentration of salt, i.e., a lower salt rejection, than without concentration polarization.

In this paper, the synthesis of prototype magnetically-responsive micromixing NF membranes is reported. It is shown, using particle image velocimetry (PIV), that the resulting movement of the polymer brushes at certain magnetic field frequencies induces mixing directly above the membrane surface. Furthermore, it is demonstrated that with such membranes the NF performance could significantly be improved (increase of flux *and* salt rejection) by a rotating magnetic field, which can be explained by a reduced concentration polarization in the boundary layer (Figure 2.1b).

A CPU-controlled alternating magnetic field apparatus consisting of two solenoids was constructed; c.f. Experimental section. For all filtration experiments, the membrane was placed inside a stirred filtration cell. This cell was placed in between the two solenoids so that the membrane barrier (topmost) layer was normal to the magnetic field generated along the longitudinal axis of the solenoids (see Figure 2.2). Since the brushes are concentrated on the membrane surface, the perpendicular magnetic field will impart its maximum torque and force. This will lead to maximum polyHEMA brush movement.

2.2. EXPERIMENTAL SECTION

2.2.1. Materials

Polyamide 20 μm neutrally buoyant seeding particles were obtained from Dantech Dynamics (Skovlunde, Denmark). Iron oxide magnetite superparamagnetic nanoparticles with 15 nm core diameter and 5 nm coating layer modified with carboxylic acid groups were purchased from Ocean Nanotech (Springdale, AR, USA).

2.2.2. Chemicals

Purified water was from a Milli-Q system from Millipore. All chemicals were at least 97% purity unless otherwise noted. Sulfuric acid was from Fisher Scientific; potassium permanganate, diisopropylcarbodiimide, N,N’,N’,N’’,N’’-pentamethyldiethylenetriamine, ethanolamine, triethylamine, N-hydroxybenzotriazole, and 4-N’,N’-dimethylaminopyridine were from Fluka; ethanol, methanol, acetonitrile, and hydrochloric acid (6 M) were from VWR; α-bromoisobutyrylbromide, bipyridine (Reagent Plus), copper (I) and copper (II) chloride, 2-

hydroxyethylmethacrylate (HEMA), 1-ethyl-3-(3-dimethylaminopropyl)carbodiimide, hydrazine hydrate, and N-hydroxysuccinimide were from Sigma-Aldrich.

2.2.3. Membrane

NF 270 flat-sheet membranes were obtained from Dow Filmtec. 25 mm diameter membrane discs were cut from the membrane sheets. Before use, the membranes were washed with Milli-Q water and then dried overnight at 40°C. Between uses the discs were stored in plastic zip-top bags containing a small amount of sodium azide to prevent bacterial growth.

2.2.4..Initiator Immobilization

The initiator immobilization solution consisted of 2.76 g α-bromoisobutyrylbromide, 1.515 g triethylamine, and 91.5 mg 4-N',N'-dimethylaminopyridine in 150 mL of dried acetonitrile. The membrane discs were placed in small glass vials to which 5 mL of this reaction solution was added. The samples were allowed to react for 2 hours at room temperature on a shaker table. This was followed by one acetonitrile wash, two methanol washes, and two deionized water washes. The membranes were dried overnight at 40^{o}C and returned to storage.

2.2.5 SI-ATRP

The monomer 2-hydroxyethylmethacrylate (HEMA) was purified through distillation and always used within 12 hours. The reaction solution for SI-ATRP consisted of HEMA (2 M), CuCl, $CuCl_2$, and bipyridine (BPy) dissolved in equal parts (v/v) water and methanol; the molar ratios HEMA : CuCl : $CuCl_2$: BPy were 100 : 0.5 : 0.1 : 1.5. First, HEMA and BPy were added to the solvent, and the stirred solution was degassed for 15 minutes. CuCl and $CuCl_2$ were then

sequentially added to the solution with strong stirring and degassing in between. Membrane discs had been placed in vials and three times evacuated under vacuum and then filled with nitrogen gas. Immediately after preparation, 6 mL of reaction solution was injected into each of the sealed vials containing a membrane disc. Reaction time was 4 hours at room temperature. Thereafter, the membranes were placed in a quenching solution (500 mg $CuBr_2$ and 1250 μL N,N',N',N'',N''-pentamethyldiethylenetriamine in 100 ml methanol / water, 50 / 50, v / v) to stop polymerization and ensure the end of each polymer chain was capped with a bromine group. After 10 minutes in the quenching solution the membranes were washed with Milli-Q water for 2 minutes, washed with methanol for 1 minute, and allowed to rest in Milli-Q water for 2 hours with shaking. The membranes were then dried at 40°C overnight and returned to storage.

2.2.6 Gabriel Synthesis Procedure

To convert the alkyl halide ends of the polymer chains to primary amines, a Gabriel synthesis protocol similar to Monge et al.[20] was used. For the first step, 1 g potassium phthalimide salt was dissolved into 20 mL ethanol. 4.5 mL of this solution was placed into a small glass vial containing one membrane disc. The vials were sealed and placed in a 40°C oil bath with shaking for 6 hours. After the reaction, the membrane was rinsed with ethanol, then with Milli-Q water twice for two minutes, and finally with ethanol before being dried. The second step consisted of dissolving 7 mL of hydrazine hydrate into 25 mL of 6 M HCl. 4 mL of this solution was placed into each small glass vial containing a membrane disc. The vials were placed in a 40^{o}C oil bath with shaking for 6 hours. Upon completion of reaction, the membranes were washed twice with Milli-Q water, then methanol, water, ethanol, and water again to ensure that no phthalimide precipitate remained. Membranes were then dried and returned to storage.

2.2.7. Nanoparticle Coupling

Carbodiimide-activated amide formation was used. 31.2 mg 1-ethyl-3-(3-dimethylaminopropyl)carbodiimide and 38.7 mg N-hydroxysuccinimide were added to 10 mL Milli-Q water and shaken vigorously on a vortex mixer. Then 0.3 mL carboxyl shell Fe_3O_4 nanoparticles in buffer solution (5 g/L) were added, but not agitated. 1.5 mL of this solution was then added to a plastic jar containing a membrane disc. This was sealed and incubated in the dark for 4 hours. Then, the membrane was removed, washed twice in Milli-Q water for 5 minutes, briefly with ethanol, and finally in Milli-Q water for 10 minutes. The membrane was then dried overnight at 40^oC and returned to storage.

2.2.8. Membrane Surface Characterization by XPS

Membranes were washed and dried before analysis. A Physica Electron 5800 ultra-high vacuum XPS-Auger spectrometer was used at a 45^o take-off angle. 20 high-resolution scans focusing on the carbon (282-292 eV), nitrogen (394-406 eV), and iron (705-730 eV) regions were averaged to observe changes during the sequential modification steps.

2.2.9. Membrane Surface Visualization by FESEM

Field emission scanning electron microscopy (FESEM) was used to image the filtration surface of the membranes. To prevent pore collapse, critical point drying was performed prior to analyzing samples with a JEOL field-emission scanning electron microscope (JSM-6500F, JEOL Ltd., Tokyo, Japan). Small membrane samples were placed into specimen holder vials. The vials were placed directly into a liquid transfer boat filled with absolute ethanol, and the boat placed into the critical point drying apparatus. Cold tap water was run to the jacket of the chamber, after

which the chamber was filled with liquid carbon dioxide and allowed to sit for approximately 7 minutes. The vent valve was then slightly opened to maintain the liquid carbon dioxide level. The drain valve was opened to remove the absolute ethanol for approximately 4 minutes. The vent valve and drain valve were then closed for approximately 7 minutes after which the vent and drain valves were open again for approximately 4 minutes. These two steps were repeated 7 times (a total of 8 flushes), until the absolute ethanol had completely displaced the water.

After flushing was complete, the chamber was again filled with liquid carbon dioxide. The temperature of the chamber was increased to 38°C by replacing the cold water in the jacket with warm water. The carbon dioxide gas was slowly vented off. Samples were removed from the chamber and the vials and mounted on microscope stubs. Samples were sputter-coated with a 10 nm gold layer before imaging.

2.2.10. Monitoring of Mixing by PIV

A time-resolved PIV system (Lavision Inc.) was used. The membranes were placed in a 90 mm diameter glass Petri dish that was filled with a mixture of 3.25% (w/w) 20 μm polyamide particles (to aid in observation of reflected light) and 0.02% (w/w) hand soap acting as a surfactant to minimize polyamide particle aggregation in water. A permanent 2 kG (field strength roughly 50 G at the membrane surface) neodymium-iron-boron magnet was attached to the shaft of a variable speed motor and placed underneath the Petri dish. Observations were made at various motor speeds, as well as when the magnet was stationary. A green laser (527 nm) illuminated the fluid above the membrane. A high-resolution lens and camera yielded an observable area of 400 x 400 μm^2 at maximum resolution, corresponding to a pixel level resolution of 0.4 x 0.4 μm^2. All data sets consisted of 1000 frames taken over 1 second. By

capturing the light reflected from the particles in the fluid, two-dimensional projections (4 μm depth of field) of the fluid velocity field were calculated over the field of view using the following procedure. First, the raw particle images of each data set were pre-processed to subtract background light. This was followed by standard PIV cross-correlation interrogation with a window size of 64 x 64 pixels with 50% overlap.[21] Window size was selected based on the size of the particles (20 μm) in the raw images. This produced a velocity vector at every 32 pixels (12.8 μm) in units of m/s.

2.2.11. Membrane Flux Measurement

The membrane discs were placed in an Amicon 8010 stirred filtration cell (Millipore). The cell was filled with Milli-Q water; pressurized nitrogen provided the driving force for fluid flow through the membrane. The membranes were allowed to equilibrate for three minutes with the permeate line closed. The permeate line was then opened and allowed to flow for three minutes before measurements began. Permeate was collected for six minutes and the flux calculated. Five measurements (6, 12, 18, 24, and 30 minutes) were taken. The fluxes were stable after 18 minutes and reported in units of $L/m^2 \cdot h$. For investigation of the stimulus-response, an apparatus designed and built to generate an oscillating magnetic field at a desired frequency and intensity was used. The cell was placed in a custom-made apparatus consisting of two stainless-steel core solenoids, see Figure 2.2. A computer-operated programmable logic controller (PLC) controlled the rate at which the two solenoids received power by alternatively activating two solid state relays. This determined the frequency of the alternating magnetic field. The solenoids were powered by an Agilent Technologies (Santa Clara, CA) 20 V, 25 A power supply. The solenoids were positioned on two opposite sides of the filtration cell so that the

magnetic field direction was parallel to the topmost selective layer of the membrane. This arrangement would yield the greatest lateral movement of the end of the nanoparticle-capped polymer brushes and thus the greatest agitation of the feed solution above the membrane surface. The output voltage and amperage of the power source and the frequency of the field were varied to generate the desired alternating magnetic field of roughly 50 G and 10 Hz to match the field used in the PIV experiments. Filtrate fractions were collected in time intervals of 30 seconds, and salt concentrations were measured with a conductivity meter (Oakton, model CON11). Salt rejection was calculated as $1-\frac{conductivity_{permeate}}{conductivity_{feed}}$. Consecutive 30 second intervals were averaged to yield an average flux reported at one minute intervals. Fluxes stabilized after no more than 20 minutes, and average values and standard deviations were calculated for data for up to 1 hour for the control and for up to 2 hours for the modified membranes.

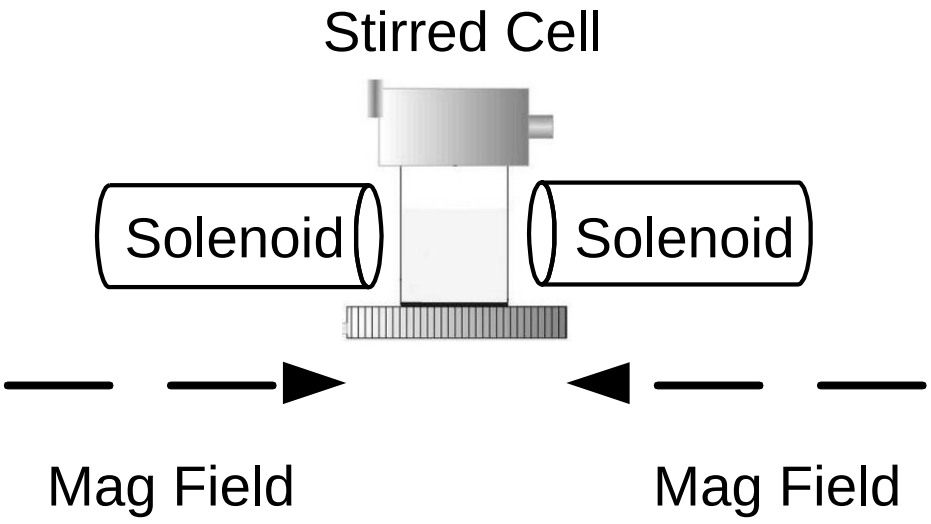

Figure 2.2. Schematic showing the orientation of the alternating magnetic field apparatus with respect to the membrane filtration cell. Only one solenoid is powered at a given time. The direction of the field generated by the solenoid, when powered, is shown by the arrow.

2.3. Results and Discussion

2.3.1. Membrane Surface Modification with Grafted Magnetic Nanoparticle-Polymer Conjugate Layers

NF membranes were chosen because they have no permanent pores in their barrier and, consequently, accumulation of rejected matter (concentration polarization) and fouling occur only on the outer surface. SI-ATRP was used to grow poly(2-hydroxyethyl methacrylate) (polyHEMA) chains from the surface of commercially available polyamide thin-film composite NF membranes. Grafting of polymer chains on membrane surfaces has been used to tailor membrane performance by this group[15,22] and others.[4,6,16] Immobilization of the SI-ATRP initiator was performed by an efficient acylation reaction[23] of amino end groups of the polyamide. The conditions for controlled SI-ATRP from polymer membrane surfaces, which retains the end-functionality of the growing polymer chain, had been established in own previous studies.[24] After polyHEMA grafting, a Gabriel synthesis reaction was used to convert the alkyl halide end group of the polymer chains to primary amines, which were capable of coupling to the carboxylic acid coated iron oxide superparamagnetic nanoparticles through an amide linkage. An overview of the entire reaction sequence is shown in Figure 2.3.

This approach differs from previous micromixer studies, which linked much larger paramagnetic particles into chains.[8-12] The grafted polyHEMA chains are more flexible in aqueous solutions than chains of linked magnetic particles, since the polyHEMA is hydrophilic. It has been shown that more flexible chains induce more effective mixing.[8,11,12] The increased flexibility and the large number of anchored mixers per surface area should lead to mixing on a larger scale than previous studies.[8-12]

In parallel SI-ATRP experiments with an established model system of track-etched PET membranes[24] it was confirmed that the chosen reaction conditions lead to controlled polymerization with a time-dependent linear increase of grafted polymer mass and corresponding linear growth of polyHEMA layer thickness. After 4 hours of SI-ATRP a chain length of at least 60 nm had been estimated (see Appendix A1).

Since the density of amino end groups is known to be low, although the exact density is unknown, the grafting density on the polyamide membranes should be relatively low. The NF composite membranes have a thin (< 50 nm) layer of a semi-aromatic poly(piperazinamide) on top of a porous polysulphone membrane and a non-woven polyester support.[25] The characterization of the surface modification of this membrane with a thin grafted layer is challenging. X-ray photoelectron spectroscopy (XPS) is one of the very few suitable methods because it provides information about chemical composition and structure for the top 1 to 10 nm of the sample.[26] Consequently, XPS was used to follow all the reaction steps; data are shown in Figure 2.4.

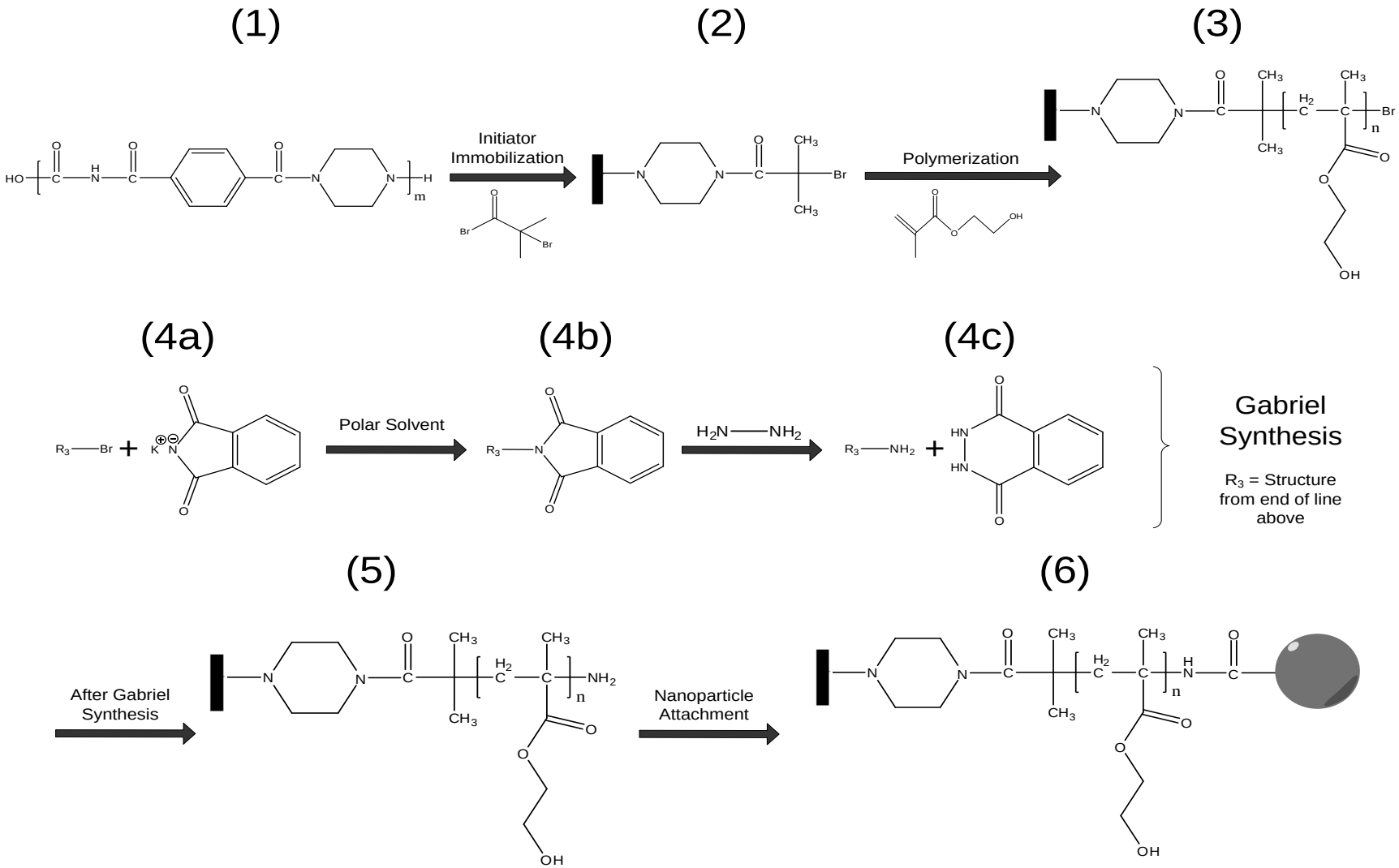

Figure 2.3. Overview of the reaction sequence for modification of nanofiltration membranes: (1)→(2) initiator immobilization, (2)→(3) SI-ATRP, (4) Gabriel synthesis, and (5)→(6) nanoparticle attachment by peptide coupling.

Figure 2.4 (a) presents a high-resolution spectrum of the 1s carbon region for various stages of modification. The peak associated with the C-OH bond appears at roughly286.4 eV after polyHEMA grafting. This functionality is not present in the base membrane. The pronounced development of this peak with polymerization indicates that polyHEMA has been successfully grafted from the membrane surface. The peaks at 288 and 289 eV are also of note. These correspond to carbonyl (C=O) and ester groups (O–C=O) respectively. The topmost surface of NF 270 membranes is rich in amide groups,[25] which explains the strong peak for both the base and initiator-immobilized membranes at 288 eV. The excitation energy of the carbon atoms of carbonyl in the amide group introduced during initiator immobilization is roughly 288.2 eV; however, a distinct peak does not appear because of the small number of these groups compared to the various other carbonyl groups associated with the membrane matrix. After polymerization, however, the peak at 288 eV reduces to almost zero while the peak at 289 eV, assigned to ester groups, becomes quite defined. Thus, the presence of grafted polyHEMA, covering the polyamide, is further confirmed.

Figure 2.4 (b) is a high-resolution spectrum for the nitrogen region. The amine peak (399.5 eV) is present for the unmodified polyamide top layer. This peak is suppressed somewhat after immobilization of the initiator (containing no nitrogen) and then disappears completely after polyHEMA grafting. This suggests that the dry grafted polyHEMA layer is of significant thickness (> 10 nm) so that the polyamide layer of the base membrane can no longer be detected with XPS. This is in line with the estimated chain length of at least 60 nm (see Appendix A1) and a sufficient grafting density to fully cover the polyamide surface with collapsed polyHEMA. After the Gabriel synthesis the amine peak appears again, confirming the generation of amine functionalities on the ends of the polyHEMA chains.

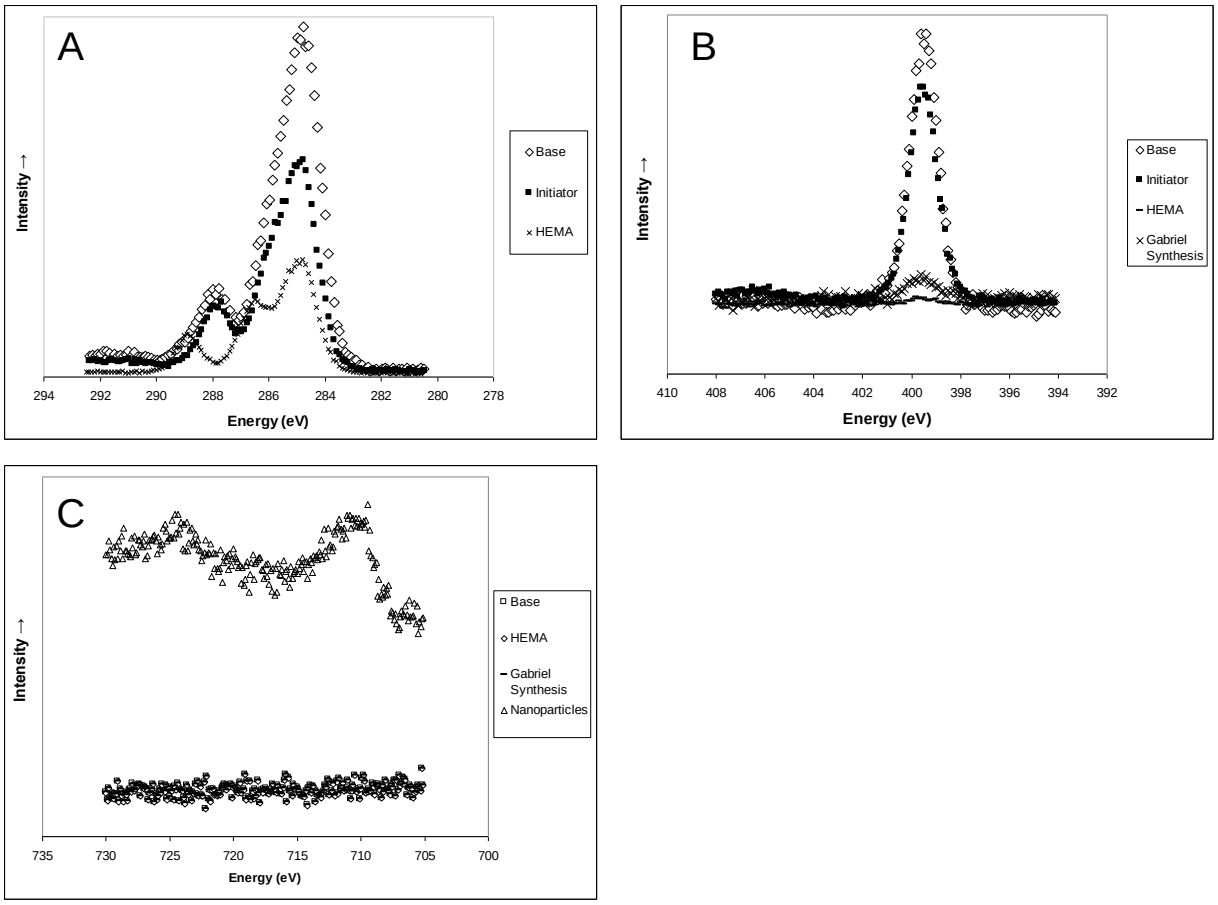

Figure 2.4. High resolution XPS spectra for carbon (2a), nitrogen (2b), and iron (2c) regions during various stages of modification (corresponding to Figure 1: Base = (1), Initiator = (2), HEMA = (3), Gabriel synthesis = (5), Nanoparticles = (6)).

Figure 2.4 (c) is a high-resolution spectrum for the iron region. This was used to verify the presence of iron oxide nanoparticles after modification. No iron was detected until after attaching the nanoparticles, via carbodiimide activation, to amino-capped grafted polyHEMA. Strong peaks appeared at 710 and 725 eV, which are associated with Fe(II).

Field-emission Scanning electron microscopy (FESEM) was used to visually confirm nanoparticle attachment. FESEM creates 2-D images of the membrane surface topography by bombarding the surface with an electron beam. The membrane surface is coated with a thin film of conductive material (here 10 nm of Au), which scatters the incoming electrons. These backscattered electrons can be analyzed to generate an image of the topmost few nm of the

membrane surface. FESEM is useful because it can verify nanoparticle attachment visually, and also give some indication of nanoparticle density on the membrane surface.

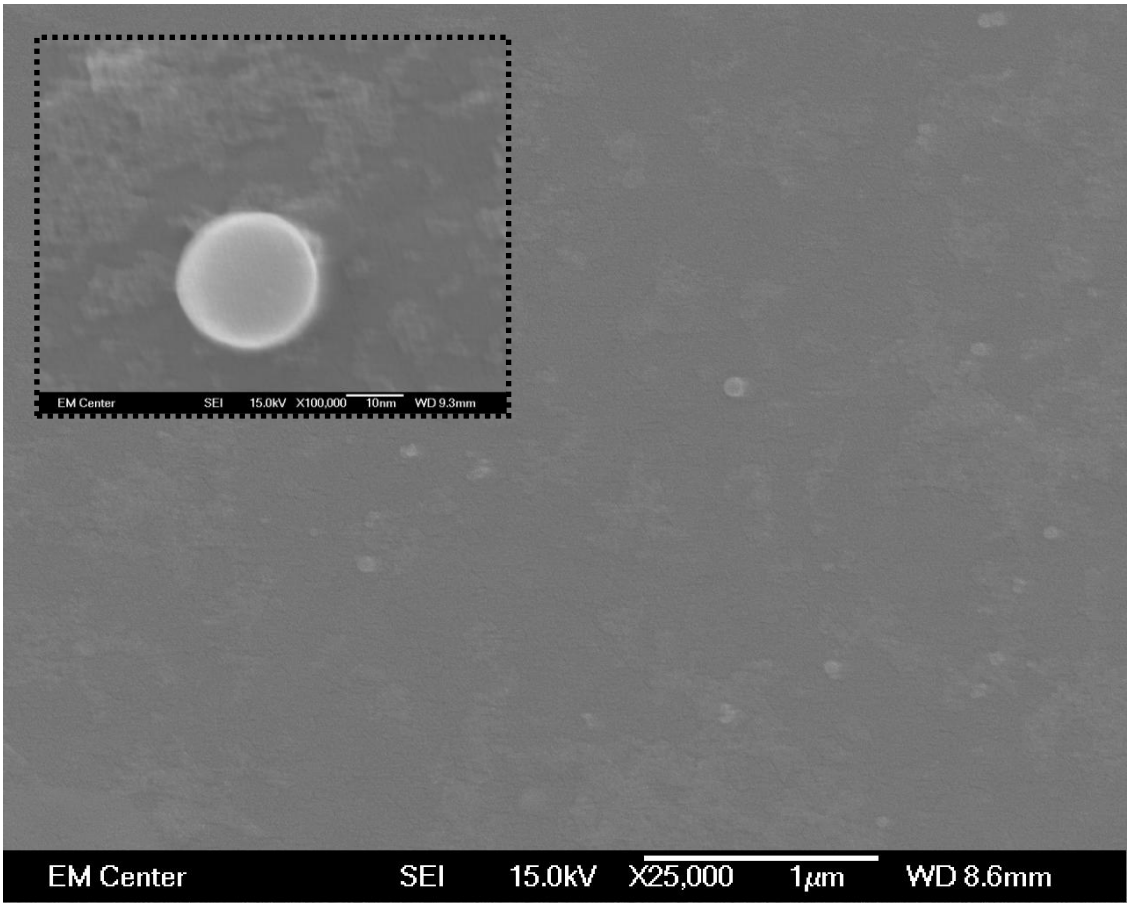

Figure 2.5. FESEM images showing isolated nanoparticles distributed across the membrane surface (25,000x magnification) as well as a single nanoparticle (inset : 100,000x magnification).

Figure 2.5 shows two FESEM images for a modified membrane. The larger image depicts the membrane surface at a 25,000x magnification. A number of nanoparticles, the bright gray circles, can be seen on the membrane surface. It is important to note that the nanoparticles are distributed across the membrane surface; i.e. they are not present in aggregates of multiple particles. This is critical because an aggregate of nanoparticles would not fully respond to a magnetic field, leading to inefficient mixing or no mixing at all. This image shows that the modification protocol was successful at attaching superparamagnetic nanoparticles to the end of

polyHEMA chains in a semi-controlled manner. The smaller inset image in Figure 2.5 shows a view of a single superparamagnetic nanoparticle at 100,000x magnification. The nanoparticle cannot be mistaken for other structures on the membrane surface because it is a perfect sphere and quite bright. This image also confirms the nanoparticle diameter as roughly 20nm.

2.3.2. Mixing Induced by an Oscillating Magnetic Field

Once the polymer chains with magnetic nanoparticles were grafted to the membrane surface, the key hypothesis of this work was tested; i.e., whether an oscillating external magnetic field could induce movement of the polymer brushes. This was done using particle image velocimetry (PIV). This method tracks the movement of dispersed particles in a fluid by using a camera to record the light reflected off dispersed particles so that time-resolved flow patterns and velocity vectors of the fluid can be determined.[21] By monitoring the velocity profile of water above the membrane surface in the presence and absence of a magnetic field, macroscopic mixing due to movement of the polymer chains could be observed. The rotational speed of a permanent magnet placed below the membrane was varied to generate 3 different time-varying magnetic fields, resulting in four observed frequencies: 0 (no magnet rotation), 9, 22, and 30 Hz. The results for unmodified and modified membranes are presented in Figure 2.6.

The fluid behavior above the unmodified membrane was always well-behaved and orderly; i.e., the red field lines were orientated in the same direction and roughly parallel. The pattern above the modified membrane at 0 Hz was similar; however, for 9 and 22 Hz, the fluid behavior was noticeably different. Mixing caused the flow to change direction and/or velocity by introducing hydrodynamic disorder. This change appears as velocity vectors of varying direction and/or length as well as field lines with chaotic (non-parallel) pathways.

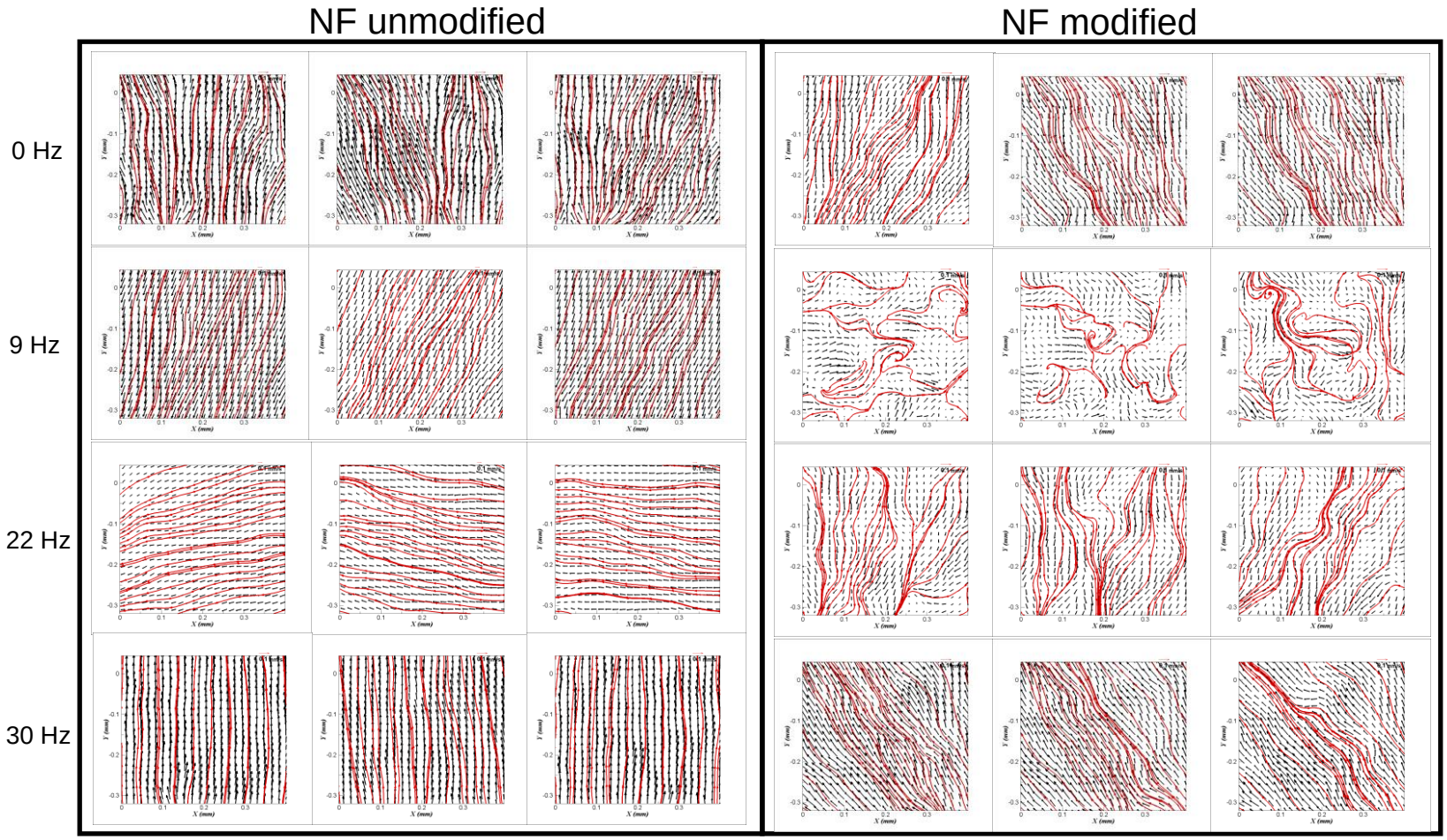

Figure 2.6. Series of 3 PIV vector diagrams for magnet rotation frequencies of 0, 9, 22 and 30 Hz. Each vector diagram is averaged over 1 ms of time.

The superparamagnetic nanoparticles in an external field will experience both a force $\vec{F} = (\vec{\mu} \cdot \vec{\nabla})\vec{B}$ and a torque $\vec{\tau} = \vec{\mu} \otimes \vec{B}$, where μ is the magnetic moment of the nanoparticle and B is the external magnetic field. The force is proportional to the gradient of the field and will induce nanoparticle lateral movement. The torque will align the magnetic moment of the nanoparticle with the external field. There are two mechanisms for this alignment: Néel relaxation time refers to the time it takes for the magnetic moments of the nanoparticles to orient randomly once an external magnetic field is removed without actual physical rotation. It is also the characteristic time for the magnetic moments of the nanoparticles to align with an external field without physical rotation. Similarly, Brownian relaxation time refers to randomization of the magnetic moments by Brownian motion once an external field is removed. Brownian motion also aligns the magnetic moments of the nanoparticles to the applied magnetic field. The nanoparticles will physically rotate only when Brownian mechanism dominates. Néel relaxation time is exponentially proportional to the magnetic volume of the particle, whereas Brownian relaxation is linearly dependent on the hydrodynamic volume of the nanoparticles. Since the movement of the nanoparticles is desired here to induce mixing, Brownian relaxation is preferred for the alignment of the magnetic moment to the external field. Besides physical rotation, the nanoparticles will also experience a magnetic force for lateral movement. Based on the size of the nanoparticle used here, 15 nm magnetic core diameter and 5 nm coating, the calculated Néel relaxation time is much larger than 1 s, significantly longer than Brownian relaxation time estimated to be on the scale of roughly 10^{-3} s. Since the oscillating frequency used here lies between 0 and 30 Hz with equivalent time scale ranging between 0.01 and 1 s, only lateral (Brownian) movement due to the presence of magnetic force will be expected to be significant.

Interesting to note is the more pronounced fluid mixing for 9 Hz compared to 22 Hz. We believe that this is due to the lateral distance traveled by the tips of the polymer chains (at least 60 nm long, at relatively low density, i.e., little mutual hindrance). The length of the polymer chains will affect particle movement by limiting the distance the particle can travel. Longer polymer chains could increase the flexibility and the distance the nanoparticles could travel, but also impart additional resistance to slow down the magnetic particle movement. The relationship between polymer chain length and magnetic particle movement was investigated in subsequent studies. Since SI-ATRP is a controlled polymerization mechanism; all grafted polymer chains will be nearly the same length. Any effect of polymer chain length should therefore be nearly identical for each polymer chain. It is for this reason that chain length is not taken into account for the explanation given below.

The faster the applied field is oscillating, the less time the polymer chains travel in a given direction. Thus the chains will not be able to cover as much distance during the lateral movement, thereby resulting in less mixing. This also explains why the 30 Hz data for the modified membrane appears so similar to the 0 Hz data. If the magnetic field is switching too quickly, then the chains can only travel a very short distance in a given direction causing ineffective mixing. The viscous drag force, which is proportional to the viscosity of the fluid and the relative velocity of the fluid and the chains, is ignored here assuming low viscosity of the solution and low relative velocity. This viscous drag force could become significant for solutions of higher viscosity and for more rapid movement of the nanoparticles. More quantitative analysis is possible only if the polymer chain length and the external magnetic field could be accurately determined. This was studied in greater detail in subsequent studies. The

distance covered by the magnetic polymer chain to a first approximation is proportional to the time squared and inversely related to the frequency squared, as shown in Equation 1.1.

$$d \sim \frac{F}{m}\left(\frac{1}{f^2}\right) = a\left(\frac{1}{f^2}\right) \tag{1.1}$$

Here F is the force the magnetic field exerts on the magnetic nanoparticles and m is the effective mass of the magnetic polymer-nanoparticle conjugate (F/m is re-labeled as the constant acceleration, a). This can be used to explain the results in Figure 2.6. The distance traveled by the chains at 9 Hz is proportional to $\frac{a}{81}$. By contrast, the maximum distance traveled for the same chain, in the same field, at 22 Hz and 30 Hz is proportional to $\frac{a}{484}$ and $\frac{a}{900}$, about five to ten times shorter, respectively, than the distance traveled with 9 Hz external field. The dramatically shortened distances at these higher frequencies would result in less turbulence created in the fluid. In fact, the resulting mixing at 30 Hz is so small, that it appears to have no clear effect on fluid behavior.

2.3.3. Influence of Membrane Modification and Magnetic Field on Separation Performance

Finally, separation performance of the membranes was investigated. The unmodified NF membrane had an average water flux of 35 L/m^{2}h at 45 psig (3.1 bar). The modified membranes exhibited a noticeably lower average flux of 15 L/m^{2}h, a decline of roughly 60%. This loss is larger than expected for an added grafted layer of a hydrophilic polymer with less than 100 nm thickness, but the conditions during chemical modification also likely reduced the flux of the polyamide layer. Filtration experiments were then performed using aqueous salt solutions to

determine the effect of membrane modification and magnetic field application on membrane flux and rejection as shown in Table 2.1.

Table 2.1. Average fluxes and salt rejections for control and modified membranes at 3.1 bar (45 psig).

	Salt Rejection (%)			
	500 ppm $CaCl_2$		**2000 ppm $MgSO_4$**	
	Unmodified	**Modified**	**Unmodified**	**Modified**
With Field	34.4 ± 0.2	40.4 ± 0.2	66.5 ± 0.2	74.4 ± 0.2
Without Field	32.5 ± 0.2	34.2 ± 0.2	66 ± 0.2	67.7 ± 0.2
	Membrane Flux (L/m^2h)			
With Field	13.4 ± 0.6	9.6 ± 0.7	5.4 ± 0.3	6.0 ± 0.4
Without Field	12.8 ± 0.6	7.8 ± 0.7	5.6 ± 0.4	4.0 ± 0.2

Salt solution fluxes were much lower than water fluxes which is explained by concentration polarization contributing additional resistance to water permeation through the membrane; this effect is larger at higher salt concentration. In line with the reduced water flux, the modified membrane had a higher salt rejection. This is due to additional resistance of the barrier structure attributable to grafted polyHEMA. While the performance of the original membrane was not influenced by the magnetic field, significant changes occurred for the modified membrane. Salt solution flux and rejection were 30% and 15% higher, respectively, for the $CaCl_2$ solution. For the $MgSO_4$ solution with a higher salt concentration, the fluxes of the modified membrane with magnetic field were identical to the ones for the original membrane, but the salt rejection was higher. All results can be explained by a significantly reduced concentration polarization within the boundary layer of the membranes triggered by the magnetic field. Because the large effects occurred only for the modified but not for the control membrane,

effects of the magnetic field alone on mixing of ions are negligible. This is strong evidence that the surface-attached micromixers indeed improve the membrane performance.

2.4. CONCLUSIONS

This study verifies proof-of-concept for the active alteration of macroscopic flow via surface-anchored micromixers based on polymer-nanoparticle conjugates. Permeable, magnetically-responsive NF membranes were successfully created by attaching superparamagnetic nanoparticles to the end of flexible hydrophilic polymer chains, which were grafted on the membrane surface using SI-ATRP. All steps of the chemical modification were confirmed using XPS. The fluid behavior above the membranes was then observed under an oscillating magnetic field. Mixing above the membrane surface was observed using a PIV system. This mixing leads to a significantly improved membrane performance in an external magnetic field that can be explained by a reduced concentration polarization. This should also lead to reduced colloidal fouling. Most likely, the specific prototype membrane reported here will not be efficient for all fouling conditions; but adaptations of the grafted polymer-nanoparticle conjugate layers are possible. Moreover, the surface-grafted polymeric cilia-like micromixers which can be activated by an oscillating magnetic field have also potential for other applications, for instance in micro-fluidic systems.

REFERENCES

1. M. Ulbricht, Advanced functional polymer membranes, Polymer, 47(2006), 2217-2262.
2. M. A. Shannon, P. W. Bohn, M. Elimelech, J. G. Georgiadis, B. J. Marinas, A. M. Mayes, Science and technology for water purification in the coming decades, Nature, 452 (2008), 301-310.
3. R. W. Baker, Membrane technology and applications, 2nd Ed. Chichester: John Wiley and Sons, 2004.
4. J. Gilron, S. Belfer, P. Väisänen, M. Nyström, Effects of surface modification on antifouling and performance properties of reverse osmosis membranes, Desalination, 140 (2001), 167-179.
5. S. Susanto, M. Ulbricht, Photo-grafted thin polymer hydrogel layers on PES ultrafiltration membranes: characterization, stability, and influence on separation performance, Langmuir, 23 (2007), 7818-7830.
6. M. A. C. Stuart, W. T. S. Huck, J. Genzer, M. Müller, C. Ober, M. Stamm, G. B. Sukhorukov, I. Szleifer, V. V. Tsukruk, M. Urban, F. Winnik, S. Zauscher, I. Luzinov, S. Minko, Emerging applications of stimuli-responsive polymer materials, Nature Materials, 9 (2010), 101–113.
7. D. Wandera, S. R. Wickramasighe, S. M. Husson, Stimuli-responsive membranes, J. Mem. Sci., 357 (2010), 6-35.
8. S. L. Biswal, A. P. Gast, Micromixing with linked chains of paramagnetic particles, Anal. Chem., 76 (2004), 6448-6455.
9. H. Singh, P. E. Laibinis, T. A. Hatton, Rigid, superparamagnetic chains of permanently linked beads coated with magnetic nanoparticles. Synthesis and rotational dynamics under applied magnetic fields, Langmuir, 21(2005), 11500-11509.
10. L. Lu, K. S. Ryu, C. Liu, A magnetic microstirrer and array for microfluidic mixing, J. Microelectromech. Syst., 11 (2002), 462-469.
11. T. Franke, L. Schmid, D. A. Weitz, A. Wixforth, Magneto-mechanical mixing and manipulation of picoliter volumes in vesicles, Lab Chip, 9 (2009), 2831-2835.
12. S. L. Biswal, A. P. Gast, Rotational mechanics of semiflexible paramagnetic particle chains, Phys. Rev. E, 69 (2004), 041406.
13. A. Lu, E. L. Salabas, F. Schüth, Magnetic nanoparticles: synthesis, protection, functionalization, and application, Angew. Chem. Int. Ed., 46 (2007), 1222-1244.
14. V. V. Khatavkar, P. D. Anderson, J. M. J. Den Toonder, H. E. H. Meijer, Active micromixer based on artificial cilia, Physics of Fluids, 19 (2007), 083605.
15. M. Ulbricht, H. Yang, Porous polypropylene membranes with different carboxyl polymer brush layers for reversible protein binding via surface initiated graft-copolymerization, Chem. Mater., 17 (2005), 2622-2631.
16. L. Ying, E. T. Kang, K.G. Neoh, Characterization of membranes prepared from blends of poly(acrylic acid)-graft-poly(vinylidene fluoride) with poly(N-isopropylacrylamide) and their temperature- and pH-sensitive microfiltration, J. Membr. Sci., 224 (2003), 93-106.
17. C. Schlemmer, W. Betz, B. Berchtold, J. Rühe, S. Santer, The design of thin polymer membranes filled with magnetic particles on a microstructured silicon surface, Nanotechnology, 20 (2009), 255301.

18. T. Hoare, J. Santamaria, G. F. Goya, S. Irusta, D. Lin, S. Lau, R. Padera, R. Langer, D. S. Kohane, A magnetically-triggered composite membrane for on-demand drug delivery, Nano Lett., 9 (2009) 3651-3657.
19. E. R. Edelman, J. Kost, H. Bobeck, R. J. Langer, Regulation of drug release from porous polymer matrices by oscillating magnetic fields, Biomed. Mat. Res., 19 (1985), 67-83.
20. S. Monge, O. Giani, E. Ruiz, M. Cavalier, J. Robin, A new route for the modification of halogen end groups to amino end-modified poly(ter-butyl acrylate)s, Macromol. Rapid Commun., 28 (2007), 2272-2276.
21. M. Raffel, C.E. Willert, S. T. Wereley, J. Kompenhans, Particle Image Velocimetry: A Practical Guide, Springer, Berlin, 2007.
22. N. Tomer, S. Mondal, D. Wandera, S. R. Wickramasinghe, S. M. Husson, Modification of nanofiltration membranes by surface-initiated atom transfer radical polymerization for produced water filtration, Sep. Sci. Technol., 44 (2009), 3346-3368.
23. Z. Bao, M. L. Bruening, G. L. Baker, Control of the density of polymer brushes prepared by surface-initiated atom transfer radical polymerization, Macromolecules, 39 (2006), 5251-5258.
24. A. Friebe, M. Ulbricht, Cylindrical pores responding to two different stimuli via surface-initiated atom transfer radical polymerization for synthesis of grafted diblock copolymers, Macromolecules, 42 (2009), 1838-1848.
25. V. Freger, Nanoscale heterogeneity of polyamide membranes formed by interfacial polymerization, Langmuir, 19 (2003), 4791-4797.
26. J. M. Hollander, W. L. Jolly, X-ray photoelectron spectroscopy, Acc. Chem. Res., 3 (1970), 193-200.

CHAPTER 3

TOWARD REMOTE-CONTROLLED VALVE FUNCTIONS VIA MAGNETICALLY-RESPONSIVE CAPILLARY PORE MEMBRANES

Track-etched microfiltration membranes were used to characterize the modification protocol and magnetic response in a highly-controlled environment. Magnetic response was shown to be reversible and significant considering the very small size of the polymer chains.

I used a premodification protocol developed by Drs. Ulbricht and Yang to adjust the density of grafted polyHEMA. I modified the membranes at various conditions, performed the filtration experiments, and characterized the modifications with guidance from the co-authors.

SUMMARY

Polyethyleneterephthalate track-etched membranes with a pore diameter of 650 nm were modified via surface-initiated atom transfer radical polymerization with grafted poly(2-hydroxyethylmethacrylate). Grafted chain length and density were varied. Superparamagnetic nanoparticles (Fe_3O_4; core diameter 15 nm) were selectively covalently coupled to the end groups of the grafted chains. The membranes were characterized by grafting degree, X-ray photoelectron spectroscopy, electron microscopy, zeta potential, and pore size in the dry state via gas flow / pore dewetting permporometry. The results confirmed that all modification steps were well controlled. Water permeability measurements allowed estimation of the hydrodynamic pore diameter of the membranes and thus the hydrodynamic polymer layer thickness on the pore walls. The water permeability of the nanoparticle hybrid membranes was then measured in a static or an alternating external magnetic field. Significant and reversible decreases of permeability were observed, with the largest effects for membranes with high polymer grafting density and long polymer chains (hydrodynamic layer thickness up to 100 nm). The maximum change in effective pore diameter was only 6%; however, the estimated change of swollen polymer layer thickness (originally between 60 and 100 nm) was up to 13 nm. The functionality of the membranes can be tuned by variations of straightforward parameters such as pore size or grafted chain lengths. The study is also relevant as model system for altering the effective thickness of grafted polymer layers on a surface by an external magnetic field for other applications, for instance in microfluidic systems.

Experiments were performed at both the Universität Duiβburg-Essen (Essen, Germany) and Colorado State University. Financial support was provided by a DoD NDSEG graduate fellowship (USA) and the DFG Mercator Fellows Program INST 20876/119-1 (Germany).

3.1. INTRODUCTION

The demand for advanced membranes with tailored properties has led to the development of stimuli-responsive membranes. These membranes contain chemical groups or moieties that change their properties in response to changes in the external environment. Many stimuli-responsive membranes use stimuli such as pH, solution ionic strength, or temperature to evoke a response[1,2]. Such stimuli carry the unfortunate side effect that the properties of the entire feed stream must be changed to observe a response. This can be avoided by using an external physical stimulus such as light or a magnetic field[1-4].

Building upon this, an exciting new type of filtration membrane responsive to an external magnetic field was recently developed by our groups[5]. The nanofiltration behavior of these membranes can be altered without affecting the characteristics of the entire feedstream by generating small scale mixing above the membrane surface via the movement of grafted polymer chains in a magnetic field[5]. In the presence of an oscillating magnetic field both rejection and permeability increased for feed streams containing dissolved salts such as $MgSO_4$ and $CaCl_2$. Our earlier work also highlighted the importance of optimizing chain density and chain length both of which can be done independently using controlled surface-initiated atom transfer radical polymerization (SI-ATRP).

The purpose of this study was to characterize the various modification steps in a controlled environment. Track-etched poly(ethylene terephthalate) (PET) microfiltration (MF) membranes with a pore diameter of about 650 nm were used to characterize the modification chemistry in detail because of their near-uniform pore diameter, well-understood cylindrical pore structure, and isotropic construction—characteristics which make these membranes a good model system[6-9]. Poly(2-hydroxyethyl methacrylate) (polyHEMA) chains were grafted from the

membrane surface in a controlled manner using SI-ATRP. The density of the grafted polyHEMA chains was varied via the density of surface-immobilized ATRP initiator[8-13]. By varying the density of the initiation sites for polymerization, high and low density modified membranes were prepared. The membranes were modified by adapting a previous protocol, used for modification of polyamide NF membranes[5], to the modification of PET MF membranes. In this chapter, the preparation and characterization of capillary pore membranes comprising superparamagnetic nanoparticles tethered to the ends of hydrophilic chains is presented, and the response of such membranes with varied grafting densities and chain lengths to different types of magnetic fields is investigated.

3.2. Materials and Methods

3.2.1. Chemicals

Water was obtained from a Milli-Q purification system from Millipore (Billerica, MA) and had a measured conductivity of 0.054 μS/cm. All chemicals were 97+% unless otherwise noted. Sulfuric acid was from Fisher Scientific (Schwerte, Germany); potassium permanganate, N,N'-diisopropylcarbodiimide (DPCI), N-hydroxybenzotriazole, ethanolamine, triethylamine, and 4-N,N-dimethylaminopyridine (DMAP) were from Fluka (Munich, Germany); dimethylformamide (DMF) was from Acros Organics (Geel, Belgium); ethanol (pure), methanol, acetonitrile, and hydrochloric acid (6 M) were from VWR (Darmstadt, Germany); α-bromoisobutyrlbromide, 2-hydroxyethylmethacrylate (HEMA), 1-ethyl-3-(3-dimethylaminopropyl)carbodiimide (EDC), 1-hydroxybenzotriazolehydrate (HOBth), and N-hydroxysuccinimide (NHS) were from Sigma-Aldrich (Munich, Germany). Iron oxide core, oleic

acid shell superparamagnetic nanoparticles with a core diameter of 15 nm were purchased from Ocean Nanotech (Fayetteville, AR, USA).

3.2.2. Membranes

Polyethylene terephthalate (PET) 400 microfiltration (MF) membranes were obtained from Oxyphen AG (Lachen, Switzerland) in sheet form. The average pore diameter was measured to be roughly 650 nm using gas flow / pore dewetting permporometry (details below). Although 650 nm is considerably larger than the nominal pore size of 400 nm given by the manufacturer, the value agrees with previous findings[7,11]. Before modification the membranes were washed with Milli-Q water for 1 minute, then in methanol for 15 minutes, and finally in ethanol for 1 minute with gentle mixing. Membranes were dried for 30 minutes at 45^{o}C in a vacuum oven.

3.2.3. Initiator Immobilization

3.2.3.1. Overview

An overview of the entire modification process, initiator immobilization through nanoparticle coupling, is shown in Figure 3.1. Two modification protocols, high density (HD) and low density (LD), were performed. For the HD method, a four-step modification procedure was used to increase the number of possible initiation sites on the membrane surface. Briefly, ester groups and hydroxyl groups on the membrane surface were first hydrolyzed and oxidized, respectively, to carboxyl groups. These newly oxidized groups along with carboxyl groups originally present on the membrane surface were used, via amidation, to introduce hydroxyl functionalities. Finally, the bromine-terminated SI-ATRP initiator was attached via

esterification. The LD procedure consisted of immobilizing the initiator to the as-received membranes with no premodification[5]. There were fewer initiation sites on the LD membranes as compared to the HD method, since the α-bromoisobutyrylbromide only bound to the hydroxyl groups originally present on the membrane surface.

3.2.3.2. Oxidative Hydrolysis

The dry membrane sheets were placed in a solution of 7.50 g $KMnO_4$ in 150 mL 0.75 N H_2SO_4 and tightly sealed. The membranes were reacted for 2.5 hours under gentle shaking. The membranes were then washed twice with purified water, four times with 6 M HCl for two minutes, four times with water for two minutes, and finally twice with ethanol for two minutes. The membrane sheets were then dried for 3 hours at 50^{o}C.

3.2.3.3. Pre-modification

The membrane sheets were submerged in a solution of 2.30 g HOBth and 0.95 g DPCI in 150 mL DMF. The membranes were reacted for 30 minutes with gentle shaking. The membranes were washed twice with DMF and then immediately placed in a solution of 4.58 g ethanolamine in 150 mL DMF for 3 hours with gentle shaking. The membrane sheets were washed twice with DMF for two minutes and twice with ethanol for two minutes. The membranes were then dried for 30 minutes in a 45^{o}C vacuum oven.

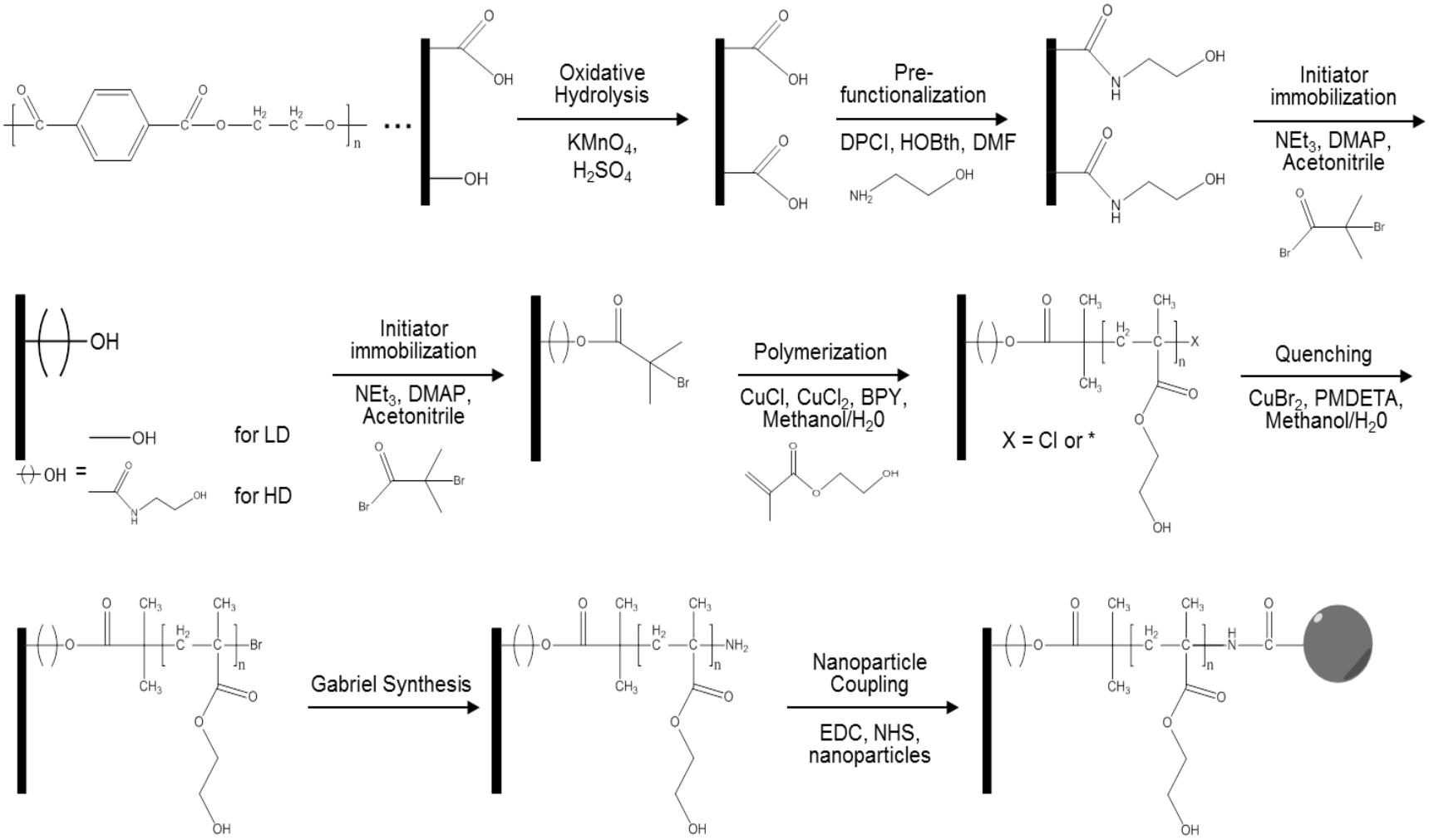

Figure 3.1. HD and LD modification schemes for PET membranes. The HD scheme increases the number of initiation sites by converting surface hydroxyl and carboxyl groups into hydroxyl terminated amides. The LD scheme generates initiation sites only at the hydroxyl groups present on the as-received membrane surface.

3.2.3.4. Initiator Immobilization

The procedure has been described in detail in previous work[5]. Briefly, the pre-modified membrane sheets were cut into 25 mm diameter discs. These discs were reacted in a solution of 1.515 g triethylamine, 91.5 mg DMAP, and 2.76 g α-bromoisobutyrylbromide in 150 mL dried acetonitrile for two hours at room temperature.

3.2.4. SI-ATRP

The HEMA monomer was purified through distillation before use in SI-ATRP to remove any inhibitors present. Purified monomer was always used within 12 hours of distillation to minimize self-polymerization. The pure monomer was degassed with argon gas for 10 minutes before use in SI-ATRP. Both LD and HD membranes followed the same SI-ATRP procedure, which has been described previously[5]. The reaction solution consisted of HEMA (2 M), CuCl, $CuCl_2$, and BPy dissolved in equal parts (v/v) water and methanol. The molar ratios of the final solution were 100 : 0.5 : 0.1 : 1.5 for HEMA : CuCl : $CuCl_2$: BPy. The reaction occurred at room temperature for a chosen reaction time, which was varied to study grafting kinetics. Thereafter, the membranes were placed in a quenching solution (500 mg $CuBr_2$ and 1250 μL PMDETA in 100 ml equal parts methanol/water (v/v)) to stop the polymerization and ensure the end of each polymer chain was capped with a bromine atom.

The amount of polyHEMA grafted from the membrane, i.e., the degree of grafting (DG), can be easily calculated by dividing the membrane mass difference before and after SI-ATRP grafting by the specific area of the membrane.

$$DG = \frac{m_{ATRP} - m_{base}}{A_{specific}} \tag{2.1}$$

Specific area is the sum of the surface area of the top and bottom of the membrane plus the surface area of the pores surface; i.e., the total area available for grafting. The surface area of the pores was calculated by using the known membrane thickness (pore length) as well as calculated pore density (see eq. 2.2) and measured average pore diameter (section 3.2.8.1). Furthermore, using a known density of grafted polyHEMA (1.15 g/cm^3) it is possible to confirm that the DG values obtained yield similar grafted layer thicknesses as those determined using PMI and the Hagen-Poiseuille equation (see eq. 2.2).

3.2.5. Gabriel Synthesis Procedure

A modified Gabriel synthesis reaction was used to convert the terminal bromide to a primary amine[5]. Because the PET 400 membranes are quite stable, DMF was used as a solvent rather than ethanol[5]; the stronger polarity of DMF is advantageous for the reaction. The discs were reacted in a 60^{o}C oil bath for six hours in a solution of 3 g potassium phthalimide salt in DMF. Gentle shaking was used to ensure good mixing. Next, the discs were reacted in a 60^{o}C oil bath in a solution of 7 mL hydrazine hydrate in 25 mL of 6 M HCl for 6 hours again with gentle shaking.

3.2.6. Nanoparticle Coupling

Carboxylic acid coated nanoparticles were covalently bound to the primary amine-capped polyHEMA chains via a proven coupling reaction resulting in an amide bond[5]. The discs were incubated in a solution of 31.2 mg EDC, 38.7 mg NHS, 0.3 mL nanoparticle stock solution, and 10 mL DI water for 4 hours in the dark. After incubation, the membrane was removed, washed, and dried.

3.2.7. Characterization of Nanoparticles via Dynamic Light Scattering

Dispersions of the Fe_3O_4 nanoparticles in water, adjusted to different pH values, were characterized using a ZetaSizer from Malvern, Inc. (Malvern, U.K.).

3.2.8. Membrane Characterization

3.2.8.1. Permporometry

A capillary flow porometer (Porous Materials, Inc., NY, USA) was used to measure the average pore diameter in dry state of the various membrane discs using a gas flow / pore dewetting procedure, with Galwick (surface tension 16 dyn/cm) as the wetting liquid, analogous to previous work[8,9,11]. Permporometry tests were performed twice for each membrane sample.

3.2.8.2. Membrane Permeability

The dry membrane discs were placed in an Amicon 8010 stirred filtration cell (Millipore, Billerica, MA) connected to an open reservoir providing a hydrostatic pressure for fluid flow through the membrane. The membranes were allowed to equilibrate for 3 minutes with the permeate line closed. The permeate line was opened and allowed to flow for 3 minutes before measurements began. Permeate was collected for 5 minutes and then returned to the reservoir to maintain equal pressure over the course of the filtration. Three measurements were taken; thereafter the membrane was removed, washed briefly with Milli-Q water, and stored. The Hagen-Poiseuille equation was used to calculate pore density for the unmodified membrane.

$$\rho_P = \frac{128 \cdot \eta \cdot l \cdot V}{A \cdot \pi \cdot \Delta P \cdot d^4 \cdot t} \tag{2.2}$$

Here ρ_p is the pore density, d is the pore diameter (from permporometry; section 3.2.8.1), ΔP is the trans-membrane pressure, *l* is the membrane thickness, η is the viscosity of water, and V/A*t

is the volume of permeate through an area of membrane per unit time, also called permeability. Assuming the calculated pore density will not change due to modification, the pore diameter for all modified membranes in the wetted state was then obtained from water permeability measurements[7]. All membrane permeabilities are reported in units of L/(m^2*hr*bar), abbreviated as Lmh/bar. Membrane permeability measurements for each membrane type were done in triplicate.

Magnetic fields were generated using a computer-controlled system comprising two iron-core solenoids located on opposite sides of the stirred cell[5], see Figure 3.2 and Appendix A4. The power supplied to the solenoids was tuned to yield a field strength of 50 G at the center of the membrane cell, measured by a probe HHG-23 Gauss/Teslameter (Omega Inc., Stamford, CN). Static fields were produced by continuously powering both solenoids. Dynamic fields were produced by alternatively powering each solenoid. Dynamic fields were operated at a frequency of 9 Hz, which was previously found to yield maximum mixing above the membrane surface[5].

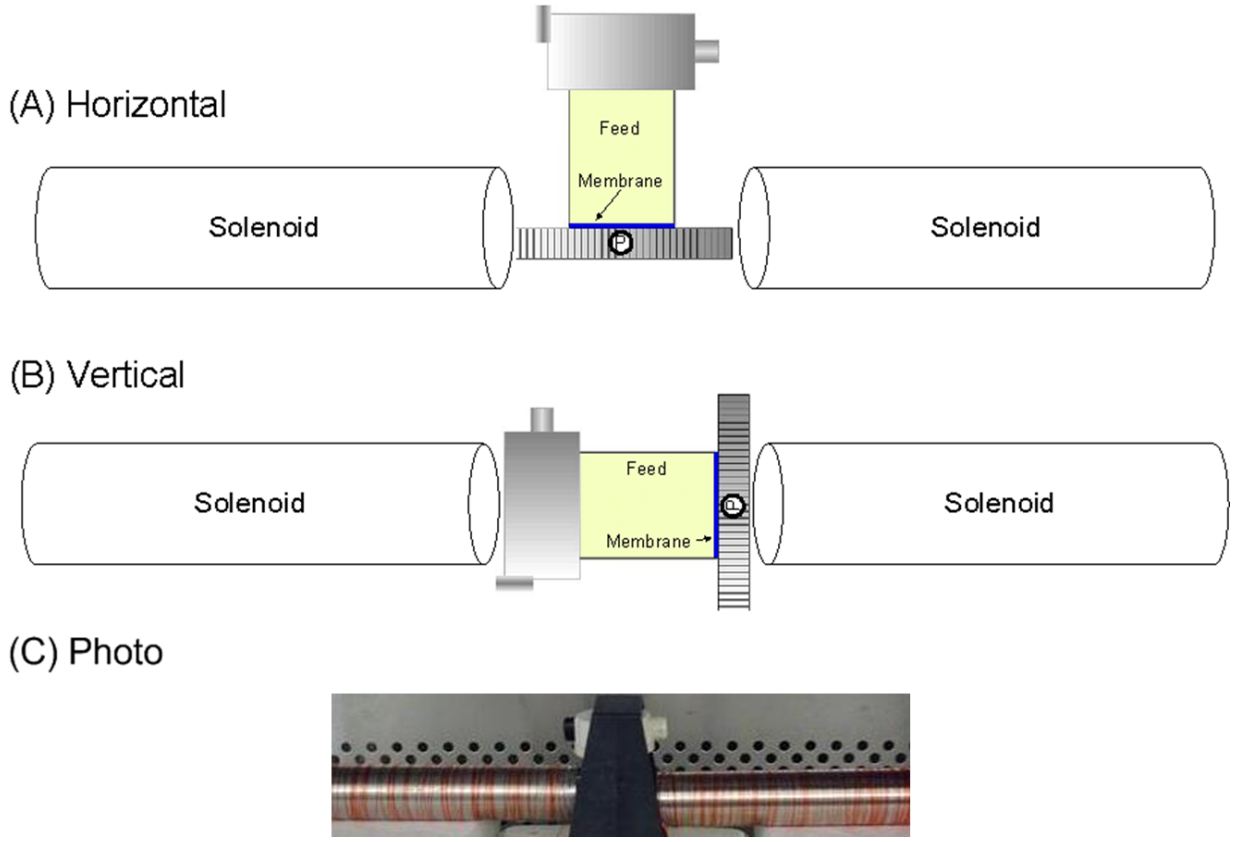

Figure 3.2. Schematic showing (A) the horizontal and (B) the vertical field orientations as well as (C) a photo of the experimental setup in the horizontal orientation. The small P at the base of the membrane cell in (A) and (B) corresponds to the permeate line coming out of the page.

3.2.8.3. Membrane Zeta potential

The zeta potential of unmodified and modified membranes was measured by using a custom built setup for streaming potential analysis, described in detail previously[16,17]. The measurements were always started at roughly pH 9 in a 10^{-3} M KCl in water solution; dilute HCl in water solution was added to obtain multiple pH values over the range 2-7. The streaming current was measured and converted to the zeta potential using the Helmholtz-Smoluchowski model.

$$\varsigma = \frac{\eta \cdot \kappa \cdot \Delta E_{SP}}{\varepsilon_o \cdot \varepsilon_r \cdot \Delta P} \qquad (2.3)$$

Here η is the viscosity of the feed, κ is the conductivity of the feed, ε_o is the permittivity of free space, ε_r is the permittivity of the feed, ΔE_{SP} is the streaming potential, and ΔP is the transmembrane pressure. All zeta potential experiments were performed in tangential flow mode, and the average value of four measurements at each pH is reported.

3.2.8.4. Field Emission Scanning Electron Microscopy (FESEM)

FESEM was used to image the surface and cross section of the membrane to visualize the presence of nanoparticles and verify that the modification did not damage the structural integrity of the membranes. To prevent pore collapse, critical point drying[5] was performed prior to analyzing samples with a JEOL field-emission scanning electron microscope (JSM-6500F, JEOL Ltd., Tokyo, Japan). Membranes for cross sectional imaging were placed in liquid nitrogen for 10 seconds and then cracked.

3.2.8.5. X-ray Photoelectron Spectroscopy (XPS)

XPS is particularly useful for studying membrane surface chemistry; i.e. the topmost 1-10 nm of the sample. A Physical Electron 5800 ultra-high vacuum XPS-Auger spectrometer (Chanhassen, MN) was used. 20 scans at a high resolution of 0.1 eV focusing on individual regions of interest were averaged to characterize small changes in the surface chemistry with respect to Br, Fe, and O.

3.3. Results and Discussion

3.3.1. Membrane Modification

Degree of grafting (DG) was calculated to determine the amount of polyHEMA grafted. Figure 3.3 shows the average DG versus time for SI-ATRP for HD and LD membranes. In both cases, grafting followed a linear trend before leveling out. This trend has been observed for SI-ATRP of other similar polymers previously[5-11]. The greater number of initiation sites for HD membranes yielded a greater DG. The LD membranes showed less variance than the HD membranes due to the lack of pretreatment to adjust the surface chemistry. The variability of data for both HD and LD increased with increasing SI-ATRP reaction time. The departure from linear growth indicates that the frequency of termination events increases at longer polymerization times[5-11].

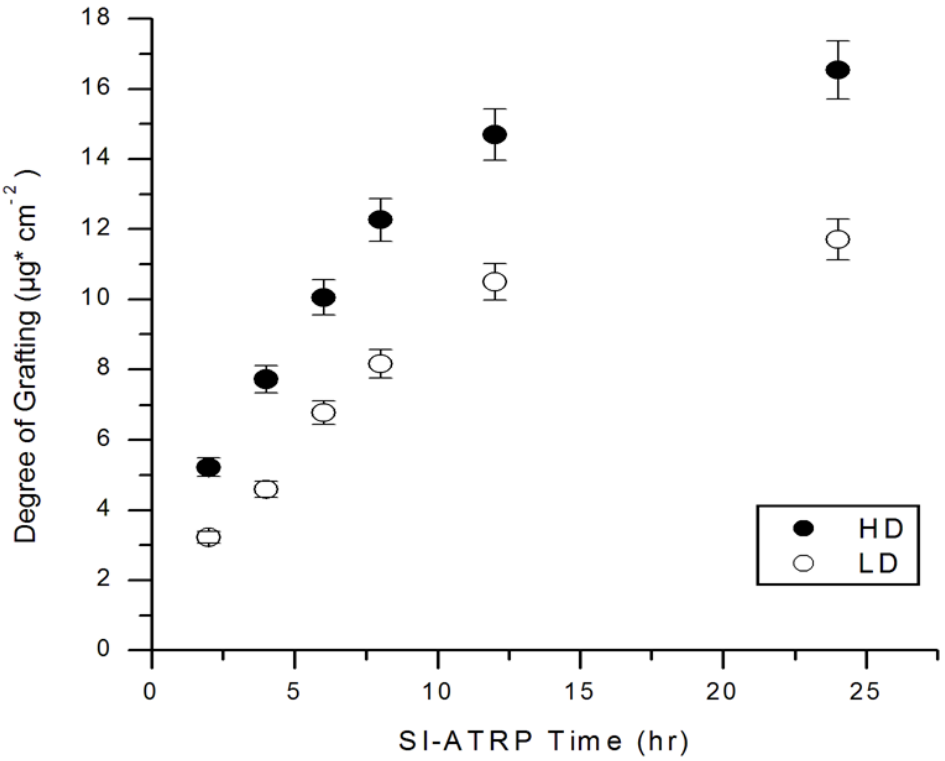

Figure 3.3. Average degree of grafting (DG) for polyHEMA SI-ATRP for both high density (HD) and low density (LD) membranes. Error bars represent one standard deviation.

All stages of membrane modification were monitored using XPS to observe compositional changes in the topmost few nm of the membrane. The regions of interest for direct evidence of the various stages of modification were bromine (Br3d) and iron (Fe3s); the oxygen (O1s) region served as supporting evidence. Spectra for the bromine region are shown in Figure 3.4 (a). Since the unmodified PET membranes contained no bromine, there was no associated peak for the base membrane. After initiator immobilization a distinct peak (71.5 eV) developed due to the presence of the bromine-capped initiator groups. The height and area of the HD peak were larger than for the LD peak, confirming that the HD protocol successfully led to greater initiator density. Following SI-ATRP, the bromine peak (only HD is shown) was practically identical to the respective data following initiator immobilization. This is to be expected since the number of bromine atoms should be equal for both the initiator immobilized and ATRP-grafted states (cf. Figure 3.1). The post Gabriel synthesis membranes showed no measurable bromine peak, which suggested that most, if not all, of the bromine sites on the end of the polyHEMA chains were successfully converted to amino groups. Analysis of the nitrogen region spectra (see previous work[5]) supports this since no nitrogen peak was observed following initiator immobilization, but a strong nitrogen peak appeared following the Gabriel synthesis.

Iron region spectra are shown in Figure 3.4 (b). A large peak (98.2 eV) was observed for both HD and LD membranes due to the presence of coupled nanoparticles. The peak for the HD membrane was slightly larger because the increased number of polyHEMA chains led to a greater number of coupled nanoparticles. All membranes from previous steps (only post Gabriel synthesis is shown) in the modification procedure showed no iron peak, as expected.

Spectra for the oxygen region, Figure 3.4 (c), showed two distinct peaks at 532.3 and 533.5 eV. The two peaks represent C-O and C=O, respectively. These are the two states of

oxygen in the membrane polymer PET. Following polyHEMA grafting, a single peak was observed for all of the other steps in the modification procedure. This suggested that the ester present in polyHEMA was the predominant observable state of oxygen along with oxygen in the many hydroxyl groups. Following the Gabriel synthesis and nanoparticle coupling the intensity of the oxygen peak was noticeably reduced since the primary amine and nanoparticle partially masked the oxygen in the polyHEMA chains (only LD is shown).

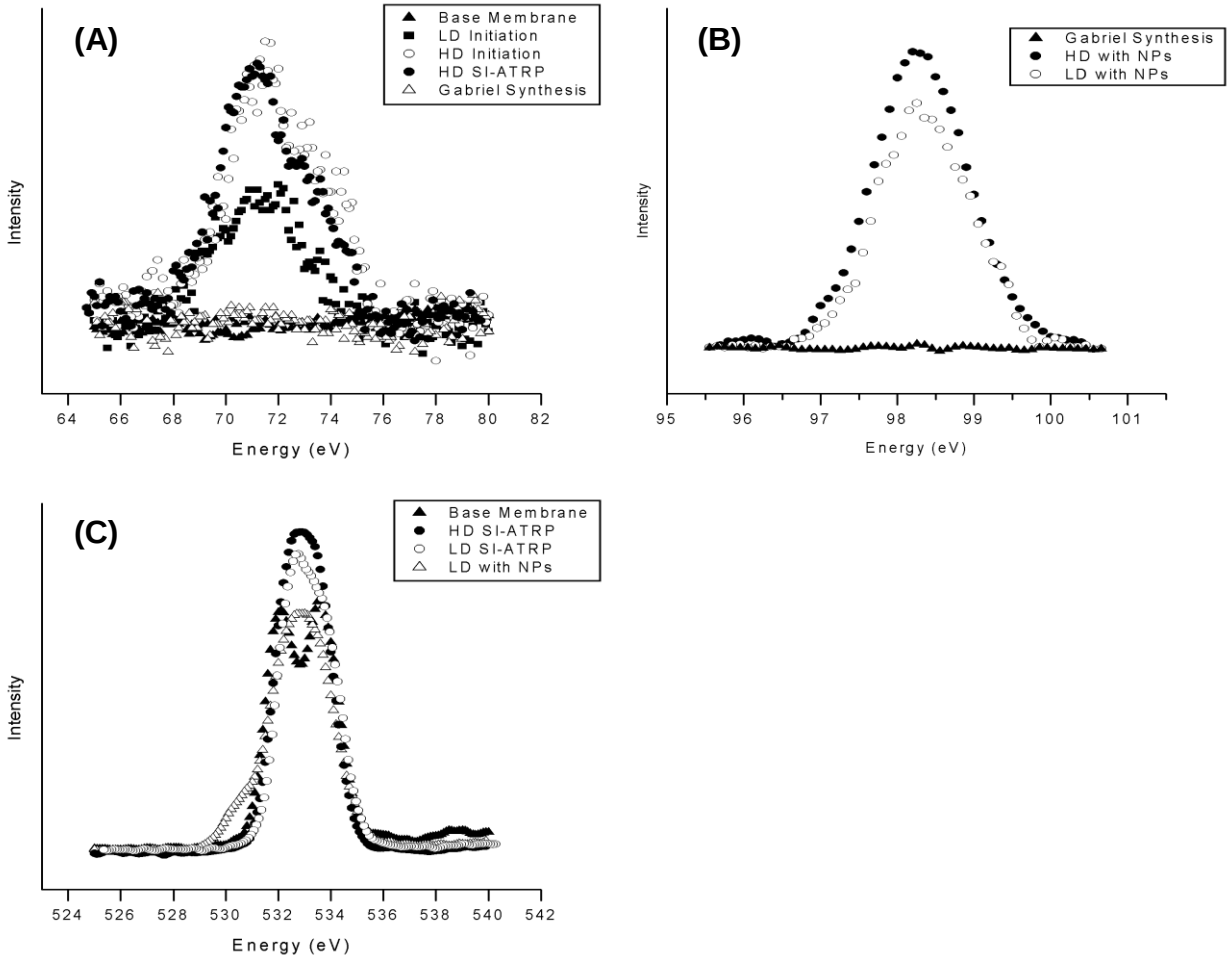

Figure 3.4. High resolution XPS spectra for bromine (A), iron (B), and oxygen (C) regions. Data for LD membranes after SI-ATRP in the bromine region and HD membranes after nanoparticle attachment in the oxygen region were excluded for ease of reading.

Figure 3.5 shows the effect of pH on zeta potential and diameter of the iron oxide nanoparticles freely dispersed in water. They had a consistent average diameter of roughly 25 nm above pH 3.8, confirming the 15 nm iron oxide core with a roughly 5 nm carboxylic acid shell as described by the manufacturer; however, the nanoparticles rapidly aggregated below pH 3.5 due to neutralization of the surface charges on the nanoparticles; thus all modification protocols and applications of the membranes remained at pH values greater than 4 to prevent aggregation. Secondly, Figure 3.5 shows that at pH values greater than 6 the nanoparticles were strongly negatively charged. The absolute zeta potential decreased with decreasing pH. This is explained by the carboxylic acid coating of the nanoparticles, which can become deprotonated (negative charge) at more alkaline conditions and protonated (neutral) in more acidic conditions.

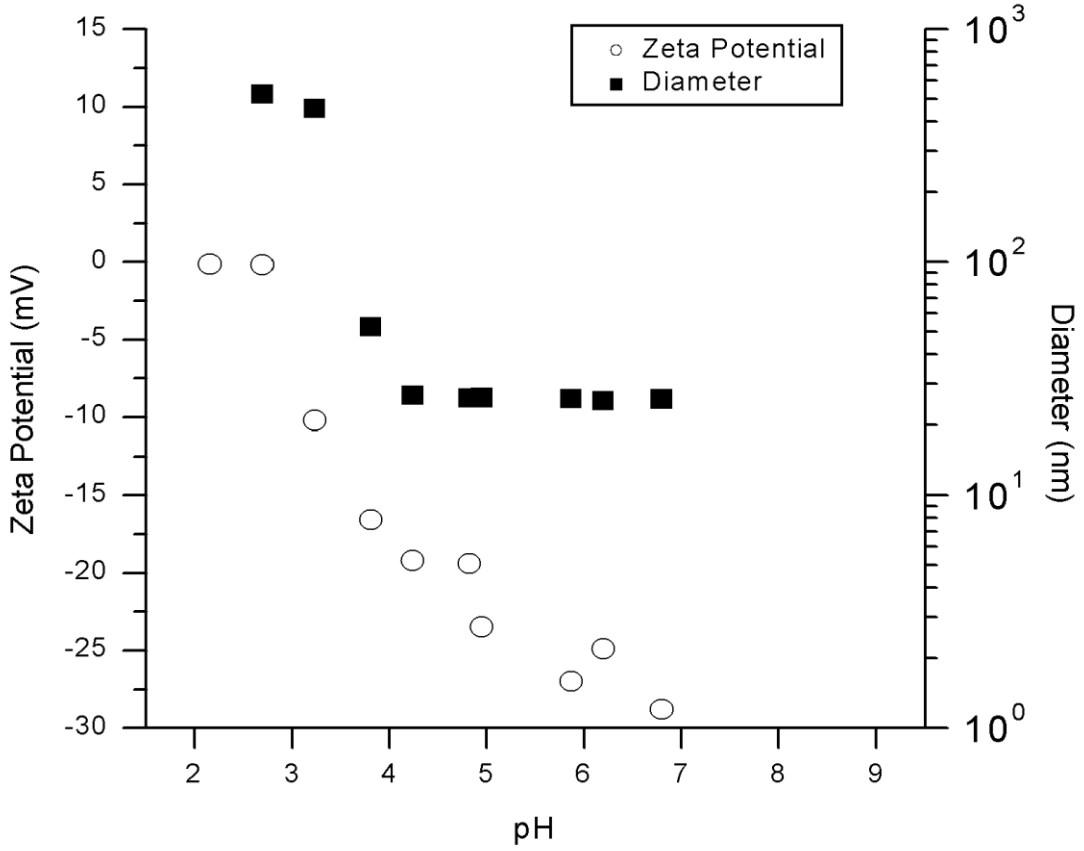

Figure 3.5. Average zeta potential and average diameter of the free nanoparticles dispersed in water as a function of pH. The size of the data points represents the measurement uncertainty.

Figure 3.6 shows the effect of pH on the zeta potential of the membrane surface at various stages of modification. The unmodified PET membrane was strongly negative above pH 6. As the pH decreased the zeta potential decreased linearly until pH roughly 5 before it became slightly positive between pH 3 and 4. The amine-capped chains following the Gabriel synthesis lead to a less negative potential which became positive around pH 4.5, matching well with known behavior for amines. Finally, the coupling of the nanoparticles to the end of the grafted chains decreased the zeta potential slightly again, agreeing with behavior for the freely dispersed particles (cf. Figure 3.5).

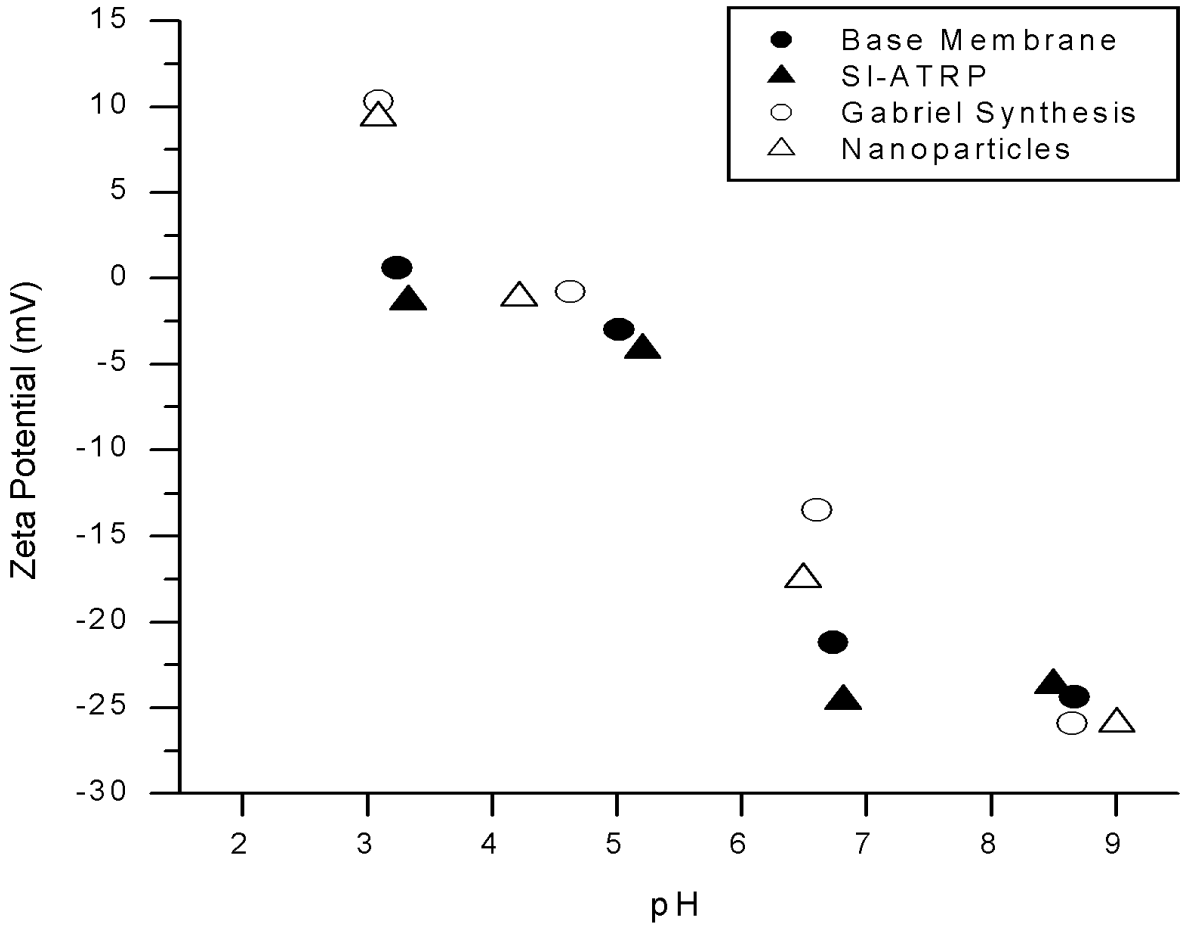

Figure 3.6. Zeta potential vs. pH after various steps in the modification procedure. The size of the data points represents the measurement uncertainty.

FESEM was performed on samples of the membranes at various stages during modification. The three images in Figure 3.7 are cross-sections of the membranes at 35,000x magnification. The highly cylindrical pores and smooth interior surface of the PET 400 membranes can be seen in Figure 3.7 (a). The apparent roughness of the membrane is noticeably increased following polyHEMA SI-ATRP, see Figure 3.7 (b). This is because the polymer chains in the dry state agglomerated on the pore wall making it appear rougher. No discernible difference was seen between LD and HD membranes at this stage. Finally, an HD membrane was imaged to observe the numerous nanoparticles present following coupling, see Figure 3.7 (c). The nanoparticles covered large areas of the pore walls. LD membranes had a similar appearance; however, they did not have as many nanoparticles present. Based on the scale bar, the size of the nanoparticles is roughly 25 nm, which agrees with manufacturer data, previous study[5], and the DLS data shown in Figure 3.5. The inset image in Figure 3.7 (c) is a higher (100,000x) magnification view of an area of the same membrane to better visualize the nanoparticles.

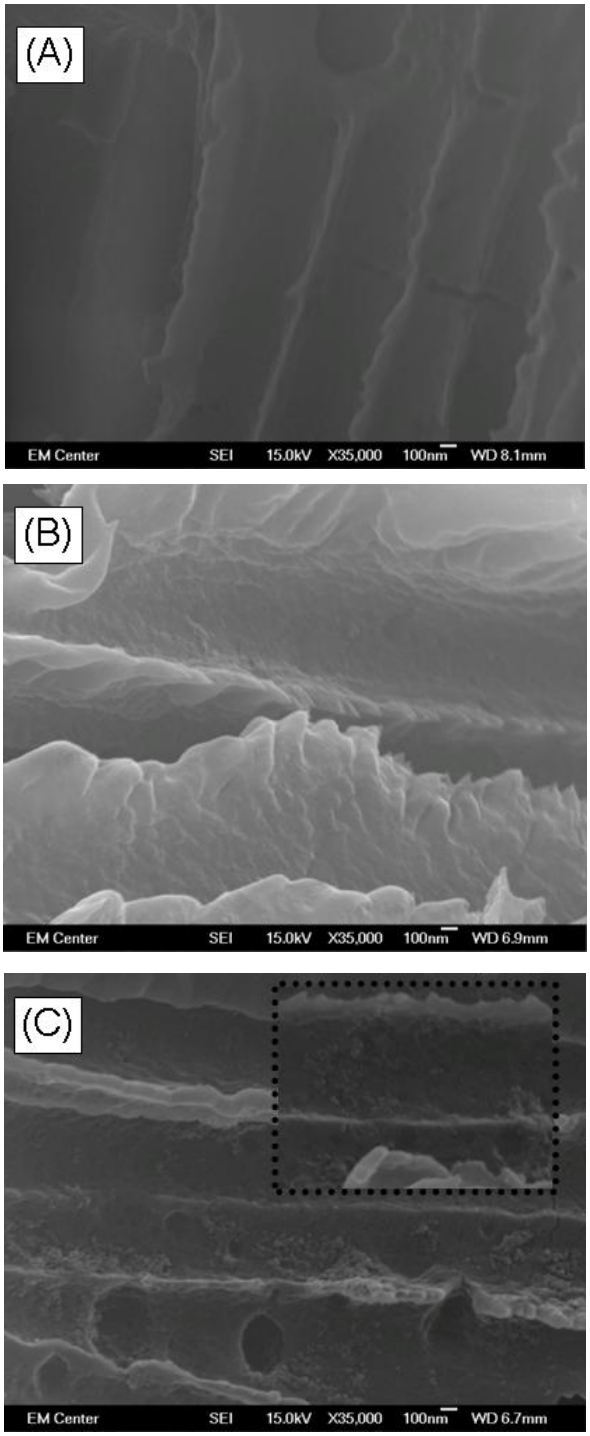

Figure 3.7. FESEM images (35,000x magnification) of membrane cross-sections for various stages in the modification procedure. (A) Unmodified PET 400 membranes as received from the manufacturer. (B) HD membrane following SI-ATRP grafting of polyHEMA. (C) HD membrane following nanoparticle coupling to the end of the polyHEMA chains. Inset image is 100,000x magnification of a section of image (C).

3.3.2. Effect of Modification on Average Pore Diameter

Eight successfully modified membranes for each high and low grafting density were used to determine the effect of modification and an external magnetic field on pore diameter and permeability. Figure 3.8 presents the average pore diameter of the dry membranes following each modification step for the HD and LD membranes, measured using gas flow / pore dewetting permporometry. Because the polyHEMA chains grew within the membrane pores, longer SI-ATRP time lead to a greater decrease in membrane pore diameter. The HD membranes showed a greater decrease in pore diameter due to the increased density of polyHEMA chains, i.e., a thicker grafted layer, for the same polymerization time (chain length). The pore diameter decreased again following the nanoparticle coupling.

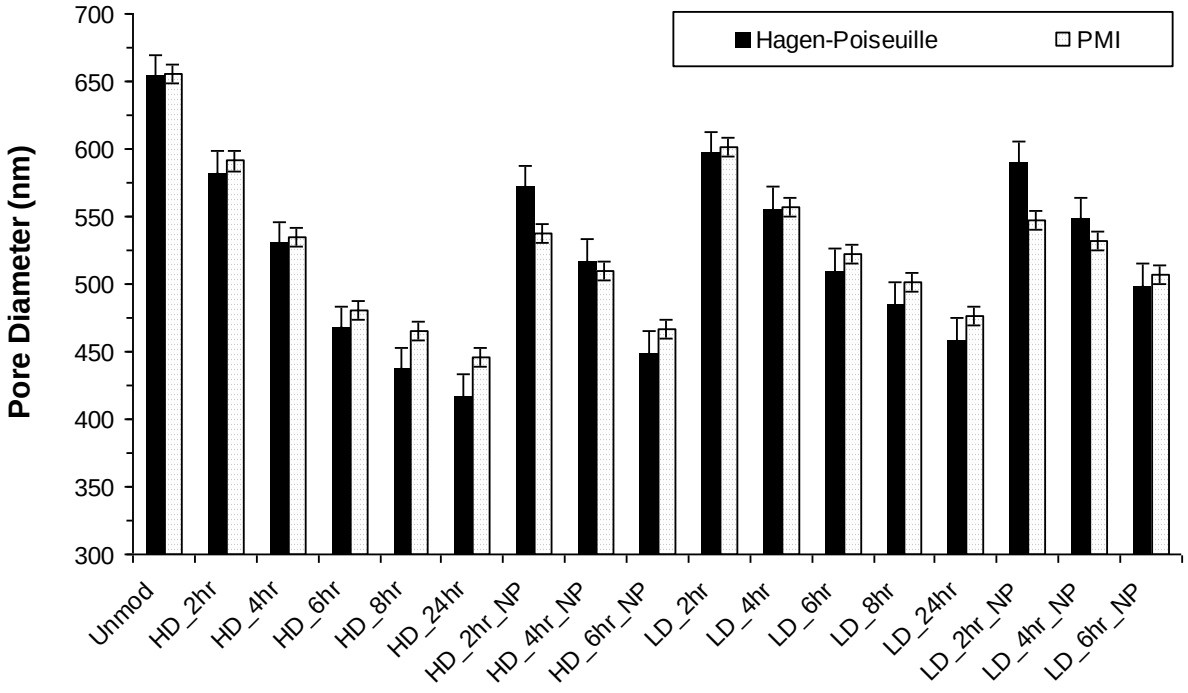

Figure 3.8. Average pore diameter measured using the Hagen-Poiseuille (HP) equation in the wet state and permporometry (PMI) in the dry state. Error bars represent one standard deviation.

The average pore diameter was then estimated by performing membrane filtration experiments with purified water. By combining the measured membrane permeability with the Hagen-Poiseuille equation (Eq. 3.2), the average pore diameter of the wetted membrane, also shown in Figure 3.8, was calculated. It is assumed that no liquid flows within the polyHEMA nanolayer; the decrease in pore radius relative to the unmodified membrane is discussed as hydrodynamic layer thickness on the pore wall. As with the permporometry data, the pore diameters decreased with increasing ATRP reaction time, with the HD membranes again having a greater decrease for the same reaction time. The difference in values obtained from the two pore diameter methods can be attributed to the swelling of the grafted polyHEMA layer in the presence of water, similar to results for capillary pore membranes with other grafted hydrophilic polymers[9-11]. The pore diameter decrease compared to the dry state data is more pronounced with increasing SI-ATRP time since the longer polyHEMA chains occupy more space when fully hydrated. Following nanoparticle coupling, the calculated pore diameter decreased slightly, in agreement with the permporometry data.

3.3.3. Effect of Magnetic Field on Membrane Performance

The average permeability through the membrane following HD and LD modification at different grafting times under different magnetic field conditions is presented in Figure 3.9. The modification procedure caused a decrease in membrane permeability due to the additional hydrodynamic resistance of the grafted polyHEMA layer. Permeability decreased with increasing SI-ATRP time (longer polyHEMA chains) and grafting density as expected. The hydrodynamic pore diameters discussed in section 3.3.2 (cf. Figure 3.8) were calculated using these “No Field” permeability data. Permeability was also measured in static and dynamic

magnetic fields in two orientations, see Figure 3.2. These are defined relative to the membrane surface: parallel/horizontal to the membrane surface and tangential/vertical to the membrane surface, respectively. The presence of a horizontal magnetic field leads to a slightly greater decrease in membrane permeability for all the membranes tested than those in the presence of a vertical field. This is due to increased hydrodynamic resistance of the extended polyHEMA chains, described in detail below. The measured permeabilities in a dynamic field were similar, but almost always slightly higher than those in a static field. Our previous work[5] showed that in an alternating field, the movement of the chains as they align with the changing field disrupted the liquid boundary layer directly above the membrane surface—via mixing generated by the moving chains—leading to a slightly higher permeability for the dynamic fields.

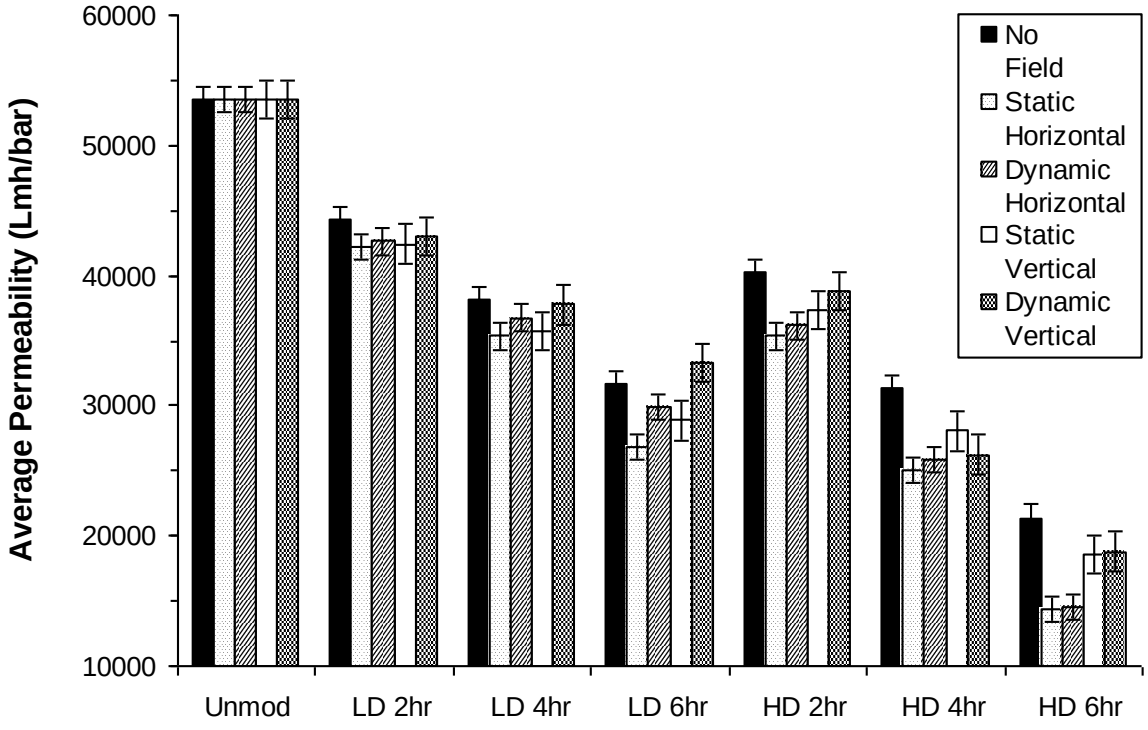

Figure 3.9. Average membrane water permeability in the presence of both static and dynamic magnetic fields, both horizontal and vertical relative to the membrane plane. Error bars represent one standard deviation.

More important is how quickly the membrane responded to the application of a field and the reversibility of this change. The permeability as a function of time in the presence and absence of static magnetic fields is shown in Figure 3.10. The permeability of unmodified membranes, roughly 54,000 Lmh/bar, is not shown since no magnetic field effect was seen for unmodified membranes. Permeability was measured for five minutes with no field present, then five minutes in a horizontal field, and finally five minutes in a vertical field. This cycle was then repeated. The magnetic field in both orientations lowered the permeability as expected; however, what is critical is that the permeability for each field orientation was the same for the two cycles. Furthermore, after the magnetic field is removed the permeability returned to its former value. This means the response was reversible, a key feature if these membranes are to be used as stimuli-responsive membranes. The response appeared to be slightly quicker for the shorter polyHEMA chains; steric hindrance of the longer chains might slow the magnetic response somewhat.

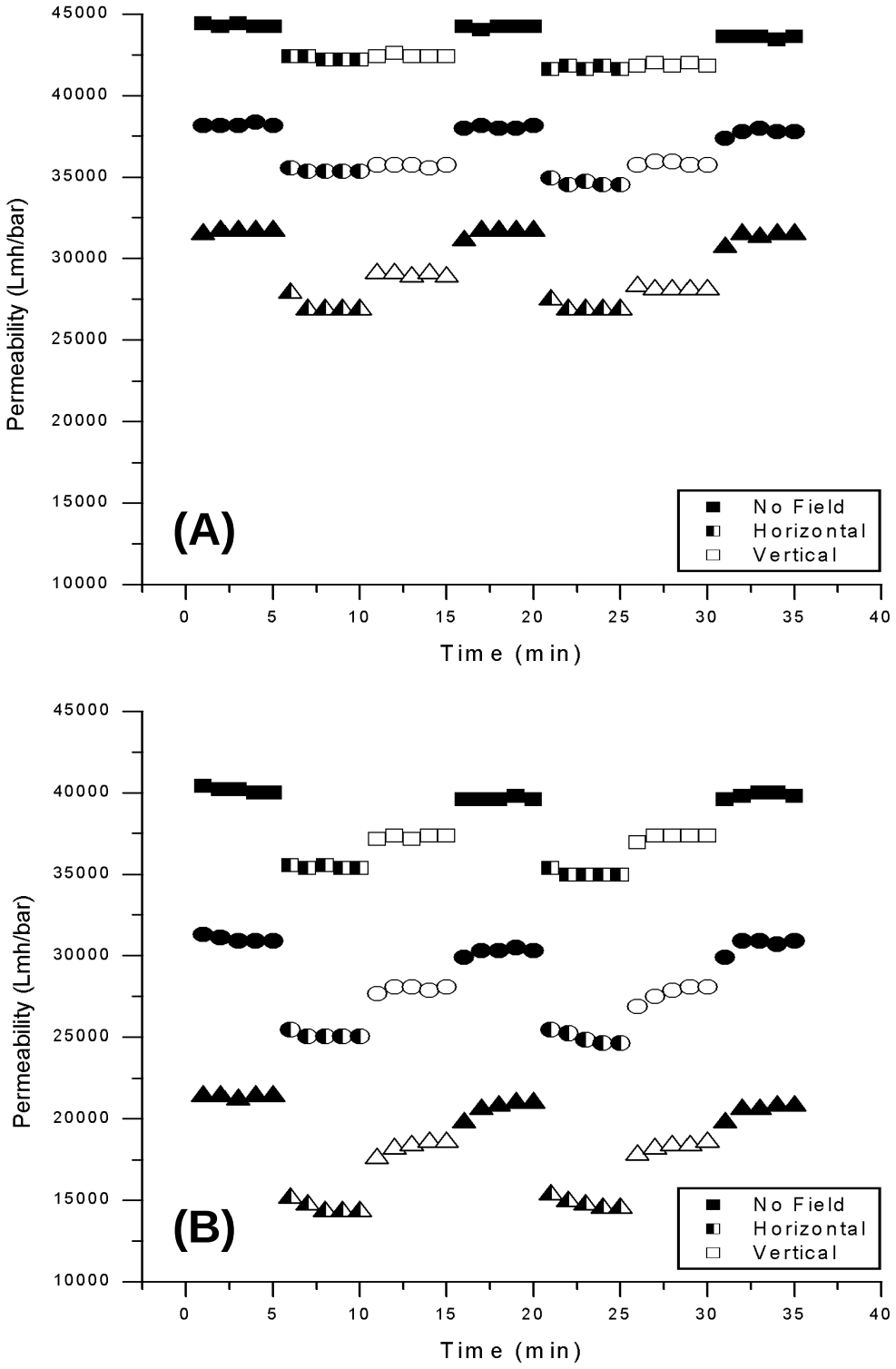

Figure 3.10. Variation in water permeability due to application of different static magnetic fields for LD (A) and HD (B) membranes, prepared by 2 (■), 4 (●), and 6 hours (▲) SI-ATRP. Permeability of unmodified membranes was constant at roughly 54,000 Lmh/bar; magnetic field application had no effect. The size of the data points represent measurement uncertainty.

3.3.4. Description of Magnetic Response

The decrease in water permeability for the modified membranes in the presence of a magnetic field can be explained by the hydrodynamic resistance associated with the physical conformation of the polyHEMA chains, conceptually illustrated in Figure 3.11. The leftmost image shows the chains when fully hydrated. Since polyHEMA is fairly hydrophilic, the chains are free to occupy space in the most favorable (lowest energy) conformation. The grafted polyHEMA chains for both LD and HD will be in the "mushroom" regime; that is, the lowest energy state will be a random coil; however, for the HD modification the chains will be slightly stretched random coils due to steric hindrance from neighboring chains[18-20], image (b). Superparamagnetic Fe_3O_4 nanoparticles have magnetic moments randomly oriented in the absence of an external field due to thermal excitation. However, in the presence of an external magnetic field, the magnetic moment of a nanoparticle will align with the applied field to minimize its energy. This alignment is achieved either by flipping the magnetic moment without physical rotation (Néel mechanism), or by rotating the particle physically (Brownian mechanism)[5,21]. In addition, this setup with two solenoids on either side of the membrane cell will create a magnetic field gradient across the membrane. In a non-uniform magnetic field, the magnetic nanoparticles will move in the direction of the gradient. The magnetic force exerted on the nanoparticle is proportional to the magnetic moment and the magnitude of the gradient with $F = \mu \nabla B$, where μ is the magnetic moment and ∇B is the gradient. This magnetic force and the subsequent movement of the nanoparticles attached to the polyHEMA chain ends will alter the conformation of the polymer chains.

The direction of the gradient produced by the twin solenoid apparatus in the horizontal and vertical configuration is not necessarily strictly horizontal or vertical with respect to all the

locations on membrane. This is particularly true towards either side of the solenoids; however, for this explanation, the fields will be assumed to be exactly horizontal and vertical. For a membrane pore surface modified with polyHEMA chains and coupled nanoparticles, all of the nanoparticles inside a pore will experience a force in the presence of a magnetic field. When applying a *horizontal* field (image (c)), with the gradient from left to right, polyHEMA chains on the left side of the pore will be stretched towards the center of the pore structure. On the other hand, polyHEMA chains on the right will move toward the pore wall causing polyHEMA structures to be more condensed. Since polyHEMA chains will encounter more resistance upon condensing due to steric hindrance, the effective pore size will be decreased. This will cause the permeability to decrease. When applying a *vertical* field (image (d)), the nanoparticles attached to the polymer chain ends will move in the direction of the gradient, and the polymer coils will be deformed in the vertical direction, possibly forcing the unfolding of some segments. Because this deformation is just slightly expanding the condensed coil conformation, a smaller decrease in permeability is observed compared to the horizontal field.

When the field is removed, the chains return to the most favorable (lowest energy) position, reducing the resistance to flow within the pore, image (b). The fact that the changes are smallest for alternating fields could be caused by the rate of polymer relaxation. On the other hand, it has recently been shown for a different responsive polymer (poly-N-isopropylacrylamide) that the change of swelling (response to temperature) of a layer of about 100 nm is in the range of milliseconds[22]. In order to clarify that point, the influence of frequency should be studied; this has not been done here because the overall effects were relatively small. Since the response is both significant and reversible, see Figure 3.10, these membranes could be used as stimuli-responsive filtration membranes.

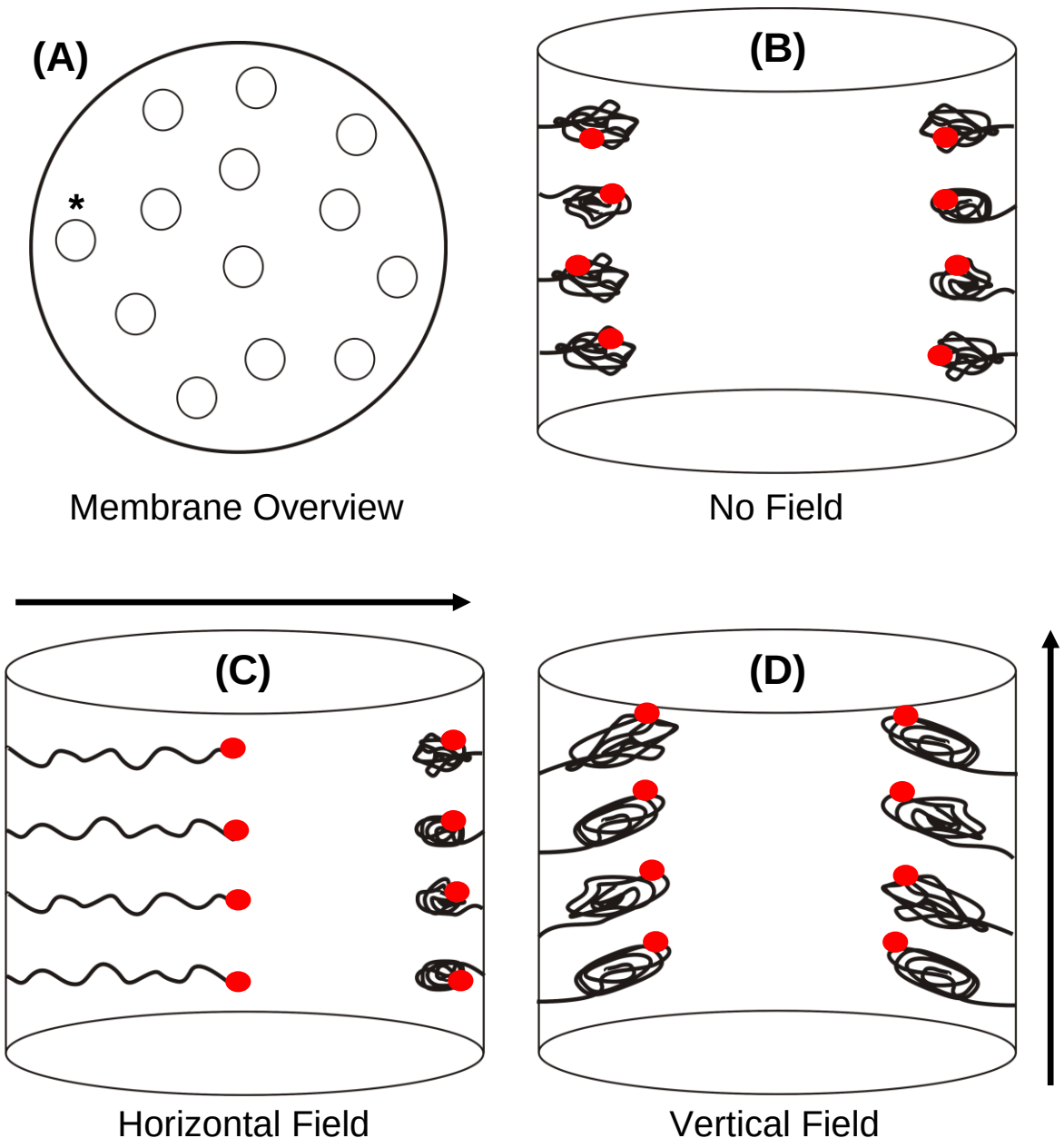

Figure 3.11. (A) A top-down view of the membrane surface with multiple pores. The response of the polyHEMA chains within the pores will vary based on the physical location of the pore. The inside of the starred pore is shown as one example. (B) The grafted polyHEMA chains are relaxed coils in the most favorable position when no field is present. (C) In a horizontal field pointing right the chains on the left side of the pore will extend towards the middle of the pore while those on the right side will contract. (D) In a vertical field pointing up the coils will extend vertically and some chain segments will probably be forced to unfold thus leading to an overall more expanded conformation compared to (B).

To quantify the degree of pore diameter change, the Hagen-Poiseuille equation (Eq. 3.2) was used to calculate the pore diameter of the wetted membranes in the presence of various magnetic fields. The average absolute decrease of pore diameter in nm and the actual calculated pore diameter for the modified membranes with no field present are shown in Table 3.1. The longer polyHEMA chains and higher grafting density (HD) impart a greater hydrodynamic resistance when extended, resulting in a greater pore diameter decrease than the LD membranes. Pore diameter decreased in both horizontal and vertical magnetic fields; however, the decrease is less drastic for vertical fields, as described above. Additionally, the slightly higher permeabilities of the dynamic fields compared to the static fields, see Figure 3.9, lead to smaller decrease in pore diameter, and even an increase in calculated pore diameter for the dynamic fields used with the LD membranes. These changes in pore diameter correspond to relative changes of up to 6% compared to when no field is present. However, for the membrane with the greatest degree of grafting and largest magnetic response, the grafted layer thickness in swollen state is 67 nm (for HD 4hr) and 100 nm (for HD 6hr)—as calculated using the hydrodynamic pore diameter of the unmodified membrane, roughly 650 nm. These layers can, on average, be "stretched" by the applied magnetic field by 12-13 nm. This corresponds to a maximum of 18% (for HD 4hr). This is remarkable and has implications toward other potential applications.

Our results indicate the unique versatility of magnetically-responsive polymer nanostructures to control membrane pore size without changing the conditions of the feed stream. The reversible response of these magnetically-responsive nanostructures could be used to selectively switch the pore size of filtration membranes. In addition, as shown in our previous work[5], in an oscillating magnetic field, these responsive polymer chains could suppress deposition of solute species on the membrane pore walls. Numerous other possible applications

exist. One could imagine "fluid steering" in microfluidic chips analogous to the work of Pappas and Holland[23] using thermally responsive phospholipids. However an advantage of our system is that all changes in resistance to flow down a given channel will be created by an external magnetic field.

Table 3.1. Average absolute decrease of membrane pore size calculated using the Hagen-Poiseuille equation. The pore diameter of the modified membranes with no field present is given as well. The negative numbers indicate an increase in calculated pore diameter corresponding to the increase in membrane permeability observed for the dynamic fields used with the LD membranes.

	Actual Pore Diameter (nm)	Pore Diameter Decrease (nm)			
	No Field	**Static Horizontal**	**Static Vertical**	**Dynamic Horizontal**	**Dynamic Vertical**
LD 2hr	590 ± 2	1 ± 1	2 ± 1	-1 ± 1	-1 ± 1
LD 4hr	548 ± 3	2 ± 1	2 ± 1	0 ± 1	-5 ± 1
LD 6hr	499 ± 5	2 ± 1	2 ± 1	-7 ± 2	-9 ± 1
	No Field	**Static Horizontal**	**Static Vertical**	**Dynamic Horizontal**	**Dynamic Vertical**
HD 2hr	572 ± 2	21 ± 1	15 ± 1	16 ± 1	9 ± 1
HD 4hr	517 ± 5	24 ± 1	12 ± 1	14 ± 1	7 ± 1
HD 6hr	449 ± 8	26 ± 2	11 ± 1	26 ± 2	7 ± 2

A few possibilities exist for increasing the magnitude of pore diameter change. SI-ATRP reaction time could be increased to maximize magnetic response. A stronger magnetic field could also be used to achieve a larger response. Additionally, applying this modification method to membranes of smaller pore diameter would yield an increased absolute change in pore diameter, and this would immediately be of interest with respect to remote control of membrane size selectivity. Hence, the membranes presented here are a versatile model system and can be tailored to give a higher magnitude of response based upon the needs of the chosen application.

3.4. CONCLUSIONS

Track-etched PET membranes were used to characterize the modification and magnetic response of magnetically-responsive filtration membranes. Permporometry and hydraulic

permeability measurements yielded effective pore diameters in both the dry and wet states. XPS, FESEM, and zeta potential characterized the membrane surface at various stages during the modification. The response of the superparamagnetic nanoparticles tethered to grafted polyHEMA chains in various magnetic field orientations showed that effective membrane pore size under filtration conditions can be changed via a "remote control" mechanism. This response is quick and reversible. The forced extension of the polyHEMA chains into the pore flow channel during application of a magnetic field introduces additional hydrodynamic resistance to fluid flow which decreases the effective pore diameter and by extension the permeability through the membrane. This decrease in membrane permeability is greater for horizontal fields. Longer chains (longer SI-ATRP times) and denser grafting (HD modification) yielded a greater decrease in permeability and pore size in a magnetic field due to the greater contributions to hydrodynamic resistance. Membranes responsive to an external magnetic field could have numerous potential applications since the pore diameter (and thus separation ability) of the membranes can be altered rapidly and at any time. Moreover, the model system presented here for altering the effective thickness of grafted polymer layers on a surface by an external magnetic field could also be used for exploring other applications, for instance in microfluidic systems.

REFERENCES

1. D. Wandera, S.R. Wickramasinghe, S.M. Husson, Stimuli-responsive membranes, J. Mem. Sci. 357 (2010) 6-35.
2. M. A. Stuart, W. T. Huck, J. Genzer, M. Müller, C. Ober, M. Stamm, G. B. Sukhorukov, I. Szleifer, V. V. Tsukruk, M. Urban, F. Winnik, S. Zauscher, I. Luzinov, S. Minko, Emerging applications of stimuli-responsive polymer materials. Nat. Mat. 9 (2010) 101-113.
3. D. M. He, H. Susanto, M. Ulbricht, Photo-irradiation for preparation, modification and stimulation of polymeric membranes. Prog. Polym. Sci. 34 (2009) 62-98.
4. K. Vanherck, S. Hermans, T. Verbiest, I. Vankelecom, Using the photothermal effect to improve membrane separations via localized heating. J. Mat. Chem. 21 (2011) 6079-6087.
5. H. H. Himstedt, Q. Yang, L. P. Dasi, X. Qian, S. R. Wickramasinghe, M. Ulbricht, Magnetically-Activated Micromixers for Separation Membranes. Langmuir. 27 (2011) 5574-5581.
6. C. Geismann, M. Ulbricht, Photoreactive functionalization of poly(ethylene terephthalate) track-etched pore surfaces with "smart" polymer systems. Macromol. Chem. Phys. 206 (2005) 268–281.
7. C. Geismann, A. Yaroshchuk, M. Ulbricht, Permeability and electrokinetic characterization of poly(ethylene terephthalate) capillary pore membranes with grafted temperature-responsive polymers. Langmuir. 23 (2007) 76–83.
8. A. Friebe, M. Ulbricht, Cylindrical pores responding to two different stimuli via surface-initiated atom transfer radical polymerization for synthesis of grafted diblock copolymers. Macromolecules. 42 (2009) 1838–1848.
9. A. Friebe, M. Ulbricht, Controlled pore functionalization of poly(ethylene terephthalate) track etched membranes via surface-initiated atom transfer radical polymerization. Langmuir. 23 (2007) 10316–10322.
10. Q. Yang, M. Ulbricht, Cylindrical membrane pores with well-defined grafted linear and comb-like glycopolymer layers for lectin binding. Macromolecules. 44 (2011) 1303-1310.
11. F. Tomicki, D. Krix, H. Nienhaus, M. Ulbricht, Stimuli-responsive track-etched membranes via surface-initiated controlled radical polymerization: Influence of grafting density and pore size. J. Mem. Sci. 377 (2011) 124-133.
12. K. Matyjaszewski, J. Xia, Atom Transfer Radical Polymerization. Chem. Rev. 101 (2001) 2921-2990.
13. V. Coessens, T. Pintauer, K. Matyjaszewski, Functional polymers by atom transfer radical polymerization. Prog. Polym. Sci. 26 (2001) 337-377.
14. S. Gabriel, Über eine Darstellung primärer Amine aus den entsprechenden Halogenverbindungen. Berichte der Deutschen Chemischen Gemeinschaft zu Berlin. A20 (1887) 2224-2240.
15. M. S. Gibson, R. W. Bradshaw, The Gabriel Synthesis of Primary Amines. Angew. Chem., Int. Ed. 7 (1968) 919-930.
16. C. Lettmann, D. Möckel, E. Staude, Permeation and Tangential Flow Zeta potential Measurements for Electrokinetic Characterization of Track-etched Microfiltration Membranes. J. Mem. Sci. 159 (1999) 243-251.
17. K. Rodemann, E. Staude. Electrokinetic Characterization of Porous Membranes made from Epoxidized Polysulfone. J. Mem. Sci. 104 (1995) 147-155.

18. P. G. de Gennes, Conformations of Polymers Attached to an Interface. Macromolecules. 13 (1980) 1069-1075.
19. S. T. Milner, Polymer Brushes. Science. 251 (1991) 905-914
20. G. Liu, L. Yan, X. Chen, G. Zhang, Study of the kinetics of mushroom-to-brush transition of charged polymer chains. Polymer. 47(2006) 3157-3163.
21. R. Kötitz, W. Weitschies, L. Trahms, W. Semmler, Investigation of Brownian and Néel Relaxation in magnetic fluids. J. Magn. Magn. Mat. 201 (1999) 102-104.
22. C. A. Naini, S. Franzka, S. Frost, M. Ulbricht, N. Hartmann, Probing the intrinsic switching kinetics of ultrathin thermo-responsive polymer brushes. Angew. Chem., Int. Ed. 50 (2011) 4513-4516.
23. T. J. Pappas, L. A. Holland. Fluid steering in a microfluidic chip by means of thermally responsive phospholipids. Sensor. Actuat. B-Chem. 128 (2008) 427-434.

CHAPTER 4

DESIGNING MAGNETIC FIELD RESPONSIVE NANOFILTRATION MEMBRANES

The effect of polyHEMA grafting density and chain length on magnetically-activated mixing is characterized. Higher grafting density yielded larger effects on membrane flux and rejection.

Drs. Yang and Wickramasinghe developed the protocol to reduce the polyHEMA grafting degree and modified all of the membranes tested. I performed the filtration tests to study the effect of grafting degree and density on salt rejection and membrane flux. I also performed XPS on the membrane samples to characterize the membrane modification.

Summary

Thin film composite, nanofiltration membranes have been modified using surface initiated atom transfer radical polymerization to graft poly(2-hydroxyethyl methacrylate) (polyHEMA) chains from the surface of the membrane. A modified Gabriel synthesis procedure was used to attach superparamagnetic (Fe_3O_4) nanoparticles to the chain ends. Chain density and chain length were independently varied by adjusting the initiator density and polymerization time. Membranes were characterized using scanning electron microscopy, X-ray photoelectron spectroscopy and contact angle measurements.

The performance of modified membranes was investigated by determining deionized water fluxes as well as fluxes and salt rejection for aqueous feed streams containing 500 ppm $CaCl_2$ and 2000 ppm $MgSO_4$. All experiments were conducted in dead end mode. Modified membranes display a reduced flux and increased salt rejection compared to unmodified membranes. Since both grafted chain density and chain length are expected to affect membrane performance differently, the decrease in permeate flux and increase in salt rejection is not directly proportional to the increase in grafted polymer molecular weight. Modified membranes do, however, display increased flux and increased salt rejection in the presence of an oscillating magnetic field compared to their performance when no field is present. Magnetically-responsive membranes could represent a new class of fouling resistant membranes.

Experiments were performed at both the Universität Duiβburg-Essen (Essen, Germany) and Colorado State University (Fort Collins, USA). Financial support was provided by the Strategic Environmental Research and Development Program WP-1670 (USA), a DoD NDSEG graduate fellowship (USA), NSF CBET 1066505 (USA), and the DFG Mercator Fellows Program INST 20876/119-1 (Germany).

4.1. INTRODUCTION

Membrane separation processes offer numerous advantages over competing technologies for water treatment applications. Pressure driven membrane filtration processes such as reverse osmosis (RO) and nanofiltration (NF) are widely applicable across a range of feeds. The membrane is a barrier for rejected components, thus the variation in feed water quality will have a minimal impact on permeate quality. Generally, no addition of environmentally harmful chemicals is required. Membranes can be used in-process to allow recycling of selected waste streams. Perhaps most importantly, membrane equipment has a smaller footprint, and energy costs are often significantly lower.

Water is a very valuable natural resource[1]. Development of new water treatment technologies is of tremendous societal importance all around the world. This work focuses on nanofiltration membranes. Nanofiltration, which originated in the 1970s, is one of the newest pressure driven membrane filtration processes[2]. Characteristics of nanofiltration membranes include greater than 99% rejection of multivalent ions, 0-70% rejection of monovalent ions and greater than 90% rejection of small organic compounds with molecular weights greater than 300 g/mol[1-6]. Initial applications of nanofiltration membranes focused on water softening[3]; however, today nanofiltration membranes find numerous uses in the areas of water treatment (e.g. removal of organics[4], pesticides[5], and pharmaceutically active compounds[6]) as well as other areas such as the dairy industry[7] and non-aqueous applications[8].

Since NF membranes operate at lower pressures and display higher fluxes than RO membranes and, consequently, require less energy, they are very attractive for treating wastewaters for beneficial uses such as livestock watering, crop irrigation, etc. However, higher

fluxes combined with exposure to feed waters containing significant amounts of suspended colloids means that membrane fouling is a major concern[9].

Membrane fouling is a major problem in numerous membrane separation processes of aqueous feed streams[10-16]. During filtration, membrane performance is compromised by the formation of a concentration polarization boundary layer consisting of rejected species at the membrane surface[17, 18]. This boundary layer provides an additional resistance to permeate flow. Further, since the concentration of rejected species is higher in the boundary layer than the bulk feed, the apparent rejection coefficient of retained species is lower. The concentration boundary layer is totally reversible. In the absence of permeate flow, the concentration boundary layer quickly dissipates. In addition, concentration polarization can lead to deposition of rejected species on the membrane surface leading to reversible as well as irreversible fouling.

Given the detrimental impact concentration polarization and fouling have on membrane performance, numerous studies have focused on minimizing concentration polarization and fouling. Three approaches have been considered: physical, chemical (surface modification of the membrane) and hydrodynamic[19]. Physical methods involve modification of the feed properties (e.g. flocculation[18], addition of seed particles) in order to suppress deposition of small highly fouling particulate matter on the membrane surface. The use of electric fields to move charged species away from the membrane surface has also been investigated[20].

Chemical methods involve changing the properties of the membrane and in particular the membrane surface that is in contact with the feed stream in order to suppress attractive interactions between rejected species in the feed and the membrane surface. Numerous methods have been investigated[21-23]. Hydrodynamic methods on the other hand, involve modifying the flow path of the fluid next to the membrane surface in order to induce mixing (usually at low

Reynolds number) in order to suppress concentration polarization. Hydrodynamic methods include the use of spacers and inserts in the flow channel[24,25], pulsation[26] and the creation of Dean vortices by using curved flow channels[27].

Stimuli-responsive membranes have been developed for many applications, perhaps some of the original being for controlled release of drugs[28]. Stimuli-responsive membranes change their physical properties in response to changes in environmental conditions such as pH, ionic strength, temperature or to changes due to photo irradiation or electric and magnetic fields[29]. Changes in the physical properties of the membrane in response to changed environmental conditions can be used to modulate membrane performance. More recently several studies have indicated that grafting stimuli-responsive nanobrushes to the surface of nanofiltration and ultrafiltration membranes can lead to enhanced performance and in particular suppression of fouling for water treatment applications[30-36].

In our previous work we proposed a radically new method of suppressing fouling during nanofiltration[37]. We developed responsive nanofiltration membranes by grafting hydrophilic poly(2-hydroxyethyl methacrylate) (polyHEMA) chains from the surface of a thin film composite nanofiltration membrane. Superparamagnetic nanoparticles were then attached to the chain ends to create a magnetically-responsive nanolayer. In an oscillating magnetic field the chains oscillate as they align with the direction of the field.

These magnetic field responsive membranes are unique for a number of reasons. Chemical modification of the membrane surface imparts fouling resistance. Movement of the magnetically-responsive nanobrushes leads to mixing at low Reynolds number at the membrane surface. Thus a hydrodynamic method is used to disrupt concentration polarization. Previous experimental and theoretical studies[38-43] show that mixing of the feed near the membrane surface

improves mass transfer by disrupting concentration polarization and reducing the rate of cake formation. By growing a magnetically-responsive nanolayer from the membrane surface mixing is induced at the membrane fluid interface thus maximizing the disruption of the concentration polarization boundary layer. Unlike many previous studies that depend on changes in the bulk feed (e.g. pH, temperature) to change the conformation of the responsive groups present, no such change is required as the grafted polymer brushes respond to an oscillating magnetic field.

Here we build upon our previous work[37]. Surface-initiated atom transfer radical polymerization (SI-ATRP) is used to graft polyHEMA chains from the surface of a commercially available thin film composite polyamide nanofiltration membrane. A modified Gabriel synthesis procedure is used to attach a superparamagnetic particle to the chain ends. The grafted chain density and chain length are changed independently by changing the concentration of active SI-ATRP initiator and polymerization time. Both variables will affect membrane performance. The results obtained here provide further evidence of the ability of these membranes to suppress concentration polarization and fouling and provide insights into further improvement of membrane performance.

4.2. EXPERIMENTAL

4.2.1. Materials

NF 270, flat-sheet, thin film, composite polyamide membranes were donated by Dow Filmtec (Edina, MN, USA). All membrane samples used in this study were cut from large sheets into circular specimens with a diameter of 25 mm. All membrane samples were washed with Milli-Q water before use to remove any protective coating layer that may be present. Iron oxide superparamagnetic nanoparticles with 15 nm core diameter and a 5 nm coating layer modified

with carboxylic acid groups, were purchased from Ocean Nanotech (Springdale, AR, USA). All of the following chemicals were obtained from Sigma Aldrich (St Louis, MO, USA). 2-Hydroxyethyl methacrylate (HEMA) was distilled under vacuum before use. Acetonitrile was purified by refluxing with boric anhydride and distillation before use. Copper (I) chloride (99.995+%) and copper (II) chloride (99.999%) were used without further purification. A-Bromoisobutyrl-bromide (BiB), propionyl bromide (PB), triethylamine (TEA), 2,2'-bipyridine (Bpy), N,N,N′,N″,N″-pentamethyl diethylenetriamine (PMDETA), potassium phthalimide salt (>99%), 4.(N′,N′-dimethylamino) pyridine (DMAP), hydrazine hydrate, hydrochloric acid (6 M), 1-ethyl-3-(3- dimethylaminopropyl)carbodiimide (EDC), N-hydroxysuccinimide (NHS), ethanol and methanol were used as received. The water used in all syntheses and measurements was from a Milli-Q system.

4.2.2. Initiator Immobilization

A reaction solution was prepared from 10 mL freshly dried acetonitrile containing DMAP (5 mM) and TEA (10 mM). NF 270 membrane samples were placed in small vials and 10 mL of the reaction solution was added to each vial. Then 100 μL BiB was added to each sample and the vial was sealed. After reaction for 2 h on a shaker at room temperature, membranes were removed and rinsed with acetonitrile and water/ethanol mixture solution (1:1, v/v), then dried in a vacuum oven at 40 ^{o}C overnight.

To decrease the initiator density on the membrane surface, a mixture (1:1, v/v) of BiB and PB was used in the initiator immobilization step. PB served as a non-initiating species to achieve diluted initiator concentration and, consequently, lower grafted polymer chain density.

4.2.3. SI ATRP of polyHEMA

Membrane samples with immobilized initiator were placed in Schlenck flasks equipped with rubber stoppers (one membrane sample per flask) and the flasks were sealed. The flasks were evacuated and back-filled with argon three times. Freshly distilled HEMA (2 M) and Bpy were dissolved in 1:1 (v/v) methanol/water mixture and purged with nitrogen for 30 min. Next, copper(I) chloride and copper(II) chloride were added to the solution with vigorous stirring under argon. The ratio between components in the ATRP reaction solution was [HEMA]/[CuCl]/[$CuCl_2$]/[Bpy] = 100:0.5:0.2:1.75. Thereafter the reaction solution was transferred into the Schlenck flasks (7 mL per flask) by a syringe and the reaction mixture was incubated at room temperature for a predetermined time. The following reaction times were investigated: 1, 2, 3, 4 and 24 hours. After SI-ATRP reaction, a 10 minute quenching procedure was used to stop the polymerization and to ensure that the polymer chain ends are terminated by an alkyl bromide. The membranes were quickly removed from the Schlenck flask and immersed in 50 mL 1:1 (v/v) methanol/water solution containing 250 mg copper (II) bromide and 625 μL PMDETA. A 1:1 (v/v) water/ethanol mixture was then used to clean the membranes. After drying in a vacuum oven at 40 ^{o}C overnight, the degree of grafting, DG (μg/cm^2), was calculated by following equation:

$$DG = \frac{W_1 - W_0}{A_m} \tag{4.1}$$

where W_0 is the mass of the unmodified membrane and W_1 is the mass of the membrane after modification and drying. A_m represents the area of the membrane (4.9 cm^2 in this study).

4.2.4. Gabriel Synthesis

To convert the alkyl bromide at the end of the polymer chains to a primary amine, a modified Gabriel synthesis similar to that of Monge *et al.*[44] was used[37]. 4.5 mL of saturated potassium phthalimide in ethanol solution was placed into a vial containing one membrane disc. The vials were sealed and placed on an incubator shaker at 40 ^{o}C for 6 h. After reaction, the membranes were rinsed twice with ethanol, then with a water/ethanol mixture, and finally with ethanol before being dried. The second step consisted of dissolving 7 mL of hydrazine hydrate into 25 mL of 6 M HCl. 4 mL of solution was placed into each vial containing a membrane disc. The vials were placed on an incubator shaker at 40 ^{o}C for 6 h. Upon completion of the reaction, the membrane samples were thoroughly washed with water/ethanol mixture to ensure no phthalimide precipitate remained. Membranes were dried under vacuum at 40 ^{o}C overnight.

4.2.5. Nanoparticle Coupling

Nanoparticles were attached to the membrane surface by reacting carboxyl groups on the nanoparticle surface to the primary amine at the polyHEMA chain ends via an amide linkage. For the coupling, a carbodiimide activated amide formation protocol was used. 31.2 mg of EDC and 38.7 mg of NHS were added to 10 mL of Milli-Q water and shaken vigorously on a vortex mixer. Next, 0.3 mL of carboxyl shell Fe_3O_4 nanoparticles in buffer solution (5 g/L) were added, but not agitated. 1.5 mL of this solution was then added to a glass vial containing a membrane disc. The concentration of nanoparticles was typically 0.015 g/L; however, 0.15 g/L (i.e. 10 fold higher concentration) was also used with membranes modified using 100 % active initiator and a 4 hour polymerization time. The vial was sealed and incubated in the dark for 4 h. Next, the membrane was removed, rinsed twice with water and then washed in a water/ethanol mixture. The membrane was finally dried in a vacuum oven overnight at 40 ^{o}C.

4.2.6. Surface Characterization

Field-emission scanning electron microscopy (FESEM) images were taken using a FEI/Philips Sirion FESEM (Hillsboro, OR, USA). Samples were coated with a 10 nm gold layer before SEM analysis.

X-ray photoelectron spectroscopy (XPS) of the membrane surface was conducted using a Physical Electron 5800 ultrahigh vacuum XPS-Auger spectrometer (Chanhassen, MN, USA) using a 45^{o} takeoff angle. Twenty high-resolution scans focusing on the carbon (282-292 eV), nitrogen (395-407 eV), oxygen (527-541 eV) and iron (705-730 eV) regions were averaged to observe changes during the sequential modification steps. All samples were measured sequentially under the same conditions (area analyzed and incidence angle).

Water contact angles were measured using an OCA20 contact angle system (Dataphysics, Filderstadt, Germany) at room temperature. The static contact angle was measured by the sessile drop method. First, a 5 µL water drop was lowered onto the membrane surface from a needle tip. Contact angles were calculated after 5 seconds using imaging software. Contact angles were measured at 7 different points on the membrane and an average value was used.

4.2.7. Membrane Performance

Each membrane was rinsed with Milli-Q water for 30 seconds per side and placed in an Amicon 8010 stirred filtration cell (EMD Millipore, Billerica, MA, USA). The cell was filled with a 1:1 (v/v) water/ethanol mixture. Pressurized nitrogen was used to supply force to flow the fluid through the membrane at 1.4 bar (20 psi) for 5 minutes. The membrane was removed, rinsed with water and then pre-compacted at 4.8 bar (70 psi) for 5 minutes with Milli-Q water. Finally, the membrane was taken from the cell and allowed to equilibrate in Milli-Q water for 2

hours. After this the membrane water flux was determined. The membrane was placed back in the stirred cell and feed solution (MilliQ or salt solution) were pumped through the membrane at 3.1 bar (45 psi). Filtration was conducted for 30 minutes, filtrate fractions were collected every 30 s. Flux values reported were averaged over a 5 min interval; thus, 6 values were obtained for each experimental run.

Membrane performance in an oscillating magnetic field was studied using a custom built system[37]. The stirred cell was placed between two stainless-steel core solenoids. A computer-operated programmable logic controller (PLC, Click Koya, Automation Direct, Cumming, GA, USA) controlled the rate at which the two solenoids receive power by alternatively activating two solid-state relays. This determined the frequency of the alternating magnetic field. The solenoids were powered by an Agilent Technologies (Santa Clara, CA, USA) 20 V, 25 A power supply. The solenoids were positioned on two opposite sides of the filtration cell so that the magnetic field direction was parallel to the topmost selective layer of the membrane and the frequency of the oscillating magnetic field was set at 10 Hz. Previous studies indicated that this arrangement yielded the greatest lateral movement of the end of the nanoparticle-capped polymer chains and thus the greatest mixing. Salt concentrations were measured with a conductivity meter (Oakton, model CON11, Cole Parmer, Vernon Hills, IL, USA). Salt rejection was calculated as:

$$(1-\frac{C_p}{C_f})\times 100\% \tag{4.2}$$

where C_p and C_f are the conductivity of permeate and feed solution, respectively. Modified and unmodified (control) membranes were tested.

4.3. Results and Discussion

As described in our previous work[37], polyHEMA was grafted from the membrane surface as shown in Figure 4.1 (a) using SI-ATRP. Superparamagnetic nanoparticles were then attached to the chain ends, thus the polyHEMA chains act as spacers between immobilized particles and the membrane surface. Our modification is unique in that we tether a superparamagnetic particle to the end of a polymer chain that is attached to the surface of a membrane. Previous studies have considered the use of chains of linked paramagnetic particles that are not attached to a surface[45-47]. Chains of paramagnetic particle have been shown to act as micromixers in an oscillating magnetic field. These earlier studies indicate that chain flexibility is very important to ensure effective mixing[45-47]. PolyHEMA is a highly flexible, hydrophilic polymer that is strongly hydrated in aqueous solution with well-characterized poly behavior[48-49]. Unlike earlier studies that developed chains of flexible paramagnetic particles, we use superparamagnetic particles in this work, which respond to an external field instantaneously with no hysteresis.

The use of SI-ATRP to grow polyHEMA chains from the surface of the membrane offers a number of advantages. As this is a so called "living" polymerization, the polymerization could be halted after a specified time and the terminal bromide selectively converted to a primary amine via a modified Gabriel synthesis procedure. This ensures that the nanoparticles which contain a carboxylic coating are attached only to the chain ends via an amide linkage. Attachment of the superparamagnetic particles to the chain ends is essential in order to maximize movement of the chains in an oscillating magnetic field.

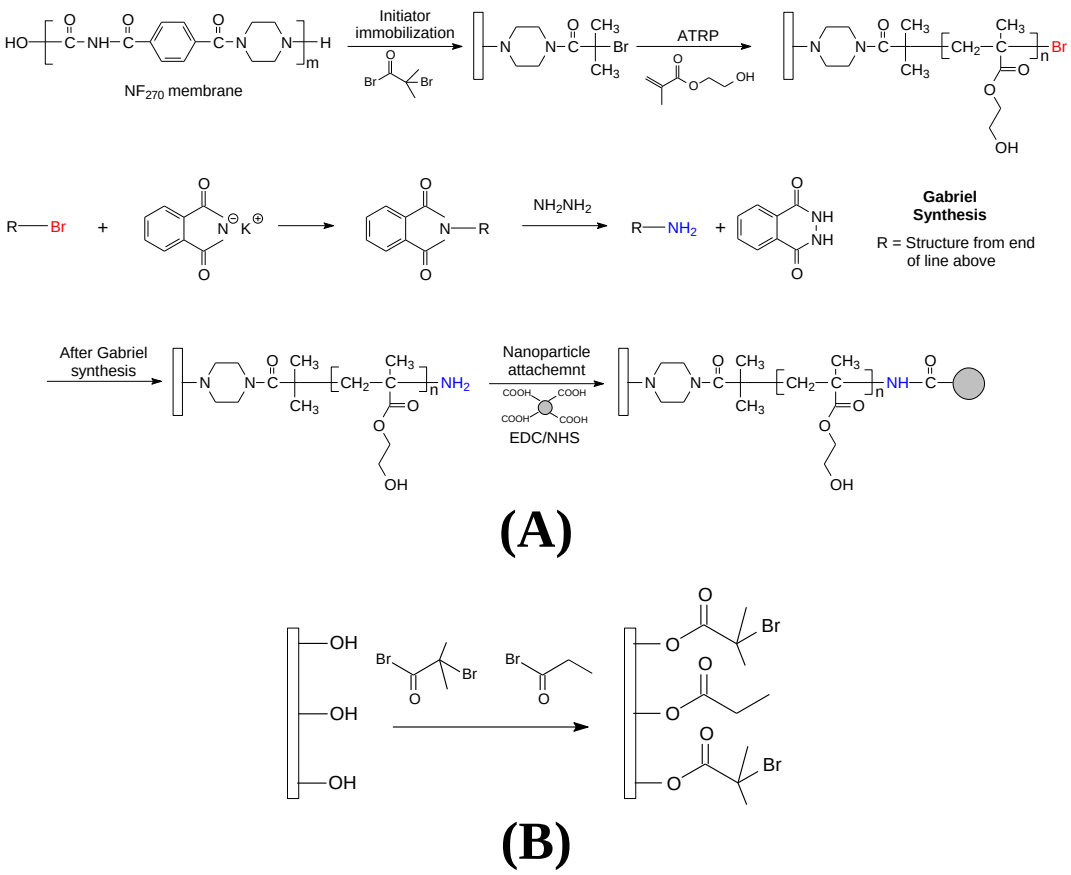

Figure 4.1. Schematic representation for (A) grafting polyHEMA and immobilization of magnetic nanoparticles and (B) diluting ATRP initiator density on the membrane surface.

SI-ATRP modification was based on our previous work using PET membranes[50,51]. As can be seen from Figure 4.2, the grafting was well controlled and the degree of grafting (DG) increased linearly with reaction time over 4 hours. Moreover, even after 24 hours reaction time we observed an obvious, though decelerated, increase in DG indicating that the chain ends were still "living". To achieve low chain density, a non-initiating species, propionyl bromide (PB), was added to the initiator immobilization solution in a 1:1 (v/v) ratio (Figure 4.1 (b)). By using a molar ratio of initiator (BiB) to non-initiating species (PB) of 1:1.4 the DG was reduced by 50% for the same polymerization time. Since the reactivities of BiB and PB are different the initiator dilution factor cannot be used to directly determine the reduction in DG[50].

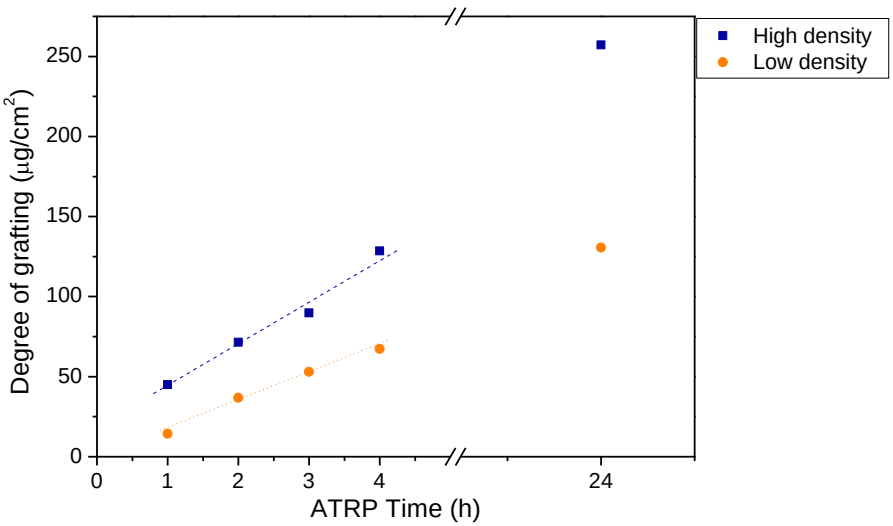

Figure 4.2. Degree of grafting of polyHEMA grafted from membranes with high (■) and low (●) initiator density.

Gabriel synthesis was used to convert the bromine at the chain ends to primary amine groups which were then used for nanoparticles coupling through formation of a carbodiimide activated amide. EDC and NHS were used as the coupling agents. XPS was used to characterize modified surfaces. XPS is a surface sensitive technique that provides chemical binding information for the top 1–10 nm from the surface. It is thus appropriate for analyzing chemical changes at the membrane surface after each of the modification steps.

Figure 4.3 (a) gives high-resolution XPS spectra of the N1s region for 4 different membrane samples: DG = 110.2 μg cm^{-2} (100 % active initiator, 4 hour SI-ATRP time); 37.2 μg cm^{-2} (100 % active initiator, 1 hour SI-ATRP time); 32.7 μg cm^{-2} (1:1.4 active initiator to PB, 4 hour SI-ATRP time); 10.2 μg cm^{-2}, (1:1.4 active initiator to PB, 1 hour SI-ATRP time). High grafting density samples showed a much smaller peak than low grafting density samples. This can be ascribed to the incomplete coverage of the base membrane surface by polyHEMA chains for the low grafting density sample. A stronger signal was detected from the bulk NF 270 membrane in which the N content is much higher than in the grafted polyHEMA layer which

contains a single N at the end of each chain after Gabriel Synthesis. For both high and low chain density samples, increasing DG resulted in a decrease of peak intensity since increasing surface coverage and layer thickness reduce the intensity of peaks associated with the barrier layer. The XPS spectra of the O1s region are shown in Figure 4.3 (b) for the same four membranes. These spectra provide additional evidence of the variation in chain density and chain length. Increasing chain density leads to a stronger peak due to the attachment of more nanoparticles and hence greater O content as a result of the carboxylic groups on the surface of the nanoparticles. Increasing DG also leads to an increase in the peak intensity due to an increasing O content as a result of greater number of HEMA monomer units.

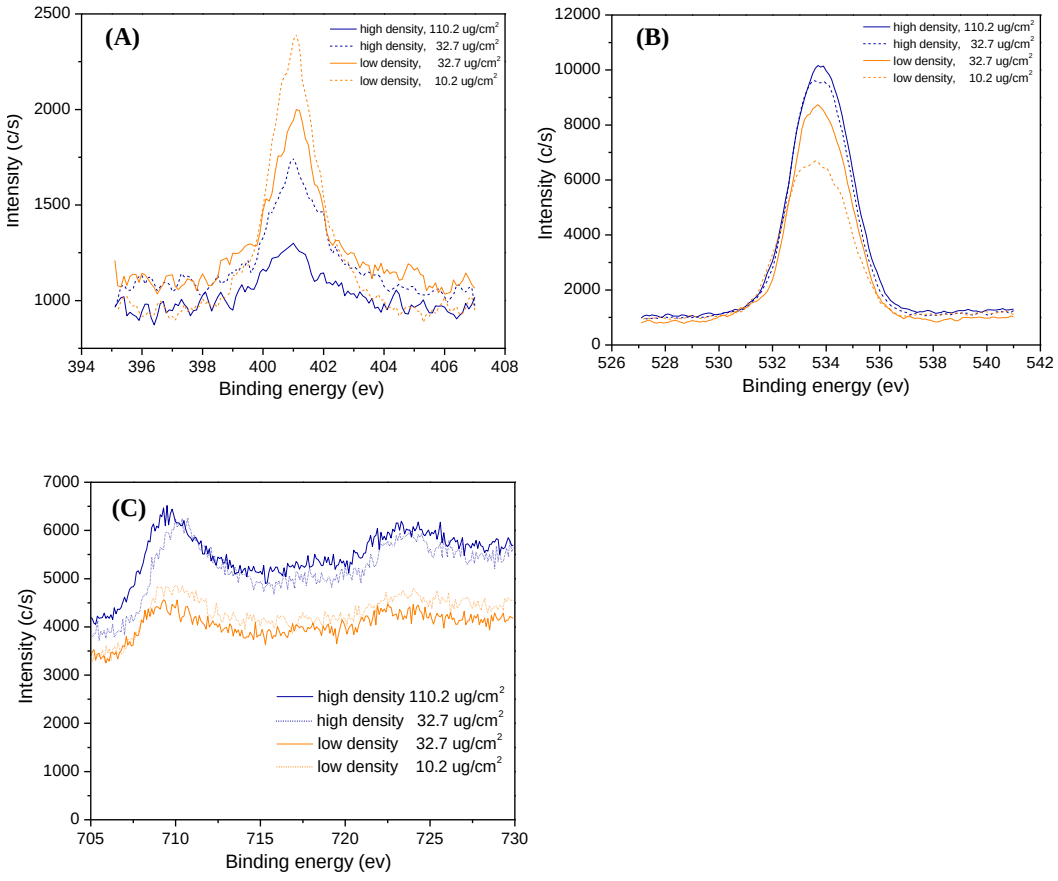

Figure 4.3. High resolution XPS spectra of polyHEMA grafted and nanoparticle immobilized membranes with different polyHEMA DG and chain density for the (A) N1s, (B) O1s, and (C) Fe2p regions.

Finally, XPS spectra of the Fe2p region are shown in Figure 4.3 (c). Two peaks associated with iron are seen at 710 and 725 eV. At higher grafting density the peak intensity increases; however, the peak intensity is insensitive to DG. This is expected as increasing the polymerization time should have no effect on the density of polyHEMA chains and hence the number of attached magnetic nanoparticles per surface area. These results highlight our ability to independently vary polymer chain length and chain density.

Figures 4.4 (a) and (b) show high-resolution spectra for the C1s region. Results are given for two of the membranes investigated in Figure 4.3 (100% active initiator, 4 hour polymerization time; 1:1.4 active initiator to PB, 1 hour polymerization time). An obvious difference in peak shape can be observed between the two samples. Using curve fitting these spectra were deconvoluted in order to distinguish the different types of functional groups present on the membrane surface. The spectra can be resolved into four peaks at binding energies of 285.0 eV, 286.2 eV, 287.2 eV and 288.5 eV which can be assigned to C-C/C-H, C-O, N-C=O and O-C=O, respectively. For high chain density and DG, a higher intensity peak at 288.5 eV can be found compared to the low density low DG sample. The presence of an ester bond is due to grafted polyHEMA. The intensity of the ester peak increases with increasing chain density and chain length. This observation may be explained by the fact that as the polyHEMA thickness increases the signal from the underlying partially aliphatic (piperazine) polyamide is reduced relative to the signal from the polyHEMA layer.

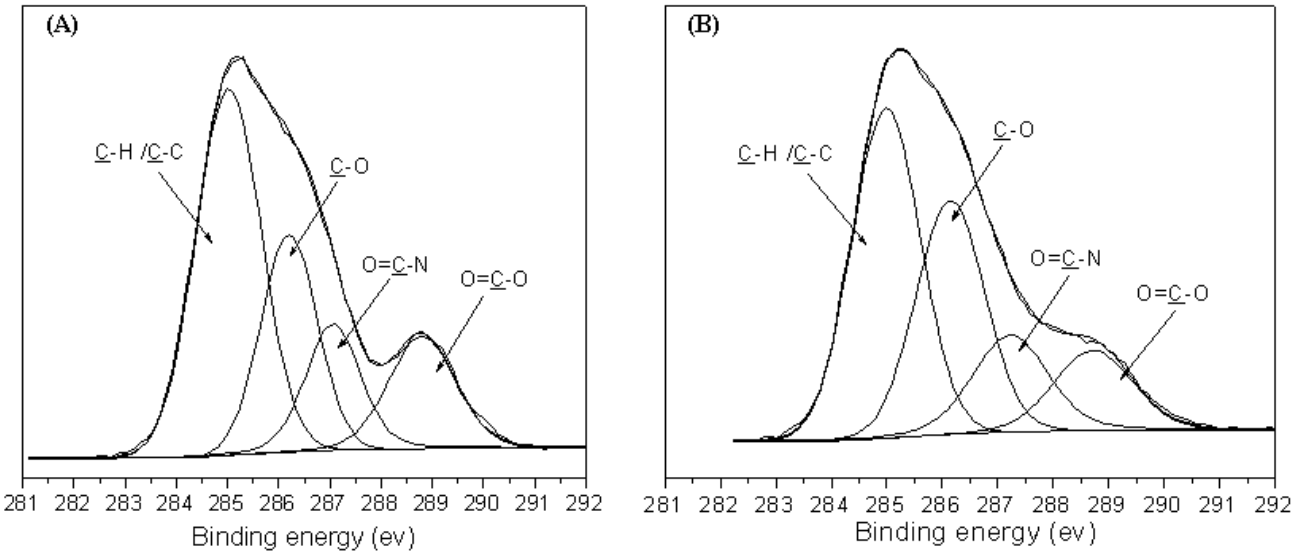

Figure 4.4. Curve-fitted high resolution C1s XPS spectra (Intensity vs. Binding energy as in Figure 4.3) of polyHEMA grafted and nanoparticle immobilized membranes (A) high density, DG = 110.2 μg/cm^2; (B) low density, DG = 10.2 μg/cm^2.

FESEM was used to visualize nanoparticles on the membrane surface as shown in Figure 4.5. Images (a) – (e) were taken at a magnification of 100,000x while images (a') – (e') were taken at a magnification of 200,000x. Images (b), (c), (d), and (e) correspond to membranes analyzed in Figure 4.3. Membranes (a) and (b) were both modified using 100% initiator and 4 hour polymerization time; however, in image (a) a 10 times higher concentration of superparamagnetic particles was used.

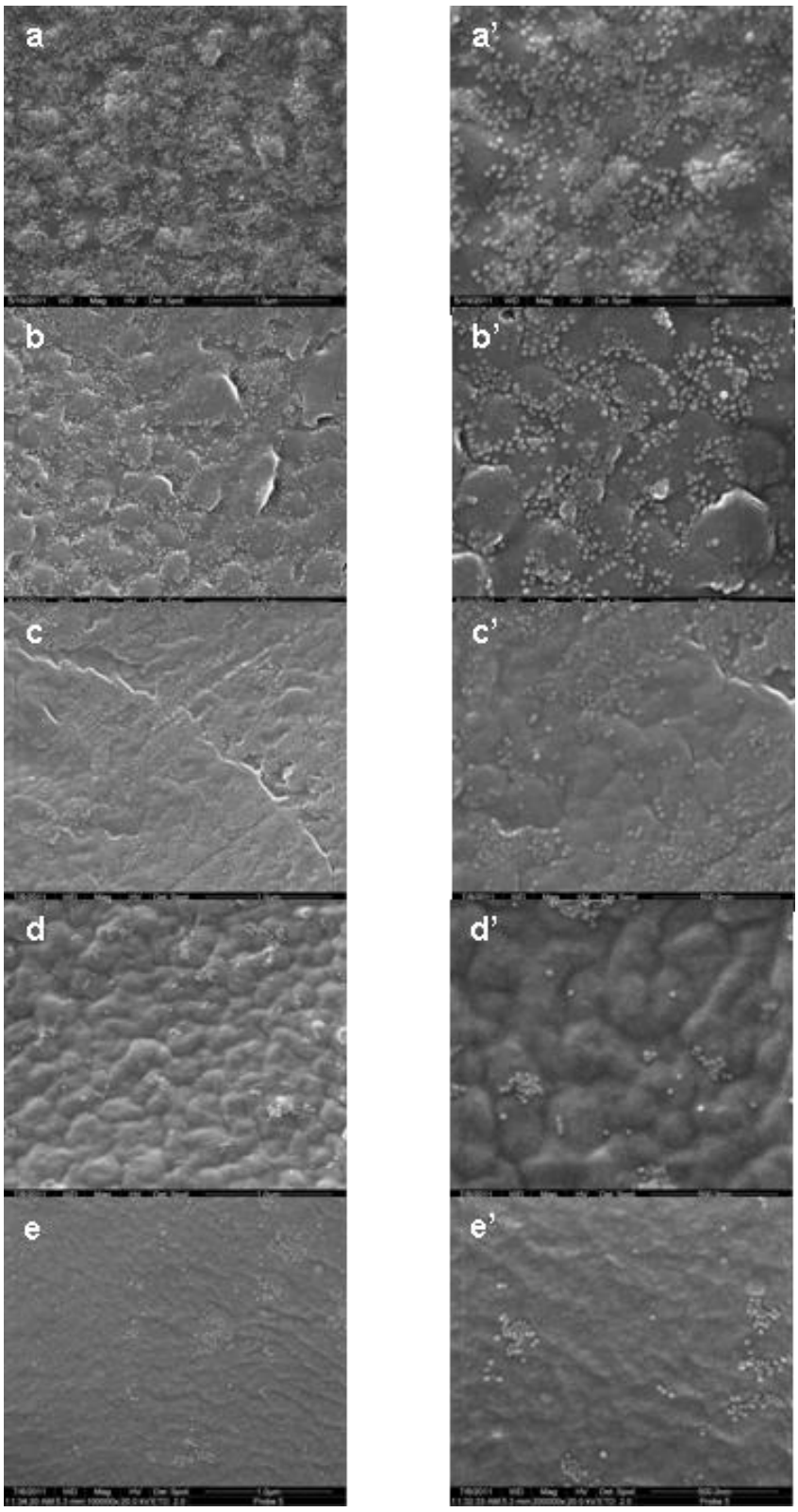

Figure 4.5. FESEM images of nanoparticle modified membrane surfaces with different density and polyHEMA DG. (a)-(c), high density, DG = 138.8, 110.2 and 32.7 μg/cm^2, respectively; (d)-(e) low density, DG = 32.7 and 10.2 μg/cm^2, respectively. The nanoparticle concentration used in coupling reaction solution was 0.15 g/L for (a) and 0.015 g/L for (b)-(e). Images (a)-(e) are 100,000x magnification and (a')-(e') are 200,000x magnification.

FESEM images confirm the XPS results. As can be seen in Figure 4.5 samples with high chain density have a greater density of coupled nanoparticles. Importantly in agreement with Figure 4.3(c), samples with same chain density but different DG exhibited no significant difference in the number of attached nanoparticles on the surface (see Figure 4.5 (b), (c) and (d), (e)). The concentration of nanoparticles in the solution used during the coupling step also affects the number of attached nanoparticles. Comparing Figures 4.5(a) and 4.5(b) it can be seen that for the same modification conditions increasing the concentration of nanoparticles in solution leads to a higher density of attached nanoparticles on the membrane surface. The results suggest that only a fraction of the amine terminated polymer chains are attached to nanoparticles. Thus the density of attached nanoparticles depends not only on chain density but also on the concentration of nanoparticles in solution. In this work we have not attempted to investigate the percentage of chain ends that are attached to nanoparticles.

Figure 4.6 gives water contact angles for unmodified and modified membranes. The unmodified NF 270 membrane showed a low water contact angle, in agreement with previous studies[31,52]. Contact angle increased after initiator immobilization. This may be ascribed to the introduction of the ATRP initiator which exposes a relatively hydrophobic alkyl bromide end group. Grafting of polyHEMA resulted in a decrease in the contact angle. PolyHEMA is a well-known hydrophilic polymer with abundant hydroxyl groups along the chain. After polyHEMA grafting the contact angle is slightly higher than for the base membrane. This could be due to increased surface roughness. Nanoparticle attachment leads to even higher contact angles. This could be due to changes in surface roughness and the relative hydrophilicity of the nanoparticle surface. Feng et al.[53] have shown that nano-structure can increase hydrophilicity of the surface. Moreover, surfaces with lower nanoparticle density exhibited lower contact angles probably due

to greater contact area with the grafted hydrophilic polyHEMA layer. This again suggests that only a fraction of the polymer chains ends are attached to nanoparticles.

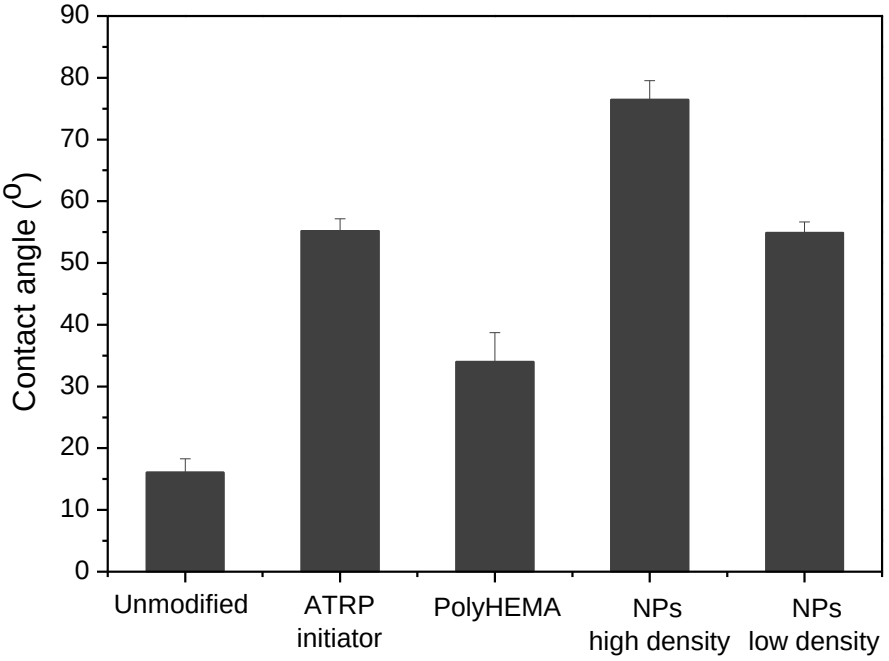

Figure 4.6. Contact angle of unmodified NF 270 membrane and membranes after each step of modification. The error bars represent the range of experimental values.

Membrane performance was investigated in the presence of an oscillating magnetic field in dead end filtration. The results are given in Table 4.1. As reported in our previous work[37], the unmodified NF membrane had an average water flux of 35 Lm^{-2} h^{-1} at 3.1 bar (45 psi). Table 4.1 indicates that the water flux for the modified membranes is less than for the unmodified membrane. This lower flux is due to the additional resistance of the grafted nanolayer and perhaps modification of the flux of the barrier layer during the modification procedure. Previously reported salt rejections for the base NF 270 membrane were 32.5 and 66.0 % for 500 ppm $CaCl_2$ and 2,000 ppm $MgSO_4$, respectively[37]. Table 4.1 indicates that rejection of $CaCl_2$ and $MgSO_4$ is slightly decreased at low grafting densities. These results suggest that the observed changes in performance are due to both the additional resistance of the grafted nanolayer as well as changes in the barrier layer during chemical modification.

Table 4.1. Average fluxes and salt rejection for modified membranes with different polymer/nanoparticle density and degree of grafting (DG) at 3.1 bar (45 psi).

DG (μg / cm^2)	Chain density	Water Flux (Lmh)		500 ppm $CaCl_2$				2000 ppm $MgSO_4$			
		With field	No field	Flux (Lmh)		Rejection (%)		Flux (Lmh)		Rejection (%)	
				With field	Without field	With field	Without field	With field	Without field	With field	Without field
38.8	High	16	14.8	9.1	5.6	35.4	32.8	5.3	4.5	68.1	64.4
116.3		13	11.1	7.6	4.7	37.2	31.5	4.3	3.7	74.1	66.4
20.4	Low	19.5	20	11.4	8.6	29.9	29.1	6.8	6	64.2	60.4
51.0		18	17.1	10.1	8.3	32.3	30.1	6	5.4	67.1	65.2

Table 4.2. Relative improvement in performance in an oscillating magnetic field for various degree of grafting (DG) and grafting densities. Percentage improvement is defined as the flux or rejection in the presence of an oscillating magnetic field minus the value in the absence of a field divided by the value in the absence of a field.

DG (μg/cm^2)	Chain Density	**DI Water**	**500 ppm $CaCl_2$**		**2000 ppm $MgSO_4$**	
		Improvement in flux (%)	Improvement in flux (%)	Improvement in rejection (%)	Improvement in flux (%)	Improvement in rejection (%)
38.8	High	8	63	8	18	8
116.3		17	62	18	16	12
20.4	Low	-3	33	3	13	6
51.0		5	22	7	11	3

Table 4.1 indicates that the water flux for a grafting degree of 38.8 μg cm^{-2} is lower than for a grafting degree of 51.0 μg cm^{-2}. The former grafting degree was obtained at higher grafting density. Consequently the increase in resistance to permeate flow depends both on the density and length of the polymer chains. At both grafting densities, the water flux decreased with increasing chain length, but much lower fluxes were observed at higher grafting density.

Closer examination of the water flux data indicates that in all cases except for a grafting density of 20.4 μg cm^{-2} the water flux increases in the presence of an oscillating magnetic field. Table 4.2 gives the percentage increase in water flux, which could be due to changes in the grafted polymer chain conformation in the presence and absence of an oscillating magnetic field. Changes in polymer conformation, e.g. unfolding enforced by the movement of the tethered nanoparticles, could lead to changes in resistance to permeate flow. The effect is greatest for the highest grafting density and non-existent for the lowest grafting density.

In previous work the unmodified NF membrane also displayed significantly lower flux than the DI water flux for aqueous feed streams containing 500 ppm $CaCl_2$ and 2000 ppm $MgSO_4$ due to concentration polarization[37]. The presence of an oscillating magnetic field had relatively little effect on the flux of unmodified membranes. However, for modified membranes a significant improvement in both flux and rejection was observed in the presence of an oscillating magnetic field.

The results of the current study, given in Table 4.1, are in agreement with these earlier results. As was the case for the DI water flux, Table 4.1 indicates that increasing the degree of grafting in general leads to a decrease in flux for $CaCl_2$ and $MgSO_4$ feed streams. Again as was observed for DI water fluxes, at a grafting degree of 38.8 μg cm^{-2}, the flux is lower than at a grafting degree of 51.0 μg cm^{-2}. The result suggests that both grafting density and grafting

degree can be tuned independently in order to minimize the decrease in flux due to the added resistance of the grafted nanolayer.

Table 4.1 indicates that in the presence of an oscillating magnetic field, for feed streams containing $CaCl_2$ and $MgSO_4$, the flux is higher than in the absence of an oscillating magnetic field. Table 4.2 gives the percentage increase in flux. It can be noted that at higher grafting density the percentage improvement is higher than at lower grafting density. Flux data for 500 ppm $CaCl_2$ show a greater percentage improvement than for 2000 ppm $MgSO_4$. In fact the flux data in the presence and absence of an oscillating magnetic field for 2000 ppm $MgSO_4$ are within the uncertainty of the readings.

A decrease in concentration polarization due to mixing of the fluid at the membrane surface will lead to lower concentration of rejected species at the membrane surface and hence an increase in the flux. The results in Tables 4.1 and 4.2 indicate that this is the case. A decrease in the concentration of rejected species at the membrane surface will also lead to an increase in the apparent rejection coefficient of the membrane. Table 4.1 indicates that in the presence of an oscillating magnetic field the rejection coefficient increases for feed streams containing 500 ppm $CaCl_2$ and 2000 ppm $MgSO_4$. Table 4.2 gives the percentage improvement in the rejection coefficient.

Closer examination of Table 4.2 indicates that the improvement in rejection is greater at higher chain density, and the improvement in performance is generally greater at lower solute concentrations. Taken together the results indicate that the increase in flux and rejection depend differently on chain density and chain length. Short chains will have less freedom of movement and will create less mixing than longer chains; however, the movement of very long chains will be limited by viscous forces and entropic resistance of the chains to movement. Low chain

densities will lead to less effective mixing while chain densities that are too high will lead to less movement due to steric hindrance.

Since the results indicate that at the highest chain density we obtain better performance it appears that even higher chain densities should be investigated. The results also indicate that at a given grafting density increasing the degree of grafting (chain length) generally improves rejection but leads to a reduced improvement in flux. Thus, the results suggest that denser, shorter chains may yield greater improvements in permeate flux at the expense of slightly lower improvements in rejection. It should be noted that in this work the frequency of the oscillating magnetic field was 10 Hz based on our previous work[37]; however, the optimum oscillation frequency will also depend on chain length and density.

In practice, modified nanofiltration membranes will be run in tangential flow mode. A number of considerations govern the economic viability of nanofiltration processes. Membrane productivity (total amount of feed that can be treated before the membrane module must be taken off line and cleaned), should be maximized. Membrane regeneration costs should be minimized by minimizing the cleaning time and the quantity of chemical cleaning agents used. Minimizing concentration polarization will suppress deposition of rejected species on the membrane surface, increase flux, and lead to an increase in the apparent rejection coefficient. Since the magnetically-responsive nanofiltration membranes developed here are able to disrupt the concentration polarization boundary layer, they have the potential to radically improve membrane performance. Any increased costs associated with the establishment of an oscillating magnetic field and membrane surface modification, must be offset by improved performance. This is studied in detail in the following chapter.

4.4. CONCLUSIONS

In this study, polyHEMA chains that act as micromixers were attached to the surface of nanofiltration membranes. Both the density and length of the polymer chains were controlled independently using SI-ATRP. Superparamagnetic nanoparticles were successfully attached to the chain ends. The results indicate that only a fraction of the polyHEMA chain ends are terminated with nanoparticles. Changes in nanoparticle density were confirmed by XPS and SEM as well as contact angle measurements.

Dead end filtration was conducted in order to determine membrane performance. Water fluxes for modified membranes were lower than for the base membrane due to the added resistance of the grafted nanolayer. Comparing performance of modified membranes in the presence and absence of an oscillating magnetic field, permeate fluxes and rejection of $CaCl_2$ and $MgSO_4$ generally increased in the former case. The increase was greater for higher densities of attached nanoparticles. The result suggest that optimization of the density of attached nanoparticles as well as the length of the polyHEMA chains is necessary to maximize the improvement in performance while minimizing the added resistance to permeate flow from the grafted nanolayer.

.

REFERENCES

1. P. H. Gleick, H. Cooley, D. Katz, E. Lee, J. Morrison, M. Palanlappan, A. Samulon, G.H. Wolff. The world's water 2006-2007, the biennial report on freshwater resources, Island Press, Washington, DC, 2006.
2. B. van der Bruggen, J. Geens, Nanofiltration, in: N.N. Li, A.G. Fane, W.S.W. Ho, T. Matsuura, Advanced Membrane Technology and Applications, John Wiley & Sons, Inc., Hoboken, NJ, 2008, 271-295.
3. W. J. Conlon, S. A. McClellan, Membrane softening; A treatment process comes of age, J. AWWA, 81(11) (1989) 47-51.
4. S. Chellam, Effects of nanofiltration on trihalomethane and haloacetic acid precursor removal and speciation in waters containing low concentrations of bromide ion, Environ. Sci. Technol. 34(9) (2000) 1813-1820.
5. Y. Kiso, Y. Nishimura, T. Kiato, K. Nishimura, Rejection properties of non-phenylic pesticides with nanofiltration membranes, J. Membr. Sc. 171(2) (2000) 229-237.
6. L. D. Nghiem, A. I. Schäfer, M. Elimelech, Removal of natural hormones by nanofiltration membranes: measurement, modeling and mechanisms. Environ. Sci. Technol. 38(6) (2004) 1888-1896.
7. G. Bargeman, M. Timmer, C. van der Horst, Nanofiltration in the food industry, in A.I Schäfer, A.G. Fane, T.D. Waite (Eds.), Nanofiltration principles and applications, Elsevier, Oxford, 2005.
8. D. Bhanushali, S. Kloos, D. Bhattacharyya, Solute transport in solvent-resistant nanofiltration membranes for non-aqueous systems: Experimental results and the role of solute-solvent coupling, J. Membr. Sc. 208(1-2) (2002) 343-359.
9. T. Rizwan, S. Bhattacharjee. Initial deposition of colloidal particles on a rough nanofiltration membrane. Can. J. Chem. Eng. 85(5) (2007) 570-579.
10. W. Yuan, A. L. Zydney, Humic acid fouling during microfiltration, J. Membr. Sci. 157(1) (1999) 1-12.
11. K. L. Jones, C. R. O'Melia, Protein and humic acid adsorption onto hydrophilic membrane surfaces: effects of pH and ionic strength, J. Membr. Sci. 165(1) (2000) 31-46.
12. K. O. Agenson, T. Urase, Change in membrane performance due to organic fouling in nanofiltration (NF)/reverse osmosis (RO) applications, Sep. Purif. Technol. 55(2) (2007) 147-156.
13. R. Deppisch, M. Storr, R. Buck, H. Gohl, Blood material interactions at the surfaces of membranes in medical applications, Sep. Purif. Technol. 14(1-3) (1998) 241-254.
14. R. W. Field, D. Wu, J. A. Howell, B. B. Gupta, Critical flux concept for microfiltration fouling, J. Membr. Sci. 100(3) (1995) 259-272.
15. P. Czekaj, F. López, C. Güell, Membrane fouling during microfiltration of fermented beverages, J. Membr. Sci. 166(2) (2000) 199-212.
16. S. T. Kelly, A. L. Zydney, Mechanisms for BSA fouling during microfiltration, J. Membr. Sci. 107(1-2) (1995) 115-127.
17. J. E. Kilduff, S. Mattaraj, M. Zhou, G. Belfort, Kinetics of membrane flux decline: the role of natural colloids and mitigation via membrane surface modification, J. Nanoparticle Res. 7(4.5) (2005) 525-544.

18. J.-S. Kim, S. Akeprathumchai, S. R. Wickramasinghe, Flocculation to enhance microfiltration, J. Membr. Sc. 182(1-2) (2001) 161-172.
19. G. Belfort, R. H. Davis, A. L. Zydney, The behavior of suspensions and macromolecular solutions in crossflow microfiltration, J. Membr. Sc. 96(1-2) (1994) 1-58.
20. J. M. Radovich, N. S. Mason, R. E. Sparks, Coupling electrophoresis with ultrafiltration for improved processing of plasma-proteins, Sep. Sci. Technol. 15(8) (1980) 1491-1498.
21. M. Ulbricht, Advanced functional polymer membranes, Polymer 47(7) (2006) 2217-2262.
22. Q. Yang, N. Adrus, F. Tomicki, M. Ulbricht, Composites of functional polymeric hydrogels and porous membranes, J. Mater. Chem. 21(9) (2011) 2783-2811.
23. D. Rana, T. Matsuura, Surface modifications for antifouling membranes, Chem. Rev. 110(4) (2010) 2448-2471.
24. J. Schwinge, D. E. Wiley, A. G. Fane, Novel spacer design improves observed flux, J. Membr. Sc., 229(1-2) (2004) 53-61.
25. J. Schwinge, P. R. Neal, D. E. Wiley, D. F. Fletcher, A. G. Fane, Spiral wound modules and spacers - Review and analysis, J Membr. Sc., 242(1-2) (2004) 129-153.
26. S. H. D. Silalahi, T. Leiknes, High frequency back-pulsing for fouling development control in ceramic microfiltration for treatment of produced water, Desalination and water treatment, 28(1-3) (2011) 137-152.
27. H. B. Winzeler, G. Belfort, Enhanced performance of pressure driven membrane filtration processes: the argument for flow instabilities, J. Membr. Sci. 80(1-3) (1992) 35-47.
28. R. P. Shaikh, V. Pillay, Y. E. Choonara, L. C. du Toit, V. M. K. Ndesendo, P. Bawa, S. Cooppan, A review of multi-responsive membrane systems for rate-modulated drug delivery, AAPS Pharm. Sci. Tech. 11(1) (2010) 441-459.
29. D. Wandera, S. R. Wickramasinghe, S. M. Husson, Stimuli-responsive membranes, J. Membr. Sci. 357(1-2) (2010) 6-35.
30. C. Gorey, I. C. Escobar, C. Gruden, M. Coleman, O. Mileyeva-Biebesheimer, Development of smart membrane filters for microbial sensing, Sep. Sci. Technol. 43(16) (2008) 4056-4074.
31. H. H. Himstedt, K. M. Marshall, S. R. Wickramasinghe, pH-responsive nanofiltration membranes by surface modification, J. Membr. Sci. 366(1-2) (2011), 373-381.
32. C. Gorey, I. C. Escobar, N-isopropylacrylamide (NIPAAM) modified cellulose acetate ultrafiltration membranes, J. Membr. Sci. 383(1-2) (2011) 272-279.
33. S. Mondal, S. R. Wickramasinghe, Photo-induced graft polymerization of N-isopropyl acrylamide on thin film composite membrane: Produced water treatment and antifouling properties, Sep. Purif. Technol. 90 (2012) 231-238.
34. D. Wandera, S. R. Wickramasinghe, S. M. Husson, Modification and characterization of ultrafiltration membranes for treatment of produced water, J. Membr. Sci. 373(1-2) (2011) 178-188.
35. N. Tomer, S. Mondal, D. Wandera, S. R. Wickramasinghe, S. M. Husson, Modification of nanofiltration membranes by surface-initiated atom transfer radical polymerization for produced water filtration, Sep. Sci. Technol. 44(14) (2009) 3346-3368.
36. D. Wandera, H. H. Himstedt, M. Marroquin, S. R. Wickramasinghe, S. M. Husson, Modification of ultrafiltration membranes with block copolymer nanolayers for produced water treatment: The roles of polymer chain density and polymerization time on performance, J. Membr. Sc. 403 (2012) 250-260.

37. H. H. Himstedt, Q. Yang, L.P. Dasi, X. Qian, S. R. Wickramasinghe, M. Ulbricht, Magnetically-activated micromixers for separation membranes, Langmuir 27(9) (2011) 5574-5581.
38. C. Rosén, C. Trägårdh, Computer simulations of mass transfer in the concentration boundary layer over ultrafiltration membranes, J. Membr. Sci. 85(2) (1993) 139-156.
39. E. Pellerin, E. Michelitsch, K. Darcovich, S. Lin, C.M. Tam, Turbulent transport in membrane modules by CFD simulation in two dimensions, J. Membr. Sci. 100(2) (1995) 139-153.
40. F. Li , G. W. Meindersma, A. B. de Haan, T. Reith, Optimization of non-woven spacers by CFD and validation by experiments, Desalination, 146(1-3) (2002) 209-212.
41. C. Pozrikidis, Boundary conditions for shear flow past a permeable interface modeled as an array of cylinders, Comput. Fluids 33(1) (2004) 1-17.
42. J. Lipnizki, G. Jonsson, Flow dynamics and concentration polarization in spacer-filled channels, Desalination 146(1-3) (2002) 213-217.
43. M. Gimmelshtein, R. Semiat, Investigation of flow next to membrane walls, J. Membr. Sci. 264(1-2) (2005) 137-150.
44. S. Monge, O. Giani, E. Ruiz, M. Cavalier, J. J Robin, A new route for the modification of halogen end groups to amino end-modified poly(tert-butyl acrylate)s, Macromol. Rapid Commun. 28(23) (2007) 2272-2276.
45. S. L. Biswal, A. P. Gast, Micromixing with linked chains of paramagnetic particles, Anal. Chem. 76(21) (2004) 6448-6455.
46. S. L. Biswal, A. P. Gast, Rotational dynamics of semiflexible paramagnetic particle chains, Phys. Rev. E 69(4) (2004) 041406.
47. T. Franke, L. Schmid, D. A. Weitz, A. Wixforth, Magneto-mechanical mixing and manipulation of picoliter volumes in vesicles, Lab Chip 9(19) (2009) 2831-2835.
48. Q. Yang, J. Tian, M.-X. Hu, Z.-K. Xu, Construction of a comb-like glycosylated membrane surface by a combination of UV-induced graft polymerization and Surface-Initiated ATRP, Langmuir, 23(12) (2007) 6684.6690.
49. Q. Yang, M. Ulbricht, Cylindrical membrane pores with well-defined grafted linear and comblike glycopolymer layers for lectin binding, Macromolecules 44(6) (2011) 1303-1310.
50. F. Tomicki, D. Krix, H. Nienhaus, M. Ulbricht, Stimuli-responsive track-etched membranes via surface-initiated controlled radical polymerization: Influence of grafting density and pore size, J Membr. Sci. 377(1-2) (2011) 124.133.
51. H. H. Himstedt, Q. Yang, X. Qian, S. R. Wickramasinghe, M. Ulbricht, Toward remote-controlled valve functions via magnetically-responsive capillary pore membranes, J. Mem. Sci. J. Mem. Sci. 423-424 (2012), 257-266.
52. M. Mänttäria, T. Pekurib, M. Nyströma, NF 270, a new membrane having promising characteristics and being suitable for treatment of dilute effluents from the paper industry, J. Membr. Sci. 242(1-2) (2004) 107-116.
53. L. Feng, S. Li, Y. Li, H. Li, L. Zhang, J. Zhai, Y. Song, B. Liu, L. Jiang, D. Zhu, Super-hydrophobic surfaces: From natural to artificial, Adv. Mater. 14(24) (2002) 1857-1860.

CHAPTER 5

MAGNETICALLY-RESPONSIVE MEMBRANES FOR TREATMENT OF MODEL AND REALISTIC OILY PRODUCED WATERS

Filtration of a model PW and a realistic PW showed the fouling resistant properties of modified membranes. Filtration was performed over many hours with multiple washing cycles. The energy costs of unmodified and modified membranes were calculated as well.

I modified the membranes at various conditions to test the effect of polyHEMA chain length on magnetic response. The basis for the model produced water composition came from a previous collaboration with another research group. I performed all of the filtration experiments to determine if the magnetically-responsive membranes improved membrane performance over lengthy filtration periods with multiple washings.

SUMMARY

Produced water is the largest by-product of oil and gas production; billions of barrels are produced annually. Treatment of produced water is difficult using traditional unit operations. The high levels of contaminants and the widely varying composition of produced water force engineers to develop tailored treatments for each composition. Membrane filtration has been studied as an alternative to traditional methods; however, success has been limited due to membrane fouling. Novel fouling resistant magnetically-activated micromixing nanofiltration membranes have been developed. In an alternating magnetic field, alignment of grafted polymer chains, coupled to superparamagnetic nanoparticles, generate mixing above the membrane surface. This mixing disrupts the filtration boundary layer, leading to less membrane fouling. These membranes are used to treat a simple model produced water as well as a realistic produced water. The modified membranes resulted in better permeate quality. Membrane flux compared to unmodified membranes, although initially lower, was higher after some time due to reduced membrane fouling on the modified membranes. A simple washing step restored the modified membrane performance quite well; however, it was ineffective at restoring unmodified membrane performance. The modified membranes also reduced total energy costs per volume of treated water. Although the magnetic field contributes an additional energy cost, this is more than offset by the reduced pumping costs attributable to improved membrane flux. Use of these membranes to treat realistic produced waters appears promising and could lead to a clean, beneficial water product from a source previously discarded as waste.

Financial support by the Strategic Environmental Research and Development Program WP-1670 (USA) and a DoD NDSEG graduate fellowship (USA). We thank Mr. Troy Bauder, Mrs. Julie Kallenberger, and Mr. Reagan Waskom for helping us obtain the realistic PW used.

5.1. INTRODUCTION

Synthetic membranes have become important tools for separation and reaction engineering because they can perform continuously with reduced operating costs and a smaller footprint compared to traditional unit operations[1-3]. However, in many applications, concentration polarization and fouling limit membrane selectivity, capacity, and productivity[1-3]. Fouling can be reduced by limiting the propensity of interactions between the membrane and rejected species in the feed via modification of the membrane surface chemistry, altering the composition of the feed, or by hydrodynamically disrupting the boundary layer near the membrane surface. Modification of membrane surface chemistry is frequently investigated as a means to reduce fouling[4-8]. An exciting subclass of modified membranes receiving much attention is membranes whose properties can be altered via application of a stimulus. These so-called responsive membranes can combat fouling by changing their properties, such as conformation, hydrophilicity or charge, under the influence of a stimulus such as pH, ionic strength, or temperature[4, 5, 9]. Such stimuli carry the unfortunate side effect that the properties of the entire feed stream must be changed to observe a response. This can be avoided by using an external physical stimulus such as light or a magnetic field[5, 9-13].

Based on this principle, we have developed an exciting new type of filtration membrane responsive to an external magnetic field[12, 13]. The filtration behavior of these membranes can be altered without affecting the characteristics of the entire feedstream by generating small scale mixing above the membrane surface via the movement of grafted polymer chains in a magnetic field[12, 13]. Superparamagnetic nanoparticles are covalently bounded to polymer chains grown from the membrane surface via surface-initiated atom transfer radical polymerization (SI-ATRP). In an alternating magnetic field, the nanoparticles generate a torque and force on the

polymer chains, causing them to move. This movement disrupts the boundary layer, alleviating concentration polarization near the membrane surface.

One potential use of these magnetically-activated mixing membranes is the treatment of oily wastewaters known as produced water (PW). PW is a co-product of oil and gas production including alternative fuel sources such as coal bed methane, tar sand, and oil shale. Although PW composition varies widely with location, common concerns are high levels of total dissolved solids (TDS), high electrical conductivity, numerous fouling species such as fatty acids, oils, and numerous other organics and inorganics[14-17]. This large volume of wastewater has traditionally been discarded as waste because it is very difficult to treat; however, both discharge to surface waters and reinjection are problematic[13-19]. It is desired to treat PW to obtain beneficial waters such as irrigation or chemical process makeup water rather than simply dispose of the PW. PW reuse could greatly alleviate increasing water demands in arid or heavily populated regions[16].

Magnetically-activated nanofiltration membranes were used to filter an idealized model PW as well as an authentic PW obtained from a local oil production operation. The most beneficial magnetic field application interval and SI-ATRP modification time were determined using the model PW. Additionally, the ability of the modified membranes to combat fouling and ease membrane cleaning was investigated over numerous filtration and washing cycles. Finally, the best performing membranes were used to treat the realistic PW to test if the modified membranes were able to produce a clean water permeate even after numerous hours of harsh filtration and repeated cleanings.

5.2. MATERIALS AND METHODS

5.2.1. Materials and Chemicals

NF 270 flat-sheet membranes were obtained from Dow Filmtec. 45 mm diameter membrane discs cut from the membrane sheets were used for all filtration experiments. Before use, the membranes were washed thoroughly with DI water and dried overnight at 40°C. When not is use, the discs were stored in zip-top plastic bags containing a dilute sodium azide in water solution to prevent microbial growth. Iron oxide core, oleic acid shell superparamagnetic nanoparticles with a core diameter of 15 nm were purchased from Ocean Nanotech (Springdale, AR, USA). Purified water was from a Siemens ELGA Purelab Ultra DI system. All chemicals were at least 97% purity unless otherwise noted. Diisopropylcarbodiimide, triethylamine, N,N',N',N'',N''-pentamethyldiethylenetriamine, and 4-N',N'-dimethylaminopyridine were from Fluka; ethanol, methanol, acetonitrile, and hydrochloric acid (6 M) were from VWR; α-bromoisobutyrylbromide, bipyridine (Reagent Plus), copper (I) and copper (II) chloride, 2-hydroxyethylmethacrylate (HEMA), sodium chloride, calcium chloride, magnesium sulfate, humic acid salt, hydrazine hydrate, 1-ethyl-3-(3-dimethylaminopropyl)carbodiimide (EDC), and N-hydroxysuccinimide (NHS) were from Sigma-Aldrich. Before polymerization HEMA was purified via column chromatography, and always used within 12 hours to minimize self-polymerization. Soybean oil was purchased from a local grocery store. PW was obtained from an operating oil production site in northern Colorado. The PW was stored away from direct sunlight and was not treated before use.

5.2.2. Membrane Modification

The full modification procedure has been described in detail previously[12, 13]. Briefly, the initiator was first immobilized on the membrane surface by reacting the membrane discs at room temperature for 2 hours on a shaker table in a solution of 2.76 g α-bromoisobutyrylbromide, 1.515 g triethylamine, and 91.5 mg 4-N',N'-dimethylaminopyridine in 150 mL dried acetonitrile. PolyHEMA chains were then grafted from the membrane surface using SI-ATRP. The reaction solution consisted of purified HEMA monomer (2 M), CuCl, $CuCl_2$, and bipyridine (BPy) dissolved in equal parts (v/v) water and methanol; the molar ratios HEMA : CuCl : $CuCl_2$: BPy were 100 : 0.5 : 0.1 : 1.5. The solution was strongly degassed with nitrogen for at least 20 minutes before being added to the reaction vessels, which had been thrice evacuated under vacuum and back-filled with nitrogen gas, containing the membrane discs. The membrane discs reacted at room temperature for either 4, 6, or 8 hours before being removed and placed in a quenching solution consisting of 500mg $CuBr_2$ and 1250 μL N,N',N',N'',N''-pentamethyldiethylenetriamine in equal parts methanol and water. The quenching solution halted the polymerization and insured that the end of each polyHEMA chain contained a bromine atom, necessary for the following modification step. In order to convert the terminal bromide to a primary amine, which could then be bound to the superparamagnetic nanoparticles, a modified Gabriel synthesis was employed[12, 13]. The discs were placed in vials containing potassium phthalimide dissolved to saturation in ethanol. The vials were sealed and reacted at 40^{o}C on a shaker table for 6 hours. The discs were then placed in a solution of 7 mL hydrazine hydrate in 25 mL of 6 M HCl, and the sealed vials placed on a shaker table at 40^{o}C for 6 hours. Finally, the nanoparticle coupling solution consisted of 31.2 mg EDC, 38.7 mg NHS, and 3 μL carboxyl shell Fe_3O_4 nanoparticles in buffer solution (5 g/L) added to 10 mL DI water. 1.5 mL of this

solution was then added to a plastic jar containing a membrane disc. This was sealed and incubated in the dark for 4 hours.

5.2.3. Membrane Filtration

Four different feed solutions were used throughout the filtration experiments. 500 ppm $CaCl_2$ and 2000 ppm $MgSO_4$ dissolved in DI water were used as per the manufacturer's instructions. The model PW, designed to approximate the fouling tendencies of the realistic PW, was created by mixing 2 mL of soybean oil per L of water, to which 1 g/L of sodium chloride, calcium chloride, and magnesium sulfate, along with 0.05 g/L humic acid salt were dissolved. The realistic PW was obtained from an operating oil production site in northern Colorado.

A Millipore stirred cell 8050 (50 mL) with an active membrane area of 13.4 cm^2 and initial feed volume of 50 mL was used for all filtration experiments. The membranes were removed from storage in the sodium azide solution and washed thoroughly with DI water before use. The cell was first filled with a 50% ethanol/water solution and pressurized to 1.4 bar (20 psi) and the filtrate outlet opened for 10 minutes in order to wet the membrane. Next, the membrane was flushed with DI water at 1.4 bar (20 psi) for 10 minutes, then allowed to equilibrate in DI water for 2 hours. The stirred cell was then filled with feed solution, and the pressure increased to the desired operating pressure. For longer filtration experiments, the 8050 cell was connected to a reservoir of feed solution. The permeate outlet was kept closed for the first 3 minutes to allow the membrane to equilibrate, then opened, and flux measurements begun. Following the filtration experiment, the membranes were flushed with DI water at 1.4 bar (20 psi) for 20 minutes, then washed thoroughly with DI water and returned to storage. Membrane flux is reported in units of L / m^2 hr, abbreviated Lmh.

Magnetic fields were generated using a computer-controlled system comprising two iron-core solenoids located on opposite sides of the stirred cell[12,13]. The power supplied to the solenoids was tuned to yield a field strength of 50 G at the center of the membrane cell, measured by a probe HHG-23 Gauss/Teslameter (Omega Inc., Stamford, CN). Fields were operated at a frequency of 10 Hz, which was previously found to yield maximum mixing above the membrane surface[12].

Periodically during lengthy filtrations with model and realistic PW, the membranes were lightly cleaned or "washed". The membrane was not removed from the stirred cell during the washing procedure. Washing consisted of removing the feed solution from the cell, rinsing the membrane with shaken DI water for 1 minute, flushing the membrane with 0.5N NaOH at 1.4 bar (20 psi) for 2 minutes, and finally flushing the membrane with DI water at 1.4 bar (20 psi) for 2 minutes. Following the 5 minute washing procedure, 50 mL of the feed was reintroduced to the cell, and the filtration was continued.

5.2.4. Membrane Characterization

5.2.4.1. Membrane Chemical Characterization via ATR-FTIR

Membranes were characterized using ATR-FTIR (Attenuated Total Reflectance Fourier Transform Infrared) spectroscopy. ATR-FTIR provides qualitative information on the types of functional groups present at depths between 100 and 1000 nm. A Nicolet Magna 760 FTIR spectrometer, Thermo Electron Corporation (Madison, WI) equipped with a mercury-cadmium-tellurium (MCT) detector with a resolution of 4 cm^{-1} and zinc selenide (ZnSe) crystal plate with an incidence angle of 45^{o} was used. Prior to analysis, the membranes were removed from

storage and rinsed thoroughly with DI water and dried overnight at 40^{o}C. ATR-FTIR spectra were averaged over 512 scans (range: 600-4000 cm^{-1}).

5.2.4.2. Surface Visualization via FESEM

Field-emission Scanning Electron Microscopy (FESEM) was used to image the surface and cross section of the membrane to visualize the membranes following filtration of realistic PW. To prevent pore collapse, critical point drying was performed prior to analysing samples with a JEOL field-emission scanning electron microscope (JSM-6500F, JEOL Ltd., Tokyo, Japan). Prior to analysis, the membranes were removed from the zip top bags and rinsed thoroughly with DI water and dried overnight at 40^{o}C.

5.3. Results and Discussion

5.3.1. Filtration of $CaCl_2$ and $MgSO_4$ Solutions

The modified membranes were used to filter simple salt solutions at 3.1 bar (45 psi). 500 ppm $CaCl_2$ and 2000 ppm $MgSO_4$ in DI water were used to compare flux and rejection data of the modified membranes to manufacturer's data of unmodified membranes. The data in Table 5.1 show a noticeable decrease in membrane flux due to SI-ATRP modification, as seen previously[12, 13]. In the presence of an alternating magnetic field (50 G, 10 Hz)[12, 13], the flux of the modified membranes increases. The increase in flux during magnetic field application--attributable to reduced concentration polarization--is roughly equal for each of the three modification conditions. The modified membranes also exhibited increased salt rejection in the absence of a field due to the grafted polyHEMA on the membrane selective layer adding additional resistance making the membranes tighter. Similar to flux, the rejection increased for all modified membranes in the presence of a magnetic field, again due to reduced concentration

polarization. The greatest increase in rejection and flux during field application was seen for the 4 hour modified membranes. The increase in flux and rejection in the presence of a field is due to small-scale mixing generated by the modified membranes.

The mechanism of magnetically-activated mixing has been described in detail previously[12]. Briefly, in the presence of an external magnetic field, the magnetic moments of the superparamagnetic nanoparticles align with the direction of the external field. This causes the polyHEMA chains to experience both a force and a torque, which causes the chains to move in the direction of the external field. When this external field is alternated at an appropriate frequency, the polyHEMA chains move back and forth as they align with the alternating field. This movement generates small scale mixing directly above the membrane surface and disrupts the boundary layer, which contains concentrated solutes from the feed. Reducing the concentration of solutes at the membrane surface greatly improves membrane performance. Data suggests that shorter polymer chains (4 hour SI-ATRP) yield the most effective mixing.; however, it is possible that even shorter chains may yield better mixing. Shorter polymer chains will have less drag and less entropic resistance to stretching than longer polymer chains. This allows the shorter polymer chains to be more easily moved, resulting in enhanced mixing compared to longer chains.

Table 5.1. Membrane flux and rejection of simple salt solutions at 3.1 bar (45psig) for unmodified and modified membranes.

	500 ppm $CaCl_2$				2000 ppm $MgSO_4$			
	Unmodified	**4 hr**	**6 hr**	**8 hr**	**Unmodified**	**4 hr**	**6 hr**	**8 hr**
				Salt Rejection (%)				
With Field	33.4 ± 0.2	40.4 ± 0.2	41.7 ± 0.2	44.3 ± 0.2	66.5 ± 0.2	74.4 ± 0.2	76.7 ± 0.2	80.0 ± 0.2
Without Field	32.5 ± 0.2	34.2 ± 0.2	37.8 ± 0.2	41.0 ± 0.2	66.0 ± 0.2	67.7 ± 0.2	68.4 ± 0.2	75.6 ± 0.2
				Flux ($L * m^{-2} * hr^{-1}$)				
With Field	13.4 ± 0.6	9.6 ± 0.7	8.8 ± 0.5	8.0 ± 0.3	5.4 ± 0.3	6.0 ± 0.4	5.6 ± 0.3	5.0 ± 0.2
Without Field	12.8 ± 0.6	7.8 ± 0.7	7.2 ± 0.5	6.5 ± 0.3	5.6 ± 0.4	4.0 ± 0.2	3.8 ± 0.2	3.3 ± 0.2

5.3.2. Filtration of Model Produced Water

5.3.2.1. Characteristics of Model PW vs. Realistic PW

A realistic PW was obtained from an operating oil production site in northern Colorado. Characteristics of this PW, hereafter labeled realistic PW, are collected in Table 5.2. Due to the variability of PW composition and properties, a model PW needed to be created to eliminate variability between various experiments. The model PW was modified from a previously used example which was a reasonable base solution for approximating PW[20, 21]. Due to the somewhat high salinity of the particular realistic PW used here, a high concentration and variety of salts were used in the model PW so the model and realistic PW affected the membranes more similarly. Table 5.3 shows some of the characteristics of both the model and realistic PW. The conductivity and TDS of the model PW are higher than the realistic PW to make the model PW foul more similarly to the realistic PW, which contains a greater variety of foulants. It is apparent that the realistic PW will have more complex characteristics—note the high levels of total carbon and nitrogen—than the simplified model PW; however, it is only necessary that the model PW approximate the fouling tendencies of the realistic PW.

Table 5.2. Characteristics and composition of realistic PW. All units are parts per million (ppm) unless otherwise stated.

pH	7.4	**Phosphorous**	0.02
Conductivity	1080 µS/dm	**Aluminum**	< 0.01
TDS	550	**Iron**	< 0.01
Total Carbon	<5	**Manganese**	< 0.01
Calcium	1.0	**Copper**	< 0.01
Magnesium	1.2	**Zinc**	< 0.01
Sodium	164.0	**Nickel**	< 0.01
Potassium	2.6	**Boron**	0.09
Chloride	201	**Molybdenum**	< 0.01
Sulfate	1.2	**Cadmium**	< 0.01
Total Nitrogen	23	**Chromium**	< 0.01
BOD	<10	**Barium**	0.11
Oils & Grease	<10	**Lead**	< 0.01
Turbidity	1.3 NTU	**Selenium**	< 0.01
Sodium Adsorption Ratio	26.2	**Salinity Hazard**	Med
		Sodium Hazard	Med

Table 5.3. Comparison of Model and Realistic PW.

	Realistic PW	Model PW
pH	7.9	8.1
Conductivity (µS/dm)	3100	3950
TDS (ppm)	2298	2470
Turbidity (NTU)	28	35
Total Carbon (ppm)	680	<10
Total Nitrogen (ppm)	450	<10

Both PWs were filtered through unmodified membranes at 4.83 bar (70 psi) to observe their fouling tendencies, as shown in Figure 5.1. As can be seen, the overall decrease in membrane flux is similar in magnitude and behavior for both PWs, although the model PW caused a much greater initial decrease in flux. The realistic PW, however, did result in a greater decrease in flux overall. This was expected since the realistic PW contains a multitude of fouling species, which are capable of complex interspecies interactions and interactions with the membrane, compared to the extremely simple composition of the model PW. This showed that this model PW recipe is a reasonable simulation for the realistic PW.

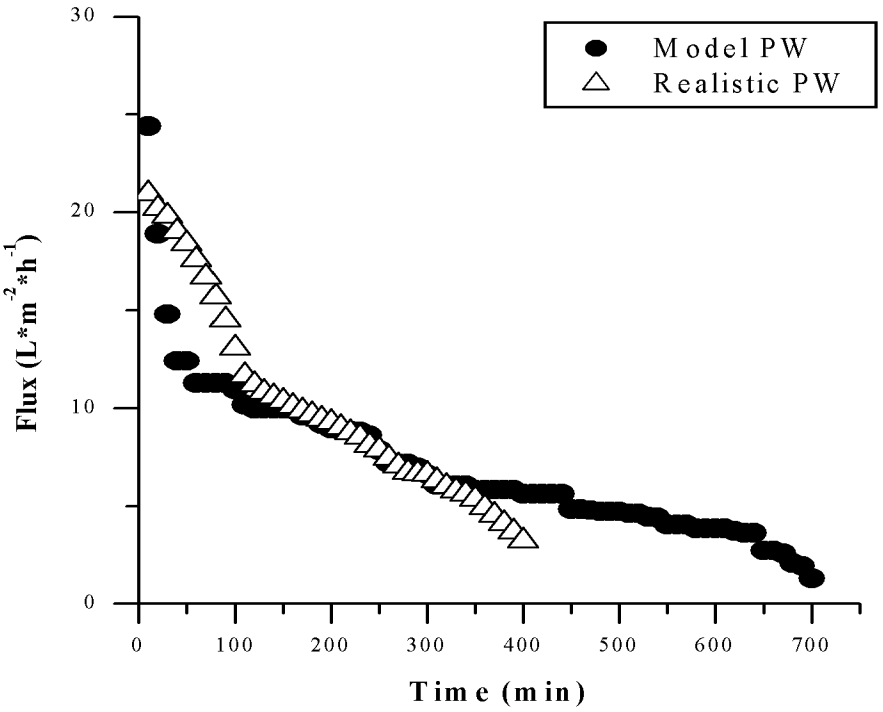

Figure 5.1. Comparison of membrane flux during filtration of model and realistic PW. Data points represent range of experimental values obtained for experiments in triplicate.

5.3.2.2. Optimization of Magnetic Field Application Interval

Table 5.1 shows that mixing in a magnetic field improved membrane performance; however, operating the field continuously would be prohibitively costly. Ideally, the system could be used sparingly as a short "cleaning" operation followed by a set time when it was off. The optimal balance between increased energy costs due to application of the field and decreased pumping costs due to increased flux during field application was needed. To determine the optimal magnetic field duration model PW was filtered 90 minutes at 3.79 bar (55 psi) with varying magnetic field durations. When the magnetic field was turned on (for 5, 10, or 30 seconds) the two solenoids were powered alternatively at a rate of 10 Hz as described above. The magnetic field was then turned off for a chosen amount of time ranging from 5 to 900

seconds before the field was turned on again. Tables 5.4 (a)-(c) show the average flux through the membrane after 90 minutes of model PW filtration for various modified membranes and magnetic field durations, along with associated energy costs. A representative pumping cost was calculated by averaging the power consumption of five commercially available pumps suitable for industrial settings. It should be noted that this analysis, although for dead-end filtration, was performed to verify that periodic field application improves membrane performance; however, tangential flow would be used in practice.

It is apparent that less off-time results in higher membrane flux, due to the surface mixing being active a greater percentage of the filtration time; however, this comes at the expense of higher energy costs to power the magnetic field. Conversely, higher flux results in lower energy costs associated with pressurizing and pumping a given volume of feed due to the quicker filtration. The ratio of flux to net energy cost (field energy costs plus pumping costs) was calculated, shown in the far-right column. The optimal field duration was 10 seconds on followed by 120 off for each of the three modification conditions; however, on/off times of 10/10, 10/30, 10/60, 30/30, and 30/60 performed almost as well. Another factor in choosing the 10/120 duration was to minimize the time the magnetic field was powered compared to the five other well-performing durations mentioned above. For the 10/120 case the flux to net energy cost ratio was 2.9, 2.4, and 1.8 times greater than the unmodified membranes for the 4, 6, and 8 hour modifications, respectively. Based on these experiments, the 4 hour modified membrane is the best modification because it yields the greatest increase in flux compared to overall cost.

Table 5.4. Membrane performance and operating costs for (A) 4 hour, (B) 6 hour, and (C) 8 hour modified membranes treating model PW for 90 minutes at 3.79 bar (55 psi). All fluxes are ± 0.15 Lmh.

Table 5.4 (A). 4 Hour SI-ATRP Modification.

Time on (s)	Time off (s)	Flux (Lmh)	Energy Cost (kWhr / 1000 L)	Pumping Cost (kWhr / 1000 L)	Net Cost (kWhr / 1000 L)	Flux / Net Cost
Unmod	Continuous	3.80	0.00	31.58	31.58	12.0
0	Continuous	3.00	0.00	40.00	40.00	7.5
5	5	5.82	17.18	20.62	37.80	15.4
5	10	5.71	11.68	21.02	32.69	17.5
5	30	5.64	5.07	21.28	26.34	21.4
5	60	5.54	2.78	21.66	24.44	22.7
10	10	8.68	11.52	13.82	25.35	34.2
10	30	7.64	6.54	15.71	22.25	34.3
10	60	7.21	3.96	16.64	20.61	35.0
10	120	6.93	2.22	17.32	19.54	35.5
10	180	5.25	2.01	22.86	24.86	21.1
10	240	4.81	1.66	24.95	26.61	18.1
10	300	4.73	1.36	25.37	26.73	17.7
30	30	8.51	11.75	14.10	25.85	32.9
30	60	7.85	8.49	15.29	23.78	33.0
30	300	5.11	3.56	23.48	27.04	18.9
30	600	3.93	2.42	30.53	32.96	11.9
30	900	3.57	1.81	33.61	35.42	10.1

Table 5.4 (B). 6 Hour SI-ATRP Modification.

Time on (s)	Time off (s)	Flux (Lmh)	Energy Cost (kWhr / 1000 L)	Pumping Cost (kWhr / 1000 L)	Net Cost (kWhr / 1000 L)	Flux / Net Cost
Unmod	Continuous	3.80	0.00	31.58	31.58	12.0
0	Continuous	2.80	0.00	42.86	42.86	6.5
5	5	4.76	21.01	25.21	46.22	10.3
5	10	4.67	14.28	25.70	39.97	11.7
5	30	4.60	6.21	26.09	32.30	14.2
5	60	4.55	3.38	26.37	29.75	15.3
10	10	7.18	13.93	16.71	30.64	23.4
10	30	6.52	7.67	18.40	26.07	25.0
10	60	6.10	4.68	19.67	24.36	25.0
10	120	5.97	2.58	20.10	22.68	26.3
10	180	4.20	2.51	28.57	31.08	13.5
10	240	4.24	1.89	28.30	30.19	14.0
10	300	4.15	1.55	28.92	30.47	13.6
30	30	7.28	13.74	16.48	30.22	24.1
30	60	6.37	10.47	18.84	29.30	21.7
30	300	4.18	4.35	28.71	33.06	12.6
30	600	3.24	2.94	37.04	39.98	8.1
30	900	3.01	2.14	39.87	42.01	7.2

Table 5.4 (C). 8 Hour SI-ATRP Modification.

Time on (s)	Time off (s)	Flux (Lmh)	Energy Cost (kWhr / 1000 L)	Pumping Cost (kWhr / 1000 L)	Net Cost (kWhr / 1000 L)	Flux / Net Cost
Unmod	Continuous	3.80	0.00	31.58	31.58	12.0
0	Continuous	2.30	0.00	52.17	52.17	4.4
5	5	3.58	27.93	33.52	61.45	5.8
5	10	3.54	18.83	33.90	52.73	6.7
5	30	3.52	8.12	34.09	42.21	8.3
5	60	3.49	4.41	34.38	38.79	9.0
10	10	5.28	18.94	22.73	41.67	12.7
10	30	4.93	10.14	24.34	34.48	14.3
10	60	4.68	6.11	25.64	31.75	14.7
10	120	4.59	3.35	26.14	29.50	15.6
10	180	3.21	3.28	37.38	40.66	7.9
10	240	3.24	2.47	37.04	39.51	8.2
10	300	3.19	2.02	37.62	39.64	8.0
30	30	5.71	17.51	21.02	38.53	14.8
30	60	4.86	13.72	24.69	38.41	12.7
30	300	3.27	5.56	36.70	42.26	7.7
30	600	2.61	3.65	45.98	49.63	5.3
30	900	2.43	2.65	49.38	52.04	4.7

5.3.2.3. Long-term Performance of Membranes during filtration of model PW

The modified membranes were used to treat model PW at the optimal field conditions (50 G, 10 Hz, 10 s on, 120 s off) for extended periods to test the long-term benefits of the activated mixing. The model PW was filtered for 700 minutes at 4.83 bar (70 psi), as shown in Figure 5.2. It should be noted that the data points for the 6 hour ATRP modification were omitted to ease legibility of the figure. The 6 hour modification flux, both with and without the field, was roughly halfway between the 4 and 8 hour modifications. When the magnetic field is applied the flux of all three modified membranes increases by roughly 25% or more. The increase is roughly equal throughout the experiment. This confirms that not only the modification but also the response of the modified membranes is permanent and is reliable over long filtration times.

The data show that the flux through the unmodified membranes was initially higher than the 3 modified membranes; however, the unmodified flux decreased extremely rapidly so that the flux of all 4 membranes with no field was roughly equal between 30 and 240 minutes. After 240 minutes, the flux of the unmodified membrane is lower than all of the unmodified membranes, even in the absence of a field. The flux through the modified membranes decreases much less than the unmodified membrane, confirming that the magnetically-activated mixing is capable of reducing membrane fouling. Although the modification process decreases the membrane flux, the benefits of modification and mixing lead to greater membrane performance over time.

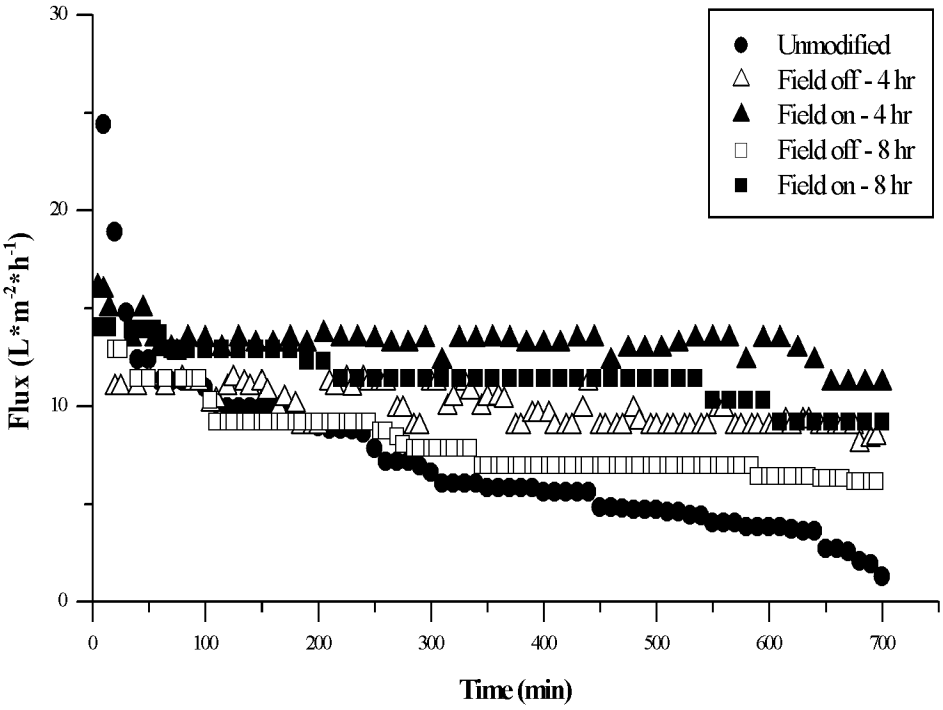

Figure 5.2. Membrane flux during filtration of model PW for unmodified and modified membranes. The magnetic field was applied for 10 seconds, followed by 120 seconds of non-application. 6 hr data was omitted for legibility. Data points represent range of experimental values obtained for experiments in triplicate.

Figures 5.3 and 5.4 plot the TDS concentration and conductivity of the model PW permeate of each of the four membranes tested during the 700 minute filtration experiments. Initially, the permeate quality is identical for the four membranes; however, as with the membrane flux, the permeate quality of the unmodified membrane rapidly decreases. The three modified membranes performed better than the unmodified membrane, showing less decline in permeate quality. The 4 hour modified membrane showed the least permeate quality decrease, in agreement with the least flux decline in Figure 5.2, confirming that the 4 hour modified membrane exhibits the best improvements in membrane performance due to mixing.

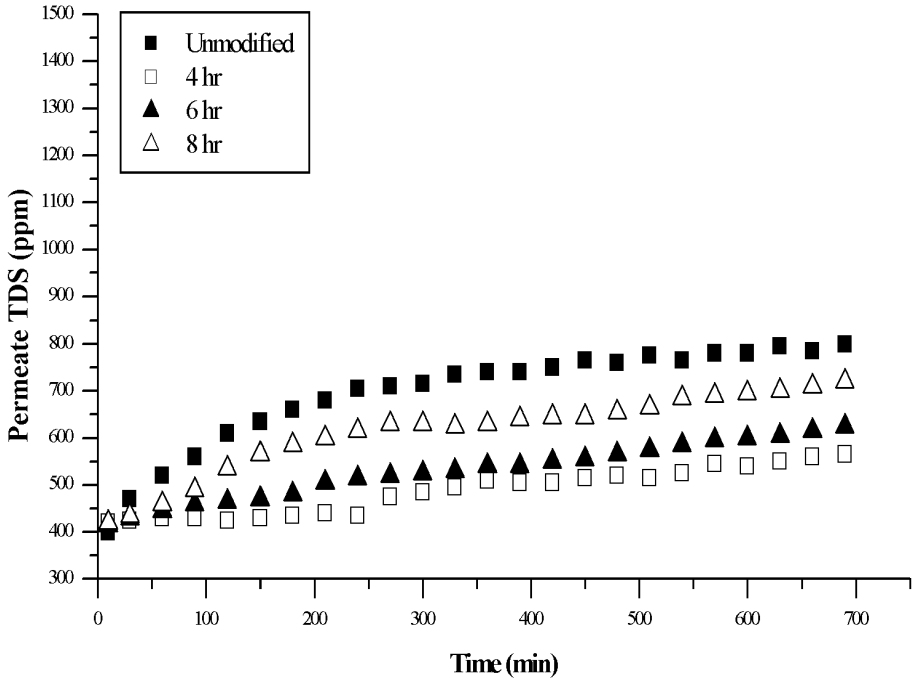

Figure 5.3. Total dissolved solids (TDS) concentration of permeate during filtration of model PW. Data points represent range of experimental values obtained for experiments in triplicate.

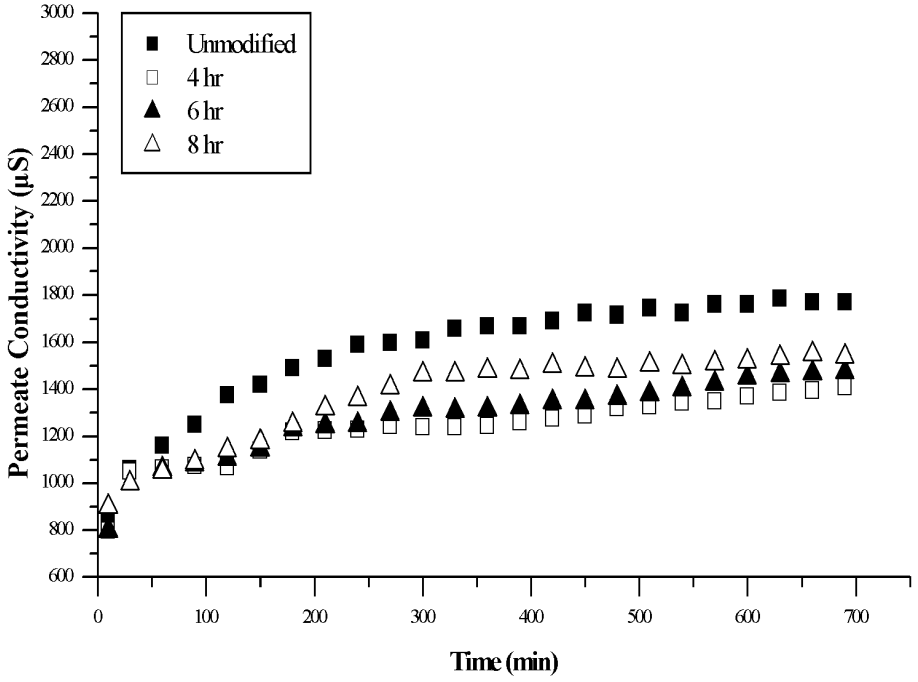

Figure 5.4. Conductivity of permeate during filtration of model PW. Data points represent range of experimental values obtained for experiments in triplicate.

Following the 700 minute filtration, the membranes were washed using the protocol described above. This washing step was not exhaustive, but designed to approximate a short, basic, periodic maintenance procedure in a membrane operation, for example back flushing. Ideally, this procedure would remove loosely deposited contaminants on the membrane surface and restore the membrane performance (flux and solute rejection) to a high percentage of their original, pre-fouled values. The washing cycle was applied following 700 minutes of filtration, an additional 180 minutes of filtration (880 minutes total), and finally after another 180 minutes of filtration (1060 minutes total). Figures 5.5 – 5.7 show the membrane flux, permeate TDS, and permeate conductivity following the repeated washings. The four membranes had roughly the same membrane flux immediately following the first washing procedure. The unmodified membrane showed the worst flux recovery, only achieving 40% recovery of its original flux (10 Lmh post-washing vs. 25 Lmh initially). The three modified membranes fared much better, with flux recoveries near 70%. Additionally, the unmodified flux decreased steadily with increasing filtration time while the modified fluxes remained almost constant, mirroring the behavior seen in Figure 5.2. Similar behavior is seen following the second and third washings. Importantly, the flux of the modified membranes returns to the same value (roughly 10 Lmh) following the first two washing cycles while the flux of the unmodified membrane continues to decrease. Following the third washing, the unmodified flux is only 25% of its value at time zero, while the flux of the three modified membranes remains at roughly 65% of their initial values. Also of note is that the magnetic response of the modified membranes (flux with field on vs. off) is still present following the multiple washings, and is practically identical to the response seen throughout the first 700 minutes of filtration. Both the modification and the response are permanent and can withstand lengthy use with multiple washings.

The permeate quality of the four membranes following multiple washings and subsequent filtration follow a similar pattern as the membrane flux, compare Figures 5.6 and 5.7 with Figures 5.3 and 5.4. The rejection of the unmodified membrane was permanently affected by the fouling caused by the lengthy filtration, and the permeate quality markedly suffers. The 4 and 6 hour modified membranes faired much better. The permeate quality shows only a roughly20% decrease following the first washing. The permeate quality following the two subsequent washings is practically equal to those following the first washing (roughly500 ppm and roughly1000 μS). Curiously, although the 8 hour modified membrane exhibited good flux recovery following repeated washings, its permeate quality is noticeably poorer than the 4 and 6 hour membranes. Based upon these results, the 4 and 6 hour modified membranes were chosen for testing with the realistic PW. Filtration of model PW showed that the magnetically-activated mixing is able to reduce membrane fouling, leading to less flux decline, improved permeate quality, and greater flux recovery following simple washings.

These dead-end filtration results confirm that magnetically-activated mixing reduces concentration polarization, leading to improved membrane performance. In practice, membrane filtration is performed in tangential (or cross-flow) filtration. The cross-flow velocity serves to reduce concentration polarization and mix the feed. Future studies will test the magnetic effect in tangential flow. It is not known if magnetic mixing will yield the same improvements in tangential flow; however, proof of concept for magnetically-responsive membranes has been shown.

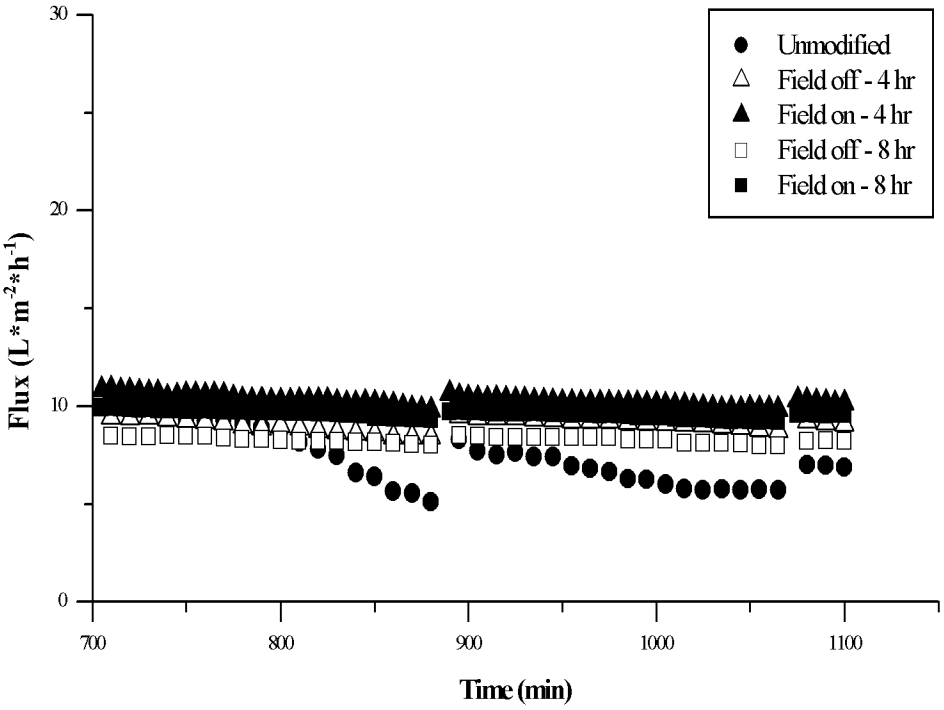

Figure 5.5. Membrane flux during filtration of model PW for unmodified and modified membranes following repeated washing procedures. The magnetic field was applied for 10 seconds, followed by 120 seconds of non-application. Data points represent range of experimental values obtained for experiments in triplicate.

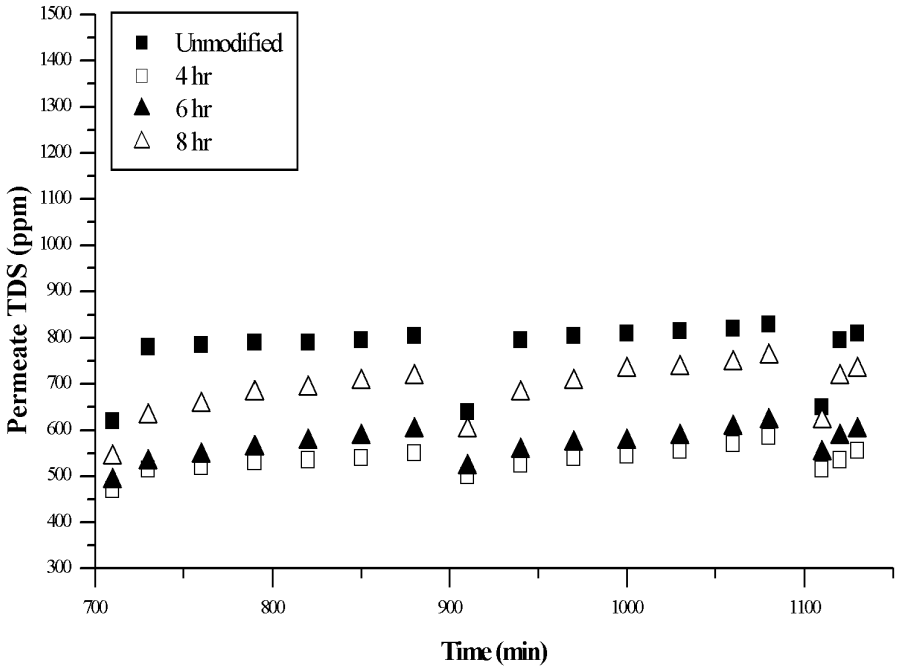

Figure 5.6. Total dissolved solids (TDS) concentration of permeate during filtration of model PW following repeated washing procedures. Data points represent range of experimental values obtained for experiments in triplicate.

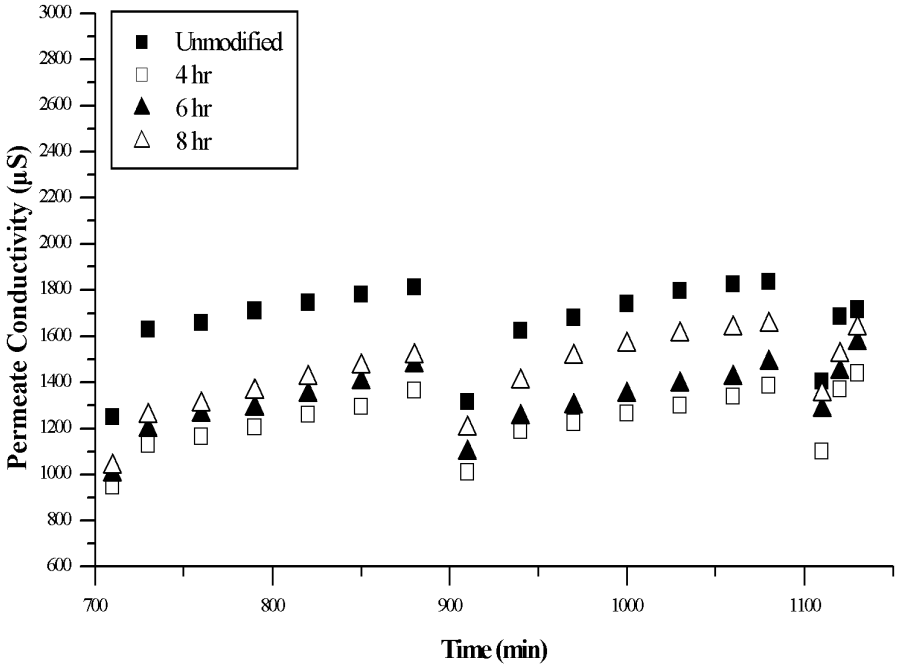

Figure 5.7. Conductivity of permeate during filtration of model PW following repeated washing procedures. Data points represent range of experimental values obtained for experiments in triplicate.

5.3.3. Filtration of Realistic PW

Unmodified membranes as well as membranes modified for 4 and 6 hours SI-ATRP were used to filter realistic PW. The 8 hour modified membranes were not used here because they did not improve membrane performance as much as the other two modifications based on the model PW tests. The same conditions as the model PW tests were used for the realistic PW—4.83 bar (70 psi), 10 seconds magnetic field on, 120 seconds field off, and the same filtration/washing procedure. The membrane flux during the initial 700 minutes of filtration is shown in Figure 5.8. The unmodified membrane was stopped early (400 minutes) because the flux had become extremely low. As with the model PW, the modified membranes showed much less flux decline than the unmodified membrane, although the gross flux decrease is slightly greater during filtration of the realistic PW. This was expected because the realistic PW has a greater fouling tendency than the model PW, see Figure 5.1. Importantly, the flux improves noticeably while the field is being applied, even at the end of the 700 minute experiment. This agrees with observations during filtration of model PW; the improvement of flux due to the magnetically-activated mixing is a permanent character of the membrane, and the magnitude of the response is roughly constant even after hours of filtration. Again, these results are for proof-of-concept dead-end filtration. Future studies will investigate the improvements of magnetically-activated mixing in tangential flow.

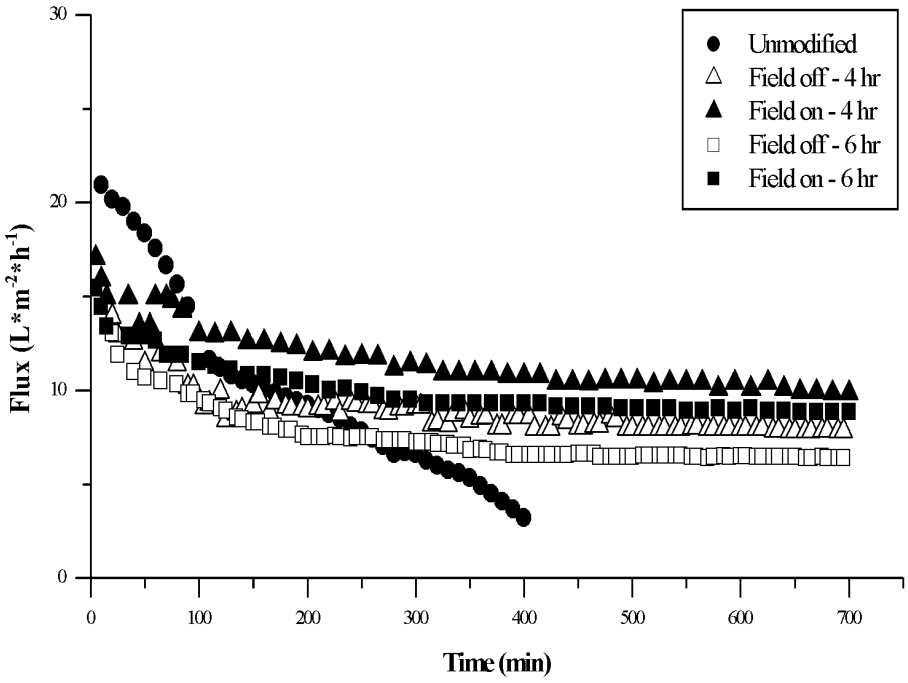

Figure 5.8. Membrane flux during filtration of realistic PW for unmodified and modified membranes. The magnetic field was applied for 10 seconds, followed by 120 seconds of non-application. Data points represent range of experimental values obtained for experiments in triplicate.

The permeate quality during filtration of realistic PW is shown in Figures 5.9 and 5.10. Again, the overall behavior is similar to what was observed for the model PW—Figures 5.3 and 5.4—confirming that the model PW was a reasonable approximation of the realistic PW. As with the model PW, the permeate quality of the unmodified membrane rapidly worsens while the modified membranes maintain a greater rejection throughout the experiment. As with the model PW, the 4 hour modified membranes performed the best during filtration of realistic PW.

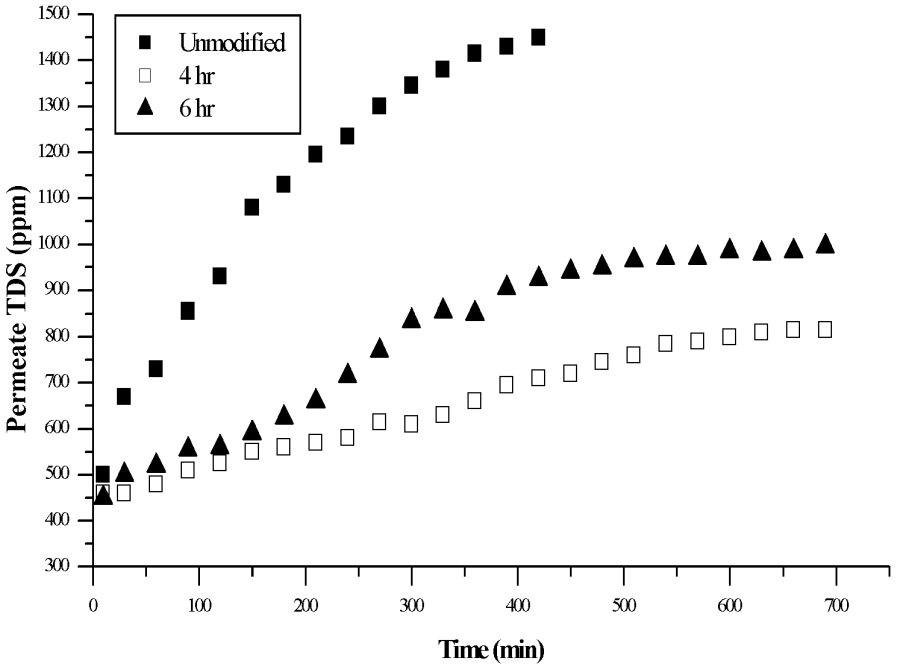

Figure 5.9. Total dissolved solids (TDS) concentration of permeate during filtration of realistic PW. Data points represent range of experimental values obtained for experiments in triplicate.

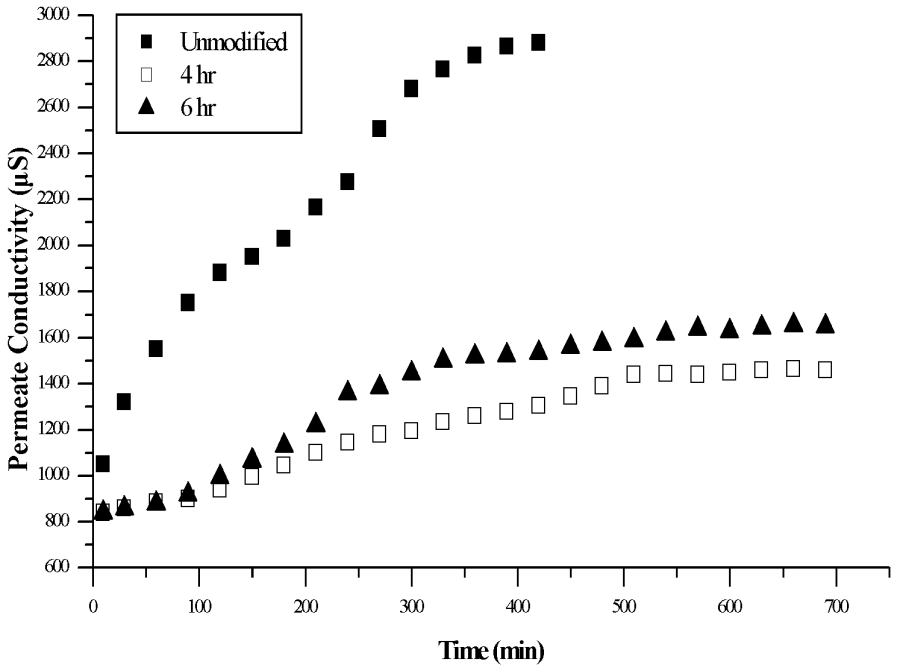

Figure 5.10. Conductivity of permeate during filtration of realistic PW. Data points represent range of experimental values obtained for experiments in triplicate.

Following the initial 700 minutes of filtration, the membranes were put through the same wash and filtration cycle as for the model PW. The effect of washing cycles and subsequent filtration on membrane flux and permeate quality, see Figures 5.11 – 5.13, are quite similar to those seen for model PW. Again the unmodified membrane performed poorly in subsequent tests exhibiting low flux and permeate quality recovery. The modified membranes performed better, showing that the magnetically-activated mixing reduces permanent deposition of foulants on the membrane surface and its effects on membrane performance. The data confirm that the model PW is a reasonable approximation of the realistic PW, which means it may be used to test future membrane modifications and/or cleaning schemes without using realistic PW, which is a limited resource. The 4 hour SI-ATRP modified membranes performed best during filtration of both model PW and realistic PW for the reasons discussed previously. It should be noted that the total time for the unmodified membrane is actually 400-760 minutes, not 700-1060, because the first filtration was stopped at 400 minutes rather than 700.

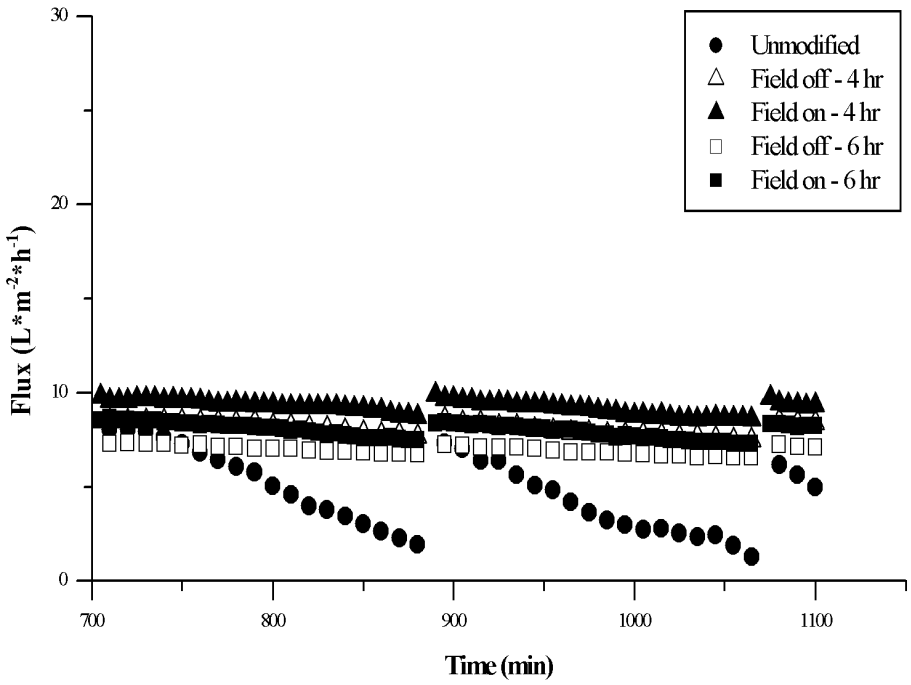

Figure 5.11. Membrane flux during filtration of realistic PW for unmodified and modified membranes following repeated washing procedures. The magnetic field was applied for 10 seconds, followed by 120 seconds of non-application. Data points represent range of experimental values obtained for experiments in triplicate.

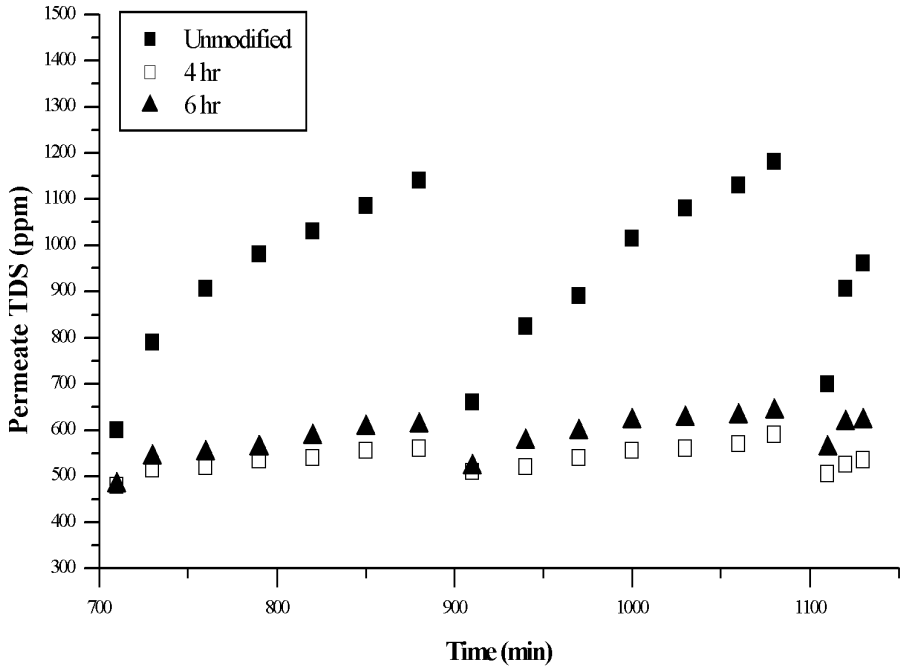

Figure 5.12. Total dissolved solids (TDS) concentration of permeate during filtration of model PW following repeated washing procedures. Data points represent range of experimental values obtained for experiments in triplicate.

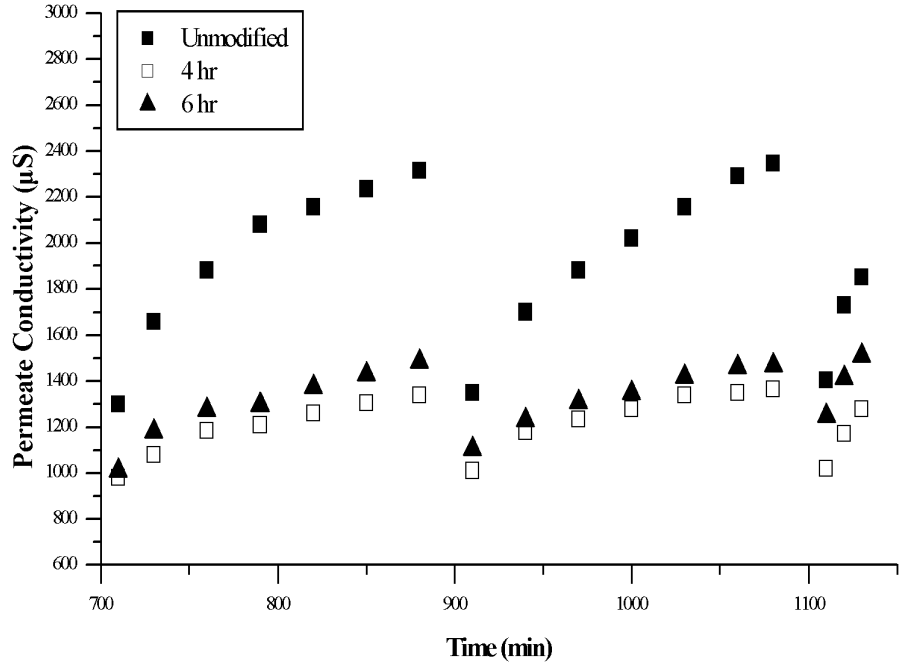

Figure 5.13. Conductivity of permeate during filtration of model PW following repeated washing procedures. Data points represent range of experimental values obtained for experiments in triplicate.

5.3.4. Effect of Realistic PW Filtration on Membranes

The 4 hour SI-ATRP modified membranes performed the best during filtration of both realistic and model PW. These membranes showed the least degree of flux and permeate quality decline as well as the greatest recovery of performance following washings. Both ATR-FTIR and SEM were used to better characterize the improvements in membrane performance of the 4 hour modified membranes compared to the unmodified membranes. These showed that the modified membranes did indeed decrease the degree of irreversible fouling on the membrane surface, which was postulated based on the filtration data.

5.3.4.1. ATR-FTIR

ATR-FTIR spectroscopy was used to characterize the chemistry of the surface of both unmodified and 4 hour modified membranes before and after washing following filtration of realistic PW. Figure 5.14 presents the spectra (from bottom to top) of the unmodified NF 270 membrane, the 4 hour modified membrane after washing, modified membrane before washing, unmodified membrane after washing, and unmodified membrane before washing. The unmodified membrane shows a number of distinct peaks between 600 and 1700 cm^{-1} corresponding to numerous C-C, C-H, and C-O bonds associated with the underlying membrane structure. There is also a series of small peaks between 2850 and 3050 cm^{-1} corresponding to symmetric CH_2 stretching and asymmetric CH_2 and CH_3 stretching, again related to the polymeric structure of the membrane. Following realistic PW filtration, see Table 5.2, a broad peak appears centered at 3300 cm^{-1} (alcohols and carboxylic acid) and sharp peaks appear at 2350 cm^{-1} (nitriles) and 3500-4000 cm^{-1} (alcohols and secondary amines)—see the two before washing (B. W.) spectra. Additionally, the sharp peaks at 2850-3050 cm^{-1} increase in

magnitude. These new peaks, and larger CH_2/CH_3 stretching peaks, confirm that fouling occurred on the membrane surface, which can be attributed to the larger number of both organic and inorganic foulants in the realistic PW.

It is apparent that the modified membranes reduced the amount of fouling on the membrane surface, particularly fouling by compounds containing nitrogen. Additionally, the modified membranes were easier to clean. Comparing the before and after washing spectra of the unmodified membranes, the peaks associated with the fouling layer, noticeably those at 2350 and 3300 cm^{-1}, were reduced, but still distinctive. In contrast, all of the peaks associated with the fouling layer on the modified membrane were almost completely removed. Only remnants of the peaks at 3300 and 3500-4000 cm^{-1} remain, and the peak at 2350 cm^{-1} is no longer present. It should be noted that the modification itself had no significant effect on the ATR-FTIR spectrum of the membranes (not shown). This was expected because only the very topmost layer of the membrane was modified, and ATR-FTIR reports the average chemical composition of the topmost 1 μm. The modification does not comprise a significant enough percentage of the total membrane to be seen on ATR-FTIR. X-ray photoelectron spectroscopy (XPS) was used previously to characterize the topmost 10 nm of the membrane to observe changes due following modification[12, 13].

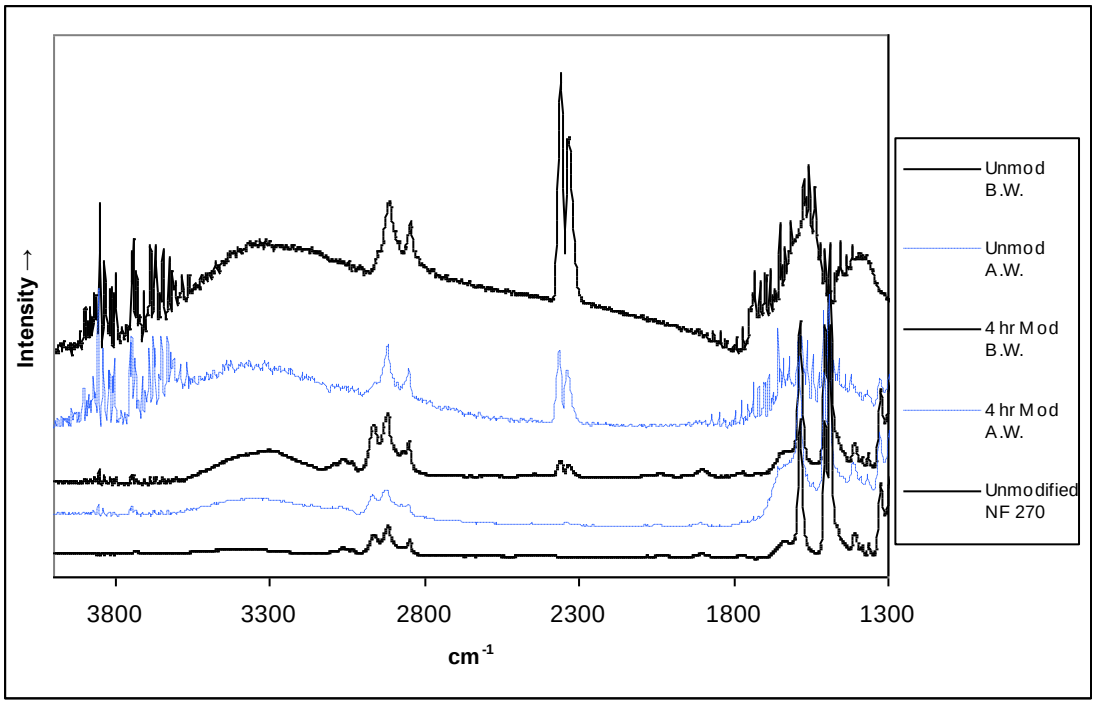

Figure 5.14. ATR-FTIR spectra showing the effect of fouling due to filtration of PW using unmodified and 4 hour SI-ATRP modified membranes. B. W. and A. W. stand for before and after washing, respectively.

5.3.4.2. FESEM

To better understand the nature of the fouling layer and why the modified membranes were easier to clean, FESEM was used to image the membrane surfaces both before and after washing. FESEM micrographs of unmodified and 4 hour SI-ATRP modified membranes following filtration of realistic PW are shown in Figure 5.15 (a)-(f). Image (a) shows an unmodified membrane (at 100x magnification) following filtration with the realistic PW. A thick film has covered the entire membrane surface. Large formations of salts, which exceeded their saturation concentration, can be seen as well as a thick underlying film consisting of various other foulants. Image (b) shows an unmodified membrane (at 100x magnification) used to filter realistic PW after it has been washed using the periodic washing procedure described above. It is clear that very little, if any, of the foulant layer has been fully removed; however, the film does

appear thinner in some areas. The resistance of the film to washing leads to the poor flux and rejection recoveries observed during the filtration experiments, see Figures 5.11 - 5.13. Images (c) and (d) show a 4 hour SI-ATRP modified membrane following filtration of realistic PW before and after washing at 100x magnification, respectively. It is readily apparent that there is less fouling on the modified membrane surface following filtration. Also, the fouling is isolated to smaller distinct areas, rather than forming a thick film over the entire surface. Following the washing procedure, the membrane surface appears rather clean, with only a small amount of deposition on the surface. The magnetically-activated mixing not only reduces fouling during filtration, but also eases membrane cleaning. The FESEM images confirm the filtration results seen earlier where the membrane flux and rejection of the modified membranes not only decreased less than the unmodified, but also recovered to a greater degree following cleaning, see Figures 5.11 – 5.13. Finally, images (e) and (f) are 10,000x magnification images of (b) and (d), respectively. Here it is seen that the fouling which occurred on the unmodified membrane is a quite dense, connected film while the fouling on the modified membrane is a collection of loosely deposited foulants. The periodic mixing appears to be sufficient to disperse foulants above the membrane surface and prevent film formation. It is for this reason that the fouling is less severe and more easily cleaned for the modified membrane.

An initial concern was that the carboxylic acid coating of the SPNPs might increase fouling. This was not seen for a few reasons. Firstly, the magnetically-activated mixing reduced concentration polarization. Secondly, previous studies (Chapters 2 and 3) showed that membrane contact angle and zeta potential were practically unchanged following modification. This suggests that neither the grafted chains nor the SPNPs had an appreciable effect on the fouling propensity of the membrane.

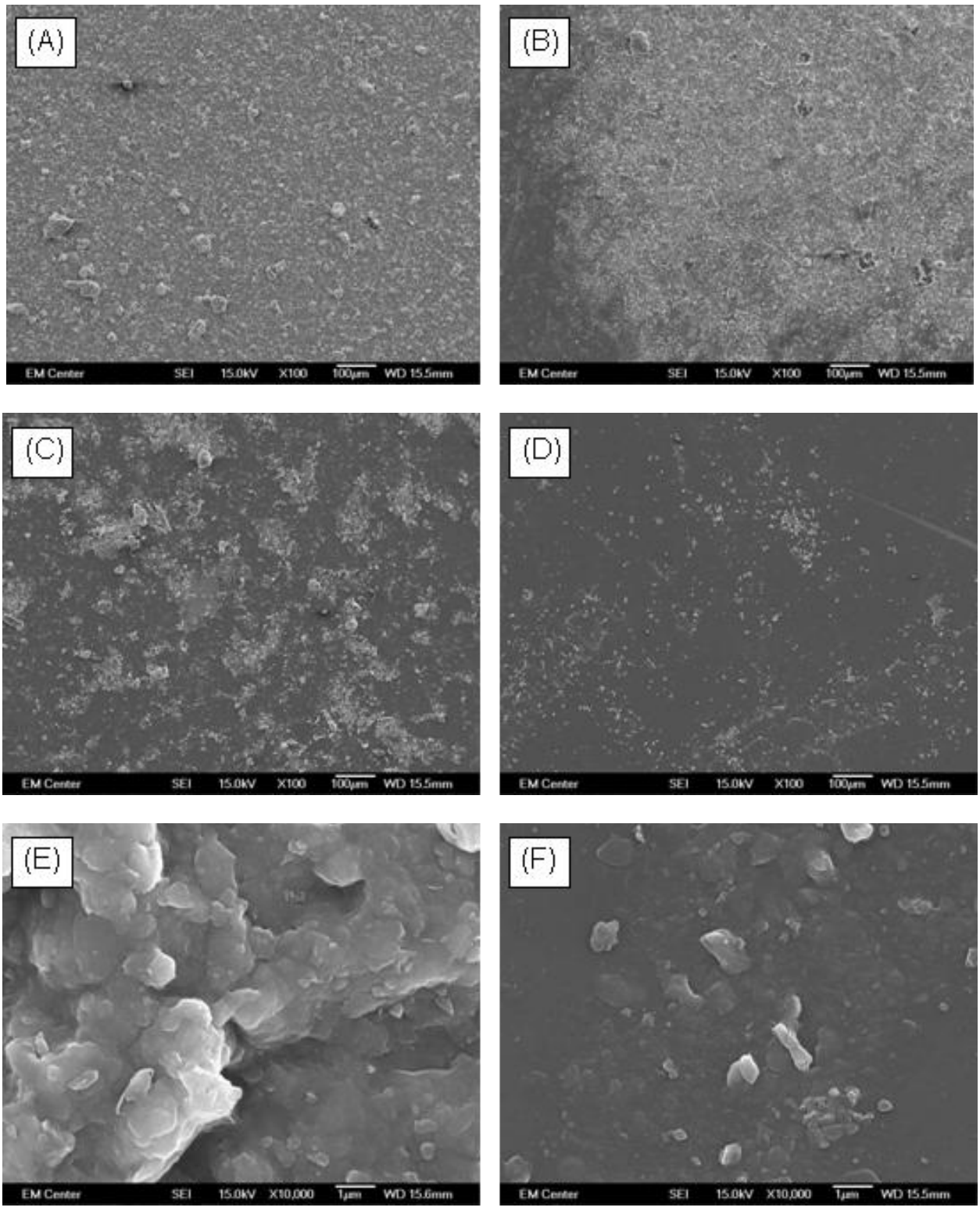

Figure 5.15. 100x magnification of unmodified (A-B) and 4 hour modified (C-D) membranes following filtration of realistic PW before washing and after washing. Additional, higher magnification (10,000x) image of both membranes following filtration as well as washing (E-F).

5.4. CONCLUSIONS

Modified nanofiltration membranes capable of generating small scale mixing in the presence of an alternating magnetic field were used to treat simple salt solutions, a model PW, and a realistic PW. The effect of various modification lengths and magnetic field durations was studied. In the proper conditions mixing generated by the modified membranes lead to less flux decline, better permeate quality, and reduced energy consumption compared to unmodified nanofiltration membranes during treatment of a model PW. The modified membranes also performed significantly better than the unmodified during treatment of a realistic PW. The improved performance of the modified membranes during the treatment of the realistic PW suggests that these membranes could be used on-site to treat PW more efficiently and to higher quality than current membrane processes. PW treated using magnetically-activated micromixer membranes could yield a new clean water permeate—which could alleviate water demand in arid regions—from a PW stream which has historically been discarded as waste.

REFERENCES

1. R. W. Baker, Membrane technology and applications, 2nd ed, 2004, Chichester: Wiley.
2. W. S. W. Ho, K. K. Sirkar, Eds. Membrane Handbook, 1992, Norwell: Kluwer.
3. N. N. Li, A. G. Fane, W. S. W. Ho, T. Matsuura, Eds. Advanced membrane technology and applications, 2008, Hoboken: J. Wiley & Sons.
4. M. Ulbricht, Advanced functional polymer membranes, Polymer, 47(2006) 2217-2262.
5. D. Wandera, S.R. Wickramasinghe, S.M. Husson, Stimuli-responsive membranes, J. Mem. Sci. 357 (2010) 6-35.
6. J. Gilron, S. Belfer, P. Väisänen, M. Nyström, Effects of surface modification on antifouling and performance properties of reverse osmosis membranes, Desalination 140 (2001) 167-179.
7. B. Van der Bruggen, L. Braeken, C. Vandecasteele, Flux decline in nanofiltration due to adsorption of organic compounds, Separation and Purification Technology. 29 (2002) 23–31.
8. L. Braeken , K. Boussu, B. van der Bruggen, C. Vandecasteele, Modeling of the Adsorption of Organic Compounds on Polymeric Nanofiltration Membranes in Solutions Containing Two Compounds, ChemPhysChem, 6 (2005) 1606 – 1612.
9. M.A. Stuart, W.T. Huck, J. Genzer, M. Müller, C. Ober, M. Stamm, G.B. Sukhorukov, I. Szleifer, V.V. Tsukruk, M. Urban, F. Winnik, S. Zauscher, I. Luzinov, S. Minko, Emerging applications of stimuli-responsive polymer materials. Nat. Mat. 9 (2010) 101-113.
10. D.M. He, H. Susanto, M. Ulbricht, Photo-irradiation for preparation, modification and stimulation of polymeric membranes. Prog. Polym. Sci. 34 (2009) 62-98.
11. K. Vanherck, S. Hermans, T. Verbiest, I. Vankelecom, Using the photothermal effect to improve membrane separations via localized heating. J. Mat. Chem. 21 (2011) 6079-6087
12. H. H. Himstedt, Q. Yang, L. P. Dasi, X. Qian, S. R. Wickramasinghe, M. Ulbricht, Magnetically-activated micromixers for separation membranes. Langmuir. 27 (2011) 5574-5581.
13. H. H. Himstedt, Q. Yang, X. Qian, S. R. Wickramasinghe, M. Ulbricht, Toward remote-controlled valve functions via magnetically-responsive capillary pore membranes, J. Mem. Sci. 423-424 (2012), 257-266.
14. M. Cakmakci, N. Kayaalp, I. Koyuneu, Desalination of produced water from oil production fields by membrane processes. Desalination, 222 (2008) 176-186.
15. K. L. Benko, J. E. Drewes, Produced water in the western United States: Geographical distribution, occurrence, and composition. Environ. Eng. Sci., 25(2008) 239-246.
16. P. Czermak. Multiphase Cross-flow Filtration Process for Efficient Treatment of Oil-field Produced Water Using Ceramic Membranes. 7th Produced Water Workshop. April 2009.
17. National Research Council of the National Academies, Management and effects of coalbed methane produced water in the western United States, 2010, Washington D.C.: The National Academies Press.
18. M. Arfie, E. Marika, E.S. Purbodiningrat, H.A. Woodard. Implementation of slurry fracture injection technology for E&P Wastes at Duri Oilfield. SPE Asia Pacific Health, Safety and Environment Conference and Exhibition, Malaysia. 2005.
19. J. W. M. de Graff, Acidic waste disposal by underground injection. Journal of Geochemical Exploration, 62 (1998) 325-329.
20. D. Wandera, S. R. Wickramasinghe, S. M. Husson, Modification and characterization of ultrafiltration membranes for treatment of produced water. J. Mem. Sci. 373 (2011) 178-188.

21. D. Wandera, H. H. Himstedt, M. Marroquin, S. R. Wickramasinghe, and S. Husson, Modification of ultrafiltration membranes with block copolymer nanolayers for produced water treatment: The roles of polymer chain density and polymerization time on performance. J. Mem. Sci. 403-404 (2012) 250-260.

CHAPTER 6

TREATMENT OF PRODUCED WATER BY MAGNETICALLY-ACTIVATED MICROMIXING MEMBRANES TO OBTAIN IRRIGATION WATER

Produced water permeate from treatment using modified nanofiltration membranes is applied as irrigation water to seeds from four crop species and two soils characteristic of Colorado. 1/3, and possibly 2/3, dilutions of treated produced water could be used as irrigation water with no significant impact on germination rates or soil properties.

I treated realistic produced water using magnetically-responsive membranes, following the same modification protocol as in Chapter 5, to treat realistic produced water. I performed all of the seedling germination and soil hydraulic conductivity experiments; however, Mr. Troy Bauder and Dr. Greg Butters guided me extensively in my experiment selection, and offered invaluable advice.

SUMMARY

Produced water is a by-product of hydrocarbon energy, including oil and gas production and alternative fuels. It is by far the largest volume stream associated with energy production. Treatment of produced water by traditional unit operations is challenging because the treatment must be tailored for each composition. Membrane filtration is a promising technique for produced water treatment due to its flexibility and lower energy costs; however, fouling and permeate quality are major concerns. A new type of fouling resistant membrane, which generates micromixing in an alternating magnetic field, is used here to treat produced water. The membranes remove a majority of the oils, metals, and other solutes resulting in a clean water permeate. Mixing generated by the modified membranes in an alternating magnetic field greatly improved performance. Membrane fouling was significantly reduced in a field, leading to greater membrane flux, easier cleaning, and cleaner treated water permeate. Dilutions of this permeate were tested as irrigation waters by studying seedling germination rates and change in soil properties when treated with the sample waters. Certain dilutions were shown to be statistically indistinguishable from control conditions, suggesting that the treated permeate could be used as irrigation water. This would reduce the volume of fresh water used for irrigation and the volume of waste discharge at alternative fuel production sites.

Financial support was provided by the Strategic Environmental Research and Development Program WP-1670 (USA) and a DoD NDSEG graduate fellowship (USA). Soil percolation studies were performed in Dr. Greg Butters' laboratory. PW filtration and seedling germination were performed in Dr. Chris Snow's laboratory. Mr. Reagan Waskom and Mrs. Julie Kallenberger helped in obtaining the PW. Jordan Driscoll and David Gleason performed the soil texture characterization and obtained the sandy soil, respectively. The Colorado Seed

Laboratory oversaw the protocols for the seedling germination study. Seeds and the loam soil were obtained via CSU ARDEC. Mr. Aaron Brown, Mr. Chris Fryrear, Mr. Mark McMillian, and Mr. Barry Ogg supplied the seeds.

6.1. INTRODUCTION

Oily wastewaters known as produced water (PW) are a co-product of all oil and gas production, including alternative fuel sources such as coal bed methane, tar sand, and oil shale. Billions of barrels of PW are produced annually in the United States, and this number is increasing each year as more alternative fuel exploration takes place[1]. Numerous oil and gas operations are located in the arid western United States, particularly Wyoming and Colorado, where water rights and clean water supply are large issues. Although PW composition varies widely with location, common concerns are high levels of total dissolved solids (TDS), high electrical conductivity, and numerous species such as fatty acids and oils as well as numerous other organics and inorganics which make treatment difficult[1,2]. This large volume of water has traditionally been discarded as waste; however, both discharge to surface waters and reinjection are problematic[1,2]. Treating PW to obtain beneficial waters such as irrigation or chemical process makeup water, rather than simply disposing of the PW, represents a great opportunity and an emerging field with the potential to provide an extremely large volume of beneficial water to the areas surrounding hydrocarbon production sites.

Synthetic membranes have become important tools for separation engineering because they can perform continuously with reduced operating costs and a smaller footprint compared to traditional unit operations[3-5]. Membranes have been used to treat PW but their performance is hampered by severe fouling—deposition of solutes on the membrane surface which decreases membrane flux and separation ability—making it necessary to develop fouling resistant membranes[1, 6-12]. This has led to the development of stimuli-responsive membranes, which contain chemical functional groups which change their properties such as conformation, charge, or hydrophilicity in response to changes in the external environment. Stimuli such as pH,

solution ionic strength, or temperature are often used; however, the entire feed stream must be modified to use these stimuli[13,14]. This is expensive and time-consuming but can be avoided by using an external stimulus such as light or a magnetic field[13-17]. An exciting new type of filtration membrane responsive to an external magnetic field has been developed by our group: small scale mixing is generated above the membrane surface via the movement of grafted polymer chains aligning with an alternating magnetic field[17]. The mechanism for this mixing is described in detail in our previous work. This reduces concentration polarization, and thus fouling, by hydrodynamically disrupting the thin boundary layer above the membrane surface[17]. Reduced fouling via mixing results in improved membrane flux, membrane longevity, and permeate quality. It is argued that improved membrane performance could lead to wider membrane usage as well as exciting new beneficial product streams by using fouling resistant membranes to treat PW[1, 6-12].

In this study PW from an operating oil production site in north-central Colorado is treated using our magnetically-activated micromixer membranes. The resulting permeate is tested for suitability as an irrigation water by measuring its effect on seedling growth and soil properties of plants and soils characteristic of Colorado. Use of treated PW (TPW) for irrigation would turn a previously discarded waste stream into a beneficial product stream which could help offset increasing water demand in the western United States and other arid areas[1,2].

6.2. Materials and Methods

6.2.1. Materials and Chemicals

NF 270 flat-sheet membranes were obtained from Dow Filmtec. 45 mm diameter membrane discs cut from the membrane sheets were used for all filtration experiments. Before use, the membranes were washed thoroughly with DI water and then dried overnight at 40°C. When not in use, the discs were stored in zip-top plastic bags containing a dilute sodium azide in water solution to prevent microbial growth. Iron oxide core, oleic acid shell superparamagnetic nanoparticles with a core diameter of 15 nm were purchased from Ocean Nanotech (Springdale, AR, USA). Purified water was from a Siemens ELGA Purelab Ultra DI system. All chemicals were at least 97% purity unless otherwise noted. Diisopropylcarbodiimide, triethylamine, N,N',N',N'',N''-pentamethyldiethylenetriamine, and 4-N',N'-dimethylaminopyridine were from Fluka; ethanol, methanol, acetonitrile, and hydrochloric acid (6 M) were from VWR; α-bromoisobutyrylbromide, bipyridine (Reagent Plus), copper (I) and copper (II) chloride, 2-hydroxyethylmethacrylate (HEMA), 1-ethyl-3-(3-dimethylaminopropyl)carbodiimide (EDC), hydrazine hydrate, and N-hydroxysuccinimide (NHS) were from Sigma-Aldrich. Before polymerization, HEMA was purified via column chromatography, and always used within 12 hours to minimize self-polymerization. PW was obtained from an operating oil production site in north-central Colorado. The PW was stored out of direct sunlight and was used as received. The composition of the PW is shown in Table 6.1.

Table 6.1. Composition of raw, untreated PW. All units are parts per million (ppm) unless otherwise stated.

pH	7.9	**Phosphorous**	0.02
Conductivity	3100 μS/dm	**Iron**	0.38
TDS	2298	**Aluminum, Cadmium, Copper, Chromium, Lead, Mercury, Molybdenum, Nickel, Selenium, Zinc**	< 0.01
Total Carbon	680		
Calcium	3.2		
Magnesium	2.1		
Sodium	651		
Potassium	5.2		
Chloride	968		
Sulfate	4.0		
Total Nitrogen	450		
BOD	27		
Oils & Grease	77	**Boron**	0.13
Turbidity	28 NTU	**Barium**	0.42
Sodium Adsorption Ratio	69.4	**Salinity Hazard**	High
		Sodium Hazard	High

6.2.2. Membrane Modification

The full modification procedure has been described in detail previously[17]. Briefly, the initiator was first immobilized to the membrane surface by reacting the membrane discs at room temperature for 2 hours on a shaker table in a solution of 2.76 g α-bromoisobutyrylbromide, 1.515 g triethylamine, and 91.5 mg 4-N',N'-dimethylaminopyridine in 150 mL dried acetonitrile. PolyHEMA chains were then grafted from the membrane surface using a controlled polymerization reaction called surface initiated atom transfer radical polymerization (SI-ATRP). The reaction solution consisted of purified HEMA monomer (2 M), CuCl, $CuCl_2$, and bipyridine (BPy) dissolved in equal parts (v/v) water and methanol; the molar ratios HEMA : CuCl : $CuCl_2$: BPy were 100 : 0.5 : 0.1 : 1.5. The membrane discs reacted at room temperature for either 4, 6, or 8 hours before being removed and placed in a quenching solution consisting of 500mg $CuBr_2$ and 1250 μL N,N',N',N'',N''-pentamethyldiethylenetriamine in equal parts methanol and water. The quenching solution halted the polymerization and insured that each polyHEMA chain was

capped with a terminal bromide; this was necessary for the following modification step. In order to convert the terminal bromides to primary amines, which could then be bound to the superparamagnetic nanoparticles, a modified Gabriel synthesis was employed[17,18]. The discs were placed in vials containing potassium phthalimide dissolved to saturation in ethanol. The vials were sealed and reacted in a shaken 40^{o}C oil bath for 6 hours. The discs were then placed in a solution of 7 mL hydrazine hydrate in 25 mL of 6 M HCl, and the sealed vials placed in a shaken 40^{o}C oil bath for 6 hours. Finally, the nanoparticle coupling solution consisted of 31.2 mg EDC, 38.7 mg NHS, and 3 µL carboxyl shell Fe_3O_4 nanoparticles in buffer solution (5 g/L) were added to 10 mL DI water. 1.5 mL of this solution was then added to a jar containing a membrane disc. This was sealed and incubated in the dark for 4 hours.

6.2.3. Membrane Filtration

A Millipore stirred cell 8050 (50 mL) with an active membrane area of 13.4 cm^2 was used for all filtration experiments with an initial feed volume of 50 mL. The membranes were removed from storage in the sodium azide solution and washed thoroughly with DI water before use. The cell was first filled with a 50% ethanol/water solution and pressurized to 1.4 bar (20 psi) and the filtrate outlet opened for 10 minutes in order to wet the membrane. Next, the membrane was flushed with DI water at 1.4 bar (20 psi) for 10 minutes, and then allowed to equilibrate in DI water for 2 hours. The stirred cell was then connected to a reservoir filled with feed solution and the pressure increased to 4.83 bar (70 psi). The permeate outlet was kept closed for the first 3 minutes to allow the membrane to equilibrate, then opened, and flux measurements begun. Following filtration, the membranes were flushed with DI water at 1.4 bar

(20 psi) for 20 minutes, then washed thoroughly with DI water and returned to storage. Membrane flux is reported in units of L / m^2 * hr, abbreviated Lmh.

Magnetic fields were generated using a computer-controlled system comprising two iron-core solenoids located on opposite sides of the stirred cell[17,18]. The power supplied to the solenoids was tuned to yield a field strength of 50 G at the center of the membrane cell, measured by a probe HHG-23 Gauss/Teslameter (Omega Inc., Stamford, CN). Fields were operated at a frequency of 10 Hz, which was previously found to yield maximum mixing above the membrane surface[17]. The magnetic mixing is envisioned as a periodic maintenance step, and was thus not applied continuously during filtration. The magnetic field was only applied periodically for 10 seconds every two minutes, the duration previously determined (results not yet published) to maximize membrane flux while minimizing energy and pumping costs.

Periodically during filtration the membranes were lightly cleaned or washed. The membrane was not removed from the stirred cell during the washing procedure. Washing consisted of removing the feed solution from the cell, rinsing the membrane with shaken DI water for 1 minute, flushing the membrane with 0.5N NaOH at 1.4 bar (20 psi) for 2 minutes, and finally flushing the membrane with DI water at 1.4 bar (20 psi) for 2 minutes. Following the 5 minute washing procedure, 50 mL of the feed was reintroduced to the cell, and the previous filtration continued. Washings were performed every three hours. Each membrane was used for five filtration/washing cycles (15 hours total) before being retired. The permeates of eight individual modified membrane discs were combined to form one treated PW source, the composition of which is shown in Table 6.2.

Table 6.2. Composition of treated PW. All units are parts per million (ppm) unless otherwise stated. This corresponds to the mixed permeate of eight membrane discs following five 3-hour filtration and washing cycles each.

pH	7.4	**Phosphorous**	0.02
Conductivity	1080 μS/dm	**Iron**	< 0.01
TDS	550	**Aluminum, Cadmium, Copper, Chromium, Lead, Mercury, Molybdenum, Nickel, Selenium, Zinc**	< 0.01
Total Carbon	< 5		
Calcium	1.0		
Magnesium	1.2		
Sodium	164.0		
Potassium	2.6		
Chloride	201		
Sulfate	1.2		
Total Nitrogen	23		
BOD	< 10		
Oils & Grease	< 10	**Boron**	0.09
Turbidity	1.3 NTU	**Barium**	0.11
Sodium Adsorption Ratio	26.2	**Salinity Hazard**	Med
		Sodium Hazard	Med

6.2.4. Seedling germination

All seedling germination studies were performed in accordance with protocols established by the Colorado Seed Laboratory. Seeds were supplied by CSU staff at the Fort Collins Agricultural Experiment Station. The following seeds were used: malt barley (*Hordeum vulgare*, L. 'Stoneham'), field corn (*Zea maize* L. 'Channel 197 14VT3'), yellow onions (*Allium capae* L. 'Colorado'), and common pinto beans (*Phaseolus vulgaris*, L. 'Pinto – Bill Z'). Barley, corn, and beans were loosely rolled in paper towels dampened with a given water; onions were placed between two sheets of blotter paper dampened with a given water. Ten seeds were placed on each paper towel or blotter paper, and three duplicate sheets (30 seeds total) of each seed were studied for each water type. The dampened papers were placed in large clear plastic bags which were loosely closed, leaving ample room for the plant shoots to grow. The plants were given eight hours of artificial sunlight per day, and the containers were rotated once per day. The

number of healthy seeds, those which had grown both a root and a shoot, were counted at either 6, 7, 8, or 10 days, depending on the Seed Lab protocol. The beans were lightly watered on day 4 using a spray bottle, and all seeds were lightly watered on day 8. The final tally was performed after 14 days, except for onions which were counted for the last time on day 10.

Ten different water types were investigated. Both city of Fort Collins tap water and water from the South Platte River in north-central Colorado were used as controls. Treated PW permeate from the modified membranes was used solely as well as in 1/3 : 2/3 and 2/3 : 1/3 dilutions with both tap water and river water. Raw PW was used as received and in corresponding dilutions with tap water. Characteristics of each of the ten waters and abbreviations used throughout this text are presented in Table 6.3.

Table 6.3. Selected characteristics of waters applied to seeds and soils as possible irrigation water. All units are parts per million (ppm) unless otherwise stated.

	Tap Water	1/3 TPW + 2/3 Tap	2/3 TPW + 1/3 Tap	TPW	Raw PW	River Water	1/3 TPW + 2/3 River	2/3 TPW + 1/3 River	1/3 Raw + 2/3 Tap	2/3 Raw + 1/3 Tap
Water Quality Abbreviation	**WQ1**	**WQ2**	**WQ3**	**WQ4**	**WQ5**	**WQ6**	**WQ7**	**WQ8**	**WQ9**	**WQ10**
pH	8.0	7.8	7.7	7.4	7.9	8.1	7.9	7.6	7.9	7.9
Conductivity (µS/dm)	110	436	777	1080	3100	657	802.6	952.7	1116	2135
TDS	55	232	402	550	2298	81	240.5	408.7	814	1577
Calcium	14.1	11.7	8.7	1.0	3.2	44.1	30.2	14.4	10.1	6.7
Magnesium	1.8	1.6	1.5	1.2	2.1	12.8	9.0	5.0	1.8	2.1
Sodium	2	59	117	164	651	42	83.4	144.7	238	470
Potassium	0.9	1.6	2.2	2.6	5.2	5	4.4	3.5	2.3	3.8
Chloride	5	74	146	201	968	34	87.7	147.4	341	663
Sulfate	43	28.3	18.4	1.2	4.0	84	58.6	34.7	32.0	21.3
Total Nitrogen	0.3	8.8	17.6	23.0	450	2.6	9.6	16.9	153.7	310.1
SAR	0.16	4.27	9.66	26.16	69.45	1.42	3.42	8.37	18.10	40.58

6.2.5. Soil column percolation

Two soils characteristic of cropland in Colorado were obtained from land at the CSU Agricultural Research, Development, and Education Center (ARDEC) in north-central Colorado. A more clay-like soil termed Garret loam (Fine-loamy, mixed, mesic Pachic Argiustolls) and more sand-like soil termed Vona loamy sand (Coarse-loamy, mixed, superactive, mesic Aridic Haplustalfs) were selected. The two soils were first sieved using a 2 mm screen; the soil texture compositions following the screening for the sandy soil were 87.5%, 7.5%, and 5.0% sand, silt, and clay, respectively and 65.5%, 10.5%, and 24.0% for the loam (clay) soil.

A diagram of the hydraulic conductivity apparatus is shown in Figure 6.1. The soils were packed into 10.2 cm (4 in.) tall, 7.6 cm (3 in.) diameter PVC cylinders to a bulk density of 1.55 ± 0.01 g/cm^3 and 1.34 ± 0.01 g/cm^3 for the sandy and loam soils, respectively. The dry soil columns were placed onto a wire frame support on top of a funnel. A one liter Mariotte bottle was filled with the desired water type. Vinyl tubing was used to convey the sample water from the Mariotte bottle to the soil cylinder; the placement of the Mariotte bottle (height relative to the top of the soil column, labeled h) determined the height of water on top of the soil. All tests were performed using the constant head method[19]. The rate of water percolation through the soil column and the pond depth were periodically measured until steady state was achieved. The saturated hydraulic conductivity (cm/hr) was then calculated using Darcy's Law.

$$HC_{sat} = \frac{Q \cdot L}{A \cdot (L + h)} \tag{6.1}$$

Q is the amount of water per time which has percolated through the column (cm^3/hr), L is the length of the packed soil in the column (cm), A is the cross-sectional area of the soil (cm^2), and h is the depth of the water pond on top of the soil (cm). Five different waters were applied to the

soil columns: a 5 mM CaCl in water control used as a standard in soil studies[19], as well as WQ 2-5 described in Table 6.3.

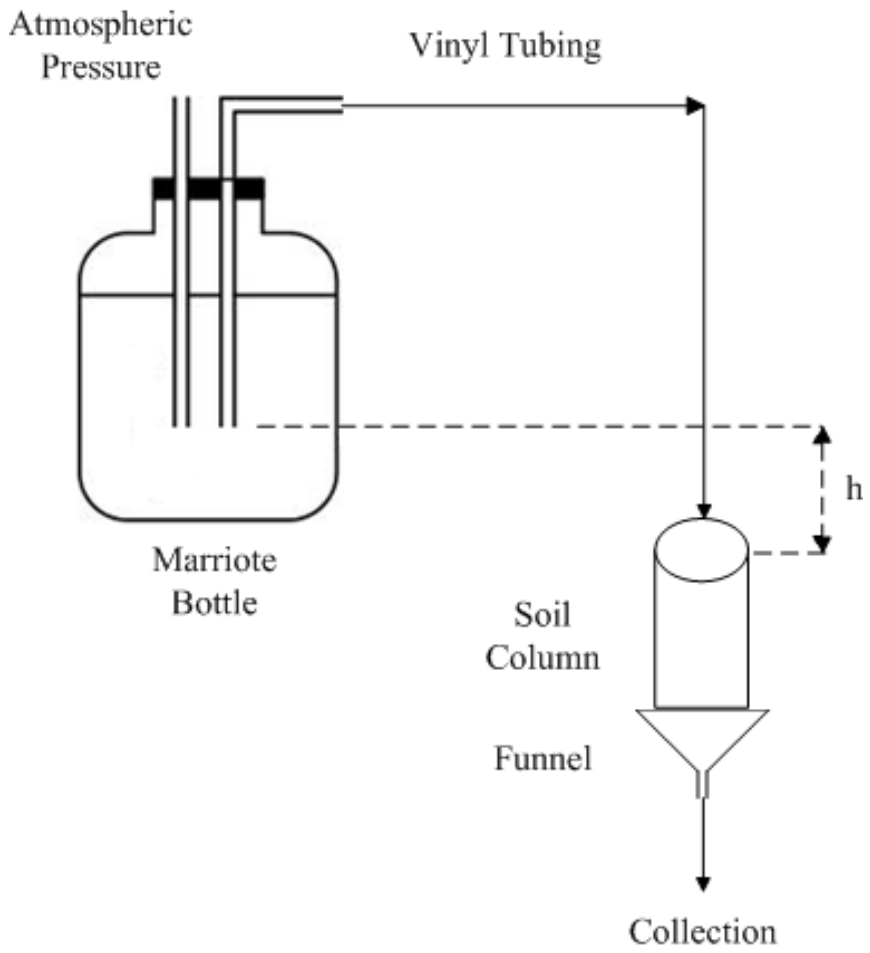

Figure 6.1. Diagram of soil percolation experimental apparatus.

6.2.6. HYDRUS-1D Modeling of Effect of Water on Soil Properties

HYDRUS-1D, an open source software package, was used to model the effect of contaminated water application on soil properties. The 1D model ignores radial flow of water as it proceeds down the soil column. The saturated hydraulic conductivity was calculated using equations and parameters present in the model[20]. Parameters fed into the model were obtained from measurements, known values for the two soils tested, and assumptions based on the nature

of the two soils. Details of the equations involved in the model are presented in the supplementary material, see Appendix A3.

6.3. Results and Discussion

6.3.1. Filtration of Produced Water

PW was filtered using both unmodified and modified membranes. Membrane flux during the five filtration/washing cycles is plotted in Figure 6.2. The flux of the unmodified membranes decreases rapidly to less than half its initial value due to fouling on the membrane surface. The flux of the modified membrane, although initially less than the unmodified membrane due to the increased resistance of the grafted polyHEMA chains[17], decreases only slightly during filtration. Previous work (not yet published) has shown that the mixing generated by the modified membranes in an alternating magnetic field can significantly reduce decline in membrane performance measured by flux and permeate quality during filtration of PW. This is because mixing reduces the degree of fouling on the membrane surface. Reduced fouling in turn allows the membranes to be more easily cleaned; that is, irreversible fouling is reduced. The washing procedures only slightly restore the flux of the unmodified membrane, and the flux rapidly declines again. Clearly some of the fouling is irreversible. The first washing restored the modified membrane flux to 85% of its previous value, and the subsequent washings all resulted in > 95% recovery. The activated mixing reduces the irreversible fouling on the membrane surface, leading to more easily cleaned membranes.

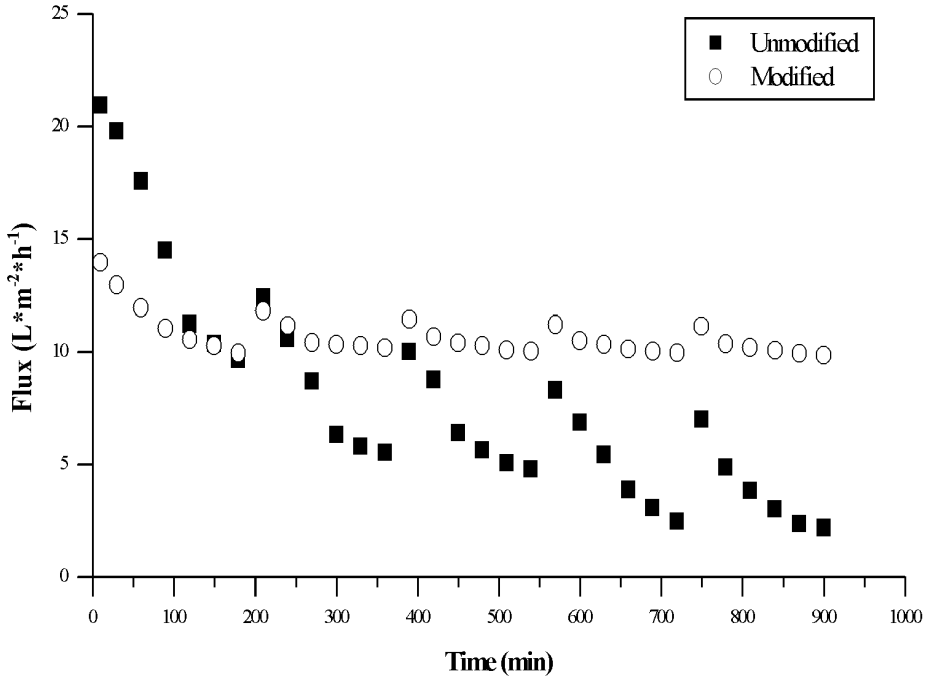

Figure 6.2. Average membrane flux for unmodified and modified membranes during filtration of PW. Data points represent range of experimental values obtained for experiments in triplicate.

The effect on permeate quality can be seen in Figure 6.3. Both TDS and conductivity of the unmodified membrane permeate rapidly increase during each filtration period, due to concentration polarization reducing the effective membrane rejection, and both quantities are slightly higher following each successive washing. This continued deterioration of permeate quality is attributable to irreversible fouling and agrees with the continually decreasing flux. The TDS and conductivity of the modified membrane permeate are both much lower than the unmodified membrane. Also, the decrease in permeate quality is only minor for each filtration cycle. Following washing, the values return to very near their previous values, indicating that the mixing is preventing irreversible fouling. In practice the modified membranes would result in improved operational lifetime and higher quality permeate.

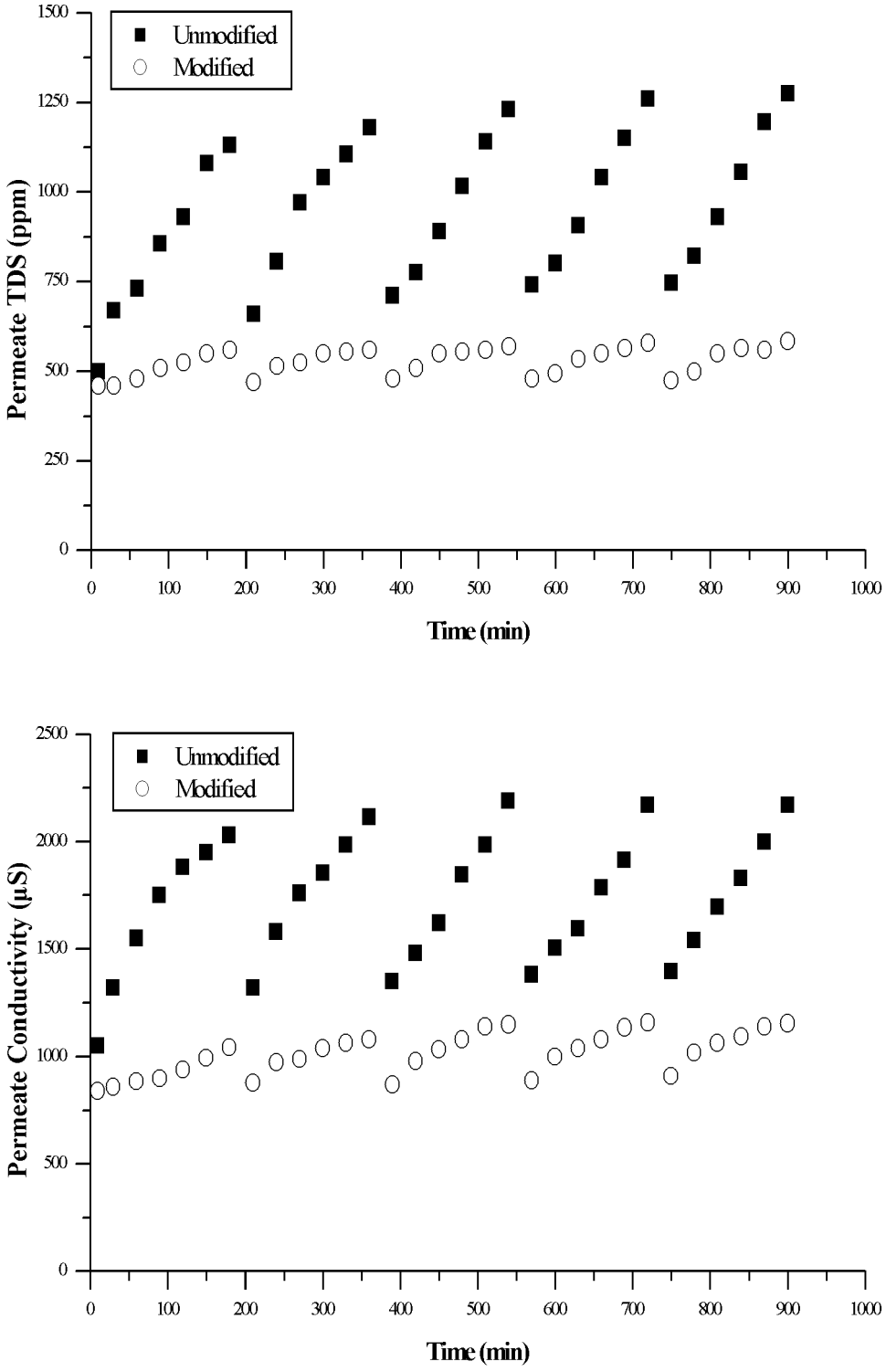

Figure 6.3. Permeate quality of PW treated by unmodified and modified membranes measured by TDS and Conductivity. Data points represent range of experimental values obtained for experiments in triplicate.

Unfortunately, nanofiltration membranes characteristically reject divalent ions (such as calcium and magnesium) more than monovalent ions (such as sodium). Although nanofiltration membranes are well-suited at removing most of the solutes found in PW, particularly oils, the resulting permeate will most likely contain a high amount of sodium. This could lead to a relatively high sodium adsorption ratio (SAR) value, see Table 6.2. Higher SAR values will impede water permeation through soil; however, the larger concern for seedling germination is water electrical conductivity (EC). EC is related to the total concentration of salts, not simply sodium salts. To reduce the EC TPW could be diluted via addition of fresh water. In practice, this would involve adding TPW to an existing nearby water source (for example a pond or stream) supplying an irrigation system. Here TPW was diluted to ratios of 1/3 : 2/3 and 2/3 : 1/3 TPW: fresh water, as shown in Table 6.3, to study the effects on seedling growth and soil characteristics.

6.3.2. Seedling Germination

6.3.2.1. Observation of Healthy Seedlings

The effects of using the TPW in Table 6.2, or some dilution thereof, on seedling growth and soil properties were tested to determine if the modified membranes could be used to obtain permeate suitable for irrigation. Barley, corn, onions, and beans were chosen as representative crops which are grown in the areas of Colorado surrounding oil production sites wells. These crops also exhibit a range of EC tolerance: barley and corn are relatively tolerant, while onions and beans are very sensitive[21,22]. The seeds were used as received with no treatment or preparation. The number of healthy, germinated seeds (those which had grown both a root and a

shoot) were tallied at numerous times during a two-week growth period. The percentage of healthy seeds is presented for each water type in Figure 6.4.

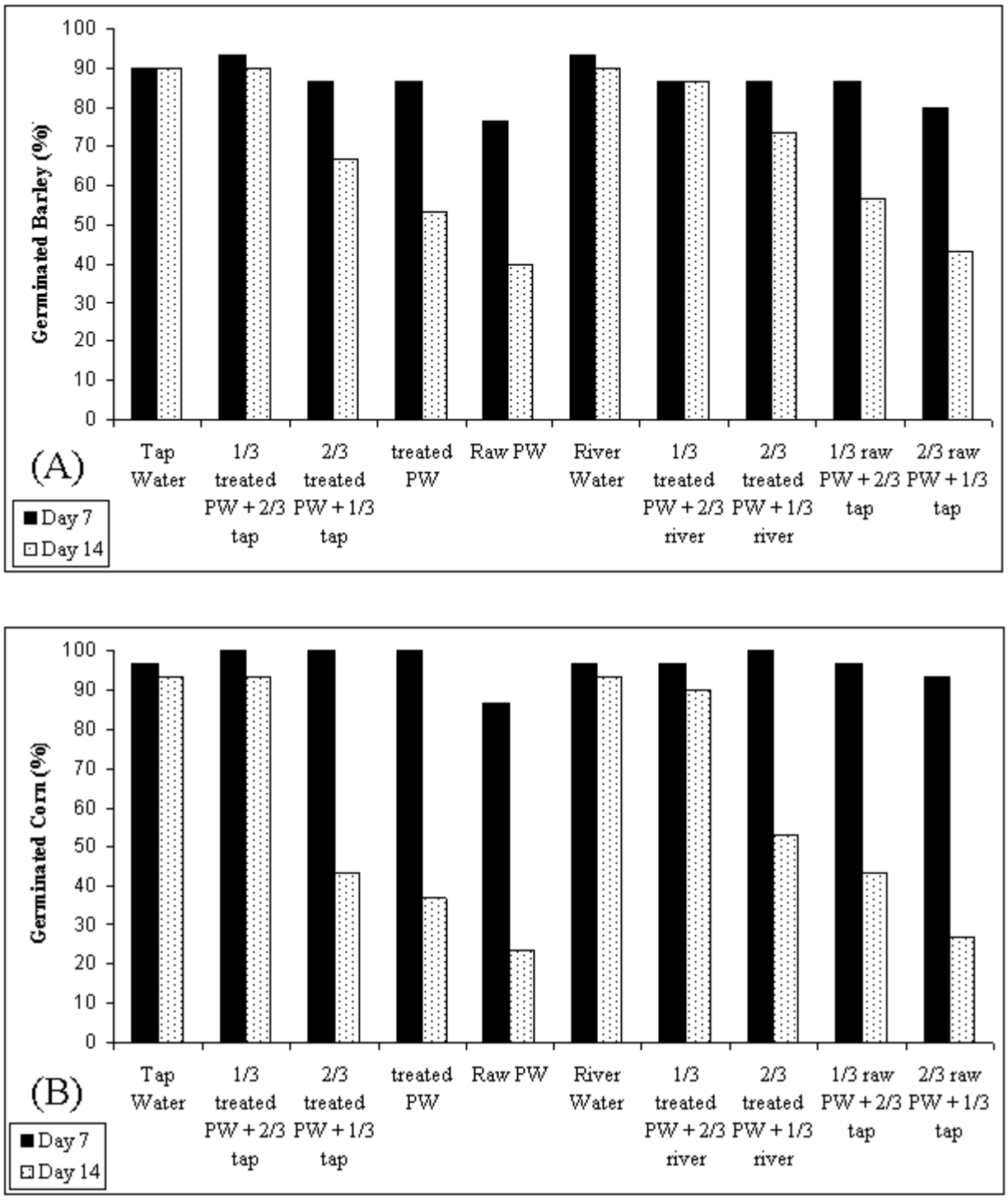

Figure 6.4. Percentage of germinated (A) barley, (B) corn, (C) onion, and (D) bean seeds watered with various waters.

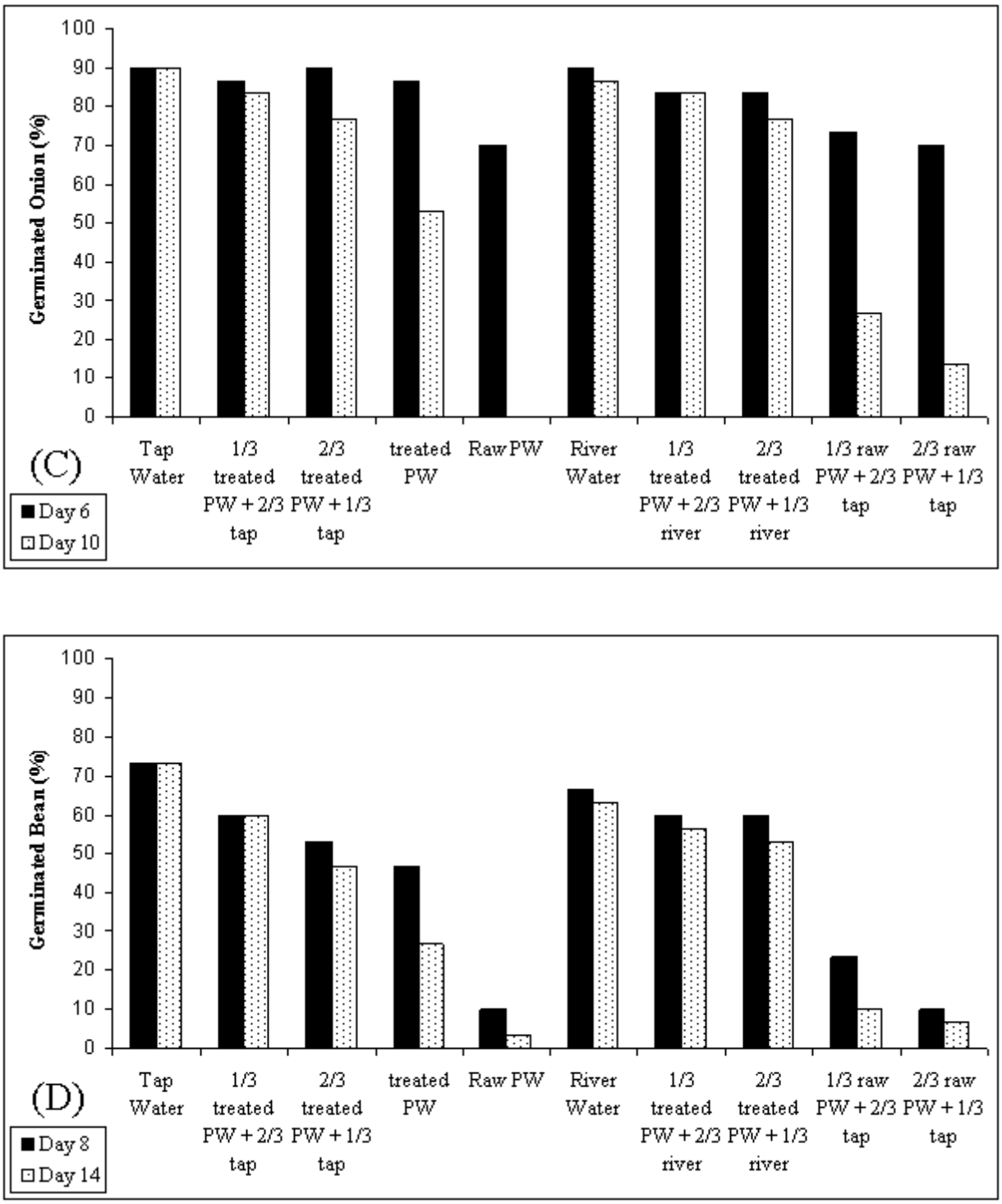

Figure 6.4. Percentage of germinated (A) barley, (B) corn, (C) onion, and (D) bean seeds watered with various waters.

Both WQ1 and WQ6 yielded roughly 90% germination for barley and onions, nearly 100% for corn, but only roughly73 and roughly65% for the beans, respectively. These values agreed with the expected germination rates of the obtained seeds. The germination rates for barley (a) and corn (b) were very similar for each water source at day 7; however, a marked decrease in healthy seeds for WQ 3-5 and 8-10 was seen at day 14. No such drop-off was seen for WQ 1, 2, 6, or 7. The data show that treated PW can be used in a 1/3 : 2/3 ratio to either tap water or river water (WQ2 or WQ6) with no adverse effect on germination.

The more salt sensitive onions (3c) and beans (3d) performed somewhat differently. The healthy onion count decreased sharply at day 10 for WQ 4, 5, 9, and 10; however, WQ 1-3 and 6-8 performed quite well. It was expected that the higher EC of the 2/3 TPW dilutions would be detrimental to the seeds; however, this was not seen. The beans, being the most salt sensitive crop, already showed a noticeable decrease in healthy seed count on day 8. The higher EC of WQ 4, 5, 9, and 10 was clearly detrimental to the seeds. WQ 2 and 7 performed comparably to WQ 1 and 6, similar to the other three seeds, while WQ 3 and 8 performed somewhat well.

The data agree with known salinity tolerances of these plant species. This is encouraging since the use of PW—treated or untreated—as irrigation water is still a young field. Three important conclusions can be drawn from the application of treated PW as irrigation water. Firstly, 1/3 TPW mixed with 2/3 tap water or river water (WQ 2 and 7) yielded statistically identical germination rates as the tap and river water controls (WQ 1 and 6) for barley, corn, and onions. This provides preliminary evidence that WQ 2 and 7 could be used as an irrigation water for these crops with no appreciable decrease in the number of seeds which mature into plants. Further field research would be beneficial to test the impact of these water on crop yield and quality. It could also be possible to use WQ 3 and 8 for certain plants, such as onions or possibly

barley. Secondly, similar dilutions of 1/3 raw PW (WQ 9 and 10) are very detrimental to seedling growth, removing doubt that merely diluting raw PW would be sufficient. Clearly, the modified membranes remove certain compounds in the raw PW which are damaging to seedling growth. Finally, there is no statistical difference, except for a slight difference for beans, in the use of water from the South Platte River and city of Fort Collins municipal tap water, either alone or used to dilute treated and raw PW. This is important because the use of river water instead of tap water for irrigation would reduce the water demand on western municipalities and make it possible for oil production sites to "mix" their own irrigation water on-site for use on nearby crop plots.

6.3.2.2. Statistical Analysis of Seedling Germination

The percentage of germinated seeds for each water was normalized to that of tap water to remove inconsistencies between the germination rates of the tap water control. A general linear model using these normalized values was constructed in R, an open source statistics package, to determine which effects on germination were significant and if any interactions between water quality, crop species, and time existed. The full data generation is presented in Appendix A2. Table 6.4 presents the average normalized percentage germinated seeds for all combinations of crop, water quality, and time. The letters represent statistically significant groupings within a given column (combination of crop, water quality, and time). The groupings mirror the behavior seen in Figure 6.4. Table 6.4 also presents the test for significance for certain interactions. Water quality had a significant effect on seedling germination for all crops on the second counting day. An effect was seen for beans and onions at time 1 as well, but a less significant effect on barley and corn at time 1. Time had a strong effect on all four crops, as expected.

Table 6.4. Average percentage of germinated seeds normalized against tap water (WQ1). Statistically significant ($p < 0.05$) groupings of means within a column are designated by letters as determined by ANOVA. The significance of experimental factors and interactions between factors are denoted as follows: $p < 0.001$ (***); $p < 0.05$ (*); $p > 0.05$ (NS).

Interaction	Barley		Corn		Onion		Bean	
	Day 7	Day 14	Day 7	Day 14	Day 6	Day 10	Day 8	Day 14
WQ 1	100 a	100 a	100 a	100 a	100 a	100 a	100 a	100 a
WQ 2	104 a	100 a	103 a	100 a	96 a	93 ab	82 b	82 b
WQ 3	96 ab	74 bc	103 a	46 bc	100 a	85 b	73 b	64 c
WQ 4	96 ab	59 c	103 a	39 c	96 a	59 c	64 c	36 d
WQ 5	85 b	44 e	90 b	25 d	78 b	0 f	14 e	5 ef
WQ 6	104 a	100 a	100 a	100 a	100 a	96 ab	91 ab	86 b
WQ 7	96 ab	96 a	100 a	96 a	93 ab	93 ab	82 b	77 b
WQ 8	96 ab	81 b	103 a	57 b	93 ab	85 b	82 b	73 bc
WQ 9	96 ab	63 c	100 a	46 bc	81 b	30 d	32 d	14 e
WQ 10	89 b	48 e	97 a	29 d	78 b	15 e	14 e	9 e
WQ	*	***	*	***	***	***	***	***
Time	***		***		***		***	
WQ x Time	***		***		***		NS	
WQ x Crop[1]	Time 1: ***				Time 2: ***			
WQ x Time x Crop[2]	All data: ***							

[1] : WQ x Crop denotes the interaction of water quality across all crop species at each day; Time 1 = Days 6-8 and Time 2 = Days 10 and 14.

[2] : WQ x Crop x Time denotes the interaction across all water qualities, crop species, and time

The interaction between water quality and time was significant for all crops except beans, the most salt sensitive seed. This interaction can be understood visually by comparing the differences in seedling germination between time 1 and 2 in Figure 6.4 (a)-(d). That is, the decrease in healthy seedlings with increasing sodium concentration was more severe for all crops at time 2 than at time 1. The interaction between water quality and crop was significant for each time. This was expected since the salt tolerance of the seeds varied. Finally, a significant three-way interaction was observed across all data.

6.3.3. Soil column percolation

The saturated hydraulic conductivity (HC) for each water in both loam and sandy soils was averaged across five soil columns. Saturated HC, deviation across the five soil columns, time required to reach steady state, and saturated water content following testing are reported in Table 6.5. As expected, the HC of the sandy soil were greater than those of the loam soil. HC for both soils decreased with decreasing water quality, i.e. increasing PW ratio. An increase in sodium ion concentration and corresponding ionic strength will cause clay particulates in the soil to become dispersed, which leads to blocking of the free volume in the soil, and thus lower water flux. HC decrease is greater and time to steady state is longer for the loam soil because of the higher fraction of clay. Application of the TPW dilutions had no significant effect on sandy soil HC; however, application of undiluted TPW would be detrimental to a clay soil such as the loam investigated here. Raw PW would not be suitable for application on either soil. Similar to the seedling study, the 1/3 TPW dilution (WQ 2) could be used as an irrigation water, while the 2/3 TPW dilution (WQ 3) could be used in certain instances.

Table 6.5. Average saturated soil hydraulic conductivity at steady state for each of the five tested waters, time to reach steady state, and saturated water content following percolation experiments. Letters represent statistically significant groupings within each column.

		Saturated HC (cm/hr)	HC Standard Deviation	Time to Reach Steady State (min)	Saturated Water Content (g/cm^3)
5 mM CaCl Control	**Clay Soil**	10.22 a	0.48	47	514.10 b
1/3 treated PW		9.22 b	0.57	58	530.86 a
2/3 treated PW		8.39 c	0.49	74	521.41 ab
Treated PW		6.47 d	0.69	130	506.49 b
Raw PW		3.60 e	0.53	228	492.32 c
5 mM CaCl Control	**Sandy Soil**	14.26 f	0.86	17	385.72 d
1/3 treated PW		14.15 f	0.42	24	384.68 d
2/3 treated PW		13.73 f	0.65	24	386.71 d
Treated PW		12.58 g	0.87	32	381.32 d
Raw PW		10.31 a	0.85	100	380.10 d

6.3.4. HYDRUS-1D modeling

An attempt to create a predictive model using HYDRUS-1D modeling software yielded limited success. As seen in Table 6.6 the model correctly predicted the trend of decreasing saturated HC with increasing water contamination and increasing clay fraction. The magnitude of HC decrease is predicted well for most of the contaminated waters; although 1/3 TPW dilutions in both soils and the 2/3 dilution in sandy soil are outliers. However, the model is not accurate beyond reporting trends. Many factors contribute to the model error, and in future studies many of these could be addressed to improve accuracy. Most importantly, the model is extremely sensitive to pH, and large changes in calculated HC result from small changes in pH which are within measurement error (± 0.1). Also, the model assumes that the pH of the soil matches the pH of the water. This is often a reasonable assumption but may not be entirely accurate here since soil pH equilibrium cannot be guaranteed at this short time scale. Finally, there are simply too many assumptions hidden within the model. The model demands many factors to be known about the soil, see Appendix A3. The soils were not fully characterized in this study because the focus was on observable effects of water chemistry. Many of the required

model inputs could be measured in future studies; however, some assumptions are still made by the model. Reasonable assumptions, verified by an expert in soil science, were given for all inputs. Due to the layered nature of the model small changes in one assumed value can have a large effect on the final saturated HC. With further study and refinement, the model could be used to reasonably predict which soils may be most amiable to irrigation with TPW dilutions.

Table 6.6. HYDRUS-1D model results. Measured HC and water pH are compared to HC calculated by HYDRUS and the pH required for the model to agree with measured HC.

		Measured HC (cm/hr)	Measured water pH	Calculated HC (cm/hr)	pH needed to match measured HC	Calculated HC error
5 mM CaCl Control	**Clay Soil**	10.22	7.0	9.61	6.8	-6.0
1/3 treated PW		9.22	7.8	6.66	7.1	-27.7
2/3 treated PW		8.39	7.7	7.03	7.3	-16.2
Treated PW		6.47	7.4	5.38	7.0	-16.9
Raw PW		3.60	7.9	4.82	8.3	33.9
5 mM CaCl Control	**Sandy Soil**	14.26	7.0	13.40	6.8	-6.0
1/3 treated PW		14.15	7.8	9.30	6.9	-34.3
2/3 treated PW		13.73	7.7	9.81	6.9	-28.5
Treated PW		12.58	7.4	11.35	7.2	-9.8
Raw PW		10.31	7.9	8.78	7.6	-14.8

6.3.5. Potential for Use as Irrigation Water

The data suggest that WQ 2 and 7, and possibly WQ 3 and 8 as well, could be used as irrigation water under certain conditions. Although encouraging, some concerns still must be addressed before these waters could be used in practice. The effects of prolonged use of these waters must be determined. Concerns include: (1) Can this water support plants to maturity and how will this affect yield and quality? (2) What is the composition of runoff from fields irrigated with these waters, and what is its effect on surface waters? (3) What are the impacts on the soil of long-term application of these waters? (4) Could the use of these waters damage equipment?. It is believed that adult plants will perform well because seedling germination is typically a more

stressful period in a plant's lifecycle. It is believed that the 1/3 TPW dilutions will not damage (i.e. scale) piping and equipment. Other remaining questions may only be answered with dedicated field studies; potential future studies are presented in Chapter 8. The seedling germination and soil property studies presented here certainly suggest that dilutions of TPW could be used as irrigation water with no significant effects. The potential to turn a large volume of wastewater into a beneficial water stream certainly warrants additional investigation.

6.4. CONCLUSIONS

Modified nanofiltration membranes were used to treat realistic PW. The magnetically-activated mixing of the modified membranes in an alternating magnetic field improved membrane performance compared to unmodified nanofiltration membranes. The permeate of modified membranes was significantly cleaner than unmodified membranes, and the modified membranes were more easily cleaned. Seedling germination studies and soil hydraulic conductivity tests suggest that the treated PW permeate, when diluted to a ratio of 1/3 : 2/3 with either tap water or river water, could be usable as irrigation water for crops and soils characteristic of Colorado and other western states where oil production is a large business. 2/3 : 1/3 treated PW dilutions are suitable for certain crops and soils as well; however, potential long-term impacts must be studied. A preliminary model to predict impacts of diluted TPW on soil properties was developed, which yielded limited results.

The treatment of PW to obtain irrigation water introduces an exciting new beneficial use for PW, which has previously been viewed as a waste and merely discarded. Using treated PW as irrigation water could alleviate the demand for fresh water in the western United States, and would reduce the volume of polluted water which is either reinjected into the ground or

discharged to surface waters. Treating PW to obtain irrigation water is a new field of study which still requires further study; however, the early results are extremely promising.

REFERENCES

1. National Research Council of the National Academies, Management and effects of coalbed methane produced water in the western United States, 2010, Washington D.C.: The National Academies Press
2. K. L. Benko, J. E. Drewes, Produced water in the western United States: Geographical distribution, occurrence, and composition. Environ. Eng. Sci., 25(2008) 239-246.
3. R. W. Baker, Membrane technology and applications, 2nd ed, 2004, Chichester: Wiley.
4. W. S. W. Ho, K. K. Sirkar, Eds. Membrane Handbook, 1992, Norwell: Kluwer.
5. N. N. Li, A. G. Fane, W. S. W. Ho, T. Matsuura, Eds. Advanced membrane technology and applications, 2008, Hoboken: J. Wiley & Sons.
6. M. Cakmakci, N. Kayaalp, I. Koyuneu, Desalination of produced water from oil production fields by membrane processes. Desalination, 222 (2008) 176-186.
7. P. Czermak. Multiphase Cross-flow Filtration Process for Efficient Treatment of Oil-field Produced Water Using Ceramic Membranes. 7th Produced Water Workshop. April 2009.
8. D. Wandera, S. R. Wickramasinghe, S. M. Husson, Modification and characterization of ultrafiltration membranes for treatment of produced water, J. Mem. Sci. 373 (2011) 178-188.
9. D. Wandera, H. H. Himstedt, M. Marroquin, S. R. Wickramasinghe, S. M. Husson, Modification of ultrafiltration membranes with block copolymer nanolayers for produced water treatment: the roles of polymer chain density and polymerization time on performance, J. Mem. Sci. 403-404 (2012) 250-260.
10. T. Bilstad, E. Espedal, Membrane separation of produced water, Wat. Sci. Tech. 34 (1996) 239-246
11. B. Van der Bruggen, C. Vandecasteele, T. Van Gestel, W. Doyen, R. Leysen, Environ. Prog. 22 (2003) 46-56.
12. E. T. Igunnu, G. Z. Chen, Produced water treatment technologies, Int. J. Low-Carbon Techn. 1 (2012) 1-21.
13. D. Wandera, S.R. Wickramasinghe, S.M. Husson, Stimuli-responsive membranes, J. Mem. Sci. 357 (2010) 6-35.
14. M.A. Stuart, W.T. Huck, J. Genzer, M. Müller, C. Ober, M. Stamm, G.B. Sukhorukov, I. Szleifer, V.V. Tsukruk, M. Urban, F. Winnik, S. Zauscher, I. Luzinov, S. Minko, Emerging applications of stimuli-responsive polymer materials. Nat. Mat. 9 (2010) 101-113.
15. D.M. He, H. Susanto, M. Ulbricht, Photo-irradiation for preparation, modification and stimulation of polymeric membranes. Prog. Polym. Sci. 34 (2009) 62-98.
16. K. Vanherck, S. Hermans, T. Verbiest, I. Vankelecom, Using the photothermal effect to improve membrane separations via localized heating. J. Mat. Chem. 21 (2011) 6079-6087.
17. H.H. Himstedt, Q. Yang, L.P. Dasi, X. Qian, S.R. Wickramasinghe, M. Ulbricht, Magnetically-Activated Micromixers for Separation Membranes. Langmuir. 27 (2011) 5574-5581.
18. H. H. Himstedt, Q. Yang, X. Qian, S. R. Wickramasinghe, M. Ulbricht, Toward remote-controlled valve functions via magnetically-responsive capillary pore membranes, J. Mem. Sci. 423-424 (2012), 257-266.
19. A. Klute, C. Dirksen. 1986. “Hydraulic Conductivity and Diffusivity: Laboratory Methods” In: A. Klute (ed), Methods of Soil Analysis, Part 1, Physical and Mineralogical Methods (2nd ed.), American Society of Agronomy, Chapter 28, 687-700.

20. J. Šimůnek, M. Šejna, H. Saito, M. Sakai, M. Th. van Genuchten, The HYDRUS-1D software package for simulating the one-dimensional movement of water, heat, and multiple solutes in variably-saturated media, January 2009, Dept. of Environ. Sci., Univ. California Riverside. Software version 4.08.
21. T. A. Bauder, R. M. Waskom, P. L. Sutherland, J. G. Davis, Irrigation water quality criteria, Fact Sheet No. 0.506, Colorado State University Extension, May 2011.
22. R. S. Ayers and D. W. Westcott, Water quality for agriculture. FAO Irrigation and Drainage Paper No. 29, Food and Agriculture Organization of the United Nations, 1976.

CHAPTER 7

SUMMARY AND CONCLUSIONS

This dissertation presented research on magnetically-activated micromixing membranes. Commercially available membranes were modified to be responsive to a magnetic field. Various feedstreams were treated with modified nanofiltration membranes, and the magnetic response was quantified using modified track-etched microfiltration membranes as a model system. Modification consisted of grafting polyHEMA chains from the membrane surface using controlled polymerization and covalently coupling superparamagnetic nanoparticles to the end of the polymer chains. The alignment of the nanoparticle-capped grafted polymer chains with an external magnetic field was used to tune membrane filtration properties. Specifically, in an alternating field the movement of the polymer chains aligning with the alternating field direction resulted in small-scale mixing above the membrane surface.

This mixing was used to improve membrane flux and rejection during filtration of simple salt solutions, a model produced water (PW) system, and a realistic PW. The use of modified membranes resulted in lower energy costs to treat a given volume of feed and resulted in a higher quality permeate, even after multiple filtration and washing cycles. This was because the magnetically-activated mixing reduced fouling, particularly irreversible fouling, on the membrane surface. PW permeate from the best-performing modified membrane showed no detrimental effect on seedling germination and soil characteristics when used in certain dilutions as irrigation water. Throughout the study certain modification and magnetic field parameters were optimized to achieve the greatest mixing; that is, the greatest improvement in membrane

performance. Additionally, a United States non-provisional patent covering this research has been filed. Deliverables obtained through this research include:

7.1. Deliverable 1.

Developed a modification protocol to covalently couple superparamagnetic nanoparticles to the end of a polymer chain grafted from the membrane surface and an apparatus capable of generating the required magnetic field strengths and frequencies.

This work is not formally presented in this dissertation; however, the products of this labor are described in detail in Chapter 2. It was known from previous work with collaborators that SI-ATRP was a viable polymerization method which resulted in highly controllable grafted chain length. HEMA was chosen as a suitable polymer due to its hydrophilicity (anti-fouling properties), flexibility in aqueous solutions, and its ease of use with SI-ATRP. The major hurdle to be overcome was to ensure the magnetic nanoparticles coupled solely to the polyHEMA chain ends; coupling along the backbone would limit the magnetic mixing. The final modification protocol involved converting the terminal alkyl halide to a primary amine through a modified Gabriel Synthesis reaction. This reaction is well-established in organic chemistry; however, the reaction conditions needed to be modified to not damage the polymeric membranes. The final modification protocol can be readily adapted to a number of membrane surface chemistries and successfully coupled the magnetic nanoparticles to only the ends of the grafted polyHEMA chains. This is, however, still a work in progress. As discussed in detail in the following chapter, the modification protocol needs refinement to be more compatible with large-scale manufacturing conditions. Additionally, a concern from the onset of this project is how to

couple exactly one nanoparticle to exactly one polyHEMA chain. This has not yet been rigorously studied; however, the modification protocols were designed to minimize this.

Designing an apparatus capable of generating the required magnetic field strengths *and* frequencies was difficult. Additionally the optimal strength and frequency were not conclusively known, only a range. Eventually the apparatus described in Chapter 2 was created. Since then the appropriate field strength for optimal micromixing has been found, and a much more refined second generation apparatus has been built.

7.2. Deliverable 2.

Determined appropriate magnetic field parameters to generate micromixing, and showed that micromixing is sufficient to impact fluid behavior.

This is covered in detail in Chapter 2. As mentioned above, only a range of possible field strengths was known. Additionally, it was not known if the anticipated mixing would even be sufficient to disrupt the filtration boundary layer. PIV experiments were performed to answer these questions. Most importantly, PIV showed that mixing does occur when modified membranes are placed in a time-varying magnetic field. Inherit in this observation is the fact that the mixing is sufficient to cause tangible differences in fluid behavior on the scale of microns. This is remarkable given that the grafted polymer chains are only tens of nanometers long. A much more narrow range of field frequencies (roughly 10 Hz) for optimal mixing was established by varying the frequency of the rotational magnetic field. Understanding of the nature of magnetic mixing was also expanded based on the observations that higher frequencies showed very little mixing due to the relation between field frequency and distance traveled by the polymer chain.

7.3. Deliverable 3.

Characterized the effect of grafted polymer chain length and density on mixing efficacy.

The details of this deliverable are covered in Chapters 3-5. The magnitude of the magnetic response as a function of chain length and grafting density, measured by change in membrane water flux, using track-etched microfiltration membranes was studied in Chapter 3. Flux decreased with increasing chain length and grafting density due to the additional resistance of the polyHEMA chains. In a static magnetic field, the flux decreased even more, and this decrease was significantly greater for the high density grafting.

The effect of grafting density on nanofiltration membranes is the focus of Chapter 4. Membrane flux and rejection of $CaCl_2$ and $MgSO_4$ solutions for high and low grafting density and degree of grafting (DG) were studied. Water flux was improved in the presence of an alternating magnetic field, except for the low density, low DG membrane. Mixing generated in an alternating field led to an increase in flux and rejection of the two salt solutions. High grafting density improved performance more strongly than low density; thus, the original protocol from Chapter 2 was chosen for future experimentation.

Improvement in membrane flux and permeate quality during filtration of a model PW and realistic PW for three polyHEMA chain lengths was shown in Chapter 5. The modified membranes yielded a more gradual and less severe decrease in membrane performance. The permeate quality for all three was better than the unmodified membrane. The flux, although initially lower than the unmodified membrane, was higher after some time due to the high rate of flux decline for the unmodified membrane. Additionally, the modified membranes were more easily cleaned as discussed below. The membrane modified at four hours SI-ATRP yielded the greatest improvements in membrane performance for both feedstreams.

7.4. Deliverable 4.

Showed that micromixing improved membrane filtration. Specifically, concentration polarization was reduced which lead to better permeate quality, less flux decline, more efficient cleaning, longer effective membrane lifetime, and lower energy costs.

This has been mentioned briefly above. Improvement in membrane performance was seen during filtration of water as well as salt solutions in Chapters 2-5, model PW in Chapter 5, and realistic PW in Chapters 5 and 6. In all cases membrane rejection improved and flux decreased following modification due to the additional resistance of the grafted polyHEMA chains. Application of an alternating magnetic field improved flux and rejection for almost every modification due to the magnetically-activated mixing reducing concentration polarization. Application of a static field to microfiltration membranes, see Chapter 3, decreased flux and increased rejection further since the chains were acting as valves to "block" flow through the membrane pores. This response is well suited for other applications beyond membranes such as microfluidic gating devices.

The second sentence in this deliverable statement is unique to Chapters 5 and 6. Colloidal fouling and deposition of solutes on the membrane surface were significantly reduced during filtration of both model PW and realistic PW. The increased fouling resistance of the hydrophilic polyHEMA chains combined with the hydrodynamic mixing generated in an alternating field led to improved permeate quality, much less severe decline in membrane flux, and more easily cleaned membranes. The end result was membranes which could recover a great degree of their original performance following a simple washing cycle allowing them to be used for extended periods with little decrease in performance; i.e. greater membrane lifetime. Use of the modified membranes in an alternating field resulted in lower energy costs to treat a given

volume of feed. The flux to net energy cost ratios for the modified membranes were 2.9, 2.4, and 1.8 times higher than that of the unmodified membrane after only 90 minutes of filtration with a model PW for 4, 6, and 8 hour SI-ATRP, respectively. The improvements would be even more drastic at longer filtration times and with realistic PW. The improved performance and increased lifetime will greatly reduce operating costs for membrane filtration systems.

7.5. Deliverable 5.

Established potential for a viable outlet for treated PW. Specifically PW permeate in certain dilutions has no adverse effect on seedling germination and soil properties when used as irrigation water.

This is covered extensively in Chapter 6. Four seed species, ranging from salt-tolerant to salt-sensitive, commonly grown in Colorado were treated with ten water quality samples, including tap water and river water as controls as well as dilutions of raw and treated PW. A dilution of 1/3 treated PW + 2/3 tap water or river water showed no statistical difference in seedling germination for barley, corn, and onions. Germination of beans was statistically higher when treated with tap water; however, the 1/3 treated PW diluted with both tap and river water were indistinguishable from treatment with pure river water. The effect of the water qualities on a clay soil (Garret loam) and sandy soil (Vona loamy sand) characteristic of northern Colorado was tested as well. The application of increasingly contaminated waters resulted in little change to the hydraulic conductivity and saturated water content of the sandy soil; however, more contaminated waters greatly affected the loam soil. Although the data are preliminary, it does appear that dilutions of 1/3 treated PW could be used as irrigation water for certain crops and soils with no detrimental effect on soil properties and seedling germination.

CHAPTER 8

FUTURE RESEARCH DIRECTIONS

The research presented in this dissertation established a strong foundation for the understanding of novel magnetically-responsive membranes and explored one possible application. The results were promising and have introduced many opportunities for future study, many of which are covered by the United States patent submitted for this research. This chapter will suggest and briefly describe areas for further investigation to advance the state of the art and understanding of these membranes.

8.1. Modification Protocol

The modification protocol requires optimization. Certain aspects of the protocol have been tuned throughout the dissertation research; however, an exhaustive effort has not been undertaken. Aspects in need of optimization include finding a less harsh alternative to 6 M HCl for the Gabriel Synthesis, optimizing the concentration of nanoparticles used during the coupling reaction, solvent choice, and others. The finalized modification protocol should be crafted to be compatible with industrial-scale manufacturing considerations, as discussed below. It is also desired to create a model (empirical for a given polymer) to determine the effect of grafted polymer chain length on disrupting concentration polarization. Modification on gold and/or silicon chips could be performed as an ideally smooth, model surface to create an initial model before advancing to modeling of rough membrane surfaces.

Grafting polyHEMA chains using SI-ATRP is also only one of any number of modification protocols which could be used. Early proof-of-concept studies showed that UV polymerization could be used to graft polyacrylic acid to nanofiltration membranes which could be capped with magnetic nanoparticles. This route was abandoned for this study because UV polymerization is not controllable. The grafted polymer chains were not uniform in length, and it was impossible to prevent nanoparticles from coupling along the polymer backbone rather than the chain end. Other types of controlled polymerizations beyond SI-ATRP include anionic polymerization, reversible addition fragmentation chain transfer (RAFT) polymerization, and nitroxide mediated radical polymerization (NMP), among others. Polymer choice depends on the chosen polymerization method; however, there are many polymers compatible with each method. In general, polymers could be chosen based on hydrophilicity and/or flexibility in solvent. Furthermore, certain polymers could be chosen to create membranes which are responsive to two different stimuli. For instance, tuning the magnetic field differently would result in a greater degree of nanoparticle heating rather than movement. If the nanoparticles were coupled to a grafted temperature-responsive polymer such as polyNIPAAm, a much quicker temperature response could be achieved without heating the entire feed solution.

PolyHEMA was chosen for this study because hydrophilic polymers tend to foul less, it is highly flexible in water, and it is straightforward to graft using SI-ATRP. The modification protocol developed during this dissertation research performed extremely well for the intended application; however, it is by no means exhaustive for the production of magnetically-responsive membranes.

8.2. Choice of Feedstream

The membranes described in this dissertation were created to be fouling resistant for use in treating PW. The characteristics of these oily wastewaters make them difficult to treat because they rapidly foul most membranes. This is far from the only potential use of magnetically-responsive membranes. Other feed streams already discussed for future research include—but by no means are limited to—other types of PW, industrial dyes, feedstreams in the food and beverage industries, naval bilge and grey water, purification of pharmaceuticals, and filtration of a number of nonaqueous solutions, specifically organic solvents. There is no limit to the feedstreams which could be investigated, provided an appropriate membrane type is selected, as discussed in the next section. The technology could be applied to other materials beyond filtration membranes, as well. As one example, microfluidic control devices could be developed using this technology to function as highly tunable valves or rudders.

Continued study into PW permeate for use as irrigation water is needed as well. The study presented here showed that PW permeate is promising as irrigation water; however, much more study is needed before it could be applied to plants in the field. Studies needed include testing a wider variety of plants and soils, the effect of PW permeate on fully grown plants and harvest yield, the method of irrigation delivery, possible effects of the PW permeate on irrigation equipment such as scaling, and perhaps, most importantly, characterizing the agricultural runoff from PW permeate irrigation. These studies would be fascinating collaborations with soil and crop scientists.

8.3. Membrane Selection

Modified Dow Filmtec NF 270 nanofiltration membranes and Oxyphen PET 400 track-etched microfiltration membranes were used to filter various feedstreams and characterize the effect of modification and magnetic response on a model membrane system, respectively. Clearly, these are not the only membranes compatible with this technology. Any membrane which contains hydroxyl groups on its surface, or another moiety which can be converted to a hydroxyl, could be used with the current modification protocol. Additionally, the modification protocol could be easily altered to be compatible with other membrane surface chemistries. Using an appropriate protocol, magnetically-responsive membranes could be produced using microfiltration, ultrafiltration, nanofiltration, reverse osmosis, forward osmosis, or even pervaporation membranes. Also, the modification is not limited to polymeric membranes. Inorganic membranes are a rapidly growing sector of membrane research, and the development of magnetically-responsive inorganic membranes would be truly novel and present numerous exciting opportunities.

8.4. Magnetic Nanoparticle Size and Magnetic Field Parameters

New applications involving magnetically-responsive membranes could be developed by adjusting the size of the magnetic nanoparticles and the parameters of the magnetic field. Paramagnetic or perhaps even larger nanoparticles would generate different amounts of mixing and/or heating at different magnetic field strengths and frequencies compared to superparamagnetic nanoparticles. It is, however, critical to minimize coupling of a single nanoparticle to multiple grafted polymer chains. Multiple couplings would limit polymer chain

flexibility and thus limit mixing. Larger particles would be at a greater risk to couple to multiple grafted chains.

For the currently used superparamagnetic nanoparticles, the effect of magnetic field strength and frequency should be studied in-depth and modeled. The 50 G field strength used throughout this dissertation research was calculated *a priori* and proved adequate; however, changing the field strength may yield better mixing or hint at possible alternative applications. The frequency of 10 Hz showed the most mixing of the three frequencies tested; however, an empirical model of the effect of field frequency and strength on mixing and/or nanoparticle heating—for a given grafted polymer—would be a powerful tool.

8.5. Modeling of PW Fouling and Imaging Polymer Chain Movement in Real-time

An interesting study which could lead to better understanding of the effect of mixing is determining the type of fouling characteristic of the PW used in this study. This would determine if the fouling is simple deposition, adhesion, or cake layer formation, and if biological fouling is a factor. Knowing the type of fouling and how it develops will help future work optimize the mixing profile to best combat fouling for a particular PW. This would also be necessary when filtering other feedstreams beyond PW as well. A related interest, especially if PW fouling is due to cake layer formation, is whether magnetically-activated mixing can break up an already established cake layer.

Another study which could lead to better understanding of magnetically-activated mixing is imaging the movement of the grafted polymer chains in real-time. This is a complicated issue, which has been considered for some time. Particle image velocimetry, although very useful, can only observe the change in fluid behavior due to mixing, but cannot directly visualize the

movement of the chains. Imaging the polymer chains, only tens of nm in length, in a solvent at a high enough resolution and frequency to capture the magnetic response will not be easy. Some technologies which have been considered and deemed incapable include fluorescence or radiation tagging of the grafted chains (resolution too low), liquid phase atomic force and scanning electron microscopy (data collection too slow to capture movement), and others. These methods could be useful, however, to determine other properties of the system. For example, atomic force microscopy could be used to determine the force constant of varying polymer chain lengths. This could be used to develop a model of magnetically-activated mixing and help optimize the chain length for optimal mixing. If a method for direct imaging is developed, it will offer unequivocal insight into the nature of magnetically-activated mixing.

8.6. Challenges to Membrane Use in Practice

In order for these membranes to be used in real-world applications, it must be proven that the membranes can survive the manufacturing process, transportation and handling, multiple cleaning cycles, and daily wear in a real world setting with no decrease in performance. It is particularly critical that the modification is not damaged resulting in leeching of superparamagnetic particles or grafted polymer chains into the permeate. If the nanoparticles leech into a permeate to be used as process water makeup, the nanoparticles could aggregate and potentially scale or plug equipment. Leeched nanoparticles could be a serious health concern if the permeate is to be used for any application which could possibly be consumed by organisms, such as irrigation or drinking water. Although Fe_3O_4 is not toxic, other nanoparticles made from Nickel or Cobalt, for example, could pose health risks. If the membranes show no sign of leeching, numerous challenges still remain before the membranes can be put into use. Adoption

of magnetically-responsive membranes into a site requires that the membranes be cheap, compact, and should not require any alterations to existing equipment or processes. Four major challenges to develop such "plug-and-play" technology are

- make the modification protocol suitable for large-scale manufacture
- craft a module which can house the membrane but not diminish—or ideally enhance—magnetic mixing
- design the magnetic field apparatus to be compact, simple to install, and safe for humans to work near—electrical shock and disruption of sensitive equipment, such as pacemakers, must be prevented
- develop a cleaning procedure which is safe for the membrane module, effective at removing rejected solutes and/or fouling on the membrane surface, and can be performed without uninstalling the module

Items 1 and 4 are currently under investigation by this group, or will be in the near future. The primary concerns with the modification on a larger scale are the need to exclude oxygen from the SI-ATRP reaction, multiple modification steps which are at least four hours in length, and handling the membranes with sufficient care to not damage them. The cleaning procedure must not only be effective at removing fouling from the membrane surface, but must also not cause any damage to the modification. Planning toward items 2 and 3 has already begun as well. Spiral-wound modules have been considered as a likely candidate for magnetically-responsive nanofiltration membranes. These would consist of large, flat sheet membranes—easy to produce and modify—placed between permeate flow spacers, which would then be rolled into a compact cylinder. Spiral-wound modules have a very large membrane area to module volume ratio, so

the footprint will be small. They are easy to incorporate into existing membrane systems, which often use spiral-wound modules, or can be easily placed in-line at sites which do not already use membrane filtration. Also, preexisting spiral-wound modules could be modified via flow-through SI-ATRP rather than risking damage to the modification by rolling modified flat sheet membranes. It will be straightforward to design a magnetic field apparatus which can fit directly around a spiral-wound module. This is tentatively envisioned as the membrane module being placed in the center of an air-core solenoid resulting in two concentric cylinders. When powered by an AC current, a magnetic field will travel along the center of the solenoid, and thus the center of the membrane module. This field will continuously change direction as the AC current alternates phases (direction along the solenoid), resulting in a continuously alternating field. The solenoid and housing for the membrane module would be permanently mounted. To replace the membrane module, one would simply remove the module from the solenoid/housing apparatus and insert a new spiral-wound module.

The economics of membrane modification must be studied as well. The cost of the membrane modification must be countered by decreased operating costs and/or lower maintenance costs. The research presented in this dissertation suggests magnetically-responsive membranes can lead to lower operating costs (higher throughput), longer membrane lifetime, and easier cleaning; however, the true cost of the modification procedure has not been considered. Work still remains to reduce this design to practice, but the foundations are laid for a compact, easy to install, and easy to maintain magnetically-responsive fouling resistant membrane filtration system.

APPENDIX A1

SI-ATRP GRAFTING OF POLYHEMA CHAINS ON TRACK-ETCHED MICROFILTRATION MEMBRANES

This chapter presents early work, as a supplement to Chapter 2, involving grafting of polyHEMA chains onto track-etched microfiltration membranes as a model membrane system. This was later expanded into the study undertaken in Chapter 3.

Track-etched polyethylene terephthalate (PET) membranes (Oxyphen GmbH, Switzerland) with a pore diameter of roughly 690 nm were modified in an analogous manner to the NF membranes. The same SI-ATRP initiator was immobilized to the surface of the pre-modified PET membranes, containing reactive hydroxyl groups in a density of about 1 nm^{-2}. By using track-etched PET membrane as model system, optimization of SI-ATRP conditions (monomer concentration, ratio between ligand and transition metal catalyst and solvent) was achieved and subsequently also applied for the surface modification of the NF membranes via SI-ATRP. Since track-etched membranes consist of well-defined, uniform, straight-through cylindrical pores, this parallel study also allowed a facile way to monitor increase of grafted polymer mass with polymerization time as well as the grafted layer thickness. A capillary flow porometer (Porous Materials, Inc., USA) was used to measure the average pore diameter of the PET membranes before and after SI-ATRP of varied time. Due to the very narrow pore size distribution, which was preserved upon controlled SI-ATRP, the change in pore radius could be directly related to the dry layer thickness of the grafted polyHEMA on the pore walls.

Figure A1.1 shows the effect of SI-ATRP time on the degree of grafting (DG) of polyHEMA. DG increased linearly with SI-ATRP time indicating the growth of polymer chains from the surface was highly controlled.

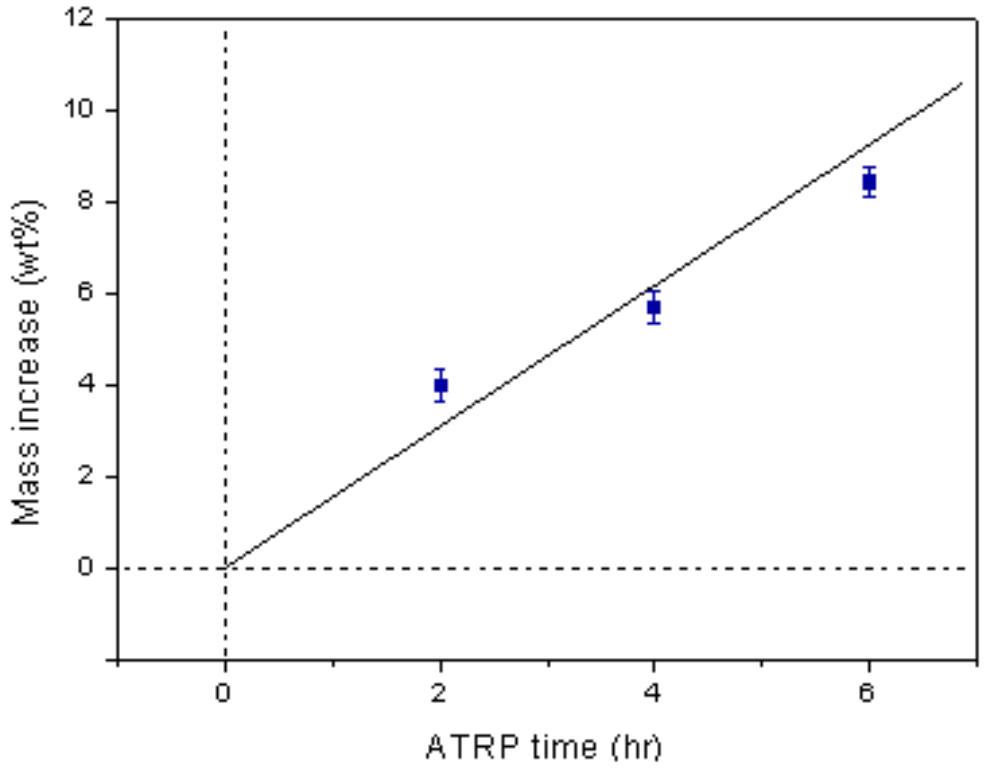

Figure A1.1. Effect of SI-ATRP time on degree of grafting of polyHEMA on track-etched PET membranes under the optimized SI-ATRP conditions to modify the nanofiltration membranes in Chapter 2.

Data from pore diameter measurement are shown in Figure A1.2. With the increase of SI-ATRP time, pore diameter decreased significantly. The pore diameter of unmodified PET membrane used in this study was roughly 690 nm and a linear decrease of pore diameter, corresponding to a linear increase of polyHEMA layer thickness, with SI-ATRP time was observed. Pore diameter after 4 hours was 570 nm, i.e., the dry grafted polyHEMA was about 60 nm thick. Because of the high initiator / grafting density on the PET surface, the grafted polyHEMA chains are in the "brush" regime and adopt a somewhat stretched conformation.

Therefore, 60 nm is a rather conservative estimate of average chain length; the fully stretched chain length, especially in water as solvent, will be larger. Since the polymerization growth conditions were the same —only the initiator / grafting density, i.e., the number of chains per area, was smaller for the NF compared to the track-etched membranes— it can be assumed that the chains on the NF membranes were also roughly 60 nm in length.

Figure A1.2. Average pore diameter (from gas flow / liquid dewetting permporometry measurement) of track-etched PET membranes after grafting of polyHEMA with different SI-ATRP time (cf. Figure A1.1).

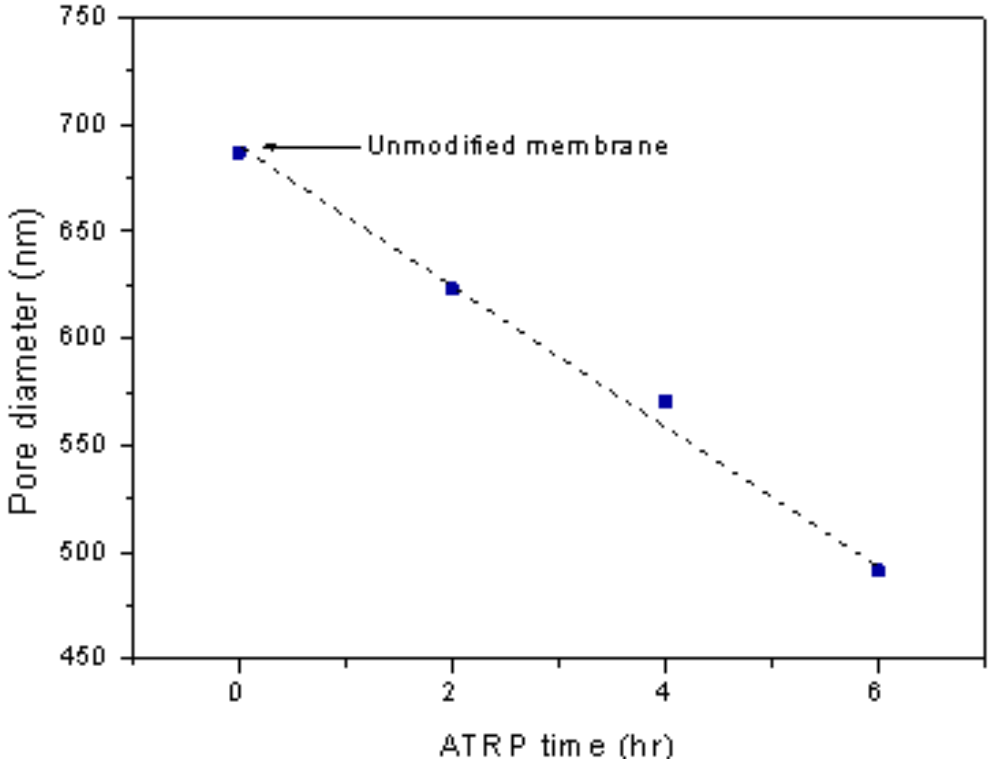

APPENDIX A2

STATISTICAL ANALYSIS OF SEEDLING GERMINATION DATA

This chapter presents the model code used in the statistical software R to calculate the various interactions terms. The full model output and selected ANOVA tables are presented as well.

DESCRIPTION

Statistical analysis on the seedling germination data was performed using R, an open source statistical package. Analysis of means was performed to determine the statistical significance of time on germination for each water quality. A linear model was generated to study the interactions of water quality, time, and crop species on seedling germination in the pairs water quality x time, water quality x crop, and the three-way interaction water quality x crop x time. The model code used in R and the resulting data output are presented here in their entirety.

MODEL CODE

```
crop=read.csv("crop.csv",header=T)
head(crop)
crop$Water.Quality=as.factor(crop$Water.Quality)
crop$Time=as.factor(crop$Time)
crop$Repetition=as.factor(crop$Repetition)
```

```
Norm.germ=lm(X..NormalizedroughlyCrop+Water.Quality+Time+Crop*Water.Quality+Water.
Quality*Time+Crop*Water.Quality*Time, data=crop)
summary(Norm.germ)
anova(Norm.germ)

c1=crop[crop$Crop=="Barley",]
c2=crop[crop$Crop=="Corn",]
c3=crop[crop$Crop=="Onion",]
c4=crop[crop$Crop=="Bean",]

s1=lm(X..NormalizedroughlyWater.Quality+Time+Water.Quality*Time, data=c1)
summary(s1)
anova(s1)
s2=lm(X..NormalizedroughlyWater.Quality+Time+Water.Quality*Time, data=c2)
summary(s2)
anova(s2)
s3=lm(X..NormalizedroughlyWater.Quality+Time+Water.Quality*Time, data=c3)
summary(s3)
anova(s3)
s4=lm(X..NormalizedroughlyWater.Quality+Time+Water.Quality*Time, data=c4)
summary(s4)
anova(s4)
```

Full Interaction Model

```
Full Model All interactions
> crop=read.csv("crop.csv",header=T)
> head(crop)

>
Norm.germ=lm(X..NormalizedroughlyCrop+Water.Quality+Time+Crop*Water.Quality+Water.
Quality*Time+Crop*Water.Quality*Time, data=crop)
> summary(Norm.germ)

Call:
lm(formula = X..Normalized roughly Crop + Water.Quality + Time + Crop *
    Water.Quality + Water.Quality * Time + Crop * Water.Quality *
    Time, data = crop)

Residuals:
    Min      1Q  Median      3Q     Max
-17.500  -4.325   0.000   3.700  18.700

Coefficients:
                                Estimate Std. Error t value Pr(>|t|)
(Intercept)                    1.000e+02  4.878e+00  20.500  < 2e-16 ***
CropBean                      -9.445e-14  6.899e+00   0.000 1.000000
CropCorn                      -1.031e-13  6.899e+00   0.000 1.000000
CropOnion                     -9.372e-14  6.899e+00   0.000 1.000000
Water.Quality2                 3.700e+00  6.899e+00   0.536 0.592474
Water.Quality3                -3.700e+00  6.899e+00  -0.536 0.592474
Water.Quality4                -3.700e+00  6.899e+00  -0.536 0.592474
Water.Quality5                -1.480e+01  6.899e+00  -2.145 0.033435 *
Water.Quality6                 3.700e+00  6.899e+00   0.536 0.592474
Water.Quality7                -3.700e+00  6.899e+00  -0.536 0.592474
Water.Quality8                -3.700e+00  6.899e+00  -0.536 0.592474
Water.Quality9                -3.700e+00  6.899e+00  -0.536 0.592474
Water.Quality10               -1.110e+01  6.899e+00  -1.609 0.109588
Time2                         -7.843e-14  6.899e+00   0.000 1.000000
CropBean:Water.Quality2       -2.217e+01  9.756e+00  -2.272 0.024415 *
CropCorn:Water.Quality2        1.175e-13  9.756e+00   0.000 1.000000
CropOnion:Water.Quality2      -6.567e+00  9.756e+00  -0.673 0.501872
CropBean:Water.Quality3       -2.310e+01  9.756e+00  -2.368 0.019093 *
CropCorn:Water.Quality3        7.400e+00  9.756e+00   0.758 0.449274
CropOnion:Water.Quality3       4.533e+00  9.756e+00   0.465 0.642807
CropBean:Water.Quality4       -3.263e+01  9.756e+00  -3.345 0.001026 **
CropCorn:Water.Quality4        7.400e+00  9.756e+00   0.758 0.449274
CropOnion:Water.Quality4       1.200e+00  9.756e+00   0.123 0.902263
CropBean:Water.Quality5       -7.210e+01  9.756e+00  -7.390 7.69e-12 ***
CropCorn:Water.Quality5        4.433e+00  9.756e+00   0.454 0.650150
CropOnion:Water.Quality5      -6.767e+00  9.756e+00  -0.694 0.488956
CropBean:Water.Quality6       -1.263e+01  9.756e+00  -1.295 0.197221
CropCorn:Water.Quality6       -3.700e+00  9.756e+00  -0.379 0.705009
CropOnion:Water.Quality6      -2.867e+00  9.756e+00  -0.294 0.769269
CropBean:Water.Quality7       -1.477e+01  9.756e+00  -1.514 0.132110
CropCorn:Water.Quality7        4.067e+00  9.756e+00   0.417 0.677363
CropOnion:Water.Quality7      -2.500e+00  9.756e+00  -0.256 0.798090
CropBean:Water.Quality8       -1.417e+01  9.756e+00  -1.452 0.148442
CropCorn:Water.Quality8        7.400e+00  9.756e+00   0.758 0.449274
CropOnion:Water.Quality8      -2.500e+00  9.756e+00  -0.256 0.798090
```

```
CropBean:Water.Quality9          -6.413e+01  9.756e+00  -6.574 6.60e-10 ***
CropCorn:Water.Quality9           4.067e+00  9.756e+00   0.417 0.677363
CropOnion:Water.Quality9         -1.370e+01  9.756e+00  -1.404 0.162189
CropBean:Water.Quality10         -7.580e+01  9.756e+00  -7.769 8.95e-13 ***
CropCorn:Water.Quality10          7.767e+00  9.756e+00   0.796 0.427170
CropOnion:Water.Quality10        -1.047e+01  9.756e+00  -1.073 0.284968
Water.Quality2:Time2             -3.700e+00  9.756e+00  -0.379 0.705009
Water.Quality3:Time2             -2.220e+01  9.756e+00  -2.275 0.024205 *
Water.Quality4:Time2             -3.700e+01  9.756e+00  -3.792 0.000211 ***
Water.Quality5:Time2             -4.080e+01  9.756e+00  -4.182 4.75e-05 ***
Water.Quality6:Time2             -3.700e+00  9.756e+00  -0.379 0.705009
Water.Quality7:Time2              9.740e-14  9.756e+00   0.000 1.000000
Water.Quality8:Time2             -1.480e+01  9.756e+00  -1.517 0.131246
Water.Quality9:Time2             -3.330e+01  9.756e+00  -3.413 0.000813 ***
Water.Quality10:Time2            -4.077e+01  9.756e+00  -4.179 4.81e-05 ***
CropBean:Time2                    8.280e-14  9.756e+00   0.000 1.000000
CropCorn:Time2                   -3.333e+00  9.756e+00  -0.342 0.733054
CropOnion:Time2                   7.892e-14  9.756e+00   0.000 1.000000
CropBean:Water.Quality2:Time2     3.700e+00  1.380e+01   0.268 0.788917
CropCorn:Water.Quality2:Time2     3.667e-01  1.380e+01   0.027 0.978832
CropOnion:Water.Quality2:Time2   -1.000e-01  1.380e+01  -0.007 0.994226
CropBean:Water.Quality3:Time2     1.267e+01  1.380e+01   0.918 0.359976
CropCorn:Water.Quality3:Time2    -3.337e+01  1.380e+01  -2.418 0.016715 *
CropOnion:Water.Quality3:Time2    7.667e+00  1.380e+01   0.556 0.579219
CropBean:Water.Quality4:Time2     9.667e+00  1.380e+01   0.701 0.484561
CropCorn:Water.Quality4:Time2    -2.523e+01  1.380e+01  -1.829 0.069285 .
CropOnion:Water.Quality4:Time2   -7.667e-01  1.380e+01  -0.056 0.955757
CropBean:Water.Quality5:Time2     3.187e+01  1.380e+01   2.310 0.022188 *
CropCorn:Water.Quality5:Time2    -2.143e+01  1.380e+01  -1.553 0.122296
CropOnion:Water.Quality5:Time2   -3.763e+01  1.380e+01  -2.728 0.007093 **
CropBean:Water.Quality6:Time2    -4.667e-01  1.380e+01  -0.034 0.973061
CropCorn:Water.Quality6:Time2     4.067e+00  1.380e+01   0.295 0.768574
CropOnion:Water.Quality6:Time2   -8.040e-14  1.380e+01   0.000 1.000000
CropBean:Water.Quality7:Time2    -4.167e+00  1.380e+01  -0.302 0.763053
CropCorn:Water.Quality7:Time2    -3.700e+00  1.380e+01  -0.268 0.788917
CropOnion:Water.Quality7:Time2   -4.667e-01  1.380e+01  -0.034 0.973061
CropBean:Water.Quality8:Time2     5.867e+00  1.380e+01   0.425 0.671262
CropCorn:Water.Quality8:Time2    -3.037e+01  1.380e+01  -2.201 0.029176 *
CropOnion:Water.Quality8:Time2    6.933e+00  1.380e+01   0.503 0.616000
CropBean:Water.Quality9:Time2     1.483e+01  1.380e+01   1.075 0.283957
CropCorn:Water.Quality9:Time2    -1.893e+01  1.380e+01  -1.372 0.171910
CropOnion:Water.Quality9:Time2   -1.940e+01  1.380e+01  -1.406 0.161645
CropBean:Water.Quality10:Time2    3.720e+01  1.380e+01   2.696 0.007765 **
CropCorn:Water.Quality10:Time2   -2.590e+01  1.380e+01  -1.877 0.062316 .
CropOnion:Water.Quality10:Time2 -2.287e+01  1.380e+01  -1.657 0.099415 .
---
Signif. codes:  0 ‘***’ 0.001 ‘**’ 0.01 ‘*’ 0.05 ‘.’ 0.1 ‘ ’ 1

Residual standard error: 8.449 on 160 degrees of freedom
Multiple R-squared: 0.948,      Adjusted R-squared: 0.9223
F-statistic: 36.89 on 79 and 160 DF,  p-value: < 2.2e-16

> anova(Norm.germ)
Analysis of Variance Table

Response: X..Normalized
                       Df Sum Sq Mean Sq  F value    Pr(>F)
Crop                    3  26215    8738 122.4068 < 2.2e-16 ***
Water.Quality           9  96441   10716 150.1036 < 2.2e-16 ***
Time                    1  32320   32320 452.7350 < 2.2e-16 ***
```

```
Crop:Water.Quality       27  17653     654   9.1585 < 2.2e-16 ***
Water.Quality:Time        9  20541    2282  31.9709 < 2.2e-16 ***
Crop:Time                 3   7042    2347  32.8806 < 2.2e-16 ***
Crop:Water.Quality:Time  27   7832     290   4.0635 1.182e-08 ***
Residuals               160  11422      71
---
Signif. codes:  0 ‘***’ 0.001 ‘**’ 0.01 ‘*’ 0.05 ‘.’ 0.1 ‘ ’ 1
>
> summary(crop$Crop)
Barley   Bean   Corn  Onion
    60     60     60     60
> c1=crop[crop$Crop=="Barley",]
>
> c2=crop[crop$Crop=="Corn",]
>
> c3=crop[crop$Crop=="Onion",]
>
> c4=crop[crop$Crop=="Bean",]
>
>
> s1=lm(X..NormalizedroughlyWater.Quality+Time+Water.Quality*Time, data=c1)
> summary(s1)

Call:
lm(formula = X..Normalized roughly Water.Quality + Time + Water.Quality *
    Time, data = c1)

Residuals:
   Min     1Q Median     3Q    Max
-7.400 -3.700  0.000  3.700  7.467

Coefficients:
                        Estimate Std. Error t value Pr(>|t|)
(Intercept)            1.000e+02  3.098e+00  32.283  < 2e-16 ***
Water.Quality2         3.700e+00  4.381e+00   0.845 0.403353
Water.Quality3        -3.700e+00  4.381e+00  -0.845 0.403353
Water.Quality4        -3.700e+00  4.381e+00  -0.845 0.403353
Water.Quality5        -1.480e+01  4.381e+00  -3.378 0.001636 **
Water.Quality6         3.700e+00  4.381e+00   0.845 0.403353
Water.Quality7        -3.700e+00  4.381e+00  -0.845 0.403353
Water.Quality8        -3.700e+00  4.381e+00  -0.845 0.403353
Water.Quality9        -3.700e+00  4.381e+00  -0.845 0.403353
Water.Quality10       -1.110e+01  4.381e+00  -2.534 0.015303 *
Time2                 -5.026e-14  4.381e+00   0.000 1.000000
Water.Quality2:Time2  -3.700e+00  6.195e+00  -0.597 0.553721
Water.Quality3:Time2  -2.220e+01  6.195e+00  -3.583 0.000911 ***
Water.Quality4:Time2  -3.700e+01  6.195e+00  -5.972 5.17e-07 ***
Water.Quality5:Time2  -4.080e+01  6.195e+00  -6.586 7.11e-08 ***
Water.Quality6:Time2  -3.700e+00  6.195e+00  -0.597 0.553721
Water.Quality7:Time2   5.229e-14  6.195e+00   0.000 1.000000
Water.Quality8:Time2  -1.480e+01  6.195e+00  -2.389 0.021705 *
Water.Quality9:Time2  -3.330e+01  6.195e+00  -5.375 3.56e-06 ***
Water.Quality10:Time2 -4.077e+01  6.195e+00  -6.580 7.24e-08 ***
---
Signif. codes:  0 ‘***’ 0.001 ‘**’ 0.01 ‘*’ 0.05 ‘.’ 0.1 ‘ ’ 1

Residual standard error: 5.365 on 40 degrees of freedom
Multiple R-squared: 0.9452,     Adjusted R-squared: 0.9192
F-statistic: 36.31 on 19 and 40 DF,  p-value: < 2.2e-16
```

```
> anova(s1)
Analysis of Variance Table

Response: X..Normalized
                   Df  Sum Sq Mean Sq F value    Pr(>F)
Water.Quality       9 10043.3  1115.9  38.766 < 2.2e-16 ***
Time                1  5778.1  5778.1 200.725 < 2.2e-16 ***
Water.Quality:Time  9  4037.5   448.6  15.584 1.627e-10 ***
Residuals          40  1151.4    28.8
---
Signif. codes:  0 ‘***’ 0.001 ‘**’ 0.01 ‘*’ 0.05 ‘.’ 0.1 ‘ ’ 1
>
> s2=lm(X..NormalizedroughlyWater.Quality+Time+Water.Quality*Time, data=c2)
> summary(s2)

Call:
lm(formula = X..Normalized roughly Water.Quality + Time + Water.Quality *
    Time, data = c2)

Residuals:
     Min       1Q   Median       3Q      Max
-10.3667  -3.7000  -0.1833   3.3333  14.0667

Coefficients:
                    Estimate Std. Error t value Pr(>|t|)
(Intercept)         1.000e+02  4.031e+00  24.806  < 2e-16 ***
Water.Quality2      3.700e+00  5.701e+00   0.649   0.5200
Water.Quality3      3.700e+00  5.701e+00   0.649   0.5200
Water.Quality4      3.700e+00  5.701e+00   0.649   0.5200
Water.Quality5     -1.037e+01  5.701e+00  -1.818   0.0765 .
Water.Quality6     -5.063e-14  5.701e+00   0.000   1.0000
Water.Quality7      3.667e-01  5.701e+00   0.064   0.9490
Water.Quality8      3.700e+00  5.701e+00   0.649   0.5200
Water.Quality9      3.667e-01  5.701e+00   0.064   0.9490
Water.Quality10    -3.333e+00  5.701e+00  -0.585   0.5620
Time2              -3.333e+00  5.701e+00  -0.585   0.5620
Water.Quality2:Time2  -3.333e+00  8.062e+00  -0.413   0.6815
Water.Quality3:Time2  -5.557e+01  8.062e+00  -6.892 2.65e-08 ***
Water.Quality4:Time2  -6.223e+01  8.062e+00  -7.719 1.91e-09 ***
Water.Quality5:Time2  -6.223e+01  8.062e+00  -7.719 1.91e-09 ***
Water.Quality6:Time2   3.667e-01  8.062e+00   0.045   0.9640
Water.Quality7:Time2  -3.700e+00  8.062e+00  -0.459   0.6488
Water.Quality8:Time2  -4.517e+01  8.062e+00  -5.602 1.71e-06 ***
Water.Quality9:Time2  -5.223e+01  8.062e+00  -6.479 1.00e-07 ***
Water.Quality10:Time2 -6.667e+01  8.062e+00  -8.269 3.43e-10 ***
---
Signif. codes:  0 ‘***’ 0.001 ‘**’ 0.01 ‘*’ 0.05 ‘.’ 0.1 ‘ ’ 1

Residual standard error: 6.982 on 40 degrees of freedom
Multiple R-squared: 0.9612,     Adjusted R-squared: 0.9427
F-statistic: 52.09 on 19 and 40 DF,  p-value: < 2.2e-16

> anova(s2)
Analysis of Variance Table

Response: X..Normalized
                   Df  Sum Sq Mean Sq F value    Pr(>F)
Water.Quality       9 14466.3  1607.4  32.970 9.158e-16 ***
Time                1 22129.9 22129.9 453.921 < 2.2e-16 ***
Water.Quality:Time  9 11651.5  1294.6  26.555 3.589e-14 ***
```

```
Residuals          40  1950.1    48.8
---
Signif. codes:  0 ‘***’ 0.001 ‘**’ 0.01 ‘*’ 0.05 ‘.’ 0.1 ‘ ’ 1
>
> s3=lm(X..NormalizedroughlyWater.Quality+Time+Water.Quality*Time, data=c3)
> summary(s3)

Call:
lm(formula = X..Normalized roughly Water.Quality + Time + Water.Quality *
    Time, data = c3)

Residuals:
    Min      1Q  Median      3Q     Max
-17.500  -7.808   0.000   6.742  18.700

Coefficients:
                       Estimate Std. Error t value Pr(>|t|)
(Intercept)           1.000e+02  6.657e+00  15.021  < 2e-16 ***
Water.Quality2       -2.867e+00  9.415e+00  -0.304 0.762342
Water.Quality3        8.333e-01  9.415e+00   0.089 0.929912
Water.Quality4       -2.500e+00  9.415e+00  -0.266 0.791963
Water.Quality5       -2.157e+01  9.415e+00  -2.291 0.027331 *
Water.Quality6        8.333e-01  9.415e+00   0.089 0.929912
Water.Quality7       -6.200e+00  9.415e+00  -0.659 0.513976
Water.Quality8       -6.200e+00  9.415e+00  -0.659 0.513976
Water.Quality9       -1.740e+01  9.415e+00  -1.848 0.071990 .
Water.Quality10      -2.157e+01  9.415e+00  -2.291 0.027331 *
Time2                -6.752e-14  9.415e+00   0.000 1.000000
Water.Quality2:Time2 -3.800e+00  1.331e+01  -0.285 0.776814
Water.Quality3:Time2 -1.453e+01  1.331e+01  -1.092 0.281579
Water.Quality4:Time2 -3.777e+01  1.331e+01  -2.836 0.007126 **
Water.Quality5:Time2 -7.843e+01  1.331e+01  -5.891 6.73e-07 ***
Water.Quality6:Time2 -3.700e+00  1.331e+01  -0.278 0.782532
Water.Quality7:Time2 -4.667e-01  1.331e+01  -0.035 0.972215
Water.Quality8:Time2 -7.867e+00  1.331e+01  -0.591 0.557966
Water.Quality9:Time2 -5.270e+01  1.331e+01  -3.958 0.000302 ***
Water.Quality10:Time2 -6.363e+01  1.331e+01  -4.779 2.39e-05 ***
---
Signif. codes:  0 ‘***’ 0.001 ‘**’ 0.01 ‘*’ 0.05 ‘.’ 0.1 ‘ ’ 1

Residual standard error: 11.53 on 40 degrees of freedom
Multiple R-squared: 0.9053,     Adjusted R-squared: 0.8603
F-statistic: 20.12 on 19 and 40 DF,  p-value: 8.536e-15

> anova(s3)
Analysis of Variance Table

Response: X..Normalized
                   Df  Sum Sq Mean Sq F value    Pr(>F)
Water.Quality       9 28770.3  3196.7 24.0418 1.853e-13 ***
Time                1 10367.5 10367.5 77.9718 6.146e-11 ***
Water.Quality:Time  9 11691.6  1299.1  9.7701 1.032e-07 ***
Residuals          40  5318.6   133.0
---
Signif. codes:  0 ‘***’ 0.001 ‘**’ 0.01 ‘*’ 0.05 ‘.’ 0.1 ‘ ’ 1
>
> s4=lm(X..NormalizedroughlyWater.Quality+Time+Water.Quality*Time, data=c4)
> summary(s4)

Call:
```

```
lm(formula = X..Normalized roughly Water.Quality + Time + Water.Quality *
    Time, data = c4)

Residuals:
    Min      1Q  Median      3Q     Max
-13.100  -5.517   0.000   5.067  13.100

Coefficients:
                       Estimate Std. Error t value Pr(>|t|)
(Intercept)            1.000e+02  5.002e+00  19.993  < 2e-16 ***
Water.Quality2        -1.847e+01  7.073e+00  -2.611 0.012656 *
Water.Quality3        -2.680e+01  7.073e+00  -3.789 0.000499 ***
Water.Quality4        -3.633e+01  7.073e+00  -5.137 7.65e-06 ***
Water.Quality5        -8.690e+01  7.073e+00 -12.285 3.72e-15 ***
Water.Quality6        -8.933e+00  7.073e+00  -1.263 0.213921
Water.Quality7        -1.847e+01  7.073e+00  -2.611 0.012656 *
Water.Quality8        -1.787e+01  7.073e+00  -2.526 0.015603 *
Water.Quality9        -6.783e+01  7.073e+00  -9.590 6.37e-12 ***
Water.Quality10       -8.690e+01  7.073e+00 -12.285 3.72e-15 ***
Time2                 -8.979e-14  7.073e+00   0.000 1.000000
Water.Quality2:Time2   6.780e-14  1.000e+01   0.000 1.000000
Water.Quality3:Time2  -9.533e+00  1.000e+01  -0.953 0.346304
Water.Quality4:Time2  -2.733e+01  1.000e+01  -2.732 0.009313 **
Water.Quality5:Time2  -8.933e+00  1.000e+01  -0.893 0.377178
Water.Quality6:Time2  -4.167e+00  1.000e+01  -0.417 0.679250
Water.Quality7:Time2  -4.167e+00  1.000e+01  -0.417 0.679250
Water.Quality8:Time2  -8.933e+00  1.000e+01  -0.893 0.377178
Water.Quality9:Time2  -1.847e+01  1.000e+01  -1.846 0.072294 .
Water.Quality10:Time2 -3.567e+00  1.000e+01  -0.357 0.723303
---
Signif. codes:  0 ‘***’ 0.001 ‘**’ 0.01 ‘*’ 0.05 ‘.’ 0.1 ‘ ’ 1

Residual standard error: 8.663 on 40 degrees of freedom
Multiple R-squared: 0.9544,     Adjusted R-squared: 0.9328
F-statistic: 44.11 on 19 and 40 DF,  p-value: < 2.2e-16

> anova(s4)
Analysis of Variance Table

Response: X..Normalized
                   Df Sum Sq Mean Sq F value    Pr(>F)
Water.Quality       9  60813  6757.1 90.0346 < 2.2e-16 ***
Time                1   1086  1086.3 14.4745 0.0004767 ***
Water.Quality:Time  9    993   110.3  1.4698 0.1925303
Residuals          40   3002    75.0
---
Signif. codes:  0 ‘***’ 0.001 ‘**’ 0.01 ‘*’ 0.05 ‘.’ 0.1 ‘ ’ 1
```

Selected ANOVA Analyses

One-way ANOVA: Barley Day 7 vs. WQ

```
Source  DF      SS     MS     F      P
C2       9   7.333  0.815  3.06  0.018
Error   20   5.333  0.267
Total   29  12.667

S = 0.5164   R-Sq = 57.89%   R-Sq(adj) = 38.95%
```

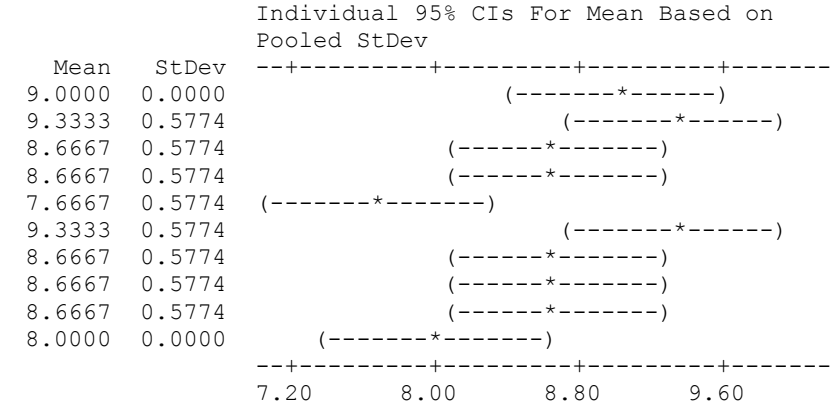


```
Pooled StDev = 0.5164
```

One-way ANOVA: Corn Day 7 vs. WQ

```
Source  DF     SS     MS     F      P
C12      9  4.667  0.519  2.59  0.036
Error   20  4.000  0.200
Total   29  8.667

S = 0.4472   R-Sq = 53.85%   R-Sq(adj) = 33.08%
```

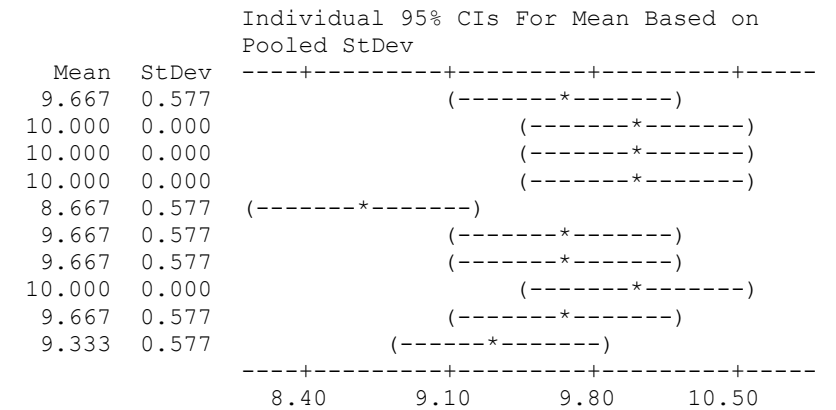


```
Pooled StDev = 0.447
```

One-way ANOVA: Onion Day 6 vs. WQ

```
Source  DF      SS     MS     F      P
C22      9  18.033  2.004  7.51  0.000
Error   20   5.333  0.267
Total   29  23.367

S = 0.5164   R-Sq = 77.18%   R-Sq(adj) = 66.90%


                          Individual 95% CIs For Mean Based on
                          Pooled StDev
Level  N    Mean   StDev  ------+---------+---------+---------+---
 1     3  9.0000  1.0000                     (-----*-----)
 2     3  8.6667  0.5774                 (------*-----)
 3     3  9.0000  0.0000                     (-----*-----)
 4     3  8.6667  0.5774                 (------*-----)
 5     3  7.0000  0.0000  (-----*-----)
 6     3  9.0000  0.0000                     (-----*-----)
 7     3  8.3333  0.5774               (-----*------)
 8     3  8.3333  0.5774               (-----*------)
 9     3  7.3333  0.5774     (-----*------)
10     3  7.0000  0.0000  (-----*-----)
                          ------+---------+---------+---------+---
                              7.0       8.0       9.0      10.0

Pooled StDev = 0.5164
```

One-way ANOVA: Bean Day 8 vs. WQ

```
Source  DF       SS      MS      F      P
C32      9  147.633  16.404  28.95  0.000
Error   20   11.333   0.567
Total   29  158.967

S = 0.7528   R-Sq = 92.87%   R-Sq(adj) = 89.66%


                          Individual 95% CIs For Mean Based on Pooled StDev
Level  N    Mean   StDev    +---------+---------+---------+---------
 1     3  7.3333  0.5774                              (--*---)
 2     3  6.0000  1.0000                         (---*---)
 3     3  5.3333  0.5774                        (--*---)
 4     3  4.6667  0.5774                   (---*--)
 5     3  1.0000  1.0000    (---*---)
 6     3  6.6667  0.5774                            (---*--)
 7     3  6.0000  1.0000                         (---*---)
 8     3  6.0000  0.0000                         (---*---)
 9     3  2.3333  0.5774           (--*---)
10     3  1.0000  1.0000    (---*---)
                            +---------+---------+---------+---------
                          0.0       2.5       5.0       7.5

Pooled StDev = 0.7528
```

One-way ANOVA: Barley Day 14 vs. WQ

```
Source  DF       SS      MS      F      P
C2       9  106.700  11.856  59.28  0.000
Error   20    4.000   0.200
Total   29  110.700

S = 0.4472   R-Sq = 96.39%   R-Sq(adj) = 94.76%


                          Individual 95% CIs For Mean Based on
                          Pooled StDev
Level  N    Mean   StDev  --------+---------+---------+---------+-
 1     3  9.0000  0.0000                                  (--*---)
 2     3  9.0000  0.0000                                  (--*---)
 3     3  6.6667  0.5774                 (---*--)
 4     3  5.3333  0.5774          (--*---)
 5     3  4.0000  0.0000  (--*--)
 6     3  9.0000  0.0000                                  (--*---)
 7     3  8.6667  0.5774                                (--*---)
 8     3  7.3333  0.5774                       (---*--)
 9     3  5.6667  0.5774            (--*---)
10     3  4.3333  0.5774    (--*--)
                          --------+---------+---------+---------+-
                                4.8       6.4       8.0       9.6

Pooled StDev = 0.4472
```

One-way ANOVA: Corn Day 14 vs. WQ

```
Source  DF       SS      MS      F      P
C12      9  234.967  26.107  87.02  0.000
Error   20    6.000   0.300
Total   29  240.967

S = 0.5477   R-Sq = 97.51%   R-Sq(adj) = 96.39%


                          Individual 95% CIs For Mean Based on
                          Pooled StDev
Level  N    Mean   StDev  ---+---------+---------+---------+------
 1     3  9.3333  0.5774                               (-*--)
 2     3  9.3333  0.5774                               (-*--)
 3     3  4.3333  0.5774          (-*--)
 4     3  3.6667  0.5774       (--*-)
 5     3  2.3333  0.5774  (-*--)
 6     3  9.3333  0.5774                               (-*--)
 7     3  9.0000  0.0000                             (--*--)
 8     3  5.3333  0.5774              (-*--)
 9     3  4.3333  0.5774          (-*--)
10     3  2.6667  0.5774   (--*-)
                          ---+---------+---------+---------+------
                           2.5       5.0       7.5      10.0

Pooled StDev = 0.5477
```

One-way ANOVA: Onion Day 10 vs. WQ

```
Source  DF       SS      MS      F      P
C22      9  305.367  33.930  92.54  0.000
Error   20    7.333   0.367
Total   29  312.700

S = 0.6055   R-Sq = 97.65%   R-Sq(adj) = 96.60%


                          Individual 95% CIs For Mean Based on
                          Pooled StDev
Level  N    Mean   StDev  --+---------+---------+---------+-------
 1     3  9.0000  1.0000                                  (-*-)
 2     3  8.3333  0.5774                                (--*-)
 3     3  7.6667  0.5774                              (--*-)
 4     3  5.3333  0.5774                    (--*-)
 5     3  0.0000  0.0000  (-*-)
 6     3  8.6667  0.5774                                 (--*-)
 7     3  8.3333  0.5774                                (--*-)
 8     3  7.6667  0.5774                              (--*-)
 9     3  2.6667  0.5774           (--*-)
10     3  1.3333  0.5774       (-*--)
                          --+---------+---------+---------+-------
                          0.0       3.0       6.0       9.0

Pooled StDev = 0.6055
```

One-way ANOVA: Bean Day 14 vs. WQ

```
Source  DF       SS      MS      F      P
C32      9  182.667  20.296  55.35  0.000
Error   20    7.333   0.367
Total   29  190.000

S = 0.6055   R-Sq = 96.14%   R-Sq(adj) = 94.40%


                          Individual 95% CIs For Mean Based on
                          Pooled StDev
Level  N    Mean   StDev  --+---------+---------+---------+-------
 1     3  7.3333  0.5774                                 (--*--)
 2     3  6.0000  1.0000                             (--*--)
 3     3  4.6667  0.5774                        (--*--)
 4     3  2.6667  0.5774              (--*--)
 5     3  0.3333  0.5774  (--*--)
 6     3  6.3333  0.5774                              (--*--)
 7     3  5.6667  0.5774                            (--*--)
 8     3  5.3333  0.5774                          (--*--)
 9     3  1.0000  0.0000      (--*--)
10     3  0.6667  0.5774    (--*--)
                          --+---------+---------+---------+-------
                          0.0       2.5       5.0       7.5

Pooled StDev = 0.6055
```

Two-way ANOVA: C14 (Norm%) versus C7(crop), C9(WQ) at time 1

Source	DF	SS	MS	F	P
C7	3	25601.1	8533.71	104.75	0.000
C9	9	16133.6	1792.63	22.01	0.000
Interaction	27	15256.5	565.06	6.94	0.000
Error	80	6517.1	81.46		
Total	119	63508.5			

S = 9.026 R-Sq = 89.74% R-Sq(adj) = 84.74%

Two-way ANOVA: C24(Norm%) versus C17(crop), C19(WQ) at time 2

Source	DF	SS	MS	F	P
C17	3	7640	2546.7	41.53	0.000
C19	9	100854	11206.0	182.73	0.000
Interaction	27	10238	379.2	6.18	0.000
Error	80	4906	61.3		
Total	119	123639			

S = 7.831 R-Sq = 96.03% R-Sq(adj) = 94.10%

Two-way ANOVA: C13 (Norm%) versus C7(crop), C9(WQ) over both times

Source	DF	SS	MS	F	P
C7	3	26305	8768.2	22.23	0.000
C9	9	96263	10695.9	27.12	0.000
Interaction	27	17788	658.8	1.67	0.025
Error	200	78890	394.4		
Total	239	219246			

S = 19.86 R-Sq = 64.02% R-Sq(adj) = 57.00%

APPENDIX A3

EQUATIONS AND ASSUMPTIONS OF THE HYDRUS 1-D MODEL

This chapter presents some of the underlying equations present in the HYDRUS-1D model used in Chapter 6.

HYDRUS-1D version 4.08 was used to model the effect of application of contaminated water on soil saturated hydraulic conductivity (HC)[1]. The 1D model does not account for radial flow of water as it moves through the soil column. When more contaminated waters are applied to soils the accumulation of cations, specifically sodium and also potassium, clay particulates in the soil can become dispersed. These dispersions can block free volume spaces in the soil and lead to soil swelling, both of which will reduce the HC of water. The amount of individual ions present as well as the pH of the soil can have a strong effect on these changes[2, 3].

In HYDRUS-1D the negative effect of water chemistry on soil HC, labeled K in the HYDRUS literature, is given by

$$K(h, pH, SAR, C_o) = r(pH, SAR, C_o)K(h) \tag{A3.1}$$

where h is the water pond height discussed in Chapter 6, SAR is the sodium adsorption ratio, C_o is the salt concentration of the solution (mmol/L), r is a scaling factor accounting for the effect of solution chemistry on the final K, and K(h) is the HC in ideal conditions with no solution chemistry effects. The factor r is further divided into two sub-factors corresponding to effects of salt concentrations and soil pH, labeled r and r_2 respectively[3, 4].

$$r(pH, SAR, C_o) = r_1(SAR, C_o)r_2(pH) \tag{A3.2}$$

Equations and assumptions present in Equations A3.3 - A3.8 were established by McNeal[4].

$$r_1 = 1 - \frac{cx^n}{1 + cx^n} \tag{A3.3}$$

where c and n are empirical parameters, and x is the interlayer swelling parameter of soil montmorillonite (a type of clay) defined as

$$x = f_{mont} \cdot (3.6E - 4)(ESP^*)(d^*) \tag{A3.4}$$

where f_{mont} is the weight fraction of montmorillonite in the soil, ESP* is the adjusted exchangeable sodium percentage (ESP) as defined below, and d* is the adjusted interlayer spacing as defined below. f_{mont} values consistent with similar soils in the area were assumed. ESP (and by extension ESP*) depends on the exchangeable sodium concentration $\overline{\text{Na}}$ (mmol/kg) and cation exchange capacity CEC (mmol/kg) as follows

$$ESP^* = \max[0, ESP - (1.24 + 11.63 \log C_o)] \tag{A3.5}$$

$$ESP = 100 \frac{\overline{Na}}{CEC} \tag{A3.6}$$

$$d^* = 0 \quad \text{for} \quad C_o > 300 \quad \text{and} \quad d^* = \frac{356.4}{\sqrt{C_o}} + 1.2 \quad \text{for} \quad C_o < 300 \tag{A3.7}$$

First approximations of the empirical factors n and c used in Equation A3.3 are given as

for	ESP < 25	n = 1	and	c = 35
for	25 < ESP < 50	n = 2	and	c = 932
for	ESP > 50	n = 3	and	c = 25,000

(A3.8)

The second reduction sub-factor, r_2, was calculated as[3]

for	pH < 6.83	$r_2 = 1$
for	6.83 < pH < 9.3	$r_2 = 3.46 - 0.36$pH
for	pH > 9.3	$r_2 = 0.1$

(A3.9)

It should be noted that HYDUS-1D assumes r_1 and r_2 are independent of pressure head—the height (h) of the water pond on the soil—see Equations A3.1 and A3.2. The software authors note that this assumption has not been validated in the literature[1].

Many of these values had to be assumed for the model study in Chapter 6. Values were chosen by Dr. G. Butters, an expert in soil science, to be consistent with similar soils, which have been characterized previously. Although reasonable, these assumptions could introduce a significant degree of error due to the multi-tiered structure of the model. If the actual soils used are fully characterized for future work, it is expected that the HYDRUS-1D model will predict changes in saturated HC more accurately.

REFERENCES

1. J. Šimůnek, M. Šejna, H. Saito, M. Sakai, M. Th. van Genuchten, The HYDRUS-1D software package for simulating the one-dimensional movement of water, heat, and multiple solutes in variably-saturated media, January 2009, Dept. of Environ. Sci., Univ. California Riverside. Software version 4.08.
2. I. Shainber, G. J. Levy, Physico-chemical effects of salts upon infiltration and water movement in soils, In: Interacting Processes in Soil Science, Ed. R. J. Wagenet, P. Baveye, B. A. Stewart, Lewis Publishers, CRC Press, Boca Raton, 1992.
3. D. L. Suarez, J. D. Rhoades, R. Lavado, C. M. Grieve, Effect of pH on saturated hydraulic conductivity and soil dispersion, Soil Sci. Soc. Am. J., 48 (1984), 50-55.
4. B. L. McNeal, Prediction of the effect of mixed-salt solutions on soil hydraulic conductivity, Soil Sci. Soc. Amer. Proc., 32 (1968), 190-193.

APPENDIX A4

DESCRIPTION OF ALTERNATING MAGNETIC FIELD APPARATUS

The complete magnetic field apparatus is shown in Figure A4.1. Two solenoids were created by wrapping two twelve inch stainless steel cores with No. 24 magnetic wire. A computer-operated programmable logic controller (PLC) controlled the rate at which the two solenoids received power by alternatively activating two solid state relays. This determined the frequency of the alternating magnetic field. The solenoids were powered by an Agilent Technologies (Santa Clara, CA) 20 V, 25 A power supply. The solenoids were positioned on two opposite sides of the filtration cell so that the magnetic field direction was parallel to the topmost selective layer of the membrane. The fields both pointed towards the filtration cell, shown by the arrows. Only one solenoid was powered at a given time. This arrangement would yield the greatest lateral movement of the end of the nanoparticle-capped polymer brushes and thus the greatest agitation of the feed solution above the membrane surface. The output voltage and amperage of the power source and the frequency of the field were varied to generate the desired alternating magnetic field of roughly 50 G and 10 Hz to match the field used in the PIV experiments.

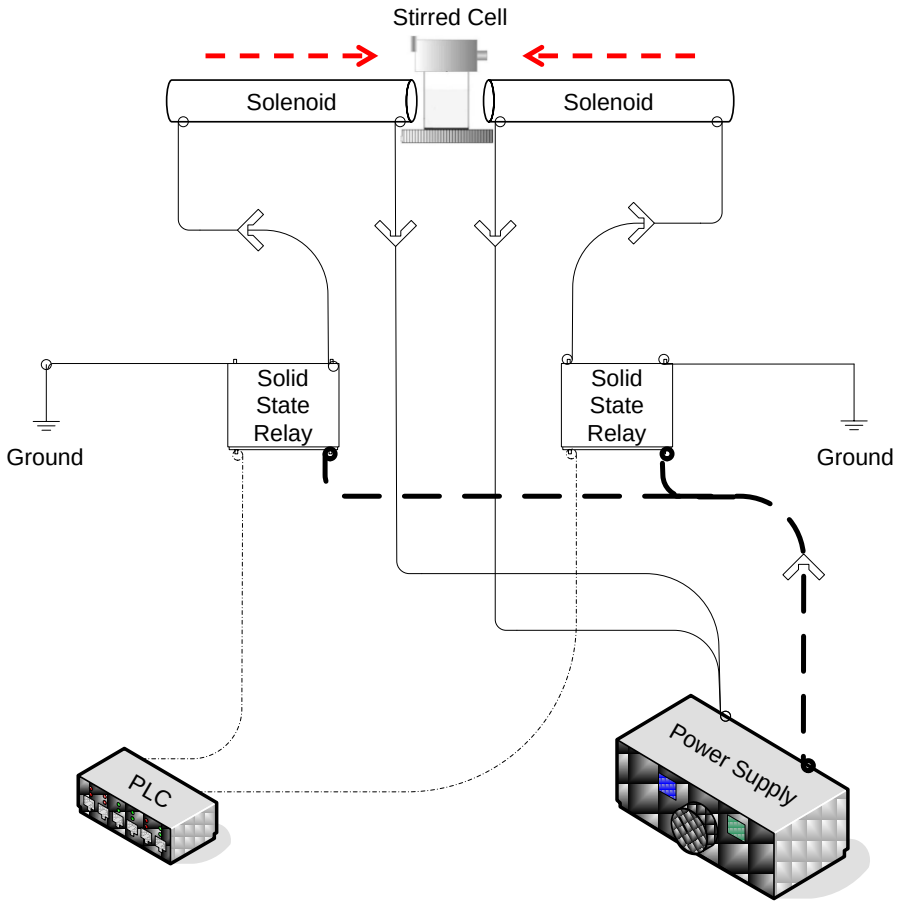

Figure A4.1. Schematic detailing the magnetic field apparatus.

The PLC was controlled using software provided by the manufacturer. An image showing one sample program is shown in Figure A4.2. The program was designed to alternatively power the two solenoids at a given frequency as well as turn the magnetic system on and off for given durations. T11 and T12 determine how long the magnetic systems is turned off and on, respectively. T1 and T2 control the rate at which the two solenoids are alternatively powered. Thus, this example generates a magnetic field alternating at 10 Hz (T1, T2), which is turned on for 10 seconds (T12) and turned off for 120 seconds (T11). This corresponds to magnetic fields used for the model and realistic PW filtration described in chapters 5 and 6.

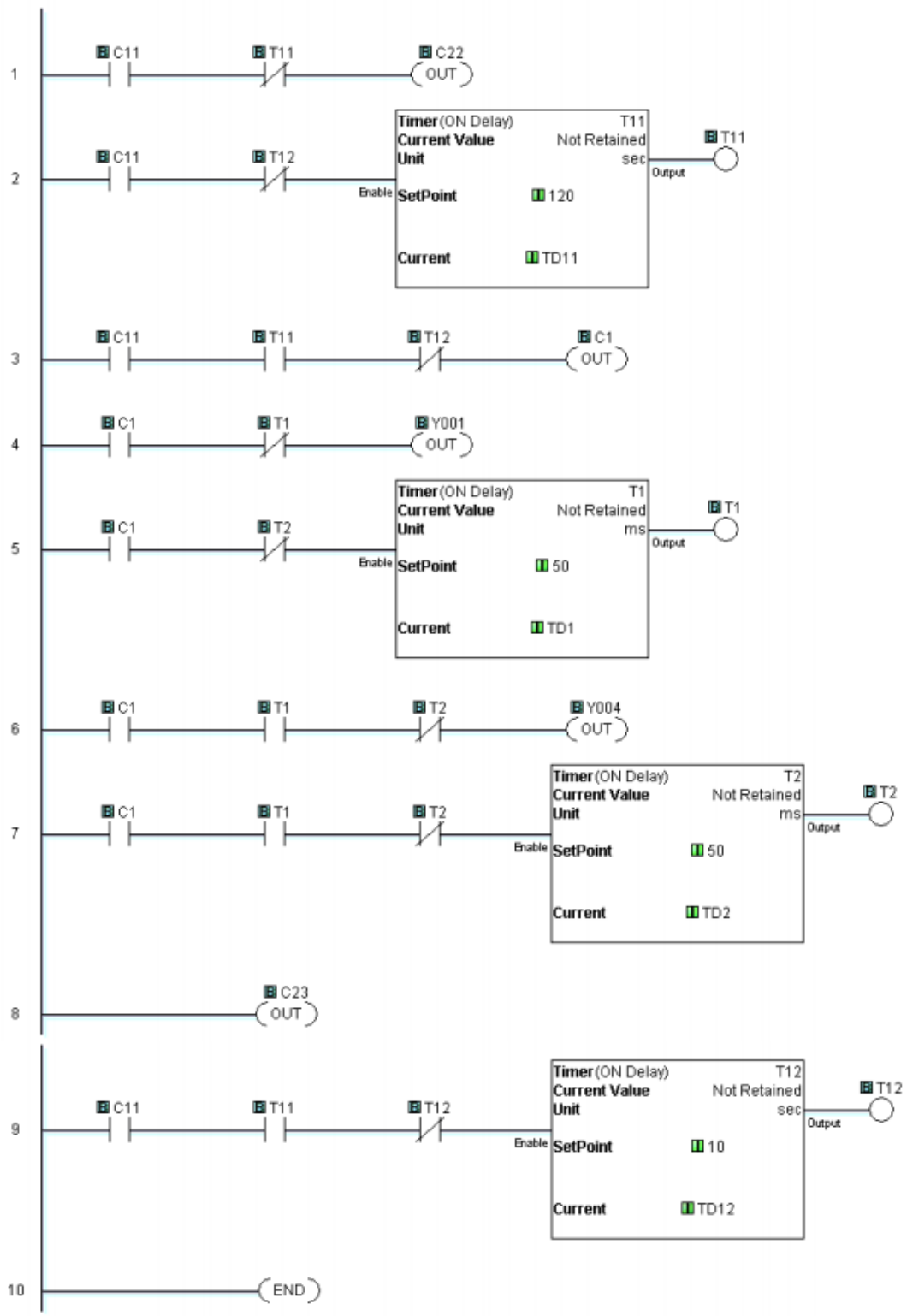

Figure A4.2. Screencapture of one possible PLC program. T1 and T2 control the frequency at which the solenoids are powered. T11 and T12 control how long the magnetic field is off and on, respectively.

APPENDIX A5

OTHER PROJECTS INVOLVING STIMULI-RESPONSIVE MEMBRANES WHICH I HAVE WORKED ON

In addition to my dissertation research, I have participated in two of side projects involving responsive membranes. The first project involved modifying nanofiltration membranes via UV-initiated polymerization to be responsive to changes in solution pH. The effect of the pH response on glucose and sucrose rejection was studied. I developed the modification protocol and designed the experiments; however, the experiments were mostly performed by Katie Marshall, and undergraduate. My role during the experimentation was predominantly an advisory role. As the study progressed, Katie was granted more independence and began to suggest experiments to perform and hypothesize explanations for the experimental findings. Additionally, another undergraduate, Sarah Williams, joined the project and performed many of the later experiments. This was a fantastic learning experience, and will help in my future career as a research professor.

The other project involved creating microfiltration membranes which were responsive to changes in solution ionic strength for hydrophobic interaction chromatography (HIC) of proteins. This work was performed as an independent study for course credit. I developed the modification protocol, and worked with another graduate student, Justin Weaver, to test the binding capacity and recovery of the modified membranes. The project was successful and is continuing in my stead. I was then responsible for training the graduate student who will be performing the future experiments.

Currently, the first part of the pH-responsive membrane study has been published (see abstract below), while the second part is in preparation for submission to *Journal of Membrane Science*. Additionally, the HIC study is in the final stages of preparation for submission to *Journal of Membrane Science* as well. The abstract for the published pH-responsive work is presented here.

pH-responsive Nanofiltration Membranes by Surface Modification.

H. H. Himstedt, K. M. Marshall, S. R. Wickramasinghe, J. Mem. Sci. 366 (2011) 373-381.

Fouling of nanofiltration membranes remains a major concern that often limits process viability. One method to minimize fouling is to modify the filtration surface and perhaps the pores of the membrane in order to minimize adsorption of dissolved solutes. Here nanofiltration membranes have been modified by growing acrylic acid nanobrushes from the surface of the membrane. If the pH of the feed is above the pKa of the grafted nanobrushes, the carboxylic groups will be deprotonated and swell. Dead end filtration experiments confirm that polyacrylic acid nanobrushes may be grafted from the surface of high flux nanofiltration membranes without significantly impacting the filtrate flux. Furthermore, swelling of the grafted nanobrushes at pH values above their pKa leads to a decrease in filtrate flux. Rejection of glucose has also been investigated. For the base membrane, glucose rejection was not affected by feed pH over the range 3–7. However for modified membranes a significant change in rejection was observed as a function of pH. Thus pH-responsive nanofiltration membranes may be designed by surface modification.

APPENDIX A6

CURRICULUM VITAE

Heath Henry Himstedt

heath.himstedt@gmail.com
501-207-1539
1370 Campus Delivery
Fort Collins, CO 80523-1370

Education

PhD Chemical Engineering, Colorado State University, expected September 2012
Thesis Advisors: Dr. S. Ranil Wickramasinghe & Dr. Xianghong Qian
Thesis title : *Magnetically-activated filtration membranes*. I chemically modified filtration membranes to generate mixing in response to a magnetic field. Using these improved-performance membranes I treated wastewater to obtain possible irrigation water.

MA German, Colorado State University, expected September 2012
Thesis Advisor: Dr. Jay Bodine
Thesis title : *The role of science in German language and culture*.
Cumulative GPA for both degrees : 3.90 on 4.00 scale

B.S. (honors) Chemical Engineering, Summa Cum Laude, University of Arkansas (Dec 2007)
Thesis Advisor: Dr. Jamie Hestekin
Honors Thesis: Transport Properties of Wafer-enhanced Electrodialysis (WE-EDI): Fundamental Determination based upon Wafer Characteristics. Defended Nov. 2007.

B.S. (honors) Physics, University of Arkansas (Dec 2007)

B.A. German University of Arkansas (Dec 2007)
Karl Franzens Universität, Graz, Austria : exchange student for two semesters (2006)
Cumulative GPA for three degrees : 3.97 on 4.00 scale

Academic Awards and Achievements

- DoD National Defense Science & Engineering Graduate (NDSEG) Fellow (2009-2012)
- American Institute of Chemical Engineers (AIChE) Separations Division Graduate Student Research Award (2012)
- North American Membrane Society (NAMS) Elias Klein Travel Award to attend NAMS National Meeting (2012)
- European Membrane Society (EMS) Travel Award to attend International Conference on Membranes (ICOM) (2011)
- North American Membrane Society (NAMS) Elias Klein Travel Award to attend International Conference on Membranes (2011)

- NSF Travel Award to attend NAMS National Meeting (2010)
- Arkansas Society of Professional Engineers (ASPE) College of Engineering Outstanding Graduating Senior (2008) : faculty-nominated and selected as top engineering graduating student
- Chemical Engineering Department Outstanding Senior Student (2008) : faculty-nominated and selected as top chemical engineering graduating student
- NSF Graduate Research Fellowship Honorable Mention (2008)
- Arkansas Student Undergraduate Research Fellowship (SURF) (2007-2008)
- AIChE National Meeting Graduate Student Division Poster Competition: selected Honorable Mention for presentation of undergraduate thesis research (2007)
- Waste-management Education and Research Consortium (WERC) environmental design competition : elected by team-members as co-leader (2007)
- WERC design competition team – First Place: Task 7 (2007)
- WERC design competition team – Oak Ridge Associated Universities (ORAU) Technological Realization award. Team design selected as most ready to be implemented. (2007)
- Goethe Institute German Proficiency Exam: Grundstuffe "First Level" (2005), Mittelstuffe "Middle Level" (2007); Middle Level corresponds to ACTFL level "Intermediate High/Advanced Low".
- UA Honors College Study Abroad Grant to study in Austria (2006)
- University of Arkansas Honors College Fellow. ~75 awarded per year (2003-2008)
- Arkansas Governor's Distinguished Scholar. One recipient per county (2003-2008)
- State-sponsored Robert C. Byrd Memorial scholarship (2003-2005)
- Valedictorian of Searcy High School : Searcy, Arkansas (2003)

Peer-Reviewed Publications

9. **Himstedt, H.H.**, Weaver, J. and Wickramasinghe, R. Responsive membranes for high-performance hydrophobic interaction chromatography. *Journal of Membrane Science*. **2012**. (In preparation).

8. **Himstedt, H.H.**, Qian, X. and Wickramasinghe, R. Magnetically-responsive membranes for treating model wastewaters. *Engineering Science and Technology*. **2012**. (In preparation).

7. **Himstedt, H.H.**, Du, H., Marshall, K., Williams, S., Qian, X. and Wickramasinghe, R. Selective sugar separation by pH-responsive nanofiltration membranes. *Journal of Membrane Science*. **2012**. (Submitted).

6. Yang, Q., **Himstedt, H.H.** Qian, X., Ulbricht, M. and Wickramasinghe, R. Designing magnetic field responsive nanofiltration membranes. *Journal of Membrane Science*. **2012**. (In revision)

5. **Himstedt, H.H.**, Yang, Q., Wickramasinghe, R. and Ulbricht, M. Toward remote-controlled valve functions via magnetically responsive capillary pore membranes. *Journal of Membrane Science*. **2012**, 423-424, 257-266.

4. Wandera, D., **Himstedt, H.H.**, Marroquin, M., Wickramasinghe, S.R. and Husson, S. Modification of ultrafiltration membranes with block copolymer nanolayers for produced water treatment: The roles of polymer chain density and polymerization time on performance. *Journal of Membrane Science*. **2012**, 403-404, 250-260.

3. **Himstedt, H.H.**, Yang, Q., Dasi, L.P., Qian, X., Wickramasinghe, R., and Ulbricht, M. Magnetically Activated Micromixers for Separation Membranes. *Langmuir*. **2011**, 27(9), 5574-5581.

2. **Himstedt, H.H.** and Hestekin, J.A. "Membrane Separation Techniques in the Dairy Industry". Invited to *Modern Applications in Membrane Science and Technology* (pg. 171-224), Edited by I. Escobar and B. Van der Bruggen, ACS Symposium Series, American Chemical Society: Washington, D.C. **2011**.

1. **Himstedt, H.H.**, Marshall, K. and Wickramasinghe, R. pH-responsive Nanofiltration Membranes by Surface Modification. *Journal of Membrane Science*. **2011**, 366(1-2), 373-381.

Grants, Patents, and Other Publications

1. Wickramasinghe, R., Qian, X., **Himstedt, H.H**, Ulbricht, M. and Semmens, M. Magnetically Responsive Membranes. U.S. Patent Application No. 13/570,003. **2012**.

Oral Presentations

17. **Himstedt, H.H.**, Bauder, T., Butters, G., Qian, X., Wickramasinghe, S.R. "Treatment of Oily Wastewater by Magnetically-Activated Filtration Membranes". American Institute of Chemical Engineers (AIChE) Annual Meeting. Oct. 28 – Nov. 2, 2012.

16. **Himstedt, H.H.**, Weaver, J., Wickramasinghe, S.R. "Environmentally-responsive Membrane Adsorbers for Hydrophobic Interaction Chromatography". AIChE Annual Meeting. Oct. 28 – Nov. 2, 2012.

15. Qian, Y., **Himstedt, H.H.**, Qian, X., Wickramasinghe, S.R. "Magnetically Responsive Membrane with Attached Nanoheaters". AIChE Annual Meeting. Oct. 28 – Nov. 2, 2012.

14. **Himstedt, H.H.**, Qian, X., Ulbricht, M., Yang, Q., Wickramasinghe, S.R. "Magnetically-responsive Membranes for Water Treatment". North American Membrane Society (NAMS) National Meeting. June 9-13, 2012.

13. Wickramasinghe, R., **Himstedt, H.H.** and Qian, X. "Responsive Membranes for Water Treatment. ECI Conference: Water Treatment and Re-Use III and the Water-Energy Nexus. Jan. 11, 2012.

12. **Himstedt, H.H.**, Qian, X., Ulbricht, M., Yang, Q., Wickramasinghe, S.R. "Responsive Membranes for Water Treatment". Invited Lecture. 6th Joint Sino-US Conference on Chemical Engineering. Nov. 6-11, 2011.

11. **Himstedt, H.H.**, Yang, Q., Dasi, L.P., Qian, X., Wickramasinghe, R., and Ulbricht, M. "Responsive Membranes for Water Treatment". International Conference on Membranes (ICOM). July 28, 2011.

10. **Himstedt, H.H.**, Yang, Q., Dasi, L.P., Qian, X., Wickramasinghe, R., and Ulbricht, M. "Responsive Membranes for Water Treatment". Network of Young Membrains. July 22, 2011.

9. **Himstedt, H.H.**, Wickramasinghe, R., Marshall, K. and Qian, X. pH responsive nanofiltration membranes by surface modification. Pacifichem. Dec. 14-20, 2010.

8. **Himstedt, H.H.**, Qian, X. and Wickramasinghe, R. "Responsive Membranes for Water Treatment". AIChE Annual Meeting. 2010. Nov 9, 2010. "pH Responsive Membranes for Water Treatment". Nov. 10, 2010

7. **Himstedt, H.H.**, Qian, X. and Wickramasinghe, R. "pH-Responsive Nanofiltration Membranes by Surface Modification". NAMS National Meeting. July 22, 2010.

6. **Himstedt, H.H.**, Marshall, K. and Wickramasinghe, R. "pH-responsive Nanofiltration Membranes for Treatment of Wastewaters". Colorado State University Hydrology Days. March 24, 2010.

5. **Himstedt, H.H.**, Marshall, K. and Wickramasinghe, R. "pH-responsive Membranes for Treatment of Wastewaters". AIChE Annual Meeting. Nov. 13, 2009.

4. **Himstedt, H.H.**, Marshall, K. and Wickramasinghe, R. "pH-responsive Membranes for Treatment of Wastewaters". NAMS Annual Meeting. June 20-24, 2009.

3. **Himstedt, H.H.**, Marshall, K. and Wickramasinghe, R. "pH-responsive Membranes for Treatment of Wastewaters". Colorado State University Hydrology Days. March 23, 2009.

2. Hestekin, J. and **Himstedt, H.H.** "Energy minimization using electrodeionization: organic acid production and separation". AIChE Annual Meeting. Nov. 4-9, 2007.

1. **Himstedt, H.H.**, Huber, S., Kincannon, A., Correnti, M., Bruick, M., Sarayath, M. Winner ORAU Technical Realization Award for most Industrially Viable Design. *Energy Efficient Removal of TDS from RO Reject and Cooling Tower Blowdown*. Task #7. WERC International Design Competition. April 1-4, 2007.

Poster Presentations

10. **Himstedt, H.H.**, Qian, X. and Wickramasinghe, R. "Magnetically-activated micromixer membranes for treatment of wastewaters". ECI Conference: Water Treatment and Re-Use III and the Water-Energy Nexus. Jan. 10, 2012

9. **Himstedt, H.H.**, Wickramasinghe, R., Qian, X., Yang, Q. and Ulbricht, M. "Magnetically Activated Membranes for Treatment of Wastewaters". NAMS National Meeting. June 6, 2011.

8. Marshall, K., Williams, S., **Himstedt, H.H.** and Wickramasinghe, R. "pH-responsive Membranes for Sugar Separation". CSU Celebrate Undergraduate Research and Creativity (CURC). April 19, 2011.

7. Marshall, K., **Himstedt, H.H.** and Wickramasinghe, R. "pH-responsive Nanofiltration Membranes for Water Treatment". CSU Celebrate Undergraduate Research and Creativity (CURC). April 20, 2011

6. **Himstedt, H.H.**, Marshall, K. and Wickramasinghe, R. "pH-responsive Nanofiltration Membranes for Water Treatment". Colorado State University Hydrology Days. March 21, 2011

5. **Himstedt, H.H.** and Wickramasinghe, R. "Magneto-responsive Membranes for Treatment of Naval Bilge Waters". Partners in Environmental Technology Technical Symposium and Workshop.2009. Dec. 1, 2009.

4. **Himstedt, H.H.**, Marshall, K. and Wickramasinghe, R. "pH-responsive Membranes for Treatment of Wastewaters". NAMS Annual Meeting. June 20-24, 2009.

3. Marshall, K., **Himstedt, H.H.** and Wickramasinghe, R. "pH-responsive Membranes for Treatment of Wastewaters". CSU Celebrate Undergraduate Research and Creativity (CURC). April 20, 2009.

2. **Himstedt, H.H.**, Marshall, K. and Wickramasinghe, R. "pH-responsive Membranes for Treatment of Wastewaters". Colorado State University Hydrology Days. March 23, 2009.

1. **Himstedt, H.H.** "Separation of Organic Acids from Fermentation Broths Using Electrodeionization: Fundamental Determination of Wafer Thickness on Transport Properties". AIChE National Meeting. November 4-9, 2007. *Honorable Mention Award.*

Collaborations

- Lab of Dr. M. Ulbricht : Universität Duisburg-Essen; Essen, Germany; Aug. - Nov. 2009
  Worked closely with Dr. Q. Yang (post-doc) to develop critical reaction.
- Symbios, Inc.; Stewart Environmental, Inc; Produced Water Development, Inc. (2010-current)
  Economic and market analysis for commercialization of technology produced by Ph.D. thesis research.
  Symbios, Inc. has purchased option license for invention
- Mr. M. Brown : The Institute of Learning and Teaching (TiLT) : CSU; 2010-current
  Surveyed undergraduates in the CBE department to assess availability and impact of undergraduate research.
  Initiated "campaign", with departmental approval, to inform more students about undergraduate research.
- Dept. of Soil and Crop Sciences : CSU; 2011-current
  Mr. T. Bauder, Dr. G. Butters : effects of treated water on soil properties.
- Mechanical Engineering Dept. : CSU; 2008-current
  Dr. X. Qian : modeling and theory of magnetic fields.
  Dr. L. P. Dasi : micro-fluidic imaging system.
- Dr. R. Waskom : CO Water Institute and CSU Water Center : CSU; 2008-current
  Helped procure various water samples and offered advice on water use issues

Teaching Experience

Colorado State University

- Instructor of Record : BIOM 543 – Membranes for Biotechnology and Biomedicine(2012)
  Online graduate course. 3 credit hours.
- Instructor of Record : CBE 543 – Membranes for Biotechnology and Biomedicine (2011)
  Resident instruction graduate course. 3 credit hours.
- Resident Graduate Mentor (2010-current)
  Drop-in mentoring of freshmen engineering students approximately four hours per week. Typically 10-12 students per week.
  Organized a forum where students could ask engineers of various disciplines what undergraduates should do to prepare for industry, academia, interviews, etc.
- Instructor of Record : ENGR 181A1 – Freshman Seminar (2010, 2011)
  Resident instruction course. 1 credit hour.
  Cover engineering careers and tips for succeeding in engineering courses.
- Teaching Assistant : CBE 442 – Separation Processes (2009, 2010, 2011)
  Lectures when professor was traveling (roughly 20% of lectures)
  Guidance for student investigating membrane systems for their semester project
- Teaching Assistant : CBE 333 – Chem. and Bio. Engineering Lab 1 (2009, 2010)
  Assisted with four sections of 12 students (8 hours per week)

University of Arkansas

- Teaching Assistant : CHEG 3232L - Chemical Engineering Laboratory II (2008)
  Instructed 3 sections of 15 students
- Teaching Assistant : PHYS 2074 University Physics II Honors Section Lab (2007)
  Instructed 1 section of 20 honors students
- Tutor for Athletic Department (2006-2008)
  Six hours per week tutoring German. Two hours per week tutoring Physics.

Certifications & Skills

- CSU The Institute of Learning and Teaching (TiLT) Certificate in College Teaching (2012) - Personal online teaching portfolio detailing courses taught and philosophy on teaching
- Engineer Intern, State of Arkansas License No. 7280 (2008). Intend to take the Principle and Practices of Engineering exam Oct. 2012
- Chromatography: FPLC, HPLC, hydrophobic interaction chromatography (HIC)
- Microscopy and Spectroscopy: SEM, XPS, ATR-FTIR, Transmission FTIR, Surface Plasma Resonance (SPR)
- Surface characterization techniques: contact angle, zeta potential, ellipsometry
- Software: ASPEN, ChemDraw suite, COMSOL Multiphysics, Java programming language, Matlab, Origin, MS Office suite
- First Aid: wilderness responder (2010-current), CPR/basic first aid (1998-current)

Memberships and Academic Involvement

- Reviewer: Separation Science & Technology (2012-current); CSU Journal of Undergraduate Research (2012-current)
- Founding co-president of the CBE Graduate Student Organization (2011-2012)
  - Outlined an organization to meet needs of graduate students
  - Registered CBEGSO as a registered student organization at CSU
  - Organize forums to help CBE graduate students with resume writing, designing experiments, and other topics for succeeding in graduate school
  - Serve CBE department by organizing prospective student tours and mediating student-faculty communication
- Member: European Membrane Society, **EMS** (2011)
- Member: American Association for the Advancement of Science, **AAAS** (2010)
- CSU Graduate Student Council: committee Member (2010-current)
- Member: North American Membrane Society, **NAMS** (2009)
- Judge for yearly CSU CURC undergraduate research poster competition (2009-current)
- Member: American Institute of Chemical Engineers, **AIChE** (2007)
  - Student Chapter: President (2007), Class representative (2006-2007)

- Member: Tau Beta Pi (2007)
  - Assisted with TBP Initiations at CSU (2010-2011)
  - Corresponding Secretary (2007-2008), National Convention Delegate (2007)
- Member: Phi Beta Kappa Honor Society (2008)
- Member: Delta Phi Alpha - National German Honor Society (2006)

Recent Volunteer and Community Involvement

- Boy Scouts of America (BSA) Eagle Scout award (2000)
- Assistant Scoutmaster and Merit Badge Instructor (adult leadership positions) for BSA Troop 116, Fayetteville, AR (2006-2008) and Troop 12, Fort Collins, CO (2008-current)
- Cook and server for weekly community meals at First Presbyterian Church (2008-current)
- Vacation Bible School at First Presbyterian Church: co-led Science module. Developed "curriculum" to teach ages 4-8 about science and easy-to-perform experiments (2011)
- Judge for Mathcounts Math Competition for local 6^{th}-8^{th} graders (2010-2012)
- CSU Engineering Days (E-days): senior design competition judge (2009-2012)
- Volunteer instructor for 4^{th} graders at CSU science, technology, engineering, mathematics (STEM) day (2008, 2010-2011).
- BSA National Jamboree Volunteer Staff (2010)
- UA Honors College Ambassador: recruitment and retention (2003-2008)